1-1-1997

Polymer surface chemistry : surface mixtures, supported polyelectrolyte multilayers and heterogeneous chemical modification.

Vipavee, Phuvanartnuruks
University of Massachusetts Amherst

Follow this and additional works at: https://scholarworks.umass.edu/dissertations_1

POLYMER SURFACE CHEMISTRY: SURFACE MIXTURES, SUPPORTED POLYELECTROLYTE MULTILAYERS AND HETEROGENEOUS CHEMICAL MODIFICATION

A Dissertation Presented

by

VIPAVEE PHUVANARTNURUKS

POLYMER SURFACE CHEMISTRY: SURFACE MIXTURES,
SUPPORTED POLYELECTROLYTE MULTILAYERS AND HETEROGENEOUS
CHEMICAL MODIFICATION

A Dissertation Presented

by

VIPAVEE PHUVANARTNURUKS

Approved as to style and content by:

_____
Thomas J. McCarthy, Chair

_____
Thomas P. Russell, Member

_____
C. Peter Lillya, Member

_____
Richard J. Farris, Department Head
Polymer Science and Engineering

To my parents Achara and Panthep Phuvanartnuruk

ACKNOWLEDGMENTS

ABSTRACT

POLYMER SURFACE CHEMISTRY: SURFACE MIXTURES,
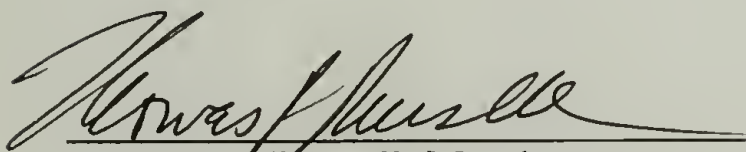SUPPORTED POLYELECTROLYTE MULTILAYERS AND HETEROGENEOUS
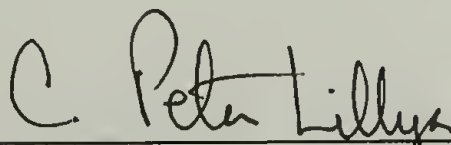CHEMICAL MODIFICATION

SEPTEMBER 1997

VIPAVEE PHUVANARTNURUKS, B.Sc., CHULALONGKORN UNIVERSITY,
THAILAND

M.S., UNIVERSITY OF MASSACHUSETTS AMHERST

Ph.D., UNIVERSITY OF MASSACHUSETTS AMHERST

Directed by: Professor Thomas J. McCarthy

This dissertation is divided into three parts that summarize three discrete projects

that are related only in their overall objective of using chemistry to rationally control

polymer surface structure and properties. Each part involves polymer surface modification,

but the three employ very different techniques to effect surface-chemical changes.

The first part (Chapter 1) involves the preparation of surfaces containing

controllable mixtures of two functionalities (alcohol/ester or hydrocarbon

ester/fluorocarbon ester) from alcohol-functionalized poly(chlorotrifluoroethylene)

(PCTFE-OH) and the studies of their wetting behavior as a function of composition and

structure. Contact angle analyses indicate that sequential and competitive esterifications

yield mixed surfaces consisting of the two functional groups distributed randomly, while

compositionally similar, patchy mixed surfaces can be prepared by partial hydrolysis/re-

esterification under some specific conditions. Greater contact angle hysteresis was

observed on the patchy surfaces.

The second part (Chapter 2) describes the layer-by-layer deposition of cationic

(polyallylamine hydrochloride (PAH)) and anionic (polysodium styrenesulfonate (PSS))

polyelectrolytes onto the PCTFE-OH substrate. XPS and contact angle data indicate that

the assembled layers are stratified even though the individual layers are extremely thin (0.3

- 4.1 Å). This thickness depends both on the charge density of the first layer of PAH (controlled using pH) and the ionic strength of the PSS adsorption solution. The stoichiometry of the assembly process also varies with the ionic strength of the PSS adsorption solution.

The third part (Chapter 3) involves the heterogeneous (gas-solid) chemical modification of poly(trifluoroethylene) (PF_3E). Chlorination of PF_3E is a surface-selective reaction and the extent of chlorination can be controlled by time and light intensity. The fluorination of PF_3E carried out using 5% F_2/N_2 yields products that exhibit similar surface properties to poly(tetrafluoroethylene) (PTFE). Very thin coatings of PF_3E on inorganic supports (Si wafers) were prepared by the adsorptions from THF:toluene solutions. The higher the toluene composition, the more polymer adsorbs and the rougher the substrate becomes. The amount of PF_3E adsorption is increased significantly by introducing a polar functional group to the polymer by maleation.

TABLE OF CONTENTS

LIST OF TABLES

xiii

xxi

PREPARATION AND STUDY OF MODIFIED POLYMER SURFACE MIXTURES

Introduction

Organic chemistry at polymer surfaces has been extensively utilized for developing superior surface properties in a number of polymers for example: adhesion, adsorption, wettability and biocompatability. Many successful methods, including polymer grafting,[1,2] plasma treatment[3,4] and corona discharge treatment[5,6] have been applied to a wide variety of polymers. Nevertheless, these types of modifications have some drawbacks. Rigorous and uncontrolled reactions can induce changes in surface morphology, changes in topography, and most certainly, chemically heterogeneous surfaces. Therefore, it becomes difficult to correlate macroscopic surface properties with microscopic surface chemical structure. In order to achieve a better understanding of surface structure-property relationships, well-controlled functionalized polymer surfaces are required. Previously, a nondestructive technique has been proposed to chemically modify polymer surfaces in a controlled manner.[7,8] With the strategy to first introduce a discrete reactive functional group to a chemically resistant polymer surface and subsequently functionalize the versatile intermediate, a series of homogeneous derivatives can be prepared.

The studies of surface properties of homogeneous functionalized polymer samples, however, are not sufficient to address some important issues concerning the "real" modified surfaces that in fact are heterogeneous in nature, for instance: how does the composition of a two component mixture affect the surface properties?, how does the two-dimensional order of two components in a heterogeneous mixed surface affect the surface properties? In order to clarify these issues, it is necessary to have polymer surface mixtures with well-defined chemical compositions and two-dimensional order.

The objectives of this research are to: (1) prepare compositionally similar mixed polymer surfaces which differ in surface structure due to their different synthetic routes and (2) determine their wetting behavior, which is profoundly sensitive to both surface functionality and surface structure, using contact angle analysis.

Surface Chemistry

Polymer Substrate

Poly(chlorotrifluoroethylene) (PCTFE), a material that is widely used for packaging applications was chosen as a substrate. This material is a thermoplastic film of 0.005 inches thickness. It was purchased from Allied-Signal as Aclar 33C which is a terpolymer composed of primarily chlorotrifluoroethylene with small amounts of tetrafluoroethylene and vinylidene fluoride. The polymer exhibits very good chemical resistance, excellent water and gas barrier properties as well as good electrical properties. It has a crystalline melting temperature of 202-204 °C and a glass transition temperature of 58-65 °C. The density is varied from d = 2.10 g/cm^3 (45% crystalline) to d = 2.13 g/cm^3 (65% crystalline) depending on its thermal history. The Aclar 33C used is highly crystalline (~65%). The refractive index is 1.435.[9]

Initial Modification

PCTFE with its chemically resistant properties has been found to react with a number of organometallic reagents.[7] Dias and McCarthy studied the modification of PCTFE powder with organolithium reagents. They proposed a mechanism involving a reduction-elimination-addition sequence (see Scheme 1.1). The polymer product contains organic chemical groups derived from the organolithium reagent and unsaturation in the polymer backbone. By utilizing the same strategy, a variety of chemical functional groups
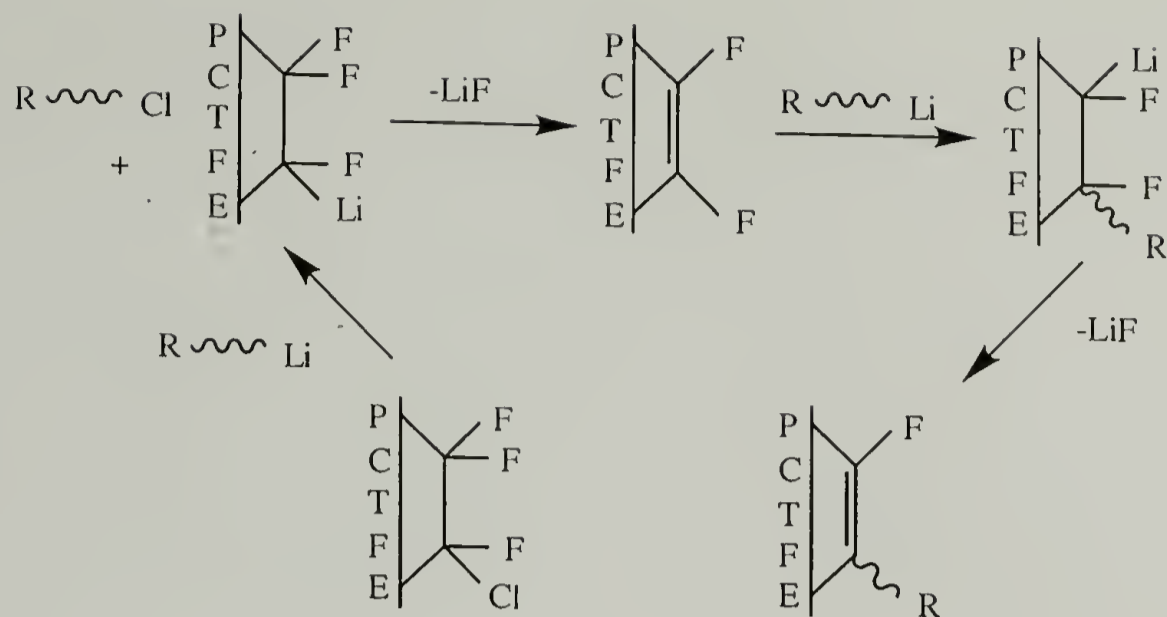
Scheme 1.1. Proposed mechanism for the reaction of organolithium reagents with PCTFE.

can be introduced by the reaction of PCTFE with organolithium reagents containing the appropriate protected functional groups.

This particular study was focused on the preparation of surface mixtures using esterification reactions of an alcohol-containing poly(chlorotrifluoroethylene) surface (PCTFE-OH) and partial hydrolysis of the ester surfaces. The hydroxyl groups can be introduced onto the polymer surface by the reaction of PCTFE film with the protected alcohol-containing organolithium reagent, (3-lithiopropyl ethyl acetaldehyde acetal), and subsequent deprotection by hydrolysis (shown below).
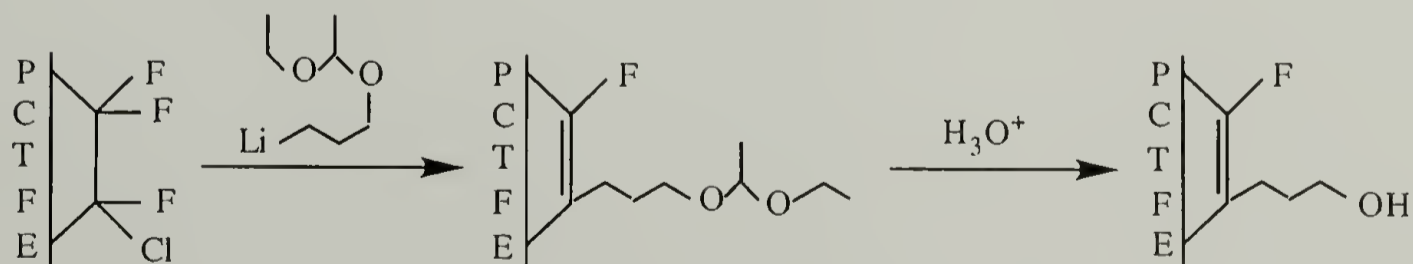
Scheme 1.2. Introduction of alcohol groups onto the PCTFE surface.

3

The depth of the initial modification reaction can be controlled by four factors: temperature, time, solvent composition and organolithium reagent concentration. The preparation and characterization have been previously discussed in detail.[8,10] The conditions selected to prepare acetal-functionalized PCTFE (PCTFE-PEAA) were reported to yield modified layer thicknesses ranging from ~50 Å to ~1000 Å for the reactions carried out between -78 °C and -15 °C, using 50:50 THF:heptane as a solvent for 30 min. Higher reaction temperatures increase surface mobility, resulting in greater modified thicknesses. The stoichiometry of acetal-functionalized PCTFE deduced from XPS atomic composition data suggests that the modified surface is composed of 80% acetal groups and 20% difluoroolefins. This structure indicates that the first step in Scheme 1.3 (formation of difluoroolefin) proceeds quantitatively, while the second step (introduction of the acetal group) proceeds in only 80% yield, likely due to steric effects.
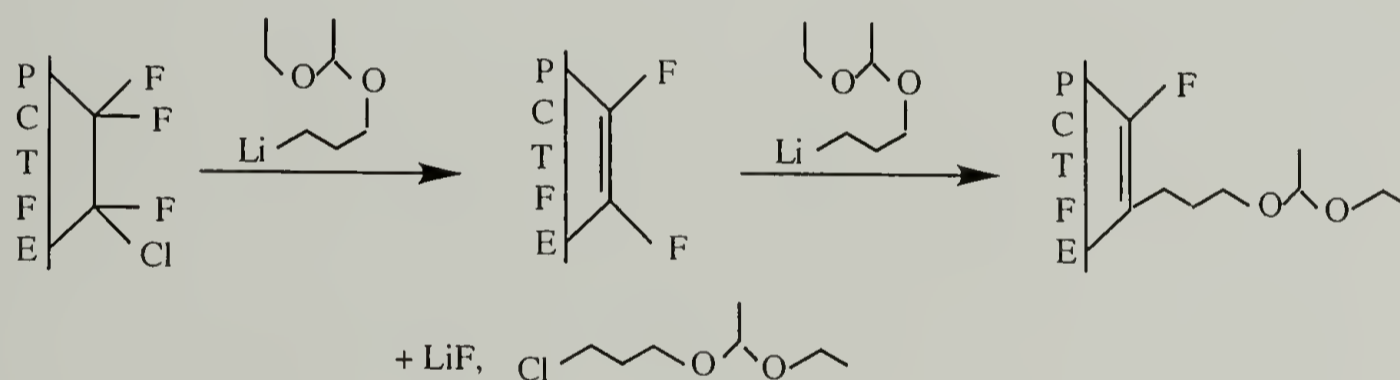
Scheme 1.3. Reaction of PCTFE with 3-lithiopropyl ethyl acetaldehyde acetal.

The alcohol-functionalized PCTFE (PCTFE-OH) can be prepared from previously made acetal-functionalized PCTFE (PCTFE-PEAA) by hydrolysis. A number of studies were conducted to determine the appropriate hydrolysis conditions that can provide the thickest possible alcohol modified layer, complete deprotection of the acetal groups and the least extent of dissolution of modified surface. It was found that the optimal condition is to reflux PCTFE-PEAA in aqueous HCl at 100 °C for 30 min.[10] Upon deprotection, the XPS

atomic composition confirms the predicted stoichiometry for a modified polymer containing 80 % hydroxyl-functionalized repeat units and 20% difluoroolefins (Figure 1.1).
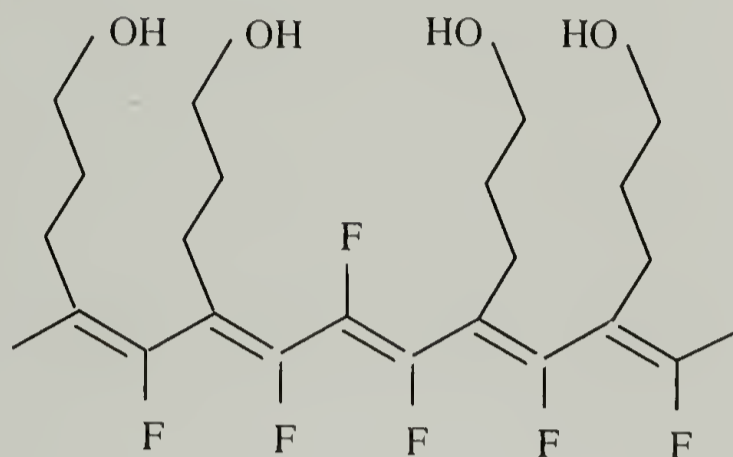
Figure 1.1. Surface structure of PCTFE-OH.

Preparation of Modified Surface Mixtures

In the research presented here, two types of surface mixtures were prepared: alcohol/ester mixed surfaces and hydrocarbon ester/fluorocarbon ester mixed surfaces. Three synthetic routes (depicted in Scheme 1.4) were used to prepare modified surface mixtures: (1) sequential esterification by partial esterification with R_1, followed by conversion of the remaining hydroxyl groups with R_2 (where R_1 and R_2 are the acid chlorides of interest), (2) partial hydrolysis/re-esterification by complete esterification of PCTFE-OH with R_1 followed by partial hydrolysis and then re-esterification of the resulting hydroxyl groups with R_2 and (3) competitive esterification of PCTFE-OH with two acid chlorides.

We conceived that sequential esterification should produce surfaces with the two functional groups randomly dispersed, while the partial hydrolysis/re-esterification approach should produce patchy surfaces (see Scheme 1.5). The hydrolysis/methanolysis of the ester surfaces may be inhibited initially since these hydrophobic surfaces are not sufficiently wet by the reaction solution. Once the hydrolysis begins at some point on

(1) Sequential Esterification
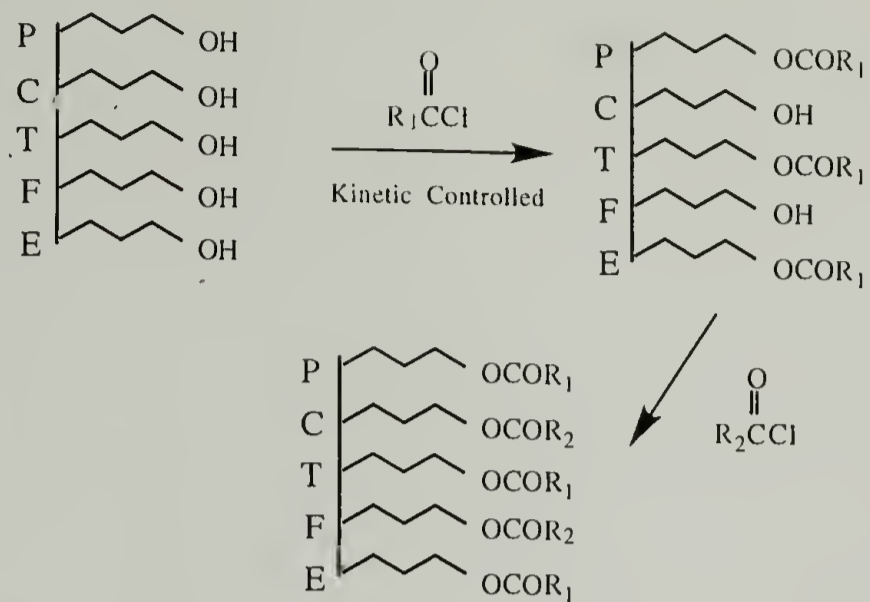
(2) Partial Hydrolysis/Re-esterification
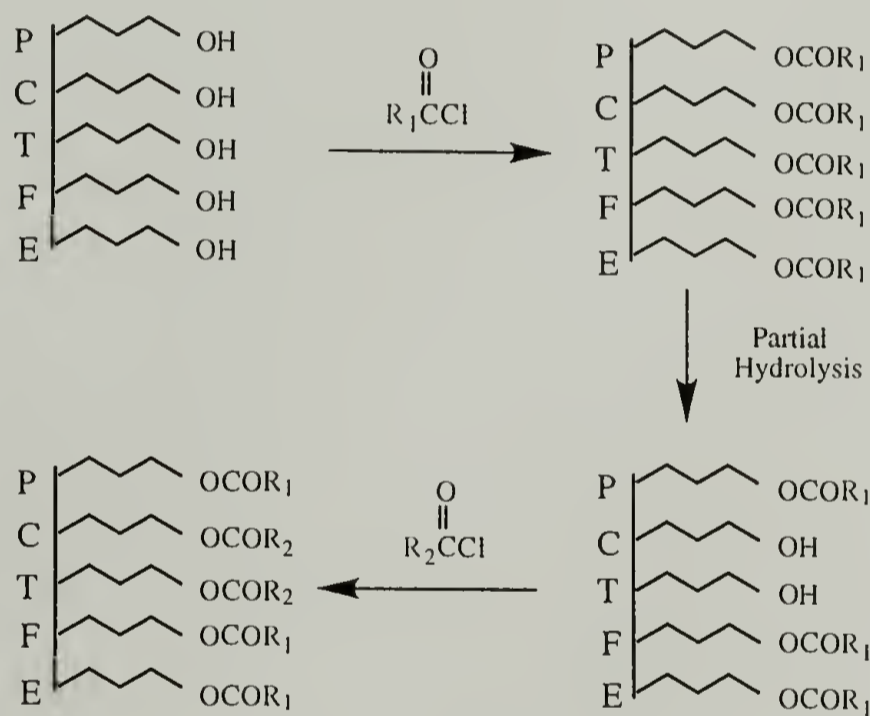
(3) Competitive Esterification
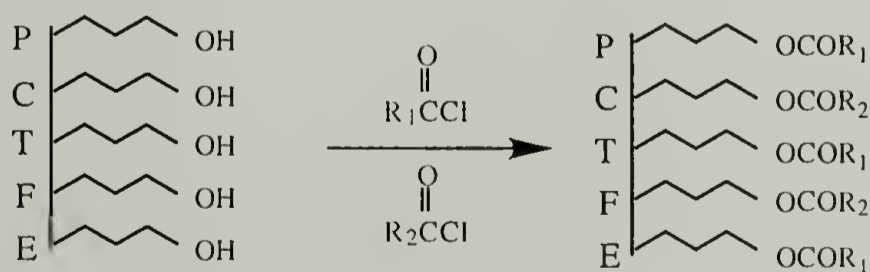
Scheme 1.4. Proposed procedures to prepare modified surface mixtures.

(1)   Randomly Mixed Surfaces
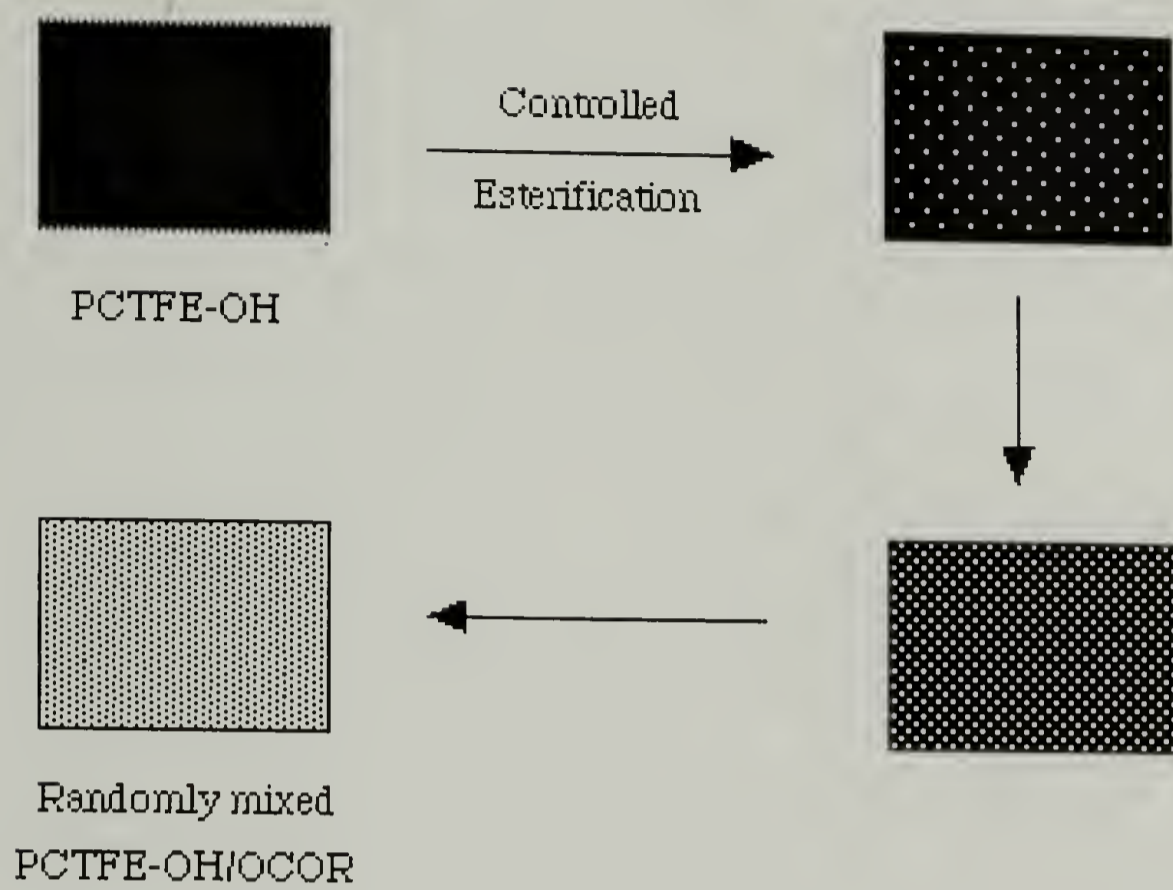
(2)   Patchy Mixed Surfaces
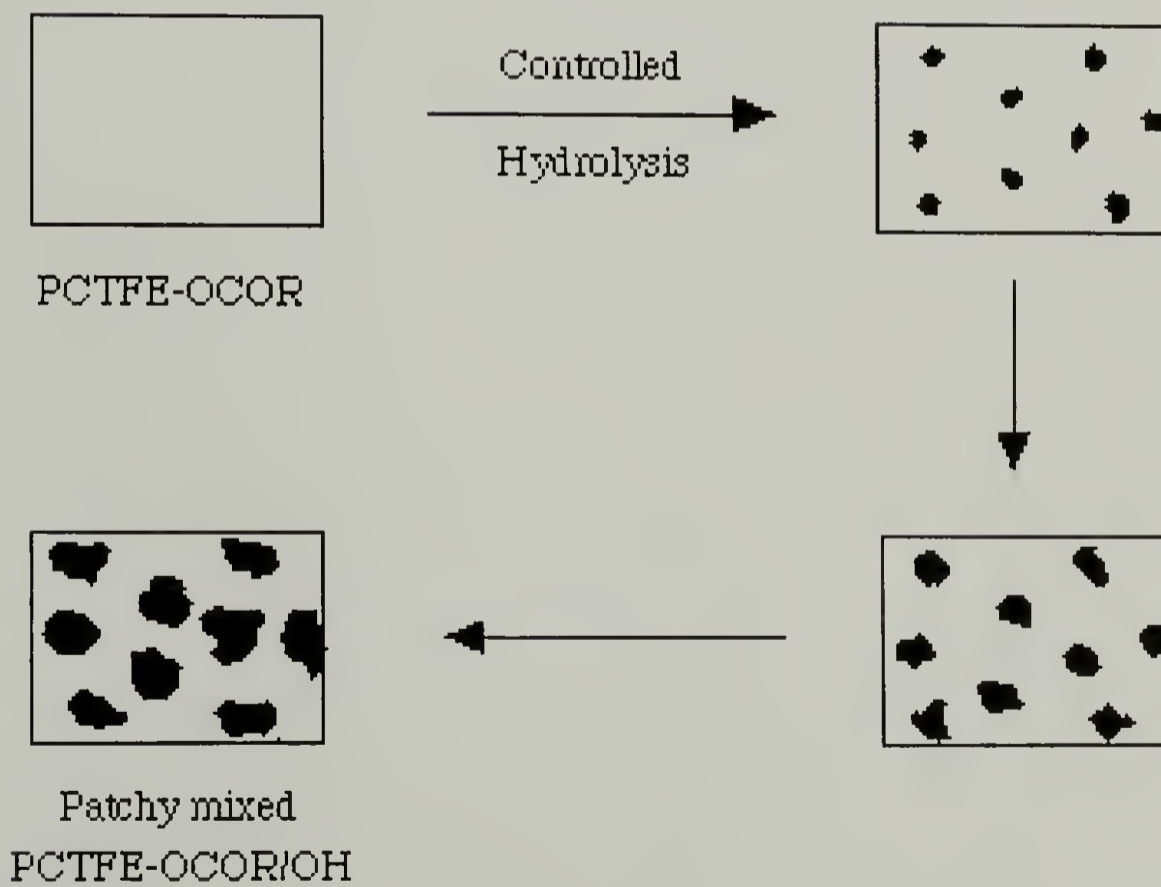
Scheme 1.5. Proposed mixed surface structures: randomly mixed surfaces and patchy mixed surfaces.

the surface (either at defects or some random position), that location will contain a hydroxyl group which will facilitate the transport of the reaction solution to the ester functionality surrounding the alcohol. The rate of hydrolysis at these points on the surface will then be enhanced, resulting in an autoaccelerative reaction and a "patchy" surface.

Kinetic control of the initial step of both synthetic routes (esterification and hydrolysis) can give rise to a series of mixed alcohol/ester surfaces with different surface compositions (randomly mixed or patchy mixed surfaces). Subsequent esterification with the desired acid chloride should then result in mixed hydrocarbon ester/fluorocarbon ester surfaces. Competitive esterification was used as an alternative to prepare mixed hydrocarbon ester/fluorocarbon ester surfaces. PCTFE-OH was reacted with acid chloride mixtures (butyryl chloride mixed with heptafluorobutyryl chloride or stearoyl chloride mixed with heptafluorobutyryl chloride). It is expected that the resulting mixed surfaces should have two ester functional groups distributed randomly throughout the surface.

Surface Analytical Techniques

X-ray Photoelectron Spectroscopy (XPS)

This technique, which is often referred to as Electron Spectroscopy for Chemical Analysis (ESCA), is generally regarded as an important technique for polymer surface characterization. The quantitative technique can provide atomic compositon of a surface with a sampling depth on the order of 10-200 Å depending on the sample and instrumental conditions.

The basic principle of XPS involves the photoelectric effect. The analysis is accomplished by irradiating a sample with monoenergetic soft x-rays and analyzing the energy of the electrons emitted. An elemental analysis can be obtained due to the unique set of core electrons for each element. The number of electrons emitted are counted as a function of their energy. Quantitative information can be calculated from peak areas and

8

atomic sensitivity factors obtained from samples with known composition. The photon energy is greater than the binding energy of the electron in the atom, and the electron ejected from the atom should have a kinetic energy (E_k) approximately equal to the difference between the photon energy and the binding energy (E_b). Therefore, the basic equation for XPS is:

$$E_b = h\upsilon - E_k - \phi \tag{1.1}$$

where h is Planck's constant, υ is x-ray frequency and ϕ is the spectrometer work function. All energies are usually expressed in electron volts (eV). Note that the results reported in this work are not corrected for sample charging.

The technique is surface selective. Although the photons can penetrate many microns deep into the sample, the electrons generated at the depth have relatively low kinetic energy (0-1000 eV) and cannot travel very large distance in matter. Only those electrons emerging from a certain depth (10-200 Å) without losing their kinetic energy from inelastic collisions comprise the main photoelectron peaks. Common anode materials used as x-rays sources are magnesium, aluminum, titanium and chromium whose K_α x-rays have energies of 1254, 1487, 4510 and 5417 eV, respectively. Although the titanium and chromium x-rays have higher energies that can eject electrons in deeper core shells and can provide information in deeper sampling region, magnesium and aluminum anodes are preferable due to their narrow line widths and lower tendency to damage samples.

The intensity of electrons detected from a specific element in a homogeneous, infinitely thick sample can be expressed by the following equation:

$$N_{i,k} = I_0 \rho_i \sigma_{i,k} \lambda_{i,k} T_{i,k} \tag{1.2}$$

where $N_{i,k}$ is the measured peak area for the kth shell of element i, I_0 is the x-ray flux, ρ_i is the volume density of element i in the surface volume examined by XPS (desired in the experiment), $\sigma_{i,k}$ is the photoionization cross-section (the probability for photoionization), $\lambda_{i,k}$ is the electron mean free path in the material and $T_{i,k}$ is the instrument transmission function (the number of electrons counted compared with the number that enter the detector). The terms in this equation are typically obtained by the calibration of the particular instrument with appropriate materials and the use of atomic sensitivity factor, $S_{i,k}$ which is equal to $I_0\sigma_{i,k}\lambda_{i,k}T_{i,k}$ is common. From equation 1.2:

$$\rho_i \;\; = \;\; N_{i,k}/S_{i,k} \tag{1.3}$$

In general, the sensitivity factor of F_{1s} electrons is assigned as 1.00 and used as a reference to calculate all other sensitivity factors by measuring relative intensities of samples with known surface composition through this equation:

$$C_j \;\; = \;\; \rho_j/\Sigma\,\rho_i \;\; = \;\; (N_j/S_j)/\Sigma(N_i/S_i) \tag{1.4}$$

where C_j is the atomic concentration of element j. There are two main advantages obtained from using this equation to calculate the relative concentration as opposed to direct calculation of ρ_i: (1) the exact x-ray flux which decays over lifetime of anode is not critical and (2) there is a small variation in the ratios of mean free paths from sample to sample, even though the mean free paths are material-dependent. Typical materials used for calibration in this work are poly(tetrafluoroethylene), poly(chlorotrifluoroethylene) and poly(ethylene terephthalate).

Practical surfaces are rarely uniform and homogeneous in composition and structure. The surface often consists of a very thin film on a semi-infinite bulk substrate. The depth profiling of samples is thus very useful. This can be accomplished by the

variable angle technique. By varying the take-off angle (θ_T) between the detector and the surface, electrons travel from similar vertical depths with different distances before reaching the detector. At small θ_T, a smaller depth is sampled than at high θ_T. The surface sensitivity is thus enhanced at low θ_T.

Anode

Detector

θ_T

t

d
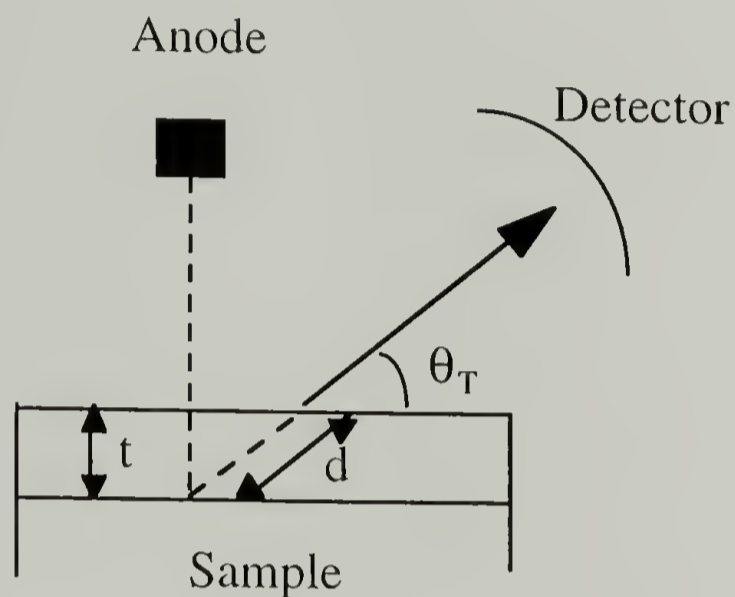
Sample

Figure 1.2. The sample/detector geometry of variable angle XPS.

The attenuation of photoelectron intensity in solids as a function of sampling depth is expressed in Equation 1.5 where N_0 is the number of electrons that originate at depth t, N is the number of photoelectrons emitted from the solid that have not been inelastically scattered, λ is the mean free path of the electron and θ is the take-off angle.

$$N = N_0 e^{-t/\lambda \sin\theta} \tag{1.5}$$

The expression indicates that 95% of detected photoelectrons originate in the outermost $3\lambda\sin\theta$. In another words, the electron should be attenuated to 5% of its original intensity when the thickness is $3\lambda\sin\theta$. The equation also indicates that the spectra

11

recorded at a 15° take-off angle assess the composition of the outermost ~27 % of the region analyzed at a 75° take-off angle.

Mean free path values have been obtained experimentally from overlayer experiments in which the decrease of signal from the substrate is measured as a function of overlayer thickness. Overlayers are normally deposited by Langmuir-Blodgett techniques,[11,12] molecular self-assembly[13] and vapor phase methods.[14,15] For organic materials, the mean free paths are somewhat controversial, ranging from the relatively low values reported by Clark et al.[14,15] to the higher values reported by others.[11-13, 16] Ashley and coworkers[17] have developed a theoretical approach for the calculation of mean free paths in organic materials. The relationship is:

$$\lambda \;=\; (ME_k/\rho n)/(13.6\ln E_k - 17.6 - 1400/E_k) \tag{1.6}$$

where E_k is the kinetic energy in eV, M is the molecular weight of molecule or repeat unit, n is the number of valence electrons in the repeat unit and ρ is the density of the material.

Attenuated Total Reflectance Infrared (ATR IR) Spectroscopy

This technique couples the method of infrared spectroscopy with the physical phenomenon of total internal reflection to enable the molecular vibrations as well as the information of molecular structure, conformation, crystallinity, functionality and secondary bonding within the surface regions of materials to be analyzed. The theoretical background has been developed by Harrick[18] and others.[19,20] The principle of this technique is based on a special case of the general phenomenon of reflection and refraction of electromagnetic radiation at an interface of two media having different refractive indices. Total internal reflection can occur at the interface of the optically transparent element and the sample only if the refractive index of the optically transparent material is greater (optically denser) than

the refractive index of the sample (optically rarer) with the incident angle above a critical angle (θ_c) which can be calculated from:

$$\theta_c = \sin^{-1}(n_{21}) \tag{1.7}$$

where $n_{21} = n_2/n_1$ and n_1 and n_2 are the refractive index of the dense material through which light propagates and the refractive index of rarer media, respectively.

In reflection spectroscopy, both dipoles oriented parallel and perpendicular to the propagating direction absorb energy, unlike normal transmission spectroscopy (dipoles oriented parallel to the propagating direction do not adsorb energy). For total internal reflection, the electric field amplitude at the interface can be expressed as:

$$E_{y0} = 2\cos\theta/(1 - n_{21}^2)^{1/2} \tag{1.8}$$

$$E_{x0} = \frac{2(\sin^2\theta - n_{21}^2)^{1/2}\cos\theta}{(1 - n_{21}^2)^{1/2}[(1 + n_{21}^2)\sin^2\theta - n_{21}^2]^{1/2}} \tag{1.9}$$

$$E_{z0} = \frac{2\sin\theta\cos\theta}{(1 - n_{21}^2)^{1/2}[(1 + n_{21}^2)\sin^2\theta - n_{21}^2]^{1/2}} \tag{1.10}$$

The right-handed coordinate system is used where the x direction is along the propagation direction and positive z direction is normal to the surface into the rarer medium. E_{y0} represents the electric field amplitude for perpendicular polarization while parallel polarization is given by:

$$E_{\parallel} = (|E_{x0}|^2 + |E_{z0}|^2)^{1/2} \tag{1.11}$$

The electromagnetic field established within the second (rarer) medium is represented by an evanescent wave. Therefore, the wave can potentially be very informative about the structure of the second medium. If the actual thickness of the second medium is greater than the distance that the electromagnetic field extends in the z-direction into the second medium, the evanescent wave decreases in amplitude exponentially from the surface:

$$E = E_0 e^{-Z/dp}$$ (1.12)

where d_p is the depth of penetration and can be defined as the distance where the electric field attenuates to $1/e$ of its original value and may be expressed by:

$$d_p = \lambda_1 / 2\pi(\sin2\theta - n_{21}^2)^{1/2}$$ (1.13)

where λ_1 is the wavelength of light in denser medium. For the research described in this chapter using PCTFE ($n_2 = 1.43$) and a germanium crystal ($n_1 = 4.00$) and entrance angle (θ) of 45°, the depth of penetration is equal to 0.2609λ or 0.9 μm at 3000 cm^{-1} and 1.7 μm at 1500 cm^{-1}.

Attenuated total reflection is a "lossy" coupling to the evanescent wave involving a loss of radiant energy associated with the electromagnetic field. The incident electromagnetic radiation is not totally reflected back into the initial medium at the interface due to an absorption of radiation by the rarer medium. Polymers are considered "lossy" materials because some radiation is irreversibly lost due to absorption. The evanescent wave amplitude is decreased without distortion or becomes attenuated as a result of reflection at the interface. Attenuated total reflection is the coupling mechanism most often used with total internal reflection for polymers. Since polymers are only weakly absorbing materials, multiple internal reflections are often used in conjunction with attenuated total

14

reflection to amplify the effects of small reflectivity decrease per reflection. Due to the weak absorption, the strength of the interaction can be expressed as an effective thickness, d_e, which is the equivalent sample thickness in transmission infrared spectroscopy (transmission through the entire thickness of the bulk sample) resulting in the same absorbance as obtained by the decrease in reflectivity per reflection (the spectra recorded in this dissertation utilized 10 reflections). The effective thickness integrated, calculated by assuming the thickness of material is much greater than the penetration depth, can be expressed as:

$$d_e = n_{21}E_0^2 d_p / 2\cos\theta \tag{1.14}$$

Upon substituting the appropriate expressions for d_p and E_0^2, the effective thicknesses for parallel and perpendicular polarizations are:

$$d_{e\parallel} = \frac{\lambda_1 n_{21}\cos\theta(2\sin^2\theta - n_{21}^2)}{\pi(1 - n_{21}^2)[(1 + n_{21}^2)\sin^2\theta - n_{21}^2](\sin^2\theta - n_{21}^2)^{1/2}} \tag{1.15}$$

$$d_{e\perp} = \frac{\lambda_1 n_{21}\cos\theta}{\pi(1 - n_{21}^2)(\sin^2\theta - n_{21}^2)^{1/2}} \tag{1.16}$$

These two equations indicate that an effective thickness is not only a function of incident angle wavelength and refractive indices of two media but also a function of the state of polarization. Inserting values of $n_1 = 4.00$ for the germanium crystal, $n_2 = 1.43$ and $\theta = 45°$ yields $d_{e\parallel} = 0.3024\lambda_1$ and $d_{e\perp} = 0.1512 \lambda_1$. $d_{e\parallel}$ and $d_{e\perp}$ are 1.0 μm and 0.5 μm, respectively at 3000 cm^{-1} and 2.0 μm and 1.0 μm, respectively at 1500 cm^{-1}. Thus the higher wavelength (low wavenumber) side of the single infrared band will have a higher absorbance than the lower wavelength (higher wavenumber) side of the band.

For surface modified materials, there are three media to be concerned: (1) the internal reflection element with refractive index n_1, (2) the modified layer with refractive index n_2 and (3) the bulk material with refractive index n_3. If the modified layer thickness (t) is much less than the penetration depth, the electric field can be assumed to be relatively constant throughout the modified layer. This assumption is valid when $2\pi t/\lambda_1 < 0.1$ (i.e. t < 800 Å when $\lambda_1 = 2000$ cm^{-1}). The effective thickness can be expressed as:

$$d_e = n_{21} E_0^2 t / \cos\theta \qquad (1.17)$$

This equation indicates that the effective thickness is proportional to the thickness of the modified layer (t), not the depth of penetration (d_p). As a result, the adsorption bands from thin modified layers are not relatively stronger at longer wavelengths and internal reflection spectra will be similar to those of transmission spectra.

Typical crystalline materials used as internal reflection elements (IRS) are germanium (Ge, n = 4.00), silicon (Si, n = 3.42), zinc selenide (ZnSe, n = 2.42) and thallium bromide-thallium iodide (KRS-5, n = 2.35).[21] The sampling depths increase for internal reflection elements having lower refractive indices. The sampling depths can also be varied for a particular internal reflection element to decrease or increase surface sensitivity by changing the incident angle. The optics of internal reflection cells are designed to have either fixed (30°, 45° or 60°) or continuously varied incident angles (20°-90°). The incident angle is actually a function of two variable angles: endface angle (β) and optics angle (ψ) (Figure 1.3). If the two variable angles are identical, then the particular angle is the incident angle ($\theta = \beta = \psi$). For a particular crystalline material, the sampling depths are increased with lower incident angles.

$\psi = \beta$
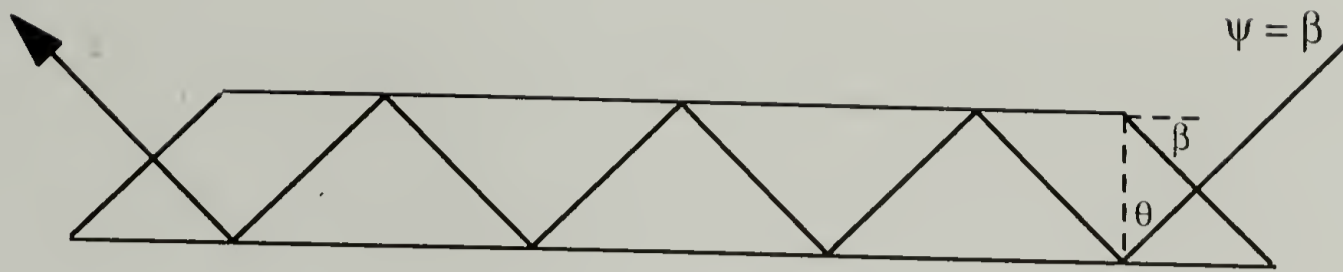
Figure 1.3. Multiple internal reflection of electromagnetic radiation within internal reflection element with equal variable angles ($\theta = \beta = \psi$).

Contact Angle

Contact angle is considered one of the most surface-sensitive techniques and can provide information on the outermost few angstroms of solids.[22] The equipment required is relatively simple and inexpensive. The basis of the contact angle technique is the three-phase equilibrium at the contact point at the solid/liquid/vapor interface (Figure 1.4).

γ^{LV}

γ^{SV}

θ

γ^{SL}
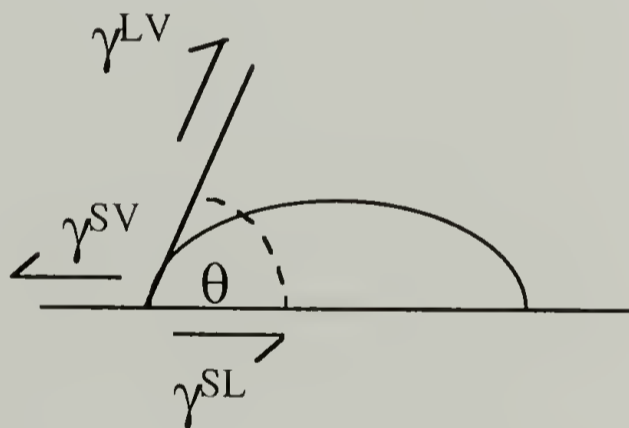
Figure 1.4. Contact angle geometry indicating the three-phase equilibrium.

The contact angle was associated to the surface energy of the solid and the liquid surface tension by Young in 1805.[23] The calculation is based on the energy balance approach to the three-phase equilibrium. The cosine contact angle ($\cos\theta$) is directly related to the surface energy by Young's equation (Equation 1.18), where γ^{sv}, γ^{sl} and γ^{lv} are the surface energy of the solid-vapor, solid-liquid, liquid-vapor interfaces, respectively.

$$\gamma^{SV} - \gamma^{SL} = \gamma^{LV} \cos\theta \tag{1.18}$$

Direct interpretations from this equation can be made based on several assumptions that predict only one intrinsic contact angle (θ_0) regardless of how that angle is measured. The assumptions are: (1) the solid surface is rigid and nondeformable (surface modulus > 3.5×10^5 dynes/cm^2), (2) the solid surface is highly smooth, (3) the solid surface is chemically homogeneous, (4) the solid surface does not interact in any way with the liquid other than the three-phase equilibrium (i.e. swelling), (5) the surface functional groups do not reorganize in response to changes in the environment during the measurement and (6) the liquid must not cause extraction or partitioning of material from the solid phase to the liquid phase.

In practice, some of these assumptions are generally not valid and the observed contact angles depend on the way they are obtained. Generally, two contact angle values are measured (see Figure 1.5). The advancing contact angle (θ_A) can be measured as the solid/liquid contact area increases. The receding contact angle (θ_R) can be measured as the solid/liquid contact area decreases.
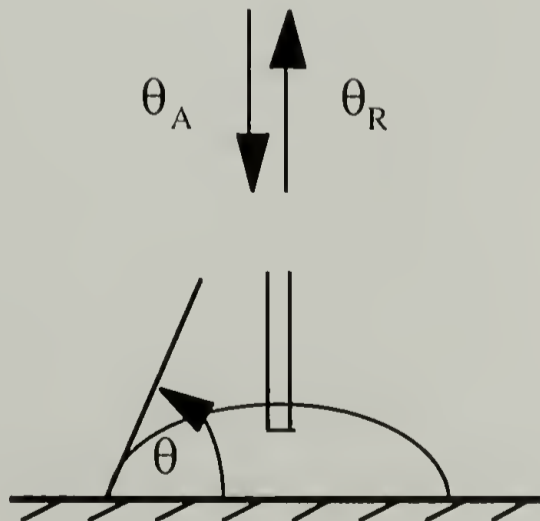
Figure 1.5. Measurement of advancing/receding contact angles (θ_A/θ_R).

In general, $\theta_A > \theta_0 > \theta_R$ and the difference between advancing angle and receding angle is defined as contact angle hysteresis. There are two classes of contact angle hysteresis: (1) thermodynamic hysteresis, where the hysteresis is reproducible over many measurements made and independent of time and (2) kinetic hysteresis, where the hysteresis changes with time and the number of repeat measurements.[24,25] The thermodynamic hysteresis is generally associated with surface roughness and chemical heterogeneity. Kinetic hysteresis is associated with breakdowns in assumptions 4-6 which can cause changes in any or all interfacial energy (γ^{sv}, γ^{sl} and γ^{lv}).

The best general study of the effect of surface roughness on contact angle was done by Johnson and Dettre.[26,27] The model consists of a liquid drop (constant volume) on a surface of concentric grooves assuming the absence of gravitational forces. The observed contact angle is given by :

$$\theta = \theta_0 + \alpha \tag{1.18}$$

where θ_0 is the intrinsic contact angle of the liquid measured on an equivalent smooth surface and α is the angle of inclination of the surface at the liquid-solid contact line. Their results show that as the surface roughness increases, the hysteresis increases (increased advancing angle and decreased receding angle) based on various experimental measurements. It has also been observed that if the surface becomes too rough, two different situations can occur. If $\theta_0 < 90°$, there is a critical roughness above which the liquid will spread spontaneously over the surface due to capillary forces. This critical roughness is reached when r = $1/\cos\theta_0$ (r is a roughness ratio which is defined as the ratio between the true surface area taking into account peaks and valleys and the apparent surface area of a plane having the same macroscopic dimensions). If $\theta_0 > 90°$, the liquid may not be able to penetrate into the crevices of the surface. The observed contact angle results

from a composite interface that consists of the solid surface and air trapped in the voids between the solid and the liquid drop.

The effect of surface heterogeneity on the contact angle was first addressed by Cassie[28] and later by Israelachvili and Gee.[29] Cassie has shown that if the components of a surface act independently, the cosine of the contact angle is a linear function of composition in cases where dispersion forces are considered the principal intermolecular interaction. The observed equilibrium contact angle (θ) was expressed in the form of following equation:

$$\cos\theta \quad = \quad Q_1\cos\theta_1 + Q_2\cos\theta_2 \qquad (1.19)$$

where Q_1 and Q_2 are the fraction of the surface area with contact angle θ_1 and θ_2, respectively.

The model proposed by Israelachvili and Gee is more applicable in the case where the heterogeneities are on the order of molecular dimension taking into account the average polarizabilities, dipole moments or surface charges of two regions. Cassie's equation is then replaced by the following equation :

$$(1 + \cos\theta)^2 \quad = \quad Q_1(1 + \cos\theta_1)^2 + Q_2(1 + \cos\theta_2)^2 \qquad (1.20)$$

For molecular sized patches, the Cassie equation predicts a larger contact angle than that of Equation 1.20.

The issue concerning the hysteresis caused by heterogeneities was not addressed by Cassie or Israelachvili and Gee. Consider a heterogeneous surface consisting of small non-wetting (high contact angle) domains in a matrix of a partially wetting continuous area (low contact angle). As the liquid advances, the edge of liquid becomes pinned at the boundaries of the non-wetting islands due to the energy barrier involved in spreading the drop from the low to high contact angle region, thus leading to an advancing angle higher than expected.

Once the surface is covered by the liquid drop, the low contact angle regions now function as pinning points to keep the liquid from receding. The result is that the advancing angle tends to represent the low surface energy (non-wetting) phase; the receding angle represents the high surface energy (wetting) phase, producing a contact angle hysteresis.

Johnson and Dettre[26,30,31] used these ideas to modulate the model for contact angle on heterogeneous surfaces containing concentric circular regions of different intrinsic contact angles, θ_1 and θ_2 with $\theta_1 > \theta_2$ where the size of each region is large compared to molecular dimensions, but small compared to the size of the drop. Figure 1.6 is the result of Johnson and Dettre's model for different drop energies. It is obvious that the advancing angle approaches θ_1 and the receding angle approaches θ_2.

Based on this model, a number of qualitative conclusions have been expressed:

(1) Advancing angles are more reproducible on predominantly low energy surfaces, whereas receding angles are more reproducible on high energy surfaces.

(2) Advancing contact angles alone cannot fully characterize a heterogeneous surface. Approximately 10% and 90% surface coverage by high (low) contact angle regions give the same advancing (receding) contact angles with very different receding (advancing) angles.

(3) The advancing angle is a measure of the wettability of the low surface energy portion and receding angle is more characteristic of the high surface energy portion.

Another cause of contact angle hysteresis is penetration of probe fluid into the solid surface. The advancing angle is measured as the liquid drop advances over the dry surface, while the receding angle is measured on a surface that is previously saturated with the liquid which is compositionally similar to the liquid itself. Thus, the receding angle becomes a much lower angle. Timmons and Zisman[32] studied the role of molecular volume and size on contact angle hysteresis using a fluorinated monolayer. They observed that the hysteresis was small for liquids with molecular volumes greater than 125 cm^3/g-mole and relatively large for liquids with small molecular volumes such as water (18 cm^3/g-mole).

It has been suggested that reorientation of functional groups at the solid-liquid interface may cause contact angle hysteresis.[33] It has been demonstrated that the functional groups tend to reorient themselves in various environments to minimize interfacial energy.[34-38] The advancing contact angle is a measure of the functional groups initially present at the solid/air interface. Since the probe fluid which is in contact with the solid may cause the reorganization of functional groups to lower the solid/liquid interface energy creating a new surface with different γ^{sv} and γ^{sl}, the receding contact angle is then an indication of the functional groups present at the surface after reorientation.

The contact angle hysteresis can be employed as a tool to indicate differences in structure of surfaces with identical composition. Obviously, there are a number of variables involving the evaluation of wetting behavior, so interpretation of the contact angles can be quite complicated. To achieve an accurate surface structure-composition relationship, results from other surface analytical techniques should be combined.
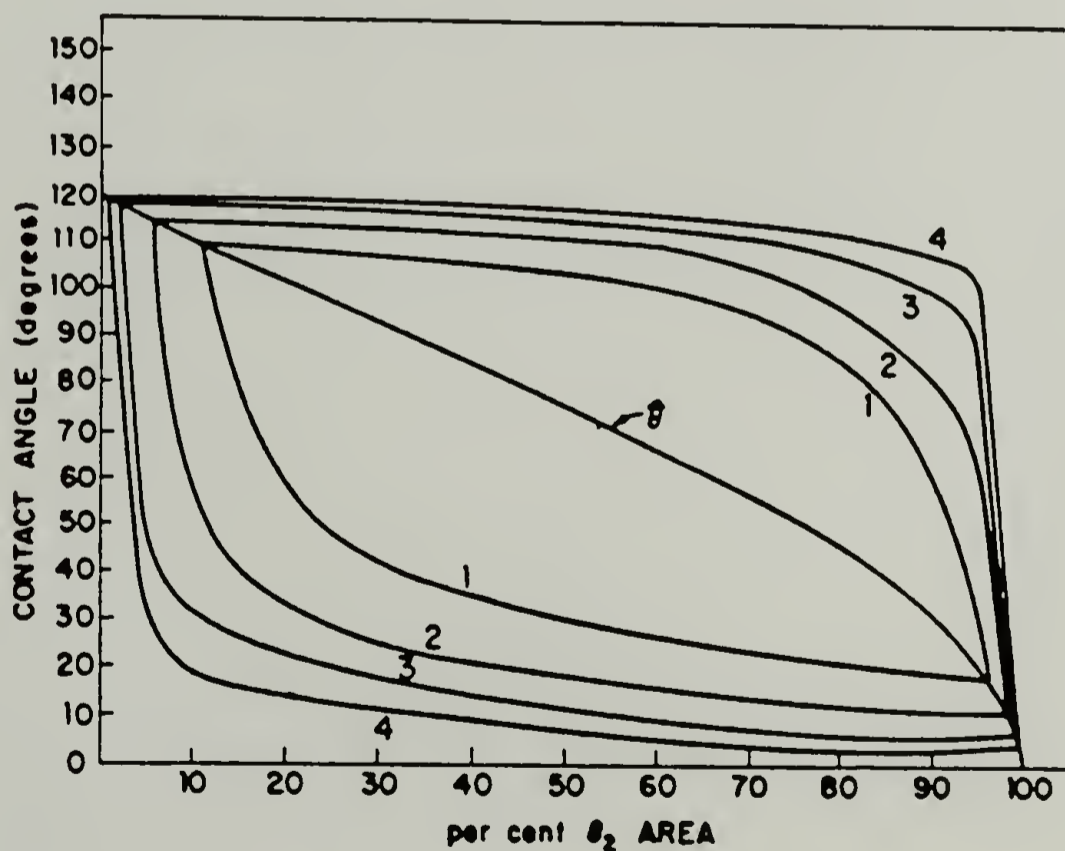
Figure 1.6. Results of the Johnson and Dettre model for contact angles on heterogeneous surfaces. Curves 1 - 4 indicate decreasing drop energies where drop energy is related to the intrinsic energy of the drop and its ability to overcome the metastable states present in the surface regions.[30]

22

Wetting Behavior of Surface Mixtures

Recently, the wettability of controlled surface mixtures has been investigated using self-assembled monolayers of long chain thiols on gold[39,40], silver[41,42], and copper[42,43].

Adsorption of long-chain thiols ($HS(CH_2)_nX$) where $X = CH_3$, OH, COOH, Br, CONHR) from solution onto gold surfaces can form ordered, oriented organic monolayers.[44] Coadsorption of two thiols of different chain length with the same[45] or different terminal functionality[46] can create surface mixtures of organic thiol monolayers. The composition and structure of the monolayer appear to be controlled by either thermodynamics or kinetics of the adsorption process, depending on the organosulfur compounds used. The chain length, nature of end groups, specific interactions within the monolayer and solvent polarity have crucial impact.

The advancing contact angles (θ_A) of water and hexadecane as a function of composition for polar/nonpolar surface mixture systems composed of $HS(CH_2)_{10}CH_3$ and $HS(CH_2)_{10}Z$ (Z = OH, COOH, Br) have been studied.[47,48] The contact angles of hexadecane for all three systems and water on the brominated surfaces, for which dispersion forces are the principal intermolecular interaction, seem to uphold Cassie's statement (see Figure 1.7). Significant deviations from linearity occur, however, for contact angles of water on surfaces containing hydroxyl and carboxylic acid groups, in which specific polar interactions (electrostatic interaction and intramonolayer hydrogen bonding) exist.

The monolayers composed of a mixture of $HS(CH_2)_{11}OH$ and $HS(CH_2)_{21}CH_3$ showed a dramatic change in advancing contact angles of water and hexadecane within a narrow range of solution composition (depicted in Figure 1.8).[46] Monolayers composed either predominantly of the long-chain methyl-terminated thiol $HS(CH_2)_{21}CH_3$ (maximizing the chain packing interactions) or the short-chain hydroxy-terminated thiol $HS(CH_2)_{11}OH$ (maximizing H-bonding with solvent and within monolayer) are more favorable than a mixture of thiols. This behavior strongly indicates that two components of the monolayer
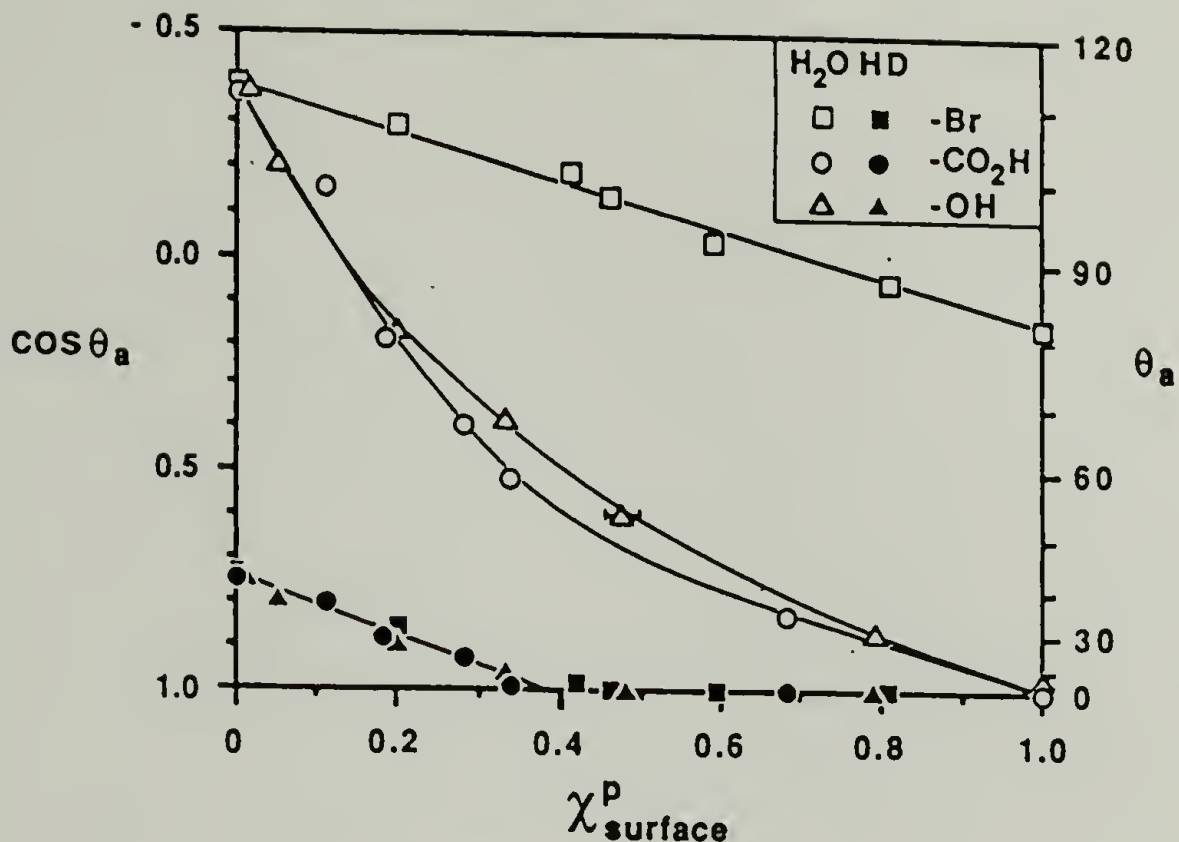
Figure 1.7. Water and hexadecane contact angle results of $HS(CH_2)_{10}CH_3/ HS(CH_2)_{10}Z$ (Z = OH, COOH, Br) where $\chi^P_{surface}$ is the mole fraction of polar components of the monolayer analyzed from XPS data.[47]
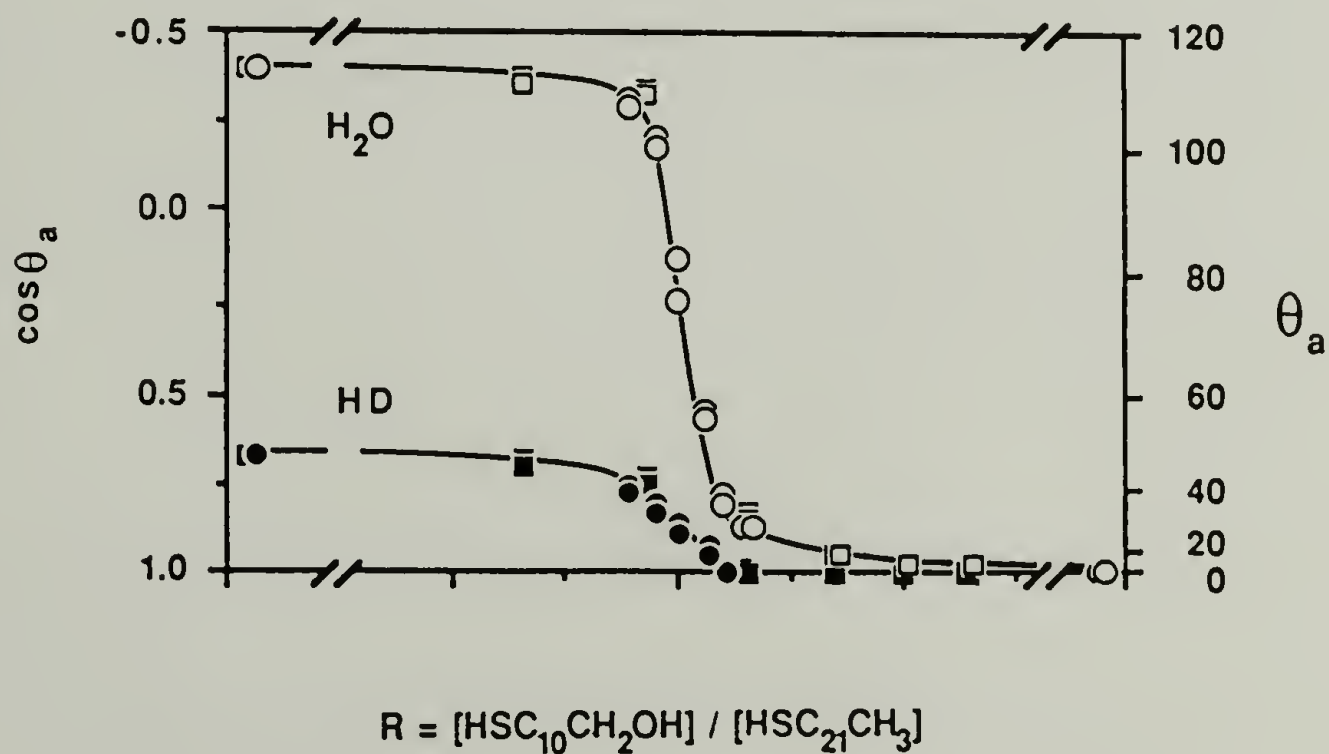
Figure 1.8. Advancing contact angles of water (open symbol) and hexadecane (HD) (solid symbol) where R is $[HS(CH_2)_{11}OH]/[HS(CH_2)_{21}CH_3]$ in solution.[46]

do not act independently but cooperatively to minimize the surface energy. The data support the idea that the two components might be segregated into small domains.

A similar investigation has been done on the same binary system produced by coadsorption of equimolar of $RS(CH_2)_{15}CH_2OH$ and $RS(CH_2)_{(15+m)}CH_3$ ($-6 < m < 6$) on gold.[49] At low m values, where methyl-terminated chains are dominated by hydroxyl-terminated chains, random distribution across the surface occurs. On the contrary, at high m values, where the longer chain methyl-terminated chains dominate, the chains are more likely to organize in the form of clusters due to favorable interchain packing.

The examination of 1:1 binary mixed monolayers formed by adsorption of unsymmetric dialkyl sulfides ($R-(CH_2)_mS(CH_2)_nR'$; R and R' represent CH_3 and COOH, respectively) having one methyl-terminated and one carboxylic acid terminated alkyl chain onto gold surfaces suggests that an excess length of five methylene units in the methyl-terminated chain can entirely screen the carboxylic acid groups on the shorter chain from being reached by water.[50] The water contact angles of mixed monolayers behave like homogeneous alkane monolayers when (m-n) > 5. The simple randomly mixed surfaces can present an unusual behavior which might lead to the misunderstanding of the real surface structure.

Experimental

General Procedures

PCTFE films (Allied 5 mil Aclar 33C) were extracted in refluxing dichloromethane for 2 h and dried (0.01 mm, room temperature, >24 h). Heptane (Aldrich) was distilled under nitrogen from calcium hydride. Tetrahydrofuran (Aldrich) was distilled under nitrogen from sodium/benzophenone. 3-Bromo-1-propanol (Aldrich) was distilled under vacuum from potassium carbonate. Ethyl vinyl ether (Aldrich) was distilled (trap-to-trap) from calcium hydride immediately before use. tert-Butyllithium (t-BuLi) (Aldrich, 1.7 M

in pentane) was standardized by titration with biphenylmethanol in THF at -78 °C. 3-Bromopropyl ethyl acetaldehyde acetal (BrPEAA) was synthesized according to a previously described procedure.[7] Butyryl chloride, and stearoyl chloride (both Aldrich) were distilled and stored under nitrogen. Heptafluorobutyryl chloride (Aldrich) was distilled (trap-to-trap) and stored under nitrogen. Methanol, dichloromethane (both Fisher, HPLC Grade), THF (Aldrich) and water (house distilled, redistilled with a Gilmont Still) were used as wash solvents. X-ray photoelectron spectra (XPS) were obtained with a Perkin Elmer-Physical Electronics 5100 with Mg K_α excitation (400 W, 15.0 kV). Spectra were recorded at two different take-off angles, 15° and 75° between the plane of the sample surface and the entrance lens of detector optics. Atomic composition data were determined using sensitivity factors obtained from samples of known composition: F_{1s}, 1.000; C_{1s}, 0.232; O_{1s}, 0.628; and Cl_{2p}, 0.655. Attenuated total reflectance infrared (ATR IR) spectra were recorded using an IBM 38 FTIR at 4 cm^{-1} resolution with a 10 x 5 x 1 mm germanium internal reflection element (45°). Dynamic advancing (θ_A) and receding (θ_R) contact angles were measured with a Rame'-Hart telescopic goniometer and a Gilmont syringe with a 24-gauge flat-tipped needle as the probe fluid was added to and withdrawn from the drop, respectively. Probe fluids used were water (purified as described above) and hexadecane (purified by vacuum distillation from calcium hydride and stored under nitrogen).

Synthesis of 3-Lithiopropyl Ethyl Acetaldehyde Acetal (LiPEAA)

BrPEAA (1.0 g, 4.8 mmol) was added via syringe to a dried nitrogen-purged reaction flask containing a glass-coated magnetic stir bar. Heptane (18 ml) was added and the solution was cooled to -78 °C. t-BuLi (1.7 M, 3.1 ml, 5.3 mmol) in heptane (14 ml), also at -78 °C, was added slowly to the BrPEAA solution via cannula. The mixture was stirred at this temperature for 30 min then placed in a -15 °C bath for 45 min. The resulting white suspension was then cooled back to -78 °C. THF (36 ml, at -78 °C) was added to dissolve the suspension yielding a clear, yellow solution. The yellow color is likely due to

a complex between the excess t-BuLi and THF. The solution temperature was then allowed to gradually increase until the excess t-BuLi reacted with THF as indicated by the disappearance of the yellow color.

Reaction of LiPEAA with PCTFE Film

A nitrogen-purged Schlenk tube containing PCTFE films was equilibrated to the desired reaction temperature (-78 °C or -15 °C). A solution of LiPEAA in heptane/THF (prepared as described above) at the same temperature was then added via cannula to cover the films. After 30 min of reaction, the solution was removed. The films were washed with methanol at the reaction temperature (1 x 100 ml), methanol (3 x 100 ml), water (3 x 100 ml), methanol (3 x 100 ml) and then dichloromethane (3 x 100 ml) and then dried (0.01 mm, room temperature, >24 h).

Hydrolysis of PCTFE-PEAA

To a nitrogen-purged, jacketed Schlenk tube containing PCTFE-PEAA films, a solution of 5 ml concentrated HCl in 50 ml water was added. The reaction mixture was then heated to reflux. After 30 min of reaction, the solution was removed. The films were washed with water (3 x 50 ml), methanol (3 x 50 ml) and dichloromethane (3 x 50 ml) and then dried (0.01 mm, room temperature, >24 h).

Kinetic Control of Esterifications of PCTFE-OH

To a nitrogen-purged Schlenk tube containing a PCTFE-OH film sample, 25 ml of dry THF was added followed by 8.8 mmol of the acid chloride of interest (butyryl chloride (C_3H_7COCl), stearoyl chloride ($C_{17}H_{35}COCl$) or heptafluorobutyryl chloride (C_3F_7COCl)). Pyridine (8.8 mmol) was also added in catalyzed esterifications. After the desired length of time, the solution was removed and the film was washed with THF (5 x 25 ml), water (5 x

27

25 ml), methanol (3 x 25 ml) and dichloromethane (3 x 25 ml) and dried (0.01 mm, room temperature, >24 h).

Partial Hydrolysis/Methanolysis of PCTFE-OCOC$_3$H$_7$, PCTFE-OCOC$_{17}$H$_{35}$ and PCTFE-OCOC$_3$F$_7$

To a teflon centrifuge tube containing a PCTFE-ester film sample, 25 ml of 0.025 M potassium hydroxide in water:methanol (0:100, 25:75, 50:50, 75:25 or 100:0 v/v) was added. The tube was then capped and placed in an oil bath at 105 °C. After the desired reaction time, the film was removed from the tube and soaked for 15 min intervals in water, methanol and then dichloromethane and dried (0.01 mm, room temperature, >24 h).

Re-esterification of PCTFE-OH/-OCOC$_3$H$_7$, PCTFE-OH/- OCOC$_{17}$H$_{35}$ and PCTFE-OH/-OCOC$_3$F$_7$

The procedure for kinetic control of esterifications was followed by reacting PCTFE-OH/-OCOC$_3$H$_7$, and PCTFE-OH/-OCOC$_{17}$H$_{35}$ with 8.8 mmol C$_3$F$_7$COCl in 25 ml of THF whereas PCTFE-OH/-OCOC$_3$F$_7$ was reacted with 8.8 mmol of C$_3$H$_7$COCl in 25 ml THF.

Competitive Esterifications of PCTFE-OH

An acid chloride mixture with the desired molar ratio was prepared by mixing 0.35 M C$_3$H$_7$COCl solution (8.8 mmol in 25 ml of THF) or C$_{17}$H$_{35}$COCl solution (8.8 mmol in 25 ml of THF) with 0.35 M C$_3$F$_7$COCl solution (8.8 mmol in 25 ml of THF), varying the w/w ratio. To a nitrogen-purged Schlenk tube containing a PCTFE-OH film sample, 25 ml of acid chloride mixture was added. The film sample was allowed to react for 24 h under nitrogen at room temperature and was then washed with THF (5 x 25 ml), water (5 x 25 ml), methanol (3 x 25 ml) and dichloromethane (3 x 25 ml) and dried (0.01 mm, room temperature, >24 h).

Results and Discussion

Preparation of PCTFE-OH

The initial modification involves the introduction of hydroxyl groups onto the polymer surface by the reaction of PCTFE film with the protected alcohol - containing lithium reagent, (3-lithiopropyl ethyl acetaldehyde acetal) and subsequent deprotection by hydrolysis. The depth of the initial modification reaction can be controlled by four factors: temperature, time, solvent composition and organolithium reagent concentration. The conditions selected to prepare acetal-functionalized PCTFE (PCTFE-PEAA) were -78 °C and -15 °C, using 50:50 THF:heptane as a solvent for 30 min to yield modified layer thicknesses of ~50 Å and ~1000 Å, respectively. The alcohol-functionalized PCTFE (PCTFE-OH) was prepared from PCTFE-PEAA by hydrolysis in aqueous HCl at 100 °C for 30 min.

Figures 1.9 and 1.10 show XPS survey and C_{1s} spectra of PCTFE (unmodified), PCTFE-PEAA (modified at -15 °C) and its hydrolyzed product, PCTFE-OH. The PCTFE-PEAA survey spectrum (Figure 1.9) shows a decrease in the intensity of fluorine, the complete removal of chlorine, an increase in the amount of carbon and the incorporation of a significant amount of oxygen into the surface of the film. The disappearance of the chlorine peak indicates that the modification proceeds entirely through the XPS sampling depth (~54 Å using a mean free path of 18 Å for Cl_{2p} photoelectrons) using this modification condition. The C_{1s} spectrum of PCTFE-PEAA (Figure 1.10) shows the disappearance of the high binding energy peak at 295 eV, assigned to unmodified PCTFE, and the emergence of a lower binding energy peak containing a high binding energy shoulder. The main peak is assigned to carbons bonded only to hydrogen or other carbons, while the shoulder peak is assigned to carbons bonded to one or two oxygens or one fluorine as expected based on the structure of modified repeat unit (see Figure 1.1). The XPS C_{1s} spectrum of PCTFE-OH is consistent with deprotection. Since only two of

29

the five carbons are bonded to an electronegative element (none are bonded to two) compared to PCTFE-PEAA, which has four of the nine carbons bonded to electronegative elements (one carbon is also bonded to two oxygens), the intensity of the high binding energy shoulder slightly decrease relative to the main peak.

Analysis of the XPS atomic composition data yields a more quantitative interpretation. The stoichiometries of PCTFE-PEAA calculated from Table 1.1 are $C_{38}F_{5.4}O_{7.6}$ (15° take-off angle) and $C_{38}F_7O_{7.2}$ (75° take-off angle) and are in good agreement with the proposed modified structure containing 80% acetal-functionalized repeat units and 20 % difluoroolefins which has a stoichiometry of $C_{38}F_6O_8$. After deprotection, the stoichiometries of the modified surface become $C_{22}F_{5.3}O_{4.5}$ and $C_{22}F_{5.2}O_{4.4}$ (15° take-off and 75° take-off angles, respectively) which are consistent with the stoichiometry predicted $(C_{22}F_6O_4)$ for a modified polymer composed of 80% hydroxyl-functionalized repeat units and 20 % difluoroolefins (See Figure 1.1).

Table 1.1. XPS atomic composition data for PCTFE, PCTFE-PEAA and PCTFE-OH.

Surface	θ_T (degrees)	Atomic Composition (%)			
		C	O	F	Cl
PCTFE	15	31.50	-	52.80	15.70
	75	32.66	-	51.80	15.54
PCTFE-PEAA	15	74.31	14.98	10.66	0.05
	75	72.50	13.72	13.42	0.06
PCTFE-OH	15	69.32	14.05	16.52	0.07
	75	69.40	14.03	16.32	0.26

Figure 1.9. XPS survey spectra (75° take-off angle) of (a) PCTFE (b) PCTFE-PEAA (modified at -15 °C) (c) PCTFE-OH (initially modified at -15 °C).
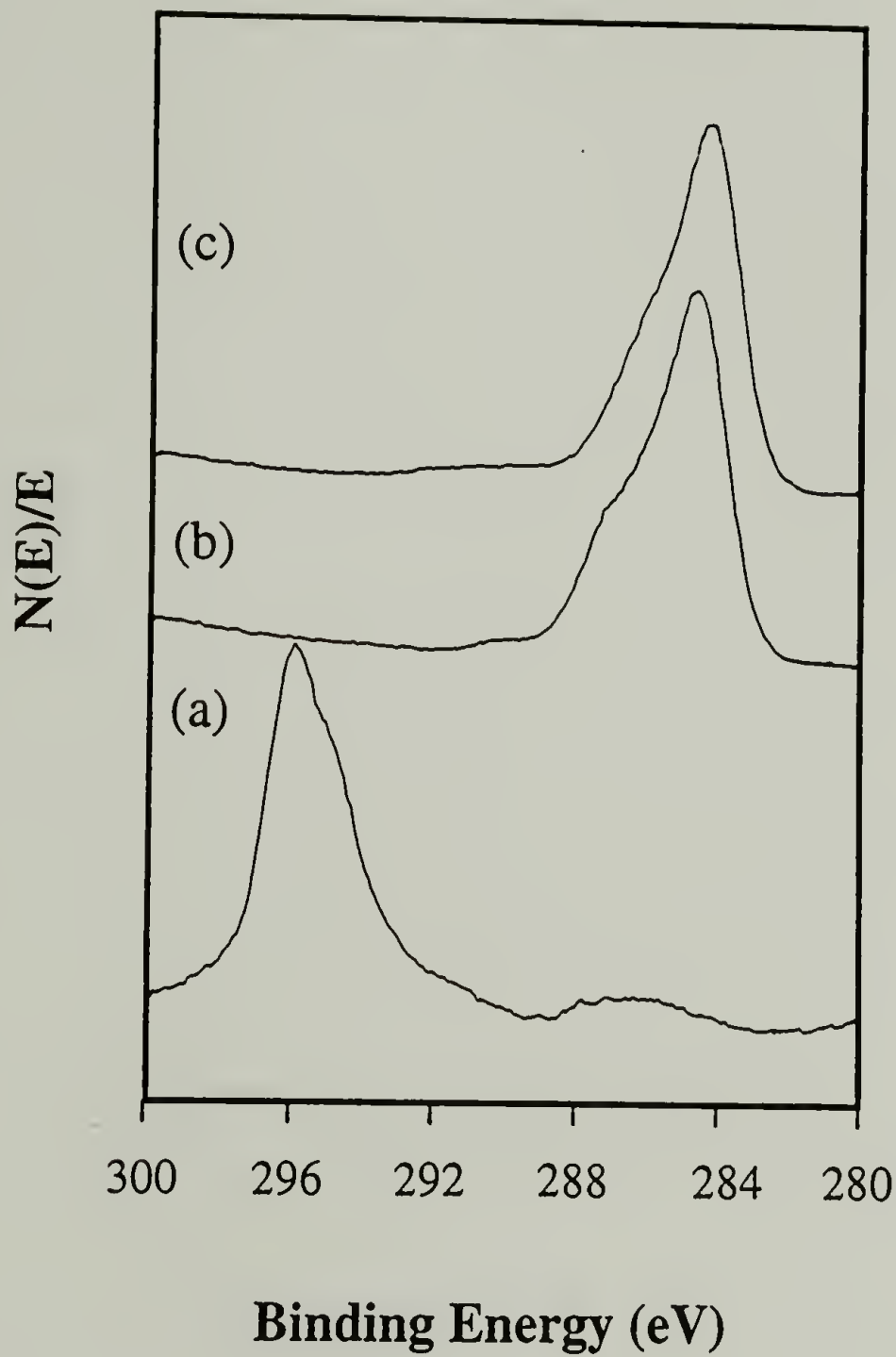
Figure 1.10. XPS C_{1s} spectra (75° take-off angle) of (a) PCTFE (b) PCTFE- PEAA (modified at -15 °C) (c) PCTFE-OH (initially modified at -15 °C).

For the thickly modified surfaces, ATR IR is a technique that can provide more qualitative information, especially about surface functionalities. A germanium crystal (45°) was used as the internal reflection element that has an approximate sampling depth of 1000 Å for all analyses. Figure 1.11 shows ATR IR spectra of PCTFE, PCTFE-PEAA (modified at -15 °C) and PCTFE-OH (initially modified at -15 °C). The appearance of C-H stretching (3000-2840 cm^{-1}) and bending (1500-1320 cm^{-1}) peaks as well as a weak, broad peak at 1675 cm^{-1} assigned to the unsaturation in the modified polymer backbone are observed. After hydrolysis, a broad hydrogen-bonded O-H stretching peak (above 3000 cm^{-1}) and the methylene C-H stretching peak appear (2990-2830 cm^{-1}) indicating the conversion of acetal groups to alcohol functionalities. As expected , the water contact angles (θ_A/θ_R) decrease from 89°/35° for PCTFE-PEAA to 69°/25° for the more polar, hydrophilic surface of PCTFE-OH. PCTFE exhibits water contact angles of $\theta_A/\theta_R =$ 104°/77°.

Esterifications of PCTFE-OH

The esterification kinetics for the reactions of PCTFE-OH with acid chlorides (butyryl chloride, stearoyl chloride and heptafluorobutyryl chloride) were studied under two sets of conditions: (1) using pyridine as an acylating catalyst (equimolar ratio of pyridine to acid chloride) and (2) uncatalyzed. The reactions of alcohol/butyrate and alcohol/stearate surfaces with heptafluorobutyryl chloride and alcohol/heptafluorobutyrate with butyryl chloride were performed not only to prepare surface mixtures but also to facilitate the quantitative determination of the unreacted hydroxyl groups since the labelled functional group is more efficiently detected by XPS. The extent of esterification was calculated from the XPS C/F ratios of the labelled surfaces.[51]
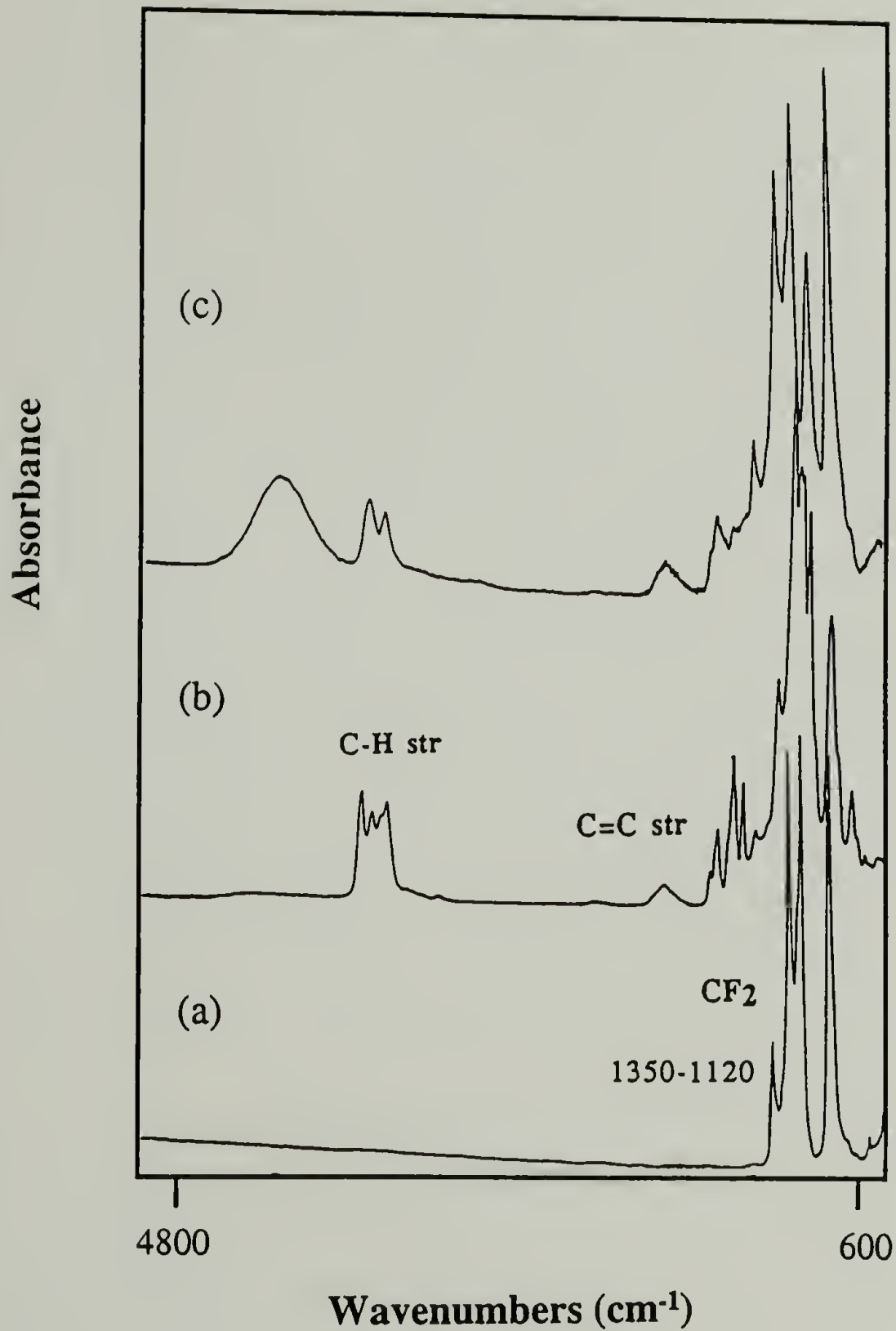
Figure 1.11. ATR IR spectra of (a) PCTFE (b) PCTFE-PEAA (modified at -15 °C) (c)
PCTFE-OH (initially modified at -15 °C).

The results presented in Figure 1.12 show that the esterifications using catalyst are very rapid and proceed in high yield (more than 90% within 2 h). The catalyzed esterifications with butyryl chloride (C_3H_7COCl) and stearoyl chloride ($C_{17}H_{35}COCl$) are rapid, but slightly slower than that of heptafluorobutyryl chloride (C_3F_7COCl).This high rate of esterification makes it difficult to kinetically regulate the extent of reaction in order to controllably prepare heterogeneous surfaces with varying compositions. Thus the study of uncatalyzed esterifications was undertaken with the hope that the reaction rate would be sufficiently slow to allow surface mixtures containing alcohol and ester with desired compositions to be formed.
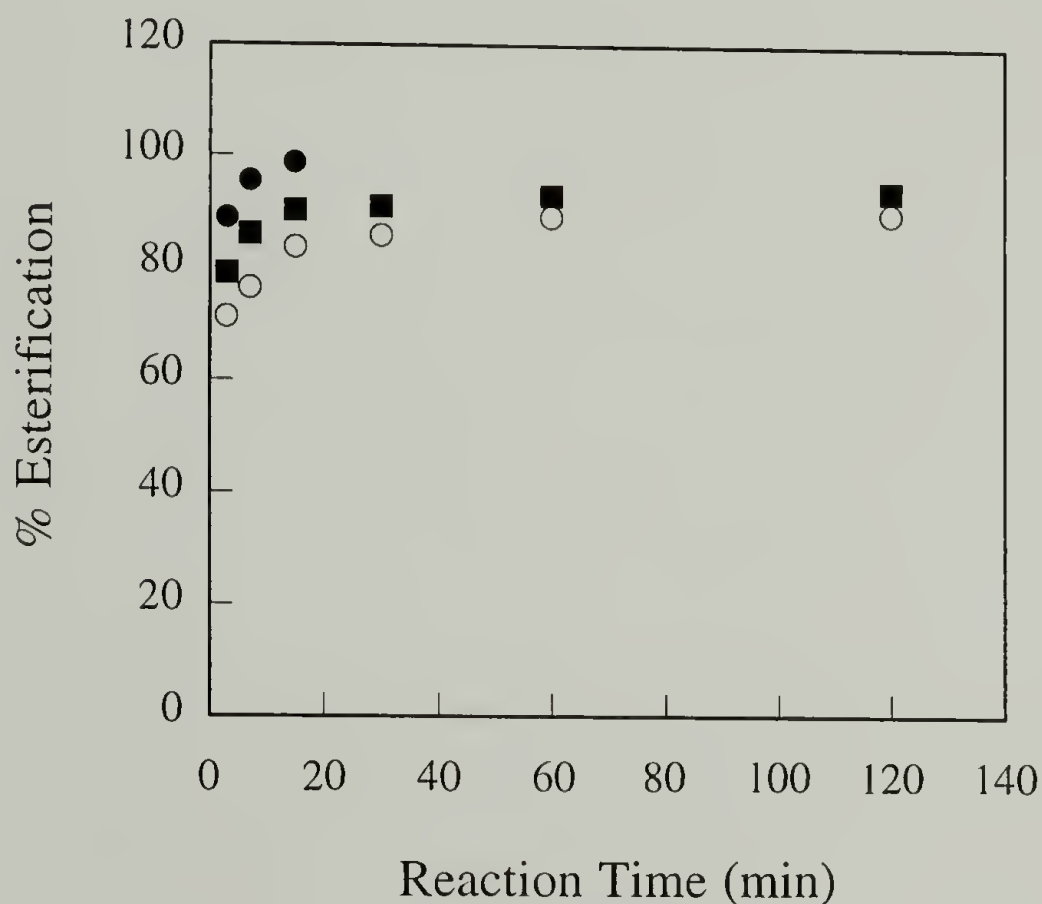
Figure 1.12. Kinetics of reactions of PCTFE-OH with C_3F_7COCl (●), C_3H_7COCl (O) and $C_{17}H_{35}COCl$ (■) using pyridine as catalyst.

Figures 1.13 and 1.14 contain the results for the initial uncatalyzed reaction of PCTFE-OH with heptafluorobutyryl chloride (C_3F_7COCl) and the subsequent treatment of these surfaces with butyryl chloride (C_3H_7COCl). The XPS data show that the initial

reaction has reached greater than 90% conversion after 15 min and is essentially complete after 30 min. The low receding water contact angle after a 15 min reaction (63° versus 68° for a completely esterified surface) indicates the presence of unreacted hydroxyl groups which form butyrate esters after labelling, resulting in a lower receding hexadecane contact angle (28°) than is observed on a surface containing only heptafluorobutyrate groups (40°). Identical results (XPS and contact angle) of the surfaces initially reacted for at least 30 min both before and after labelling indicate complete quantitative esterifications.

Results for the uncatalyzed reaction of PCTFE-OH with butyryl chloride (C_3H_7COCl) are shown in Figures 1.15 - 1.16. The C/F ratios of the initially esterified and the labelled surfaces increase with initial reaction time, indicating higher conversion of hydroxyl groups to butyrate groups as a function of reaction time. The 75° take-off angle C/F ratios of the 24 h sample after labelling indicate that the yield for the initial esterification is about 84 %, significantly less than that of the catalyzed reaction (90%). Advancing/receding water contact angles increase from 67°/17° to 90°/46° after 12 h of reaction. The receding angle of 46° remains at this value up to 24 h of reaction. Since pure $PCTFE-OCOC_3H_7$ has a receding water contact angle of 54°,[10] it can be assumed that a significant amount of hydroxyl groups remain unreacted after 24 h. This is confirmed by the lower advancing/receding hexadecane contact angles of a 24 h initially reacted surface (20°/0°) compared to a 12 h initially reacted surface (32°/5°) after labelling with heptafluorobutyryl chloride (C_3F_7COCl).

The XPS data for the uncatalyzed esterification of PCTFE-OH with stearoyl chloride ($C_{17}H_{35}COCl$) and the associated labelled surfaces are shown in Figure 1.17. Compared to the catalyzed reaction, these results show a relatively low rate of reaction and incomplete esterification even after 24 h. The C/F ratios of the labelled samples indicate that after 24 h approximately 70% of the hydroxyl groups have been converted to stearate esters. The water and hexadecane contact angle data for the initial stearoyl chloride esterification are shown in Figure 1.18. The advancing water contact angle which reflects
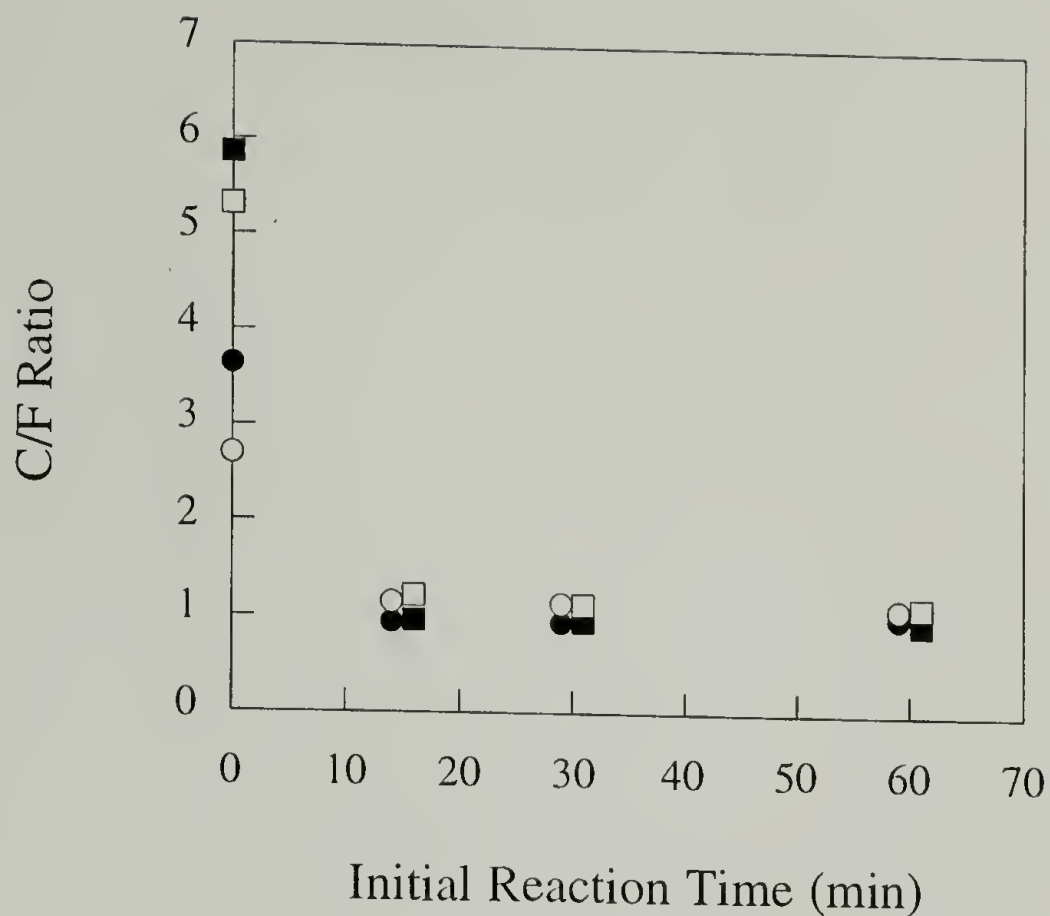
Figure 1.13. XPS C/F ratio data for uncatalyzed esterification kinetics with C_3F_7COCl: 15° (●) and 75° (O) take-off angle data after initial reaction, 15° (■) and 75° (□) take-off angle data after labelling with C_3H_7COCl.
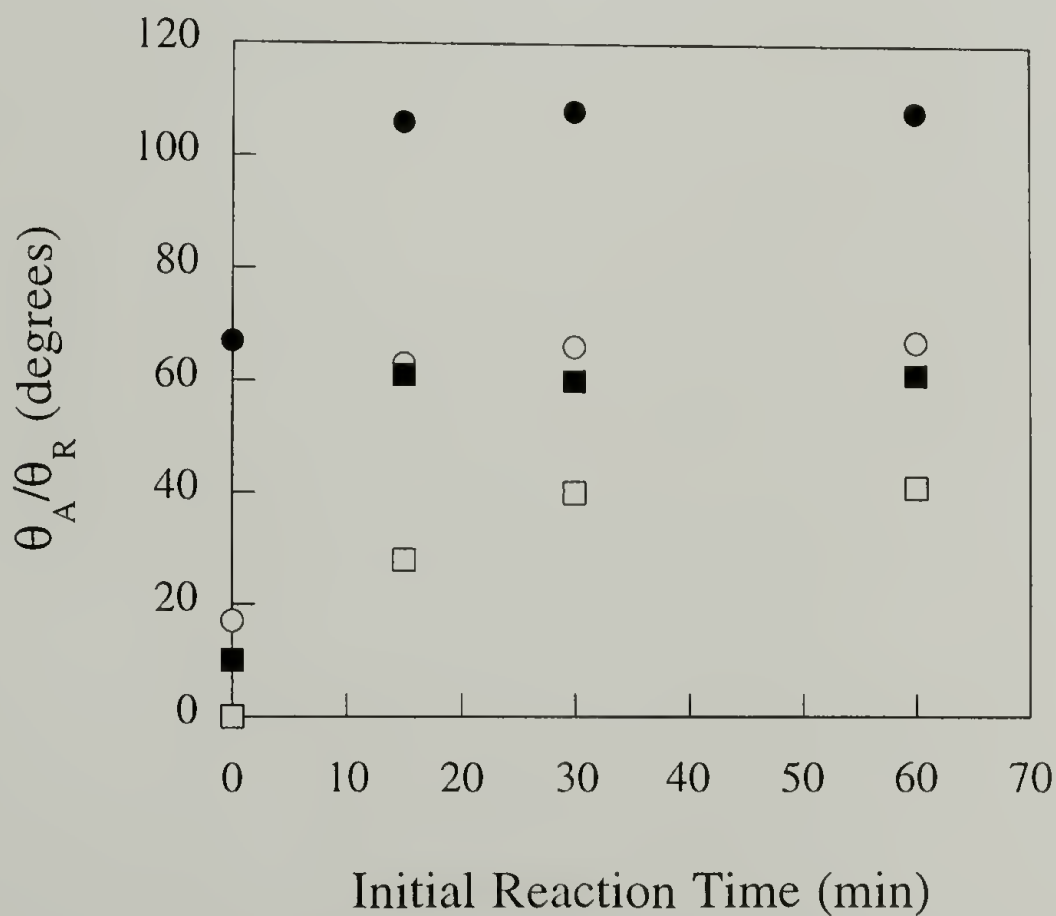
Figure 1.14. Contact angle data for uncatalyzed esterification kinetics with C_3F_7COCl: water contact angles (θ_A (●); θ_R (O)) after initial reaction and hexadecane contact angles (θ_A (■); θ_R (□)) after labelling with C_3H_7COCl.
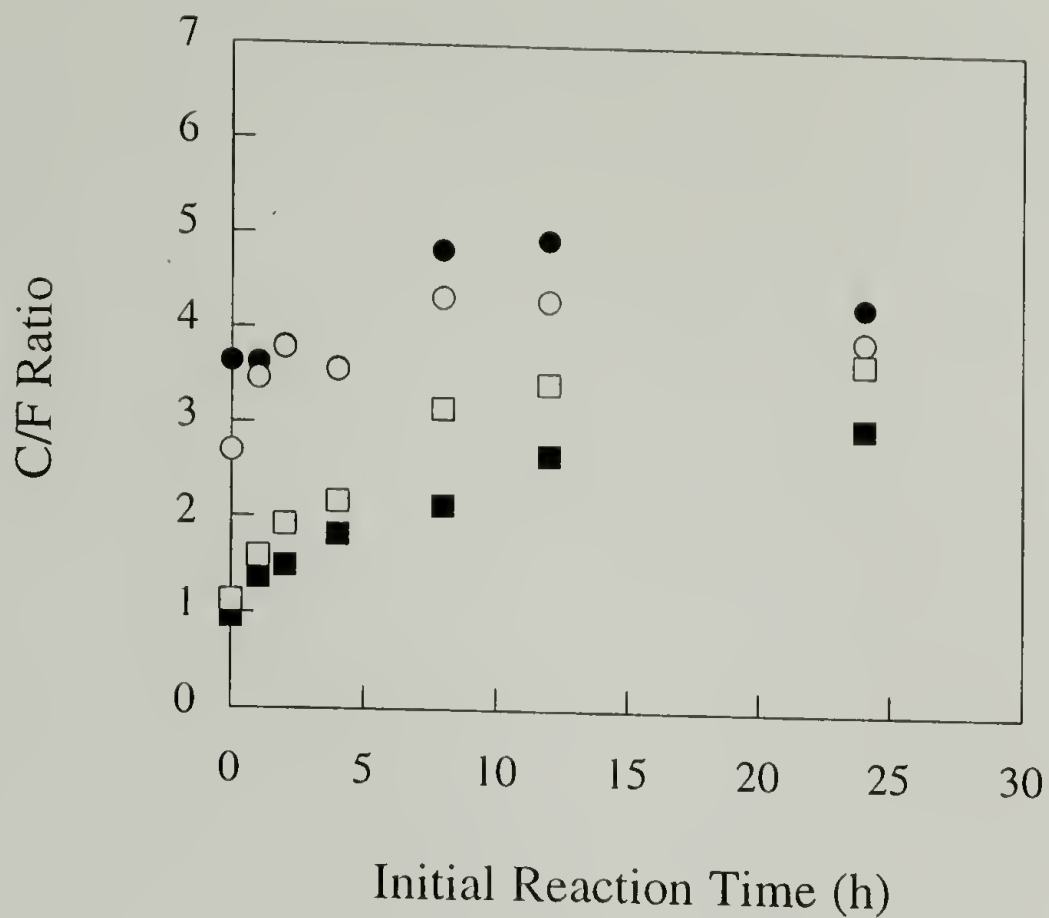
Figure 1.15. XPS C/F ratio data for uncatalyzed esterification kinetics with C_3H_7COCl: 15° (●) and 75 ° (O) take-off angle data after initial reaction, 15° (■) and 75° (□) take-off angle data after labelling with C_3F_7COCl.
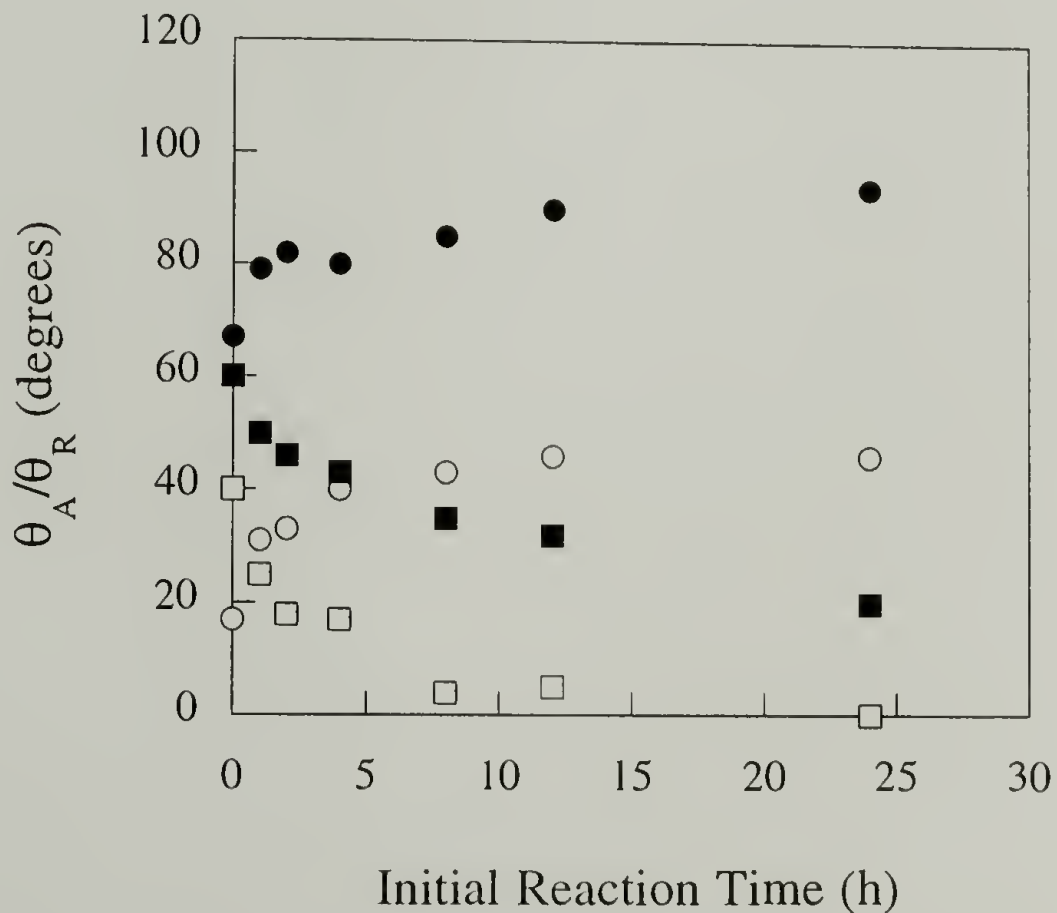
Figure 1.16. Contact angle data for uncatalyzed esterification kinetics with C_3H_7COCl: water contact angles (θ_A (●); θ_R (O)) after initial reaction and hexadecane contact angles (θ_A (■); θ_R (□)) after labelling with C_3F_7COCl.
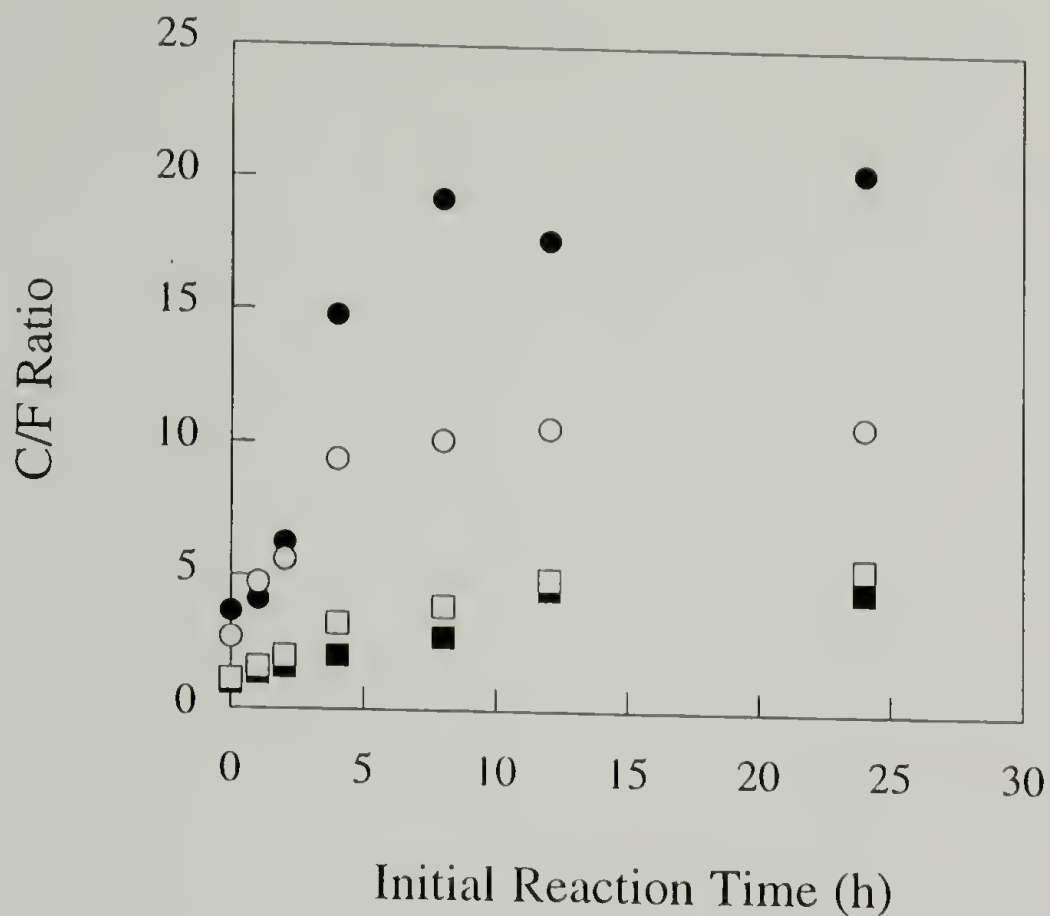
Figure 1.17. XPS C/F ratio data for uncatalyzed esterification kinetics with $C_{17}H_{35}COCl$: 15° (●) and 75 ° (O) take-off angle data after initial reaction, 15° (■) and 75° (□) take-off angle data after labelling with C_3F_7COCl.
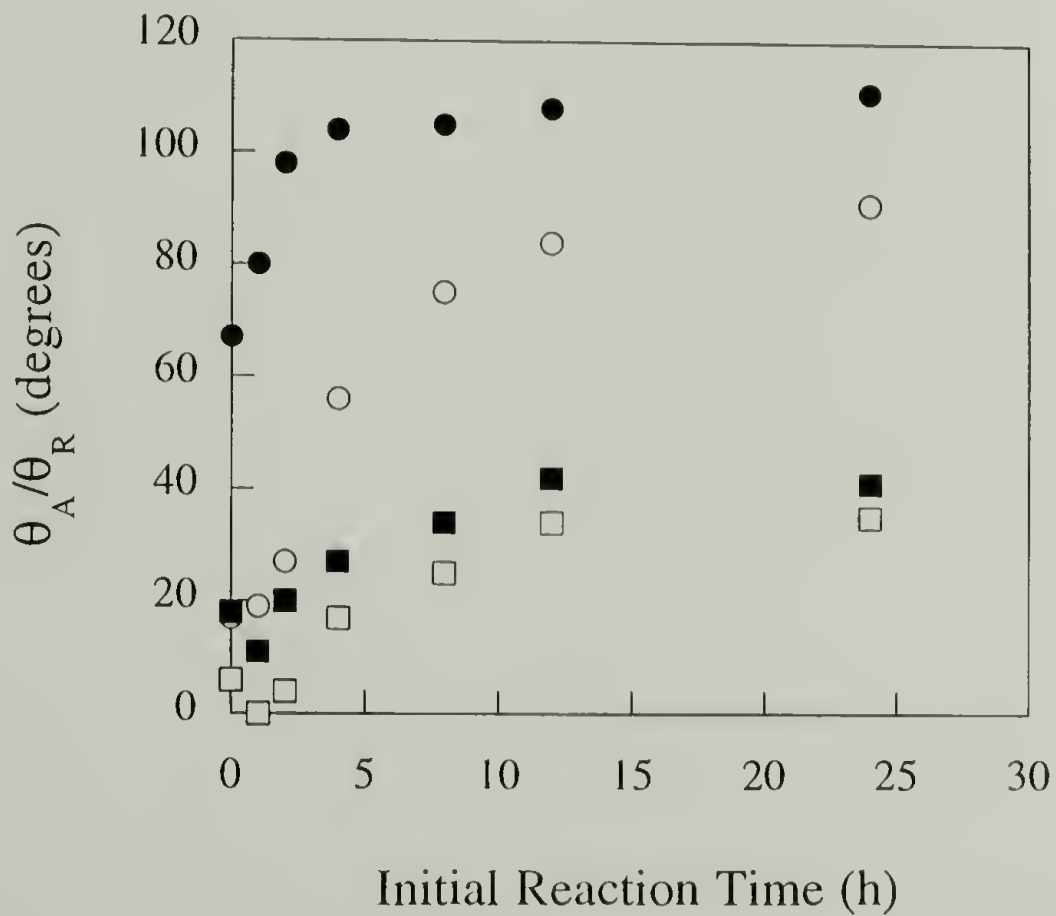
Figure 1.18. Contact angle data for uncatalyzed esterification kinetics with $C_{17}H_{35}COCl$: water contact angles (θ_A (●); θ_R (O)) and hexadecane contact angles (θ_A (■); θ_R (□)) after initial reaction.

the hydrophobic functionality at the film/air interface has increased to its maximum value (108°) after 4 h of reaction. The receding water contact angle which is more sensitive to the presence of unreacted hydroxyl groups, on the other hand, requires a 24 h reaction to reach its limiting value (90°).

The receding water contact angle is indicative of the functionality present at the film/water interface and may reflect behavior resulting from water-induced surface reconstruction and/or penetration of water into the film surface. The advancing and receding hexadecane contact angles show a decrease from 18°/6° of PCTFE-OH to 10°/0° in the first hour of reaction, followed by a gradual increase until the values of PCTFE-$OCOC_{17}H_{35}$ (42°/35°) are reached. These results can be used to interpret the structure of the modified layer at different points in the reaction. A relatively small number of stearates are formed in the first hour. The low concentration of these long chain esters makes it difficult for them to pack and orientate themselves, thus there are a significant number of methylene groups present at the film/air interface, resulting in a decrease of hexadecane contact angles. The more the reaction progresses, the more the ability of ester chains to pack together and orient themselves at the interface which can be observed by the increase of both water and hexadecane contact angles.

It has been shown that surfaces which present a closed-packed array of methyl groups exhibit higher hexadecane contact angles and have a significantly lower surface energy than surfaces consisting of predominantly methylene units.[43] The hexadecane contact angle of octadecanethiol adsorbed to gold (which has been shown to be a highly oriented closed-packed monolayer) is 48°, while hexadecane spontaneously spreads ($\theta =$ 0°) on polyethylene which contains only methylene groups. The hexadecane contact angle of PCTFE-$OCOC_{17}H_{35}$ ($\theta = 42°$) which approaches that of a pure methyl surface (48°) suggests that stearate groups may form an ordered layer at the modified polymer surface. This proposed ordering of the stearate modified surface is also supported by the ATR IR spectrum of the thick stearate surface produced by esterification of PCTFE-OH initially

modified at -15 °C (~1000 Å thickness). The surface appears slightly hazy, indicating the possible formation of microcrystalline regions. The series of bands from 1350-1215 cm^{-1} in the ATR IR spectrum of PCTFE- OCOC$_{17}$H$_{35}$ (Figure 1.19) is a characteristic of solid long chain esters.[52] The symmetric and asymmetric CH$_2$ stretching at 2853 cm^{-1} and 2919 cm^{-1} are almost the same as the 2851 cm^{-1} and 2918 cm^{-1} bands of crystalline hydrocarbon solid[53] (the symmetric and asymmetric CH$_2$ stretching of hydrocarbon liquid are 2855 cm^{-1} and 2924 cm^{-1},respectively).
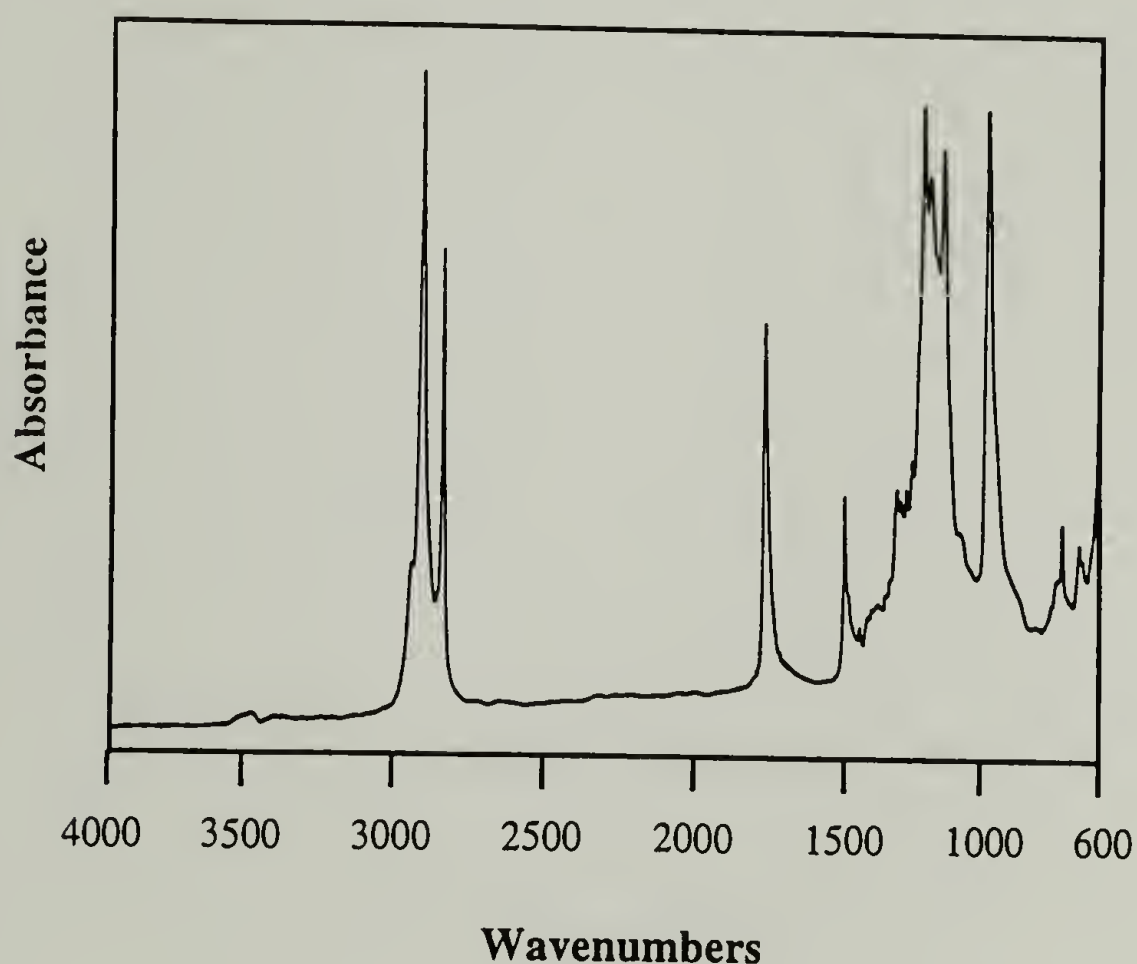
Figure 1.19. ATR IR of PCTFE-OCOC$_{17}$H$_{35}$ initially modified at -15 °C.

The hexadecane contact angle data after labelling PCTFE-OCOC$_{17}$H$_{35}$ with C$_3$F$_7$COCl are shown in Figure 1.20. The advancing angle remains relatively high within the first hour of reaction indicating that the major component of the surface is heptafluorobutyrate. The angle then decreases from a value of 59° (1 h) to 12° (24 h) over the course of reaction. As described previously, the hexadecane receding angles of stearate

surfaces before labelling reaction increase with reaction time due to the ordering of the monolayer composed mostly of methylene units. This ordered surface, however, has been disrupted by the labelling reaction with C_3F_7COCl causing a decrease in receding angles. The expected high receding angle at very low stearate content within short time of reaction or high heptafluorobutyrate content after labelling reaction was not observed. This may be influenced by surface reconstruction.

Figure 1.21 shows the kinetics of the reaction of PCTFE-OH with butyryl chloride (C_3H_7COCl), stearoyl chloride ($C_{17}H_{35}COCl$) and heptafluorobutyryl chloride (C_3F_7COCl). The heptafluorobutyrate is formed rapidly due to its high reactivity towards esterification. Mixed alcohol/heptafluorobutyrate surfaces could not be prepared by this method. On the contrary, the butyrate and stearate surfaces form more slowly and kinetics can be conveniently used to control surface composition. These results show that the uncatalyzed reactions are much slower and less quantitative than pyridine catalyzed acylations. This is explained by the fact that carbonyl carbons of the acyl pyridinium chlorides are more electropositive and susceptible to the attack of hydroxyl groups on PCTFE-OH than ones of non-acylated acid chlorides. Another possible explanation is the more favorable partitioning of acyl pyridinium salts from the solution to the previously esterified surfaces. As expected, the chain length of the acid chloride has an impact on the reaction rate and yield. Stearoyl chloride with its longer chain reacts slower and less quantitatively than butyryl chloride. Meanwhile, the heptafluorobutyryl chloride reacts much faster than the corresponding hydrocarbon due to the increased electrophilicity caused by electronegative fluorines on the carbon α to the carbonyl.

Hydrolyses/Methanolyses of PCTFE-Esters

The hydrolysis of PCTFE-Esters was used as a second method to prepare alcohol/ester mixed surfaces. Kinetics of hydrolysis/methanolysis were studied as a function of solvent composition (water:methanol) and ester chain length (butyrate or

42
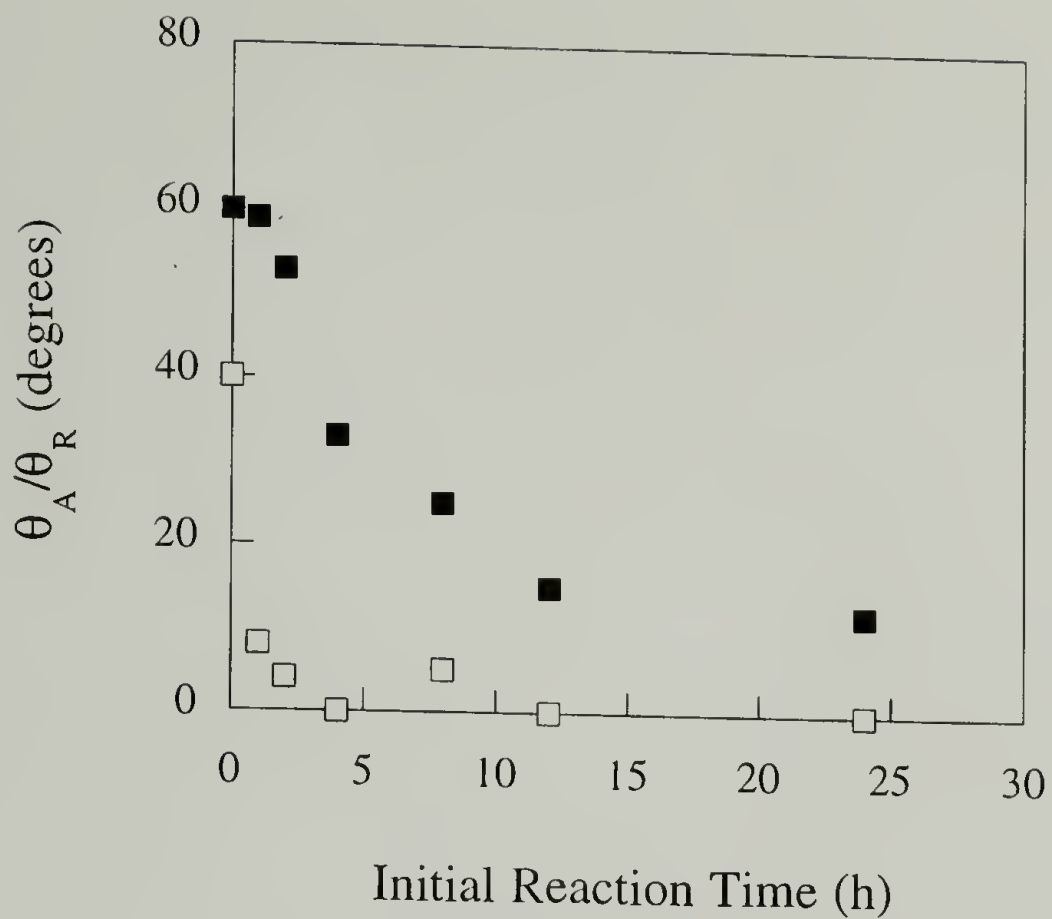
Figure 1.20. Hexadecane contact angle (θ_A (■), θ_R (□)) data for uncatalyzed esterification kinetics with $C_{17}H_{35}COCl$ after labelling with C_3F_7COCl.
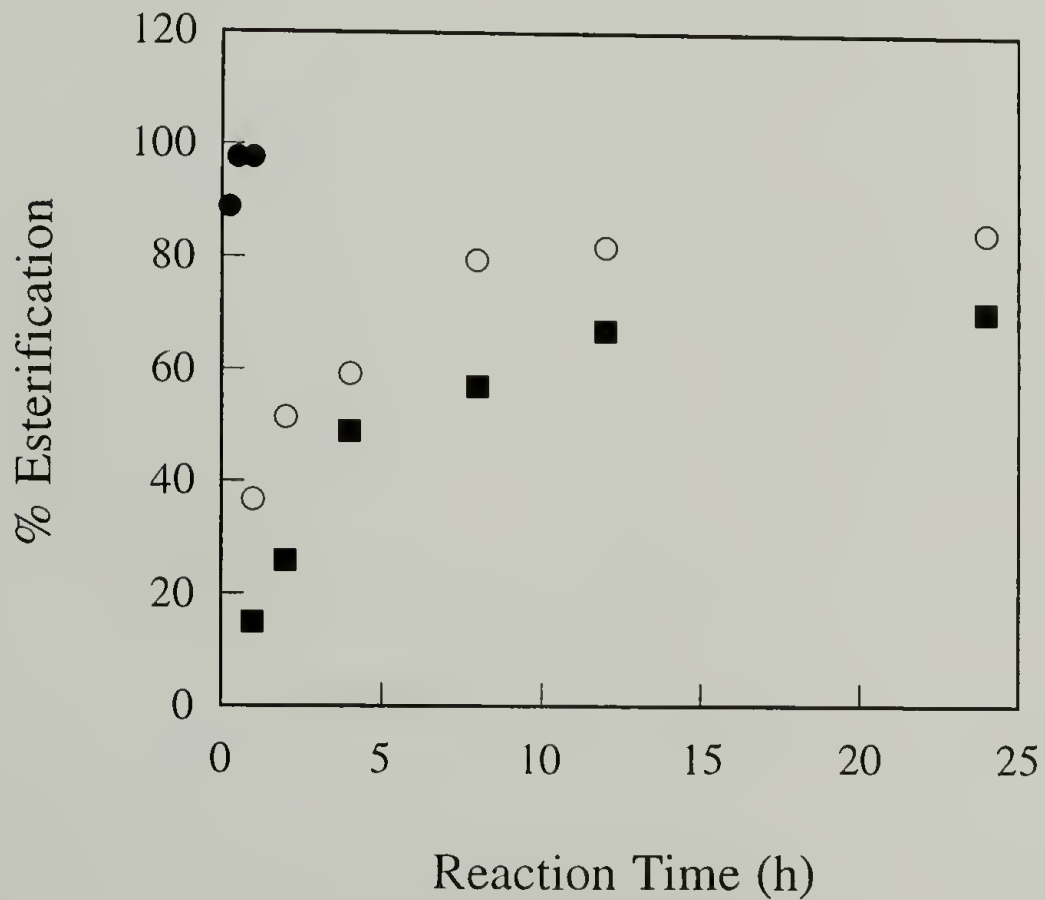
Figure 1.21. Kinetics of reactions of PCTFE-OH with C_3F_7COCl (●), C_3H_7COCl (○) and $C_{17}H_{35}COCl$ (■).

stearate). Methanol, as the less polar solvent than water, interacts more favorably with the ester surfaces as observed by contact angles of the basic solutions on the PCTFE-Esters surfaces (Table 1.2).

Table 1.2. Advancing/receding contact angles (θ_A/θ_R) of the basic hydrolysis solutions on the PCTFE-Ester surfaces.

Solution (water:methanol)	Butyrate	Stearate	Heptafluorobutyrate
0:100	23°/0°	47°/28°	30°/0°
25:75	26°/0°	-	66°/0°
50:50	39°/0°	-	82°/0°
75:25	56°/4°	-	95°/4°
100:0	78°/11°	111°/86°	108°/15°
H_2O^a	89°/54°	108°/90°	107°/68°

a - Contact angles measured with pure water (no base).

Based on their relative wettabilities, it is expected that the longer chain esters should be hydrolyzed more slowly in a given solvent mixtures than the short chain esters. Besides the expected decrease in the contact angles with an increase in the methanol content of the hydrolysis solution, the data also exhibit some interesting behavior in their hysteresis. The surfaces which hydrolyze relatively fast (PCTFE-OCOC$_3$F$_7$, PCTFE-OCOC$_3$H$_7$) show substantial hysteresis and much lower receding contact angles when the measurements were made with the basic solution (0.25 M aqueous solution of KOH) than the ones made with the neutral water. This result indicates that during the time of measurement (~1 min), some hydrolysis of these surfaces has likely occurred.

The hydrolyses of PCTFE-OCOC$_3$F$_7$ are very rapid. Under all of the solvent conditions studied, the reactions are complete within 15-30 min.[54] The water contact angles have decreased from 108°/67° of PCTFE-OCOC$_3$F$_7$ to values comparable with PCTFE-OH (67°/17°). After labelling the 0:100, 25:75 and 50:50 (water:methanol) 15 min hydrolyzed surfaces with butyryl chloride, the low hexadecane contact angles of 10°/0° indicate that surfaces contain only butyrate functionality. This is expected in cases where all heptafluorobutyrate groups were removed in the hydrolysis. The hexadecane contact angles after labelling the surfaces hydrolyzed in 75:25 and 100:0 water:methanol for 15 min with butyryl chloride are 23°/9° and 24°/12°, respectively. These results indicate a low concentration of heptafluorobutyrate groups remaining on these two surfaces. The hydrolyses of these two surfaces are complete after 30 min as indicated by the hexadecane contact angles of 10°/0° for the hydrolyzed surfaces after labelling with butyryl chloride. The slightly lower rate of hydrolyses in 75:25 and 100:0 water:methanol as compared with one of hydrolyses in 0:100, 25:75 and 50:50 water:methanol is explained by the decrease in the ability of the solvent to penetrate into the surface as the water content increases.

The control of surface composition of PCTFE-OH/-OCOC$_3$F$_7$ mixed surfaces is then difficult. These results imply that even though the fluorocarbon esters are not wet as well by the reaction solvents as are the hydrocarbon esters, the effect of the electron-withdrawing ability of the fluorines on the α carbon to the carbonyl esters is strong enough to increase the rate of hydrolysis. In an attempt to lower the reaction rate, the effect of decreasing the reaction temperature was studied for 15 min reactions conducted in pure water.[54] The results show that as the temperature is decreased, the amount of hydrolysis decreases. The rate still remains high. Almost 40 % of the heptafluorobutyrate groups have been removed within the first 15 min of reaction at as low as 30°C.

The basic hydrolysis/methanolysis of PCTFE-OCOC$_3$H$_7$ were carried out by potassium hydroxide solutions in water:methanol (0:100, 25:75, 50:50, 75:25, 100:0). The methanolysis and hydrolyses conducted in 25:75, 50:50 water:methanol solutions are

essentially complete in the first 15 min of the reaction. The hydrolysis is, however, considerably slower (10 h) when the solvent ratio is changed to 75:25 water:methanol and even slower (24 h) in pure water. The results of the hydrolyses in 75:25 and 100:0 water:methanol are discussed below.

The XPS C/F ratios (Figure 1.22) both before and after labelling with heptafluorobutyryl chloride (C_3F_7COCl) of PCTFE- $OCOC_3H_7$ hydrolyzed in 75:25 (water:methanol) solution show a large decrease in the first 2 h of reaction. The hydroxyl group content of the surface has changed from ~10% to ~60%. The labelled samples (PCTFE-$OCOC_3H_7$/-$OCOC_3F_7$) indicate 78% yield for hydrolysis after a 10 h reaction. During the first 2 h of the hydrolysis, a dramatic decrease in receding water contact angles (Figure 1.23) is observed with the increase in number of hydroxyl groups in the surface; a corresponding increase in the advancing hexadecane contact angles was observed after labelling. The advancing water and receding hexadecane contact angles which are sensitive to the presence of the butyrate groups change gradually over the course of the reaction. The receding hexadecane contact angle (35°) for a labelled sample originally hydrolyzed for 10 h is lower than that for the heptafluorobutyrate surface (40°) and indicates that butyrate groups remain on the surface after this period of time.

The hydrolysis of PCTFE-$OCOC_3H_7$ in pure water exhibit results (Figures 1.24 - 1.25) similar to those discussed for the previous case except that the changes take place over a longer reaction time. The XPS C/F ratio of the labelled sample indicates that approximately 64% alcohol groups are present after a 24 h hydrolysis in water. The receding water contact angles after hydrolysis and advancing hexadecane contact angles after labelling change rapidly in the first 5 h of the hydrolysis. The low receding hexadecane contact angle (19°) agrees with XPS data in indicating that butyrate functionality remains after a 24 h hydrolysis. It is obvious that the lower polarity of methanol can effectively decrease the surface tension of the solution and the interfacial
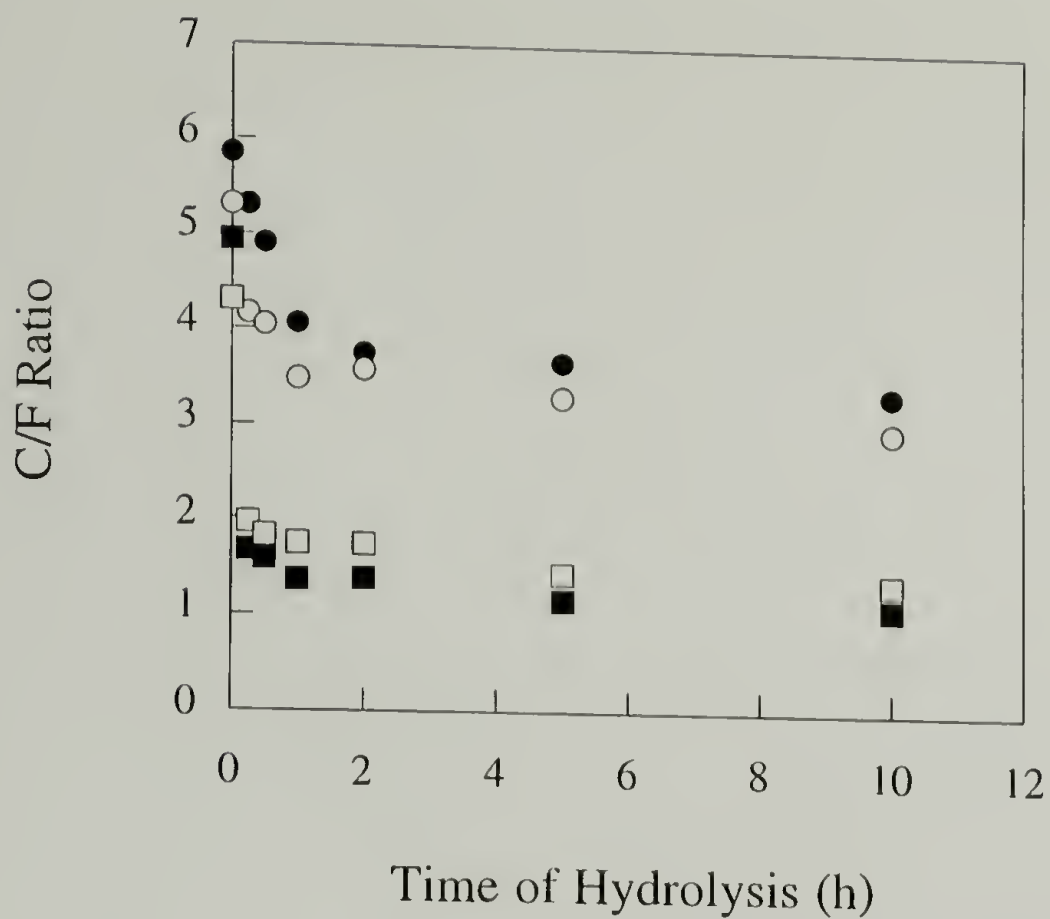
Figure 1.22. XPS C/F ratio data for the hydrolysis of PCTFE-$OCOC_3H_7$ in 75:25 water:methanol solution: 15° (●) and 75°(○) take-off angle data after hydrolysis, 15° (■) and 75° (□) take-off angle data after labelling with C_3F_7COCl.
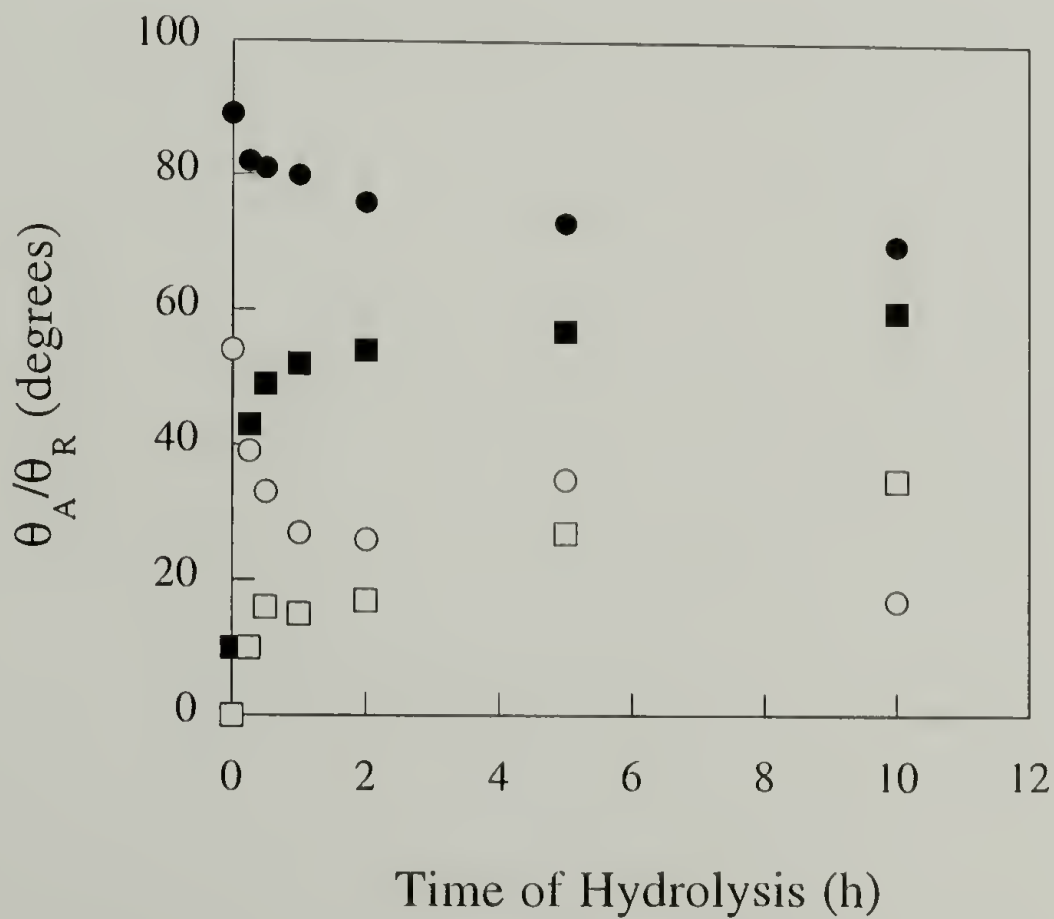
Figure 1.23. Contact angle data for the hydrolysis of PCTFE-$OCOC_3H_7$ in 75:25 water:methanol solution: water contact angles (θ_A (●); θ_R (○)) after hydrolysis and hexadecane contact angles (θ_A (■); θ_R (□)) after labelling with C_3F_7COCl.
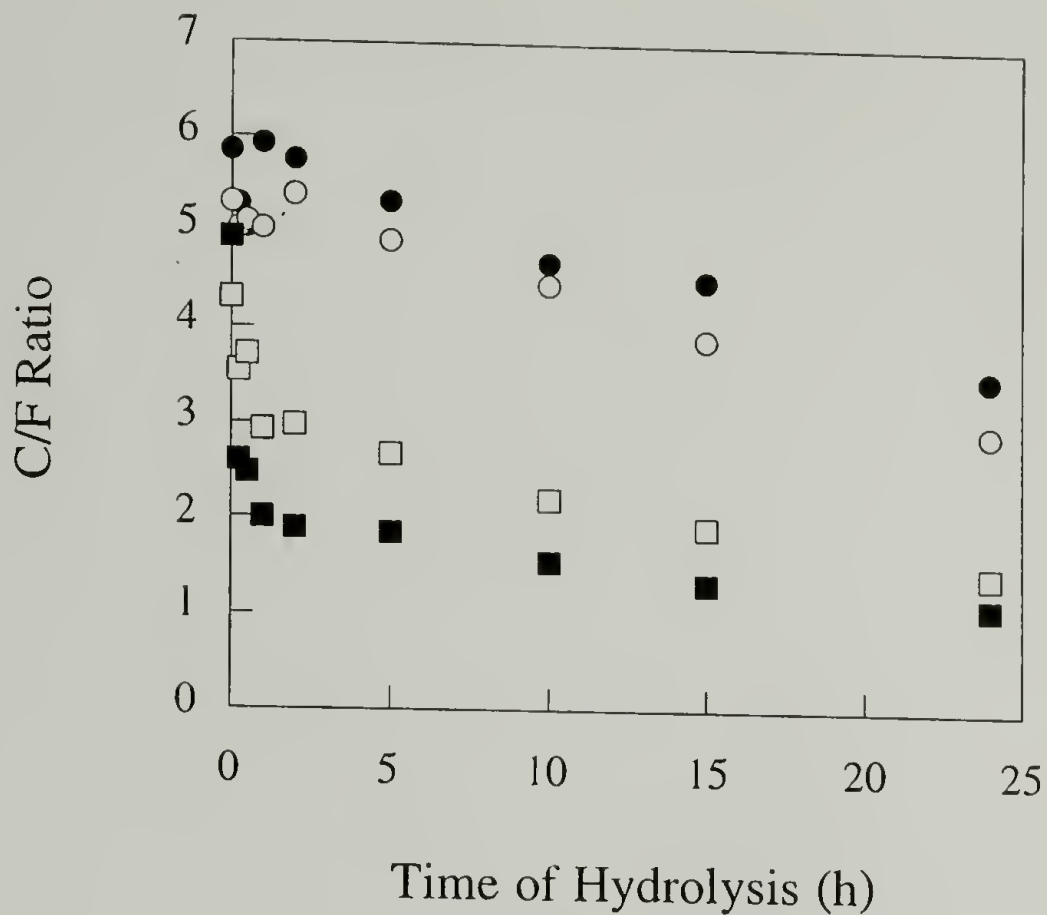
Figure 1.24. XPS C/F ratio data for the hydrolysis of PCTFE-OCOC$_3$H$_7$ in 100:0 water:methanol solution: 15° (●) and 75° (O) take-off angle data after hydrolysis, 15° (■) and 75° (□) take-off angle data after labelling with C$_3$F$_7$COCl.
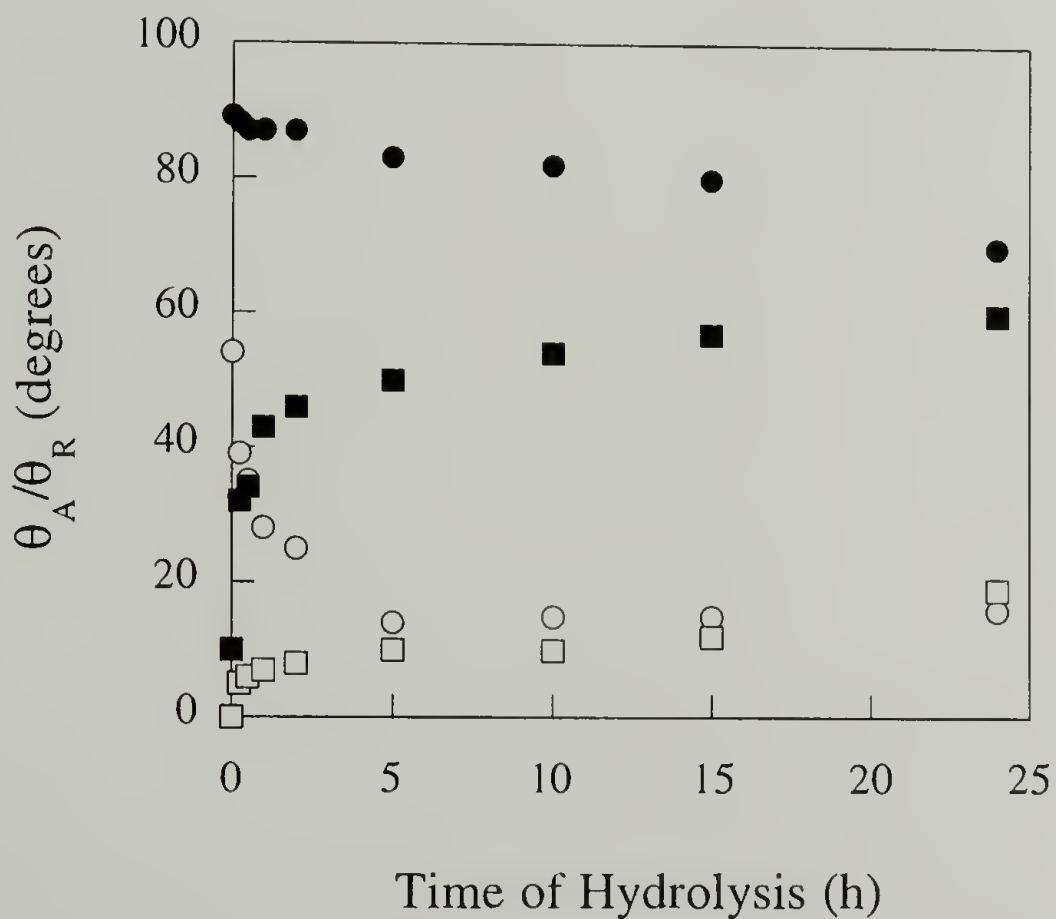
Figure 1.25. Contact angle data for the hydrolysis of PCTFE-OCOC$_3$H$_7$ in 100:0 water:methanol solution: water contact angles (θ_A (●); θ_R (O)) after hydrolysis, hexadecane contact angles (θ_A (■); θ_R (□)) after labelling with C$_3$F$_7$COCl.

energy between the hydrophobic butyrate surface and hydrolysis solution and increase hydrolysis rate.

The results of the methanolysis of PCTFE-OCOC$_{17}$H$_{35}$ (conducted in 0:100 water:methanol) are shown in Figures 1.26 - 1.27 and exhibit a number of interesting features. The extremely small decrease in receding water contact angle (from 90° to 87°) implies that a small extent of hydrolysis has occurred in the first 30 min. The XPS C/F ratio of the labelled sample indicates that the content of hydroxyl functionality has increased from 7% to 19%, whereas the yield of hydrolysis of PCTFE-OCOC$_3$H$_7$ surface was 87% for the same period of time. This low amount of hydrolysis is, however, sufficient to significantly disrupt the order of the stearate modified layer as indicated by a pronounced decrease in C/F ratios of hydrolyzed samples and a decrease in hexadecane contact angles of the labelled surfaces. In the next 30 min of reaction, C/F ratios and advancing water contact angle of the hydrolyzed samples decrease only slightly, while the receding water contact angle rapidly decreases from 87° to 57°. The concentration of hydroxyl groups has increased to 41%. At this point, the surface contains enough hydroxyl groups to be sufficiently wet by the reacting solution and thus increase the rate of reaction. Over the next 30 min of reaction, the yield of reaction rapidly increases to 90% with a corresponding large decrease in receding water contact angle. The advancing water contact angle has slightly decreased from 103° to 99° indicating the significant effect of a small percent of hydrophobic stearate functionality on the advancing contact angle. Advancing/receding water contact angles then decrease until they reach values consistent with the structure of completely hydrolyzed surface (PCTFE-OH) after 2.5 h of hydrolysis. The increase in advancing/receding hexadecane contact angles after the first 30 min of reaction are consistent with the structure and composition of the labelled surfaces.

XPS and contact angle data for the hydrolysis of PCTFE-OCOC$_{17}$H$_{35}$ conducted in a 25:75 water:methanol solution are shown in Figures 1.28 - 1.29. As expected, introducing water into the system raises the interfacial energy and decreases the ability of
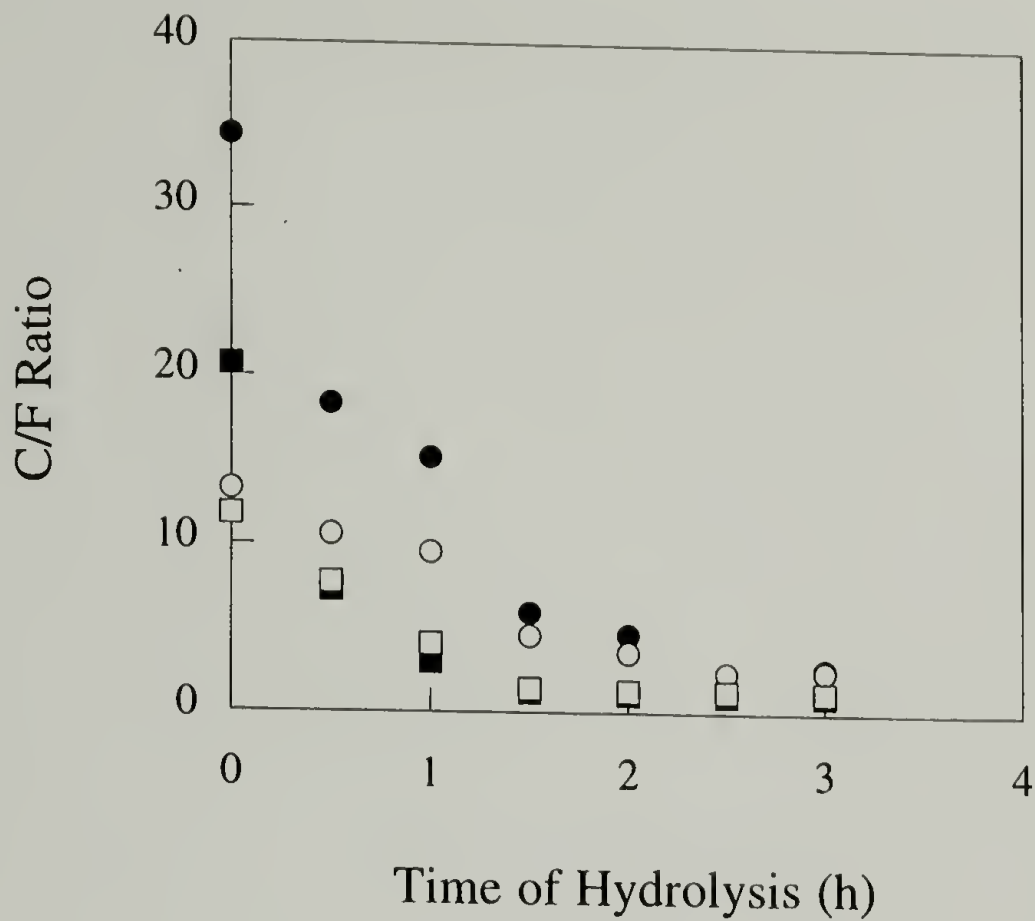
Figure 1.26. XPS C/F ratio data for the methanolysis of PCTFE-OCOC$_{17}$H$_{35}$ in 0:100 water:methanol solution: 15° (●) and 75°(○) take-off angle data after methanolysis, 15° (■) and 75° (□) take-off angle data after labelling with C$_3$F$_7$COCl.
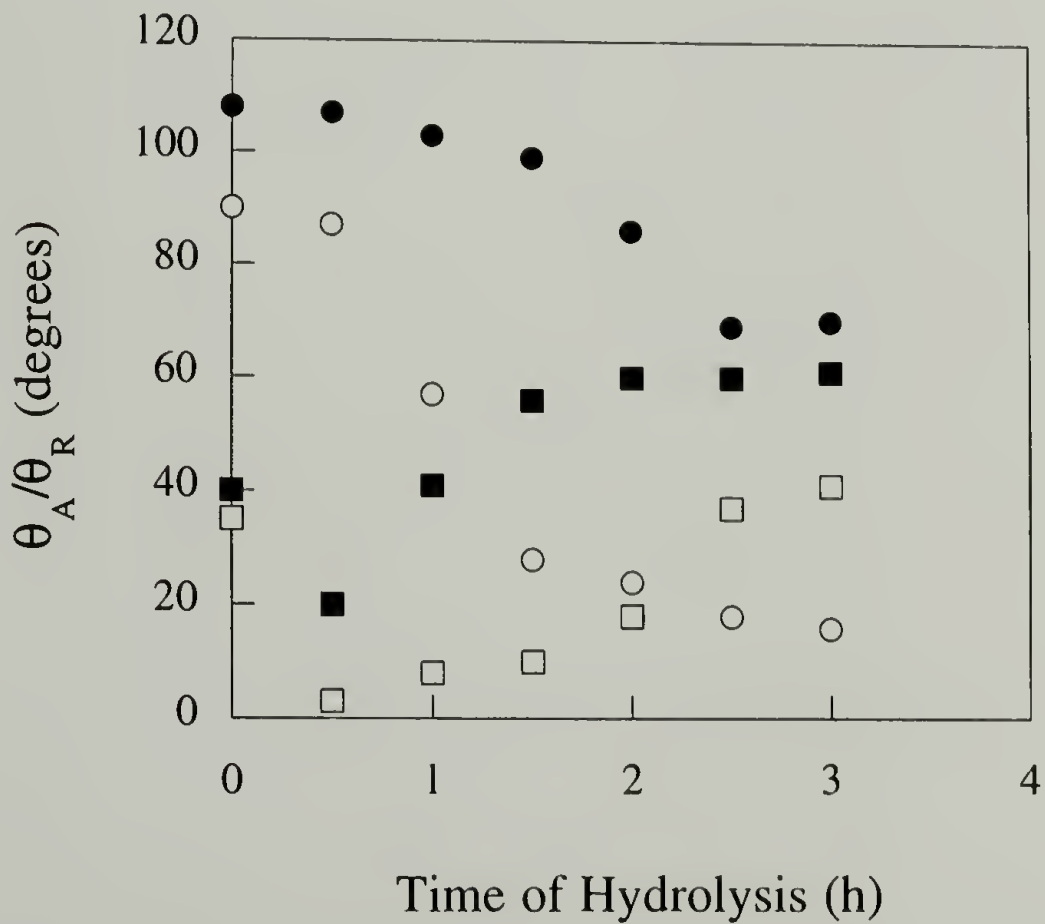
Figure 1.27. Contact angle data for the methanolysis of PCTFE-OCOC$_{17}$H$_{35}$ in 0:100 water:methanol solution: water contact angles (θ_A (●); θ_R (○)) after methanolysis and hexadecane contact angles (θ_A (■); θ_R (□)) after labelling with C$_3$F$_7$COCl.

50
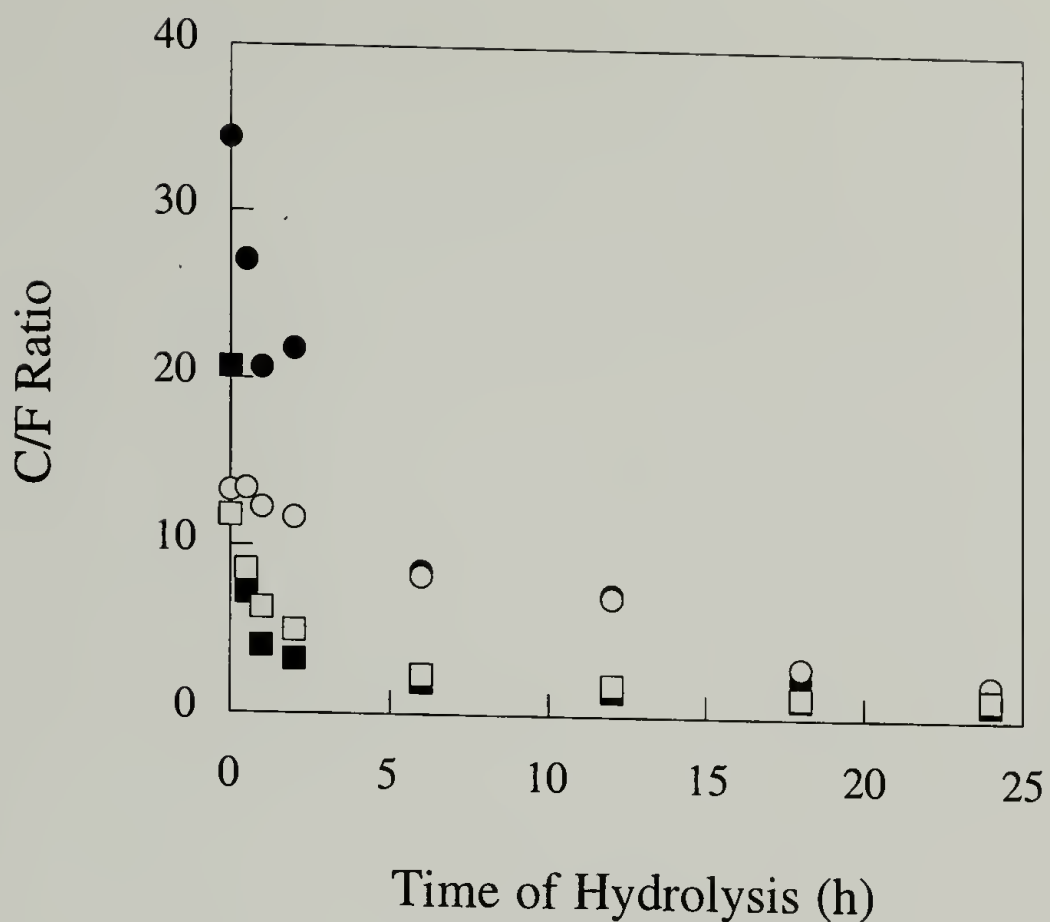
Figure 1.28. XPS C/F ratio data for the hydrolysis of PCTFE-OCOC$_{17}$H$_{35}$ in 25:75 water:methanol solution: 15° (●) and 75°(○) take-off angle data after hydrolysis, 15° (■) and 75° (□) take-off angle data after labelling with C$_3$F$_7$COCl.
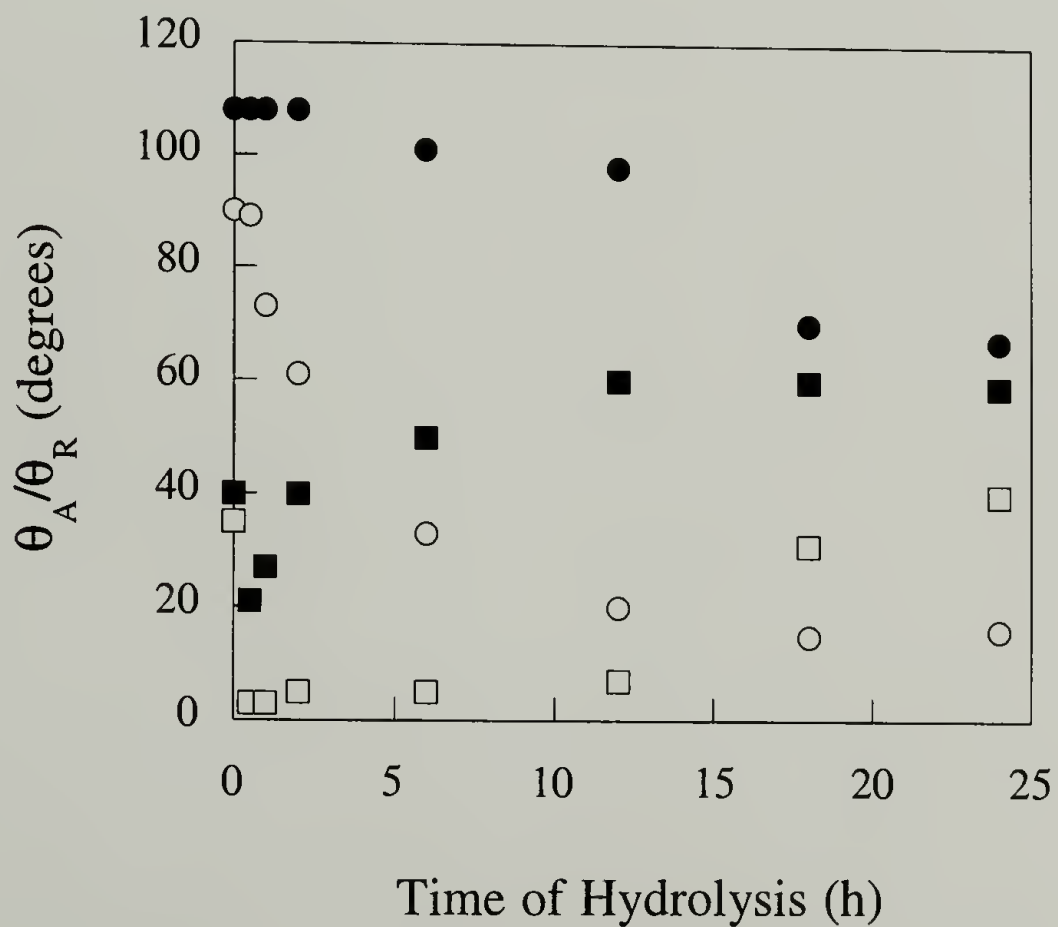
Figure 1.29. Contact angle data for the hydrolysis of PCTFE-OCOC$_{17}$H$_{35}$ in 25:75 water:methanol solution: water contact angles (θ_A (●); θ_R (○)) after hydrolysis and hexadecane contact angles (θ_A (■); θ_R (□)) after labelling with C$_3$F$_7$COCl.

51

the reacting solution to penetrate into the surface and results in a pronounced reduction in rate of hydrolysis. The data indicate that the hydrolysis is complete after 24 h, compared to 3 h for the reaction conducted in pure methanol. These results show similar trends as those discussed for methanolysis except the changes take place more slowly. Based on the results obtained, it can be imagined that the hydrolyses of PCTFE-OCOC$_{17}$H$_{35}$ in 50:50, 75:25 and 100:0 water:methanol solutions would be extremely long, so these sets of reaction were not attempted.

The extent of hydrolysis of PCTFE-OCOC$_3$H$_7$ and PCTFE-OCOC$_{17}$H$_{35}$ as a function of reaction time is plotted in Figures 1.30 - 1.31 for each of the solvent compositions studied. These figures show that as the amount of water in the hydrolysis solution increases, the reaction rate decreases due to the higher interfacial energy. The rate of hydrolysis in a given solvent mixture decreases as the length of the ester chain increases, which again is caused by an increase in the interfacial energy.

According to the speculation made earlier about the formation of patchy surfaces by the autoaccelerative hydrolysis in the presence of hydroxyl groups, the hydrolyses were expected to proceed slowly at the beginning (induction period) and then becomes faster after a certain number of hydroxyl groups were formed. Such a trend is not obvious in the hydrolysis/methanolysis of of PCTFE-OCOC$_3$H$_7$ especially when 0:100, 25:75 and 50:50 water:methanol solutions are used. There are two possible explanations: (1) the reacting solutions do not provide the interfacial energy that is high enough to induce the formation of patchy mixed surfaces, but results in randomly mixed surfaces, (2) The induction period is too small to be observed on the experimental time scale. This induction period, however, becomes longer for the systems having significantly high interfacial energy. This can be observed in the methanolysis of PCTFE-OCOC$_{17}$H$_{35}$ (see Figure 1.32 replotted for clarity from Figure 1.31). More detail about the wetting behavior that may facilitate the interpretation of these mixed surface structures is discussed below.
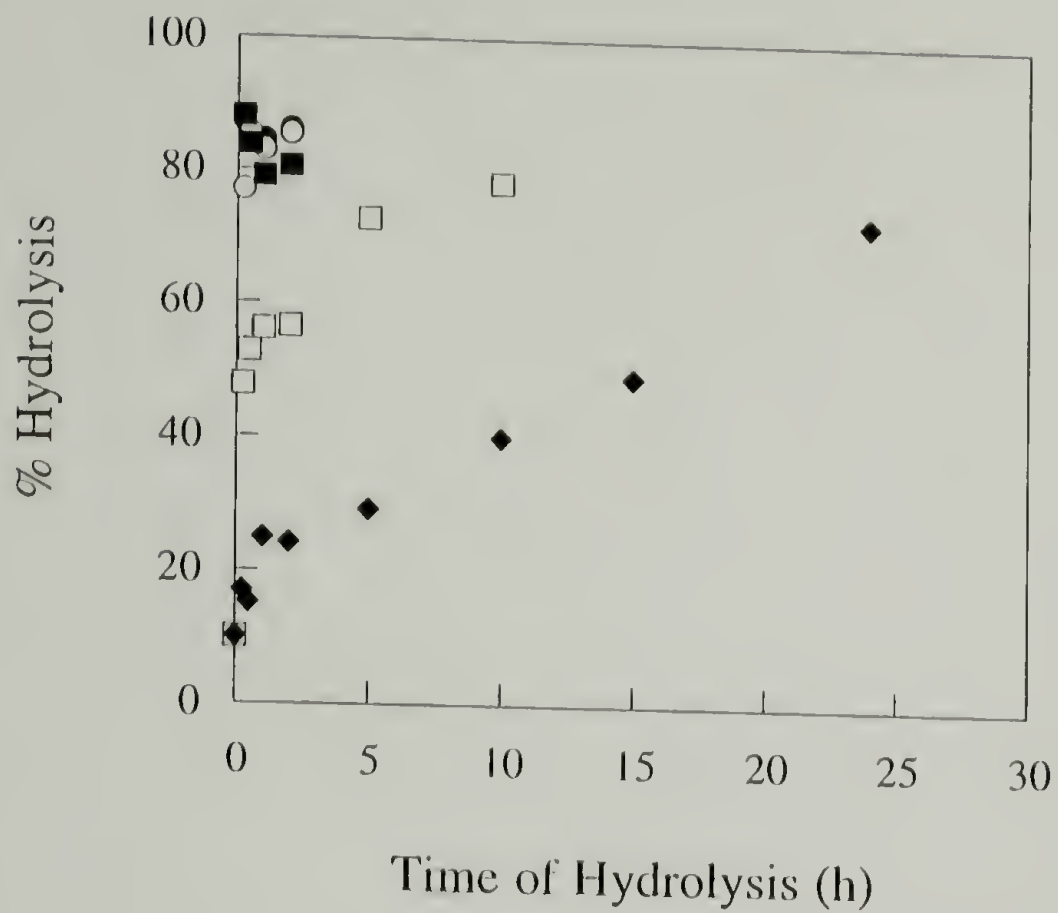
Figure 1.30. Kinetics of hydrolysis/methanolysis of PCTFE-OCOC$_3$H$_7$ using water:methanol as solvent; 0:100 (●), 25:75 (O), 50:50 (■), 75:25 (□), 100:0 (◆).
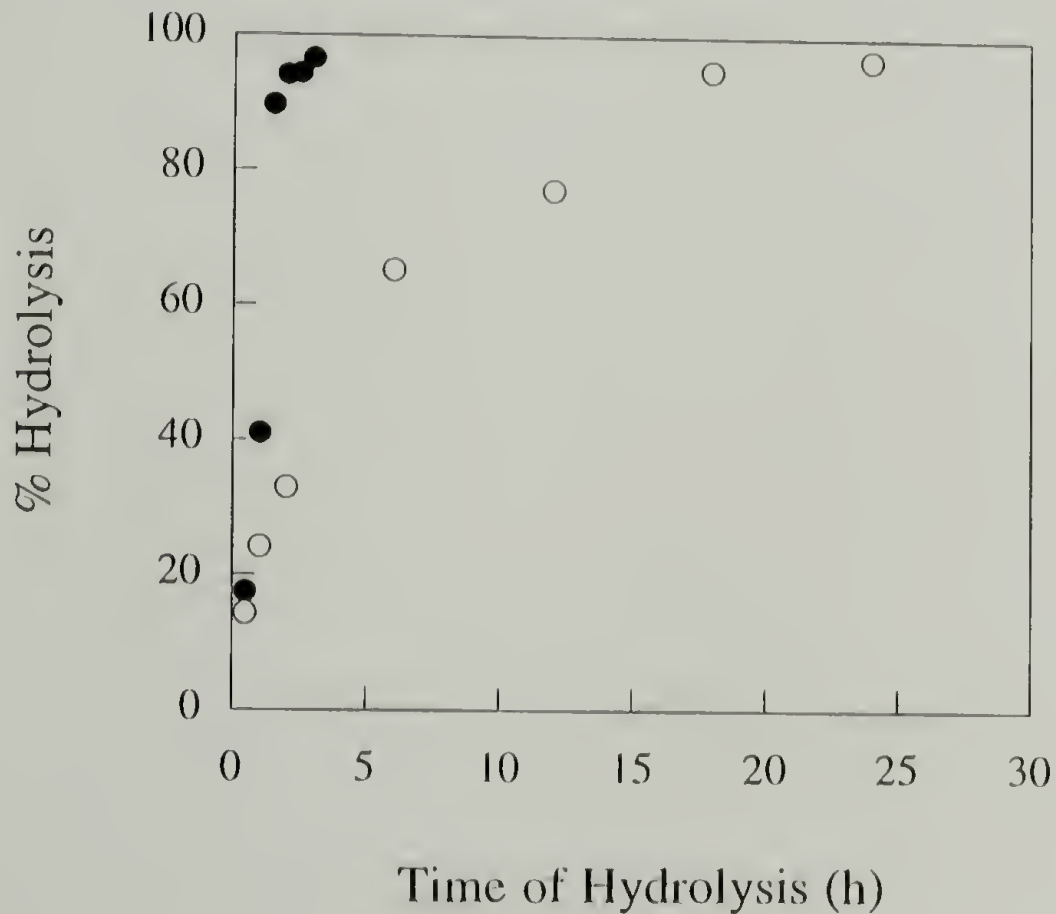
Figure 1.31. Kinetics of hydrolysis/methanolysis of PCTFE-OCOC$_{17}$H$_{35}$ using water:methanol as solvent; 0:100 (●), 25:75 (O).
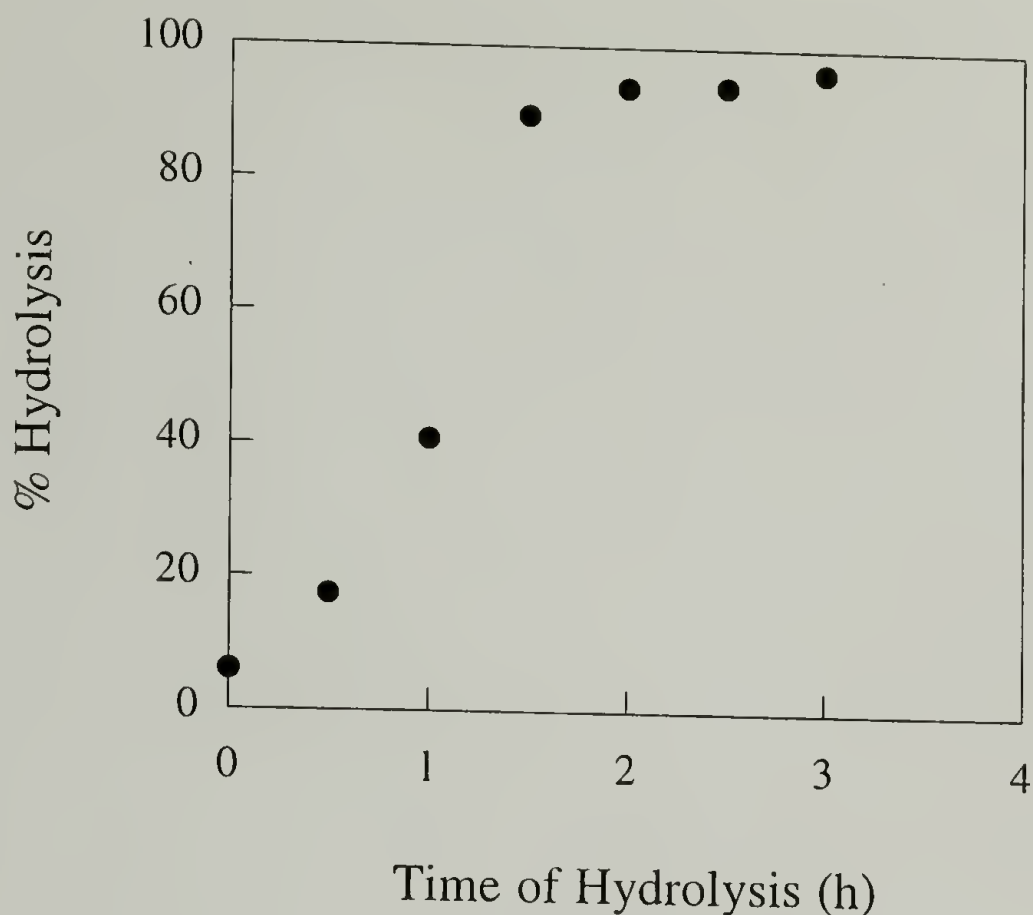
Figure 1.32. Kinetics of methanolysis of PCTFE-OCOC$_{17}$H$_{35}$.

Competitive Esterifications of PCTFE-OH

Mixed hydrocarbon ester/fluorocarbon ester surfaces can also be prepared by an alternative route, competitive esterification using a reaction of PCTFE-OH with a mixture of acid chlorides. The thickly modified (~1000 Å) PCTFE-OH surfaces prepared at -15 °C were used for this study. 75° takeoff angle XPS survey and C$_{1s}$ spectra of PCTFE-OH, PCTFE-OCOC$_3$H$_7$, PCTFE-OCOC$_{17}$H$_{35}$, PCTFE-OCOC$_3$F$_7$ are exhibited in Figure 1.33. In addition to XPS, ATR IR was used to follow the extent of esterification. Since heptafluorobutyryl chloride (C$_3$F$_7$COCl) is much more reactive than its hydrocarbon analog, butyryl chloride (C$_3$H$_7$COCl), the surfaces are composed of essentially 100% heptafluorobutyrate when the concentration of C$_3$F$_7$COCl used in the acid chloride mixtures is higher than 10%. This suggests that it is neccessary to use very low concentrations of C$_3$F$_7$COCl to allow C$_3$H$_7$COCl to effectively compete in esterification and react with PCTFE-OH.
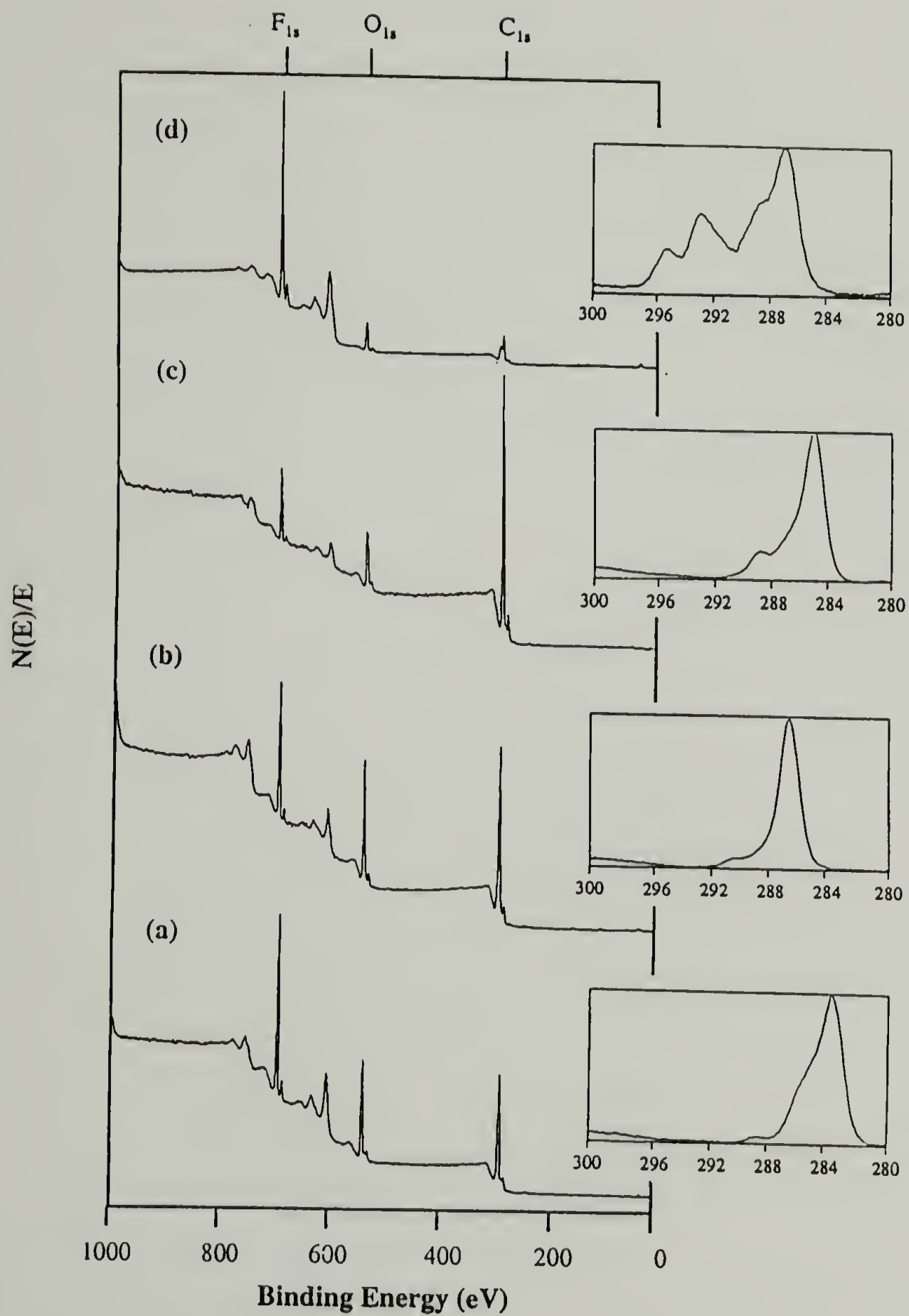
Figure 1.33. XPS survey and C_{1s} spectra ($75°$ take-off angle) of (a) PCTFE-OH (b) PCTFE-OCOC$_3$H$_7$ (c) PCTFE-OCOC$_{17}$H$_{35}$ (d) PCTFE-OCOC$_3$F$_7$.

ATR IR analysis of mixed $PCTFE-OCOC_3H_7/-OCOC_3F_7$ prepared with C_3H_7COCl/C_3F_7COCl mixtures indicate that no butyrate functionality forms until C_3F_7COCl concentration is lowered to 1.0 mole %. The small peak at 1740 cm^{-1} representing the carbonyl stretching of butyrate next to the carbonyl stretching peak at 1783 cm^{-1} assigned to the carbonyl of heptafluorobutyrate is observed (Figure 1.34). This indicates that a significant amount of butyrate is simultaneously formed at this concentration. From XPS C_{1s} spectra (Figure 1.35), the gradual decrease in intensity of the high binding energy peaks at 295 and 293 eV (assigned to carbons from CF_3 and CF_2, respectively), also confirms that the surface mixtures are produced. By assuming all alcohol groups on the surface were consumed in the reaction, butyrate composition on the surfaces can be calculated from XPS C/F ratios. Figure 1.36 shows that the mixed $PCTFE-OCOC_3H_7/-OCOC_3F_7$ can be prepared by varying the mole % of C_3F_7COCl in acid chloride mixtures over the range of 0.5 - 1.5 mole %.

The effect of heptafluorobutyryl chloride concentration on the surface composition of the mixed $PCTFE-OCOC_{17}H_{35}/-OCOC_3F_7$ surfaces appears to be similar to the case of butyrate mixed surfaces. Stearoyl chloride ($C_{17}H_{35}COCl$) begins to be able to compete with heptafluorobutyryl chloride (C_3F_7COCl) in the esterification when less than 1.0 mole % of the highly reactive C_3F_7COCl is employed (Figure 1.37). The maximum amount of C_3F_7COCl that can produce a surface mixture is slightly smaller than the previous case because of the larger difference in reactivity between $C_{17}H_{35}COCl$ and C_3F_7COCl. XPS data indicate that approximately 52% (15° take-off angle) and 67% (75° take-off angle) of stearate esters were formed when the competitive reaction was conducted in an acid chloride mixture composed of 0.4 mole % heptafluorobutyryl chloride. The existence of both stearate esters and heptafluorobutyrate esters is evidenced by ATR IR (shown in Figure 1.38). Carbonyl stretching of stearate group is represented by the peak at 1740 cm^{-1}, while the peak at 1783 cm^{-1} is assigned to carbonyl stretching of heptafluorobutyrate. The range of the amount of heptafluorobutyryl chloride used in the acid chloride mixtures
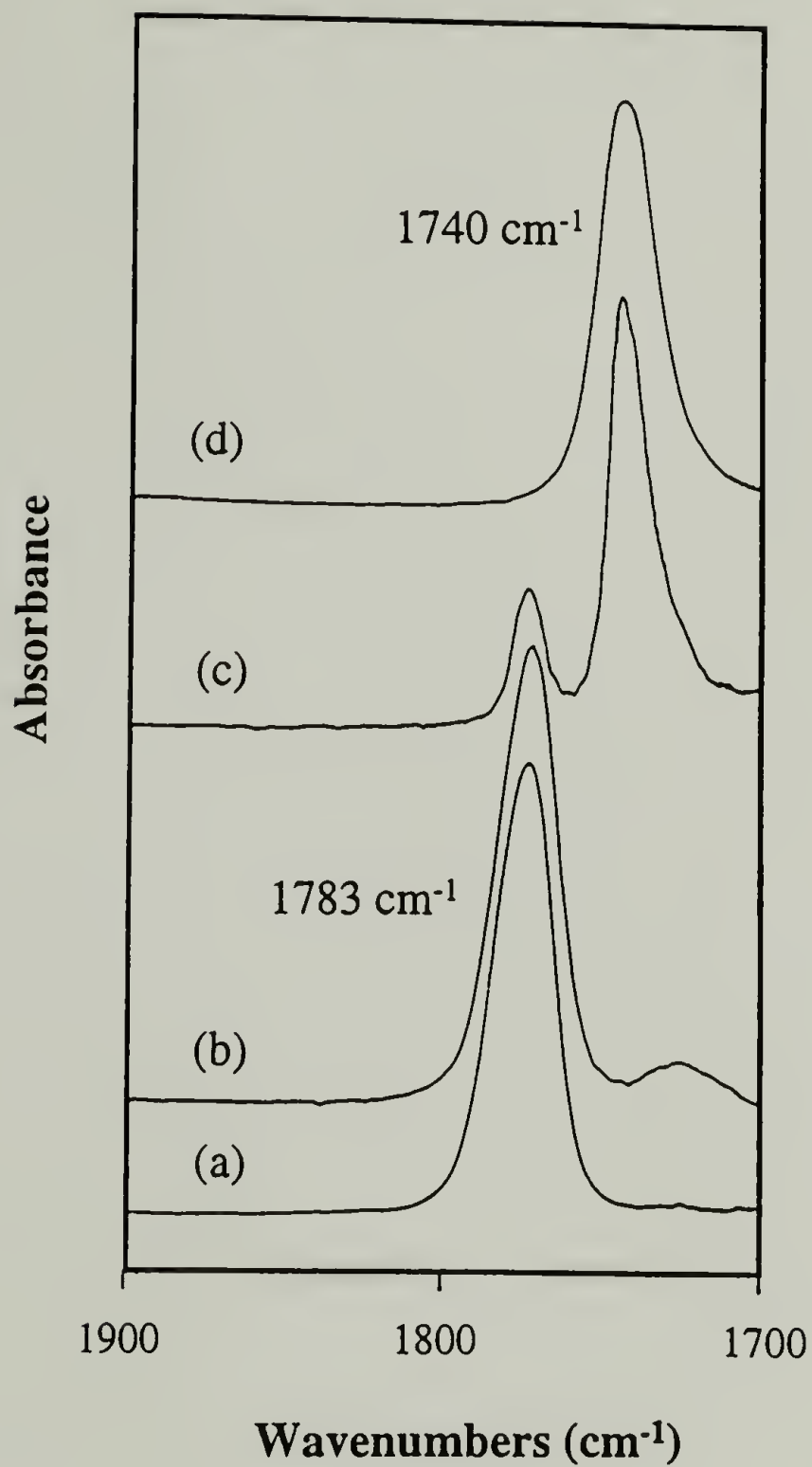
Figure 1.34. Carbonyl stretching region from ATR IR spectra of PCTFE-OCOC$_3$H$_7$/-OCOC$_3$F$_7$ prepared by competitive esterification with acid chloride mixtures containing mole % C$_3$F$_7$COCl (a) 100% (b) 1.0% (c) 0.5% (d) 0% (100% C$_3$H$_7$COCl).
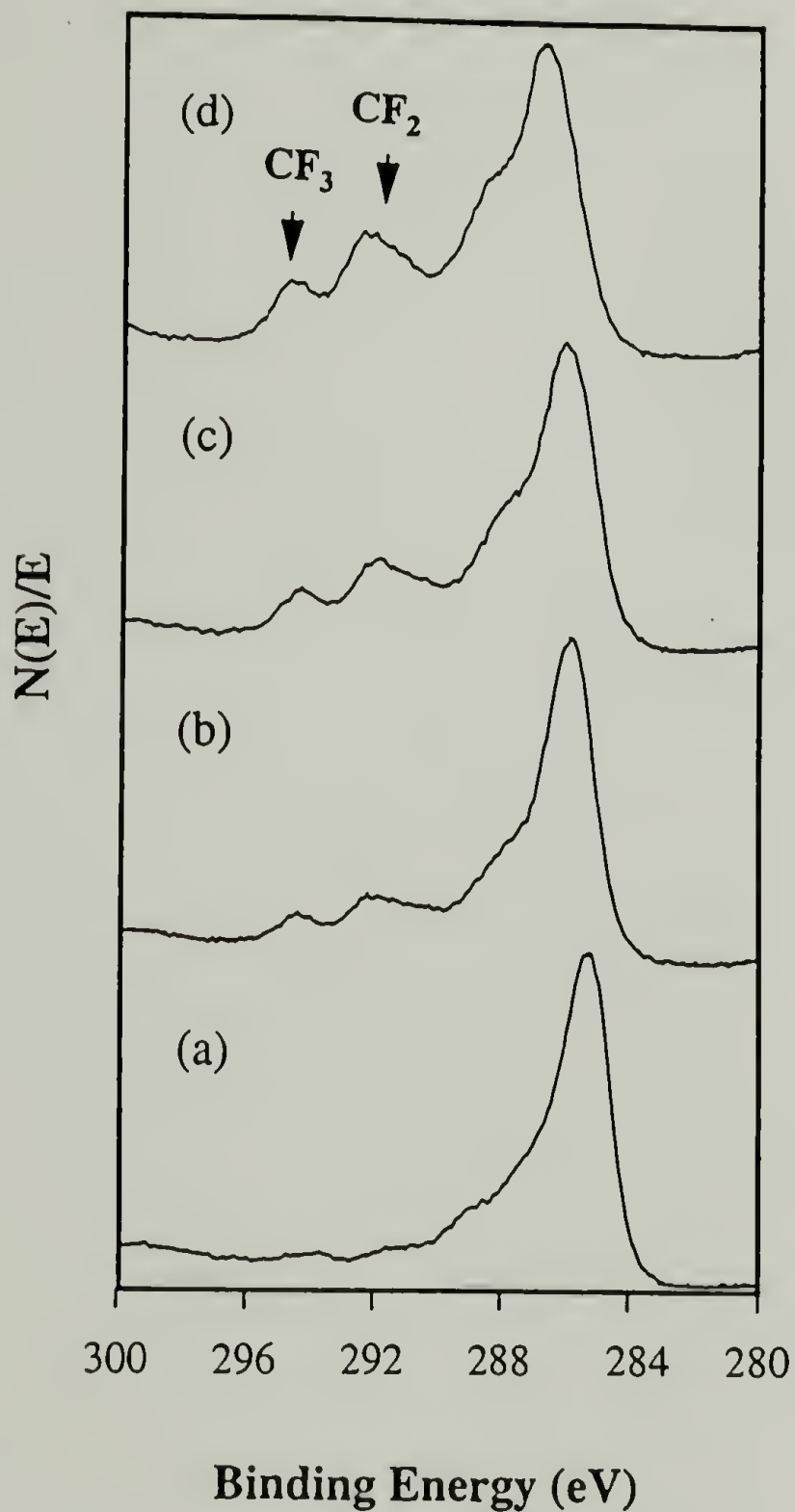
Figure 1.35. XPS C_{1s} spectra (75° take-off angle) of PCTFE-$OCOC_3H_7$/-$OCOC_3F_7$ prepared by competitive esterification with acid chloride mixtures containing mole % of C_3F_7COCl (a) 0.5% (b) 1.0% (c) 1.2% (d) 1.3%.
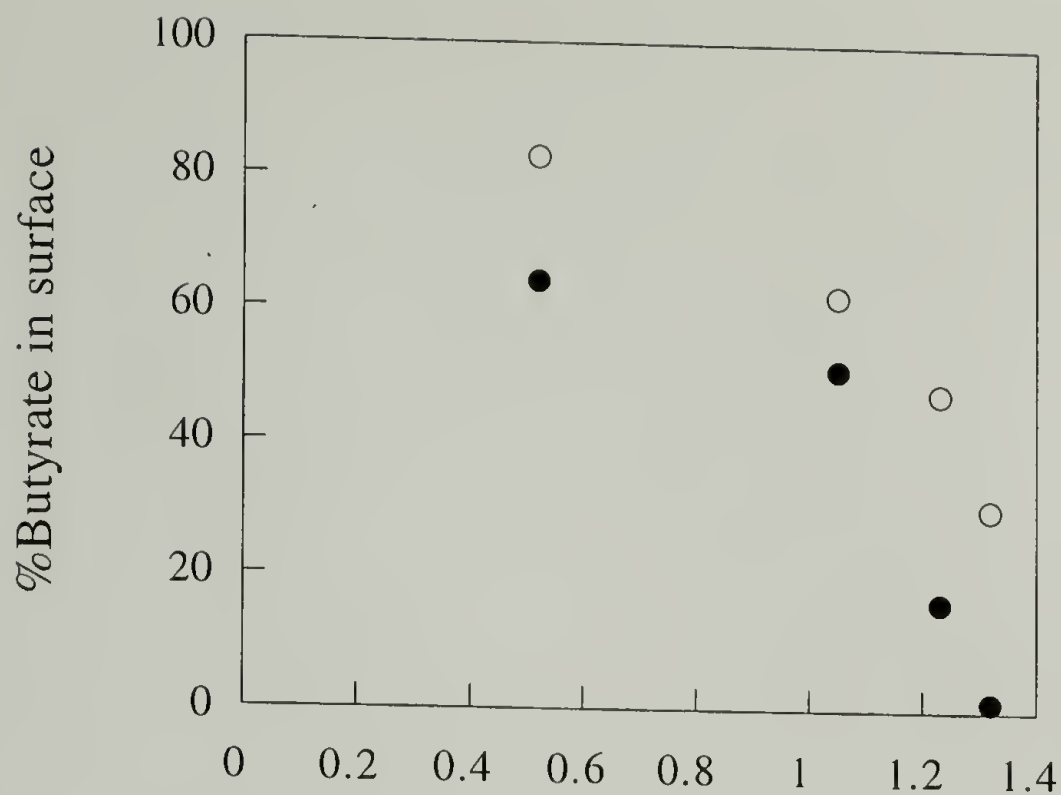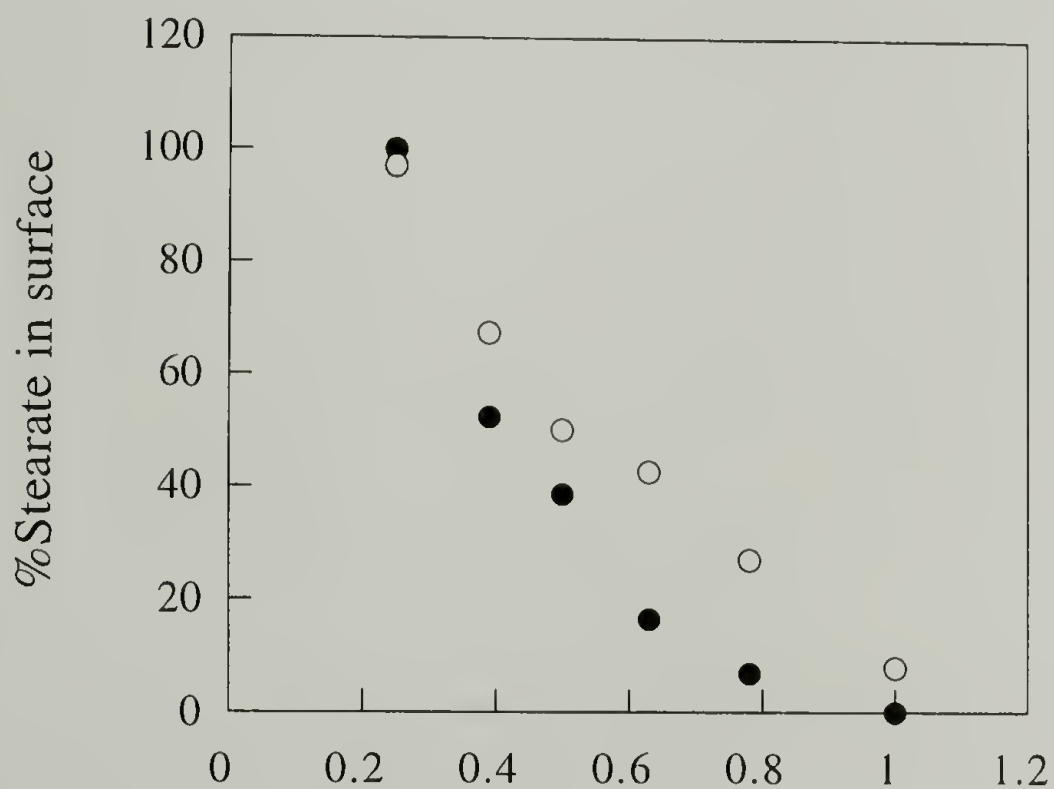
Figure 1.36. % Butyrate calculated from XPS data; 15° take-off angle (●), 75° take-off angle (O) of PCTFE-OCOC$_3$H$_7$/-OCOC$_3$F$_7$ mixed surfaces prepared by competitive esterification.

Figure 1.37. % Stearate calculated from XPS data; 15° take-off angle (●), 75° take-off angle (O) of PCTFE-OCOC$_{17}$H$_{35}$/-OCOC$_3$F$_7$ mixed surfaces prepared by competitive esterification.
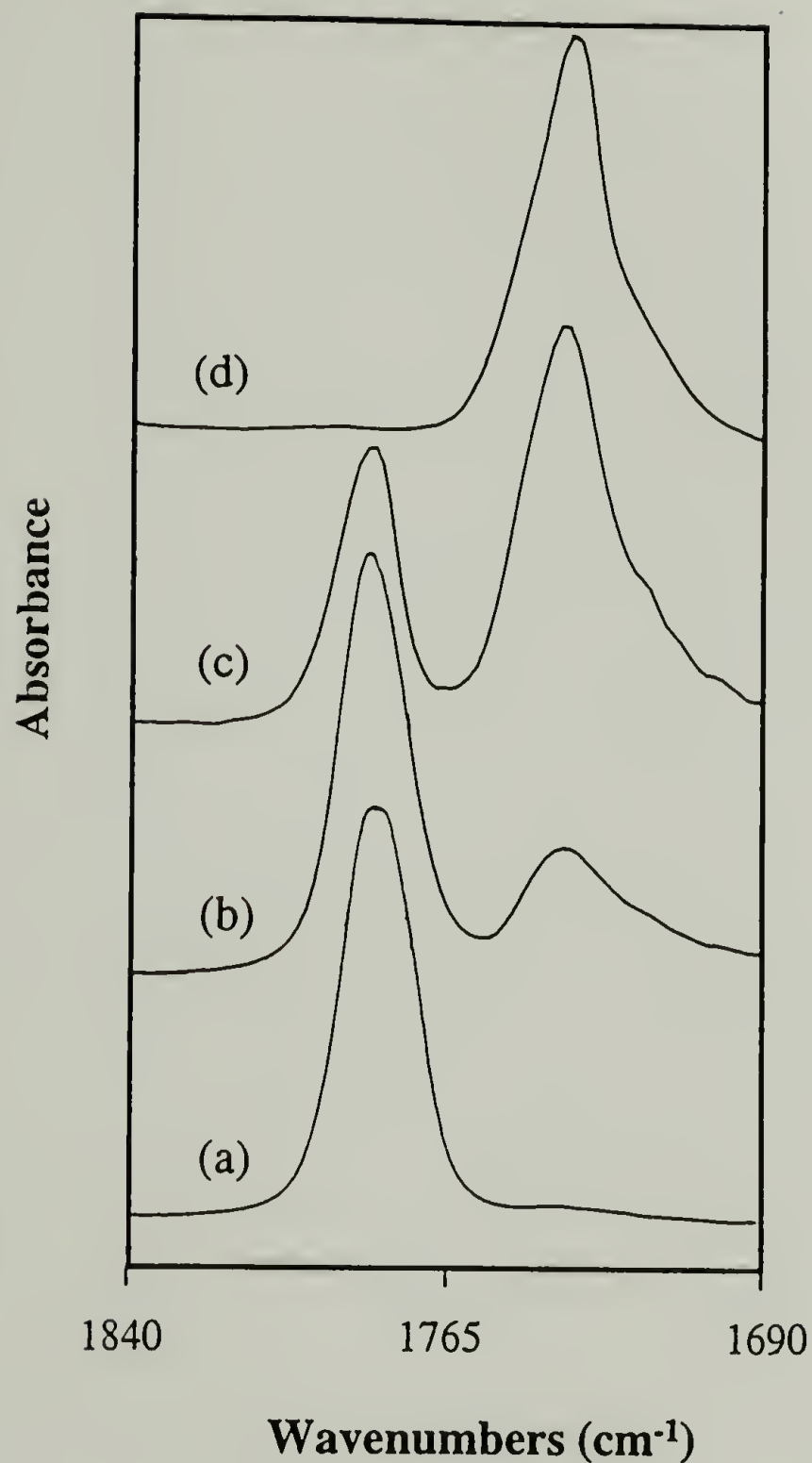
Figure 1.38. Carbonyl stretching region from ATR IR spectra of PCTFE-OCOC$_{17}$H$_{35}$/-OCOC$_3$F$_7$ prepared by competitive esterification with acid chloride mixtures containing mole % C$_3$F$_7$COCl (a) 1.00% (b) 0.6% (c) 0.4% (d) 0.25% (~100% C$_{17}$H$_{35}$COCl).

to control the surface compositions is 0.4 - 1.0 % which is narrower than the one used to control butyrate/heptafluorobutyrate mixed surfaces.

Wetting Behavior of Surface Mixtures as a Function of Surface Composition

The major goal of this study was to determine if the wetting behavior of compositionally similar surfaces varies as a function of the preparation method. Alcohol/ester mixed surfaces were synthesized either by partial esterification of PCTFE-OH or partial hydrolysis of PCTFE-Esters. Hydrocarbon ester/fluorocarbon ester mixed surfaces were produced by subsequent esterifications of alcohol/ester mixed surfaces or competitive esterification of PCTFE-OH with acid chloride mixtures. Both types of surface mixtures were prepared over a range of composition. The wettability of the former set of mixed surfaces was assessed by water contact angles, while the latter set was analyzed by hexadecane contact angles. These probe fluids were chosen to maximize the wettability differences between the two surface components. Water interacts favorably with the polar, hydrogen-bonding alcohol functionality and is repelled by the hydrophobic tails of the esters. Hexadecane, on the other hand, is attracted to the hydrocarbon esters, but repelled by the oleophobic perfluorinated groups. The contact angles of all mixed surfaces prepared were measured as a function of surface composition (calculated from XPS C/F ratios obtained at 75° take-off angle).[51] Since the surface energy directly depends on the cosine of contact angle according to Young's Equation (Equation 1.18), the following discussion are mainly based on cosine contact angle values ($\cos\theta_A/\cos\theta_R$).

Figures 1.39 and 1.40 compare the water contact angle results measured on the mixed hydroxyl/ester surfaces: PCTFE-OH/OCOC$_3$H$_7$ and PCTFE-OH/OCOC$_{17}$H$_{35}$ prepared by kinetic control of the esterification of PCTFE-OH with butyryl chloride and stearoyl chloride, respectively. The results for PCTFE-OH/OCOC$_3$H$_7$ mixed surfaces show that $\cos\theta_A$ and $\cos\theta_R$ change gradually over the composition range implying that the functional groups are dispersed randomly throughout the modified layer.

The water contact angle results for the mixed PCTFE-OH/-OCOC$_{17}$H$_{35}$ surfaces exhibit some interesting trends. A dramatic decrease of cosθ$_A$ from 0.39 to -0.14 is observed when the stearate content increases from 0% to 26% due to an excess of hydrocarbon at the film/air interface with a relatively low ester content. The behavior of cosθ$_R$ reflects the formation of an ordered, close-packed surface. Cosθ$_R$ changes slowly from 0.96 to 0.89 as the composition changes from 0% to 26% stearate. At this point, water contact angles show that as the concentration of stearate increases, the hydrocarbon tails begin to align themselves into an ordered close-packed array, oriented perpendicular to the surface. During the orientation process, the hydrocarbon tails become progressively more efficient in preventing water from reaching unreacted hydroxyl groups beneath, then cosθ$_R$ begins to drop rapidly. The ordering process seems to be complete when the stearate content reaches 70% and cosθ$_R$ remains constant. Once again, it can be interpreted that stearate and alcohol groups are dispersed randomly in the modified layers.

For comparison, the water contact angle results for the same two sets of mixed surfaces prepared by partial hydrolysis/methanolysis of PCTFE-OCOC$_3$H$_7$, and PCTFE-OCOC$_{17}$H$_{35}$ are shown in Figures 1.41 and 1.42, respectively. Partial hydrolysis/methanolysis of PCTFE-OH/OCOC$_3$H$_7$ surfaces in water:methanol mixtures (0:100, 25:75, 50:50, 75:25) all yield PCTFE-OH/OCOC$_3$H$_7$ mixed surfaces with their cosθ$_A$ and cosθ$_R$ values as a function of composition indistinguishable from the results obtained from the mixtures prepared by partial esterification (Figure 1.39). The cosine contact angle data of two series of PCTFE-OH/OCOC$_3$H$_7$ mixed surfaces hydrolyzed in water and in 75:25 water:methanol solutions are displayed in Figure 1.41. The cosθ$_R$ results for PCTFE-OH/OCOC$_3$H$_7$ mixed surfaces hydrolyzed in water cannot be superimposed on the other PCTFE-OH/OCOC$_3$H$_7$ mixed surface series, implying differences in surface structures. The significantly greater contact angle hysteresis suggests that these surfaces are "patchy" in nature. The formation of this patchiness was described previously as being the result of an initially inhibited reaction (due to high interfacial
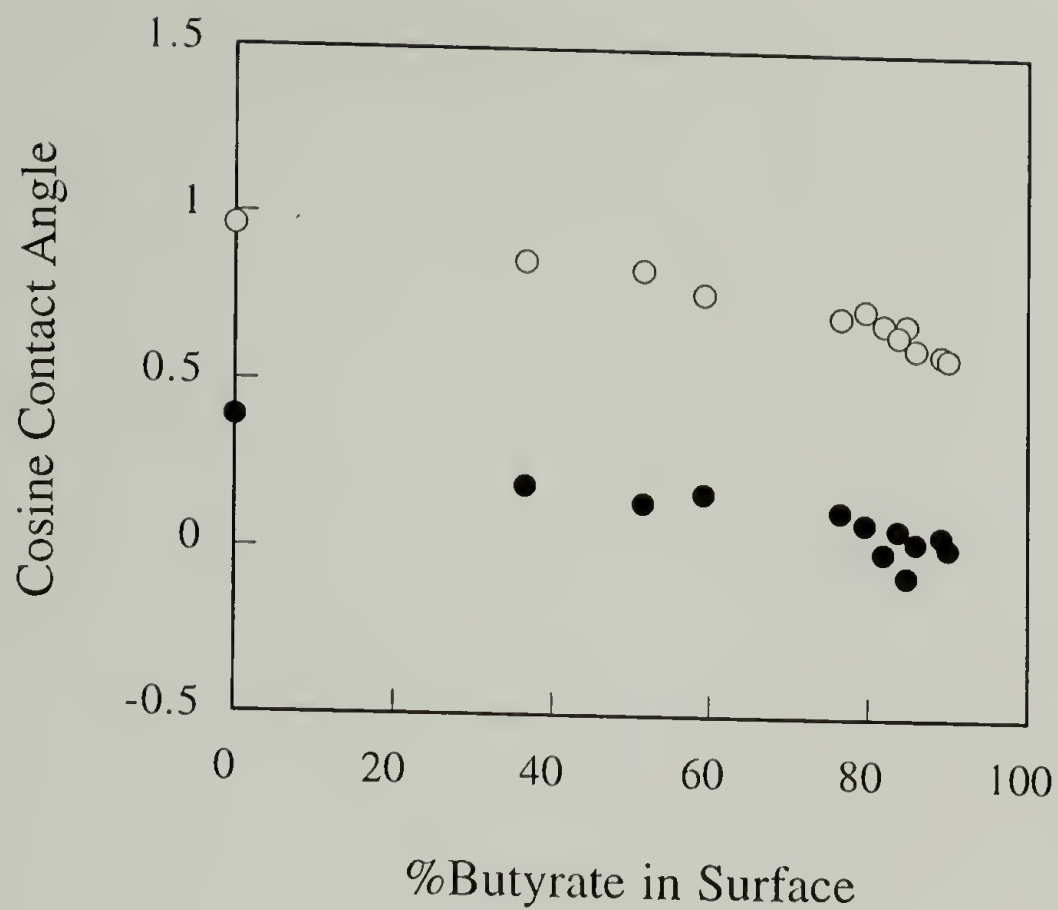
Figure 1.39. Cosine water contact angle data for PCTFE-OH/-OCOC$_3$H$_7$ prepared by partial esterification: θ_A (●); θ_R (O).
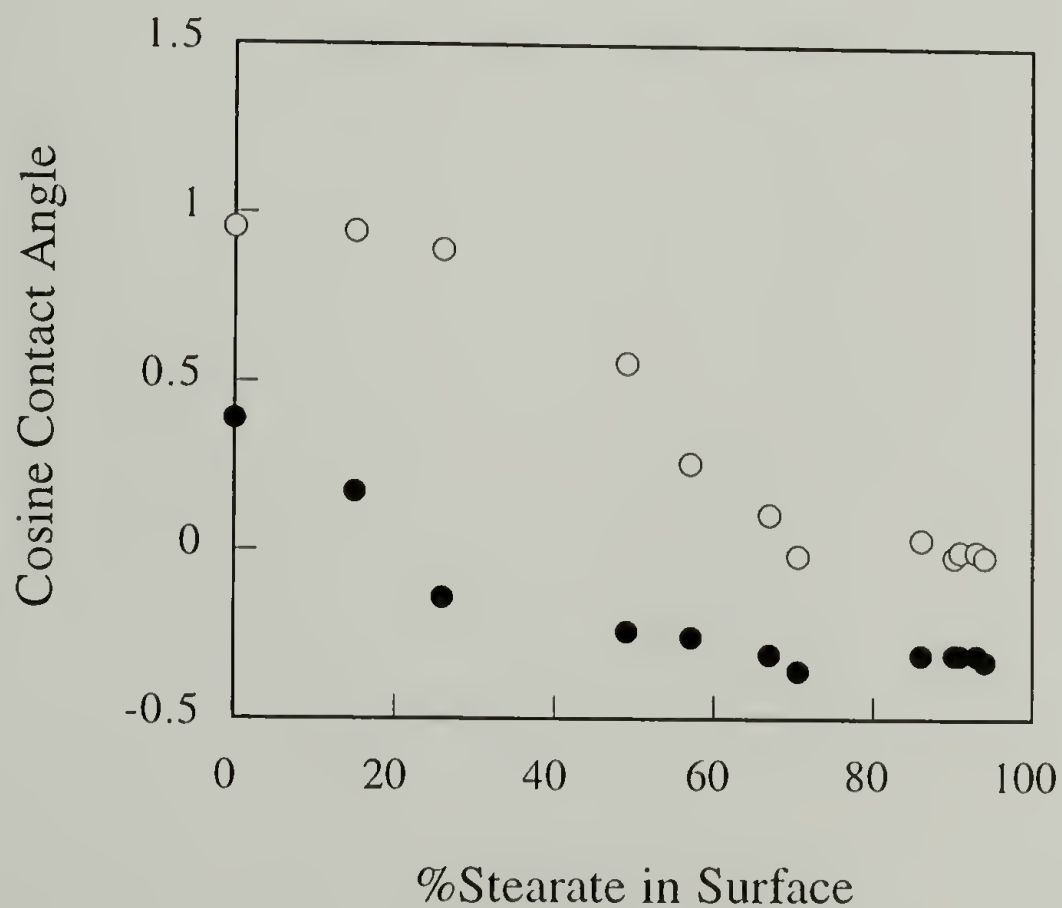
Figure 1.40. Cosine water contact angle data for PCTFE-OH/-OCOC$_{17}$H$_{35}$ prepared by partial esterification: θ_A (●); θ_R (O).
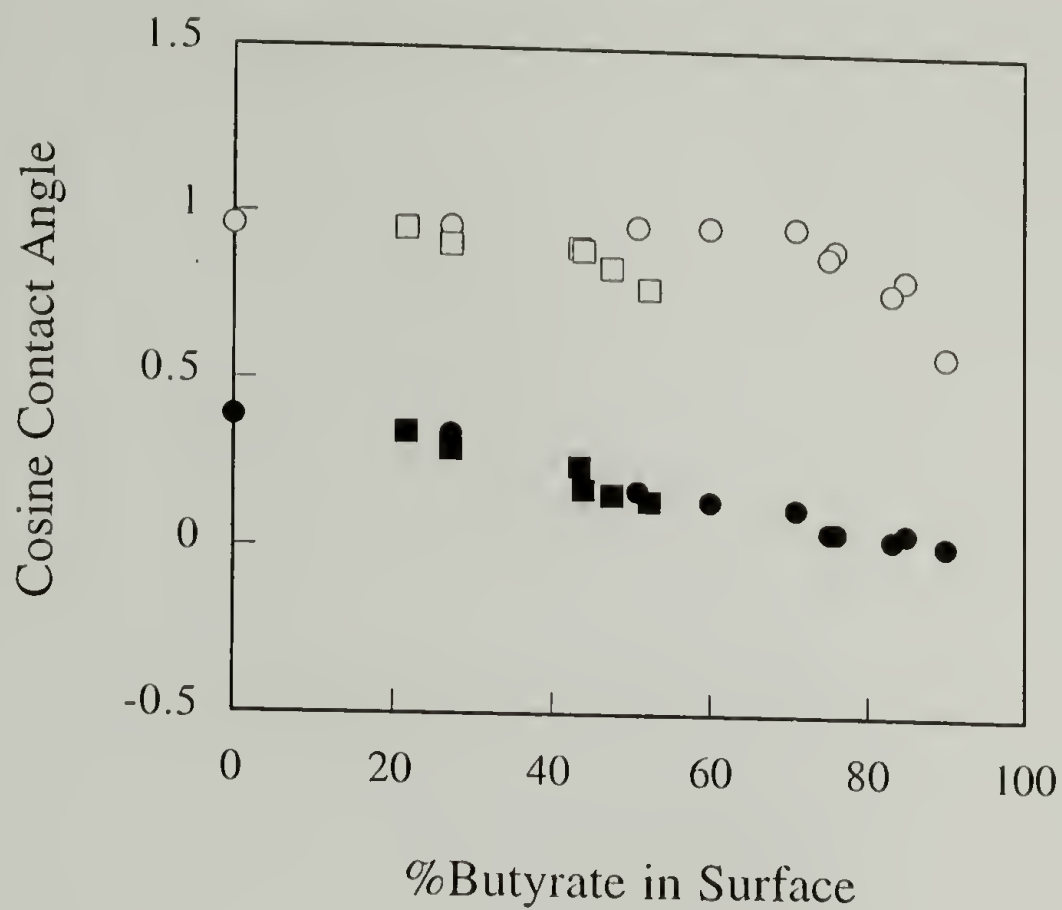
Figure 1.41. Cosine water contact angle data for PCTFE-OH/-OCOC$_3$H$_7$ prepared by partial hydrolysis in aqueous solution:θ_A (●); θ_R (O) and in 75:25 water:methanol solution: θ_A (■); θ_R (□).
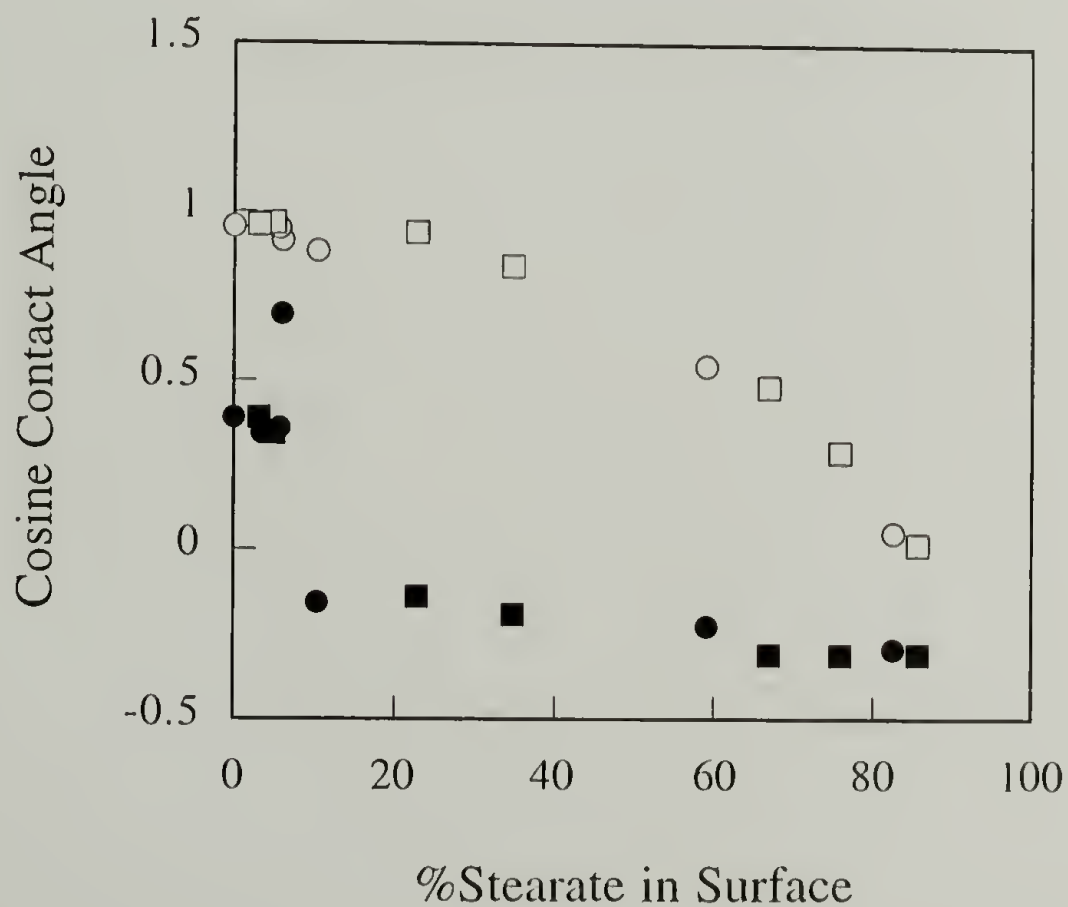
Figure 1.42. Cosine water contact angle data for PCTFE-OH/-OCOC$_{17}$H$_{35}$ prepared by partial hydrolysis/methanolysis in methanol: θ_A (●); θ_R (O) and in 25:75 water:methanol solution: θ_A (■); θ_R (□).

energy) to form isolated hydroxyl groups on the surface followed by an autoaccelerative hydrolysis radiating out from these points as the interfacial energy decreases at the reacted sites.

The water contact angle results for each of the two hydrolysis/methanolysis in water:methanol mixtures (0:100, 25:75) of PCTFE-OCOC$_{17}$H$_{35}$ are shown in Figure 1.42. The data from the two reactions are superimposable indicating similarities in the resulting mixed surface structures. For comparison with mixed surfaces obtained from kinetic control of the esterification (Figure 1.40), the relatively high values of $\cos\theta_R$ for compositionally similar surfaces indicate the formation of patchy surfaces. The rapid decrease in $\cos\theta_A$ at relatively low stearate concentration can be explained by two reasons. First, it is due to an excess of the low surface energy hydrocarbon esters at the film/air interface similar to the speculation given for the results obtained from kinetic control of esterification. Second, the patchy nature of the surface may force the advancing liquid contact line to be pinned at the boundary between two surface phases and result in a very high advancing contact angle (low $\cos\theta_A$).

The hexadecane contact angle results as a function of surface composition for the hydrocarbon ester/heptafluorobutyrate mixed surfaces prepared by sequential esterifications are shown in Figures 1.43 - 1.44. For PCTFE-OCOC$_{17}$H$_{35}$/-OCOC$_3$F$_7$ mixed surfaces (Figure 1.43), $\cos\theta_A$ increases slightly in the beginning and then linearly increases with the higher stearate content up to 67% stearate where large methylene groups are predominantly present at the film/air interface. Afterwards, $\cos\theta_A$ then begins to decrease (higher contact angle) with higher stearate content. This reflects the formation of the ordered surface which presents methyl groups to the film/air interface. At the same time, $\cos\theta_R$ initially increases and then remains relatively constant at 1.00 above 15% stearate. A rapid drop of $\cos\theta_R$ is observed as the degree of ordering increases when the stearate concentration reaches 92%.

The hexadecane wetting behavior of the PCTFE-OCOC$_3$H$_7$/-OCOC$_3$F$_7$ mixed surfaces (Figure 1.44) is also similar to PCTFE-OCOC$_{17}$H$_{35}$/-OCOC$_3$F$_7$ mixed surfaces. The only differences are in the positions of the transition points in the cosθ$_A$ and cosθ$_R$ curves. Since the sizes of the two esters in PCTFE-OCOC$_3$H$_7$/-OCOC$_3$F$_7$ mixed surfaces are comparable, the heptafluorobutyrate groups at the film/air interface can be detected by advancing angle even when the butyrate concentration is higher than 90%. As shown above, this point occurs at 67% stearate for PCTFE-OCOC$_{17}$H$_{35}$/-OCOC$_3$F$_7$ mixed surfaces. The cosθ$_R$ values remain high for butyrate concentrations greater than 59% indicating that a small number of heptafluorobutyrate functionalities are present at the film/probe fluid interface. Below this concentration, heptafluorobutyrate groups begin to be detected as shown by the decrease in cosθ$_R$.

The hexadecane contact angle results for the mixed hydrocarbon ester/heptafluorobutyrate surfaces prepared by partial hydrolysis/re-esterification of the corresponding PCTFE-Esters are shown in Figures 1.45 - 1.46. The results should be compared with those in Figures 1.43 - 1.44 where the compositionally similar surfaces were prepared by sequential esterifications. The fact that the results (Figure 1.45) from the different hydrolyses used to prepare the PCTFE-OCOC$_{17}$H$_{35}$/-OCOC$_3$F$_7$ mixed surfaces are superimposable suggests that the resulting surface structures are independent of solutions used in the initial hydrolysis. The values of cosθ$_R$ can also be superimposed on those from the randomly mixed surfaces prepared by sequential esterifications (Figure 1.43), however, at high hydrocarbon ester concentrations, the values of cosθ$_A$ are significantly lower for the surfaces prepared by partial hydrolysis/re-esterification. This greater contact angle hysteresis suggests that these surfaces are indeed patchy.

For the mixed PCTFE-OCOC$_3$H$_7$/-OCOC$_3$F$_7$ surfaces prepared by partial hydrolysis/re-esterification, the results for cosθ$_R$ from different solution compositions used in the initial hydrolysis (water:methanol, 0:100, 25:75, 50:50, 75:25 and 100:0) are superimposable on themselves and on those from Figure 1.43. The results of cosθ$_A$ for
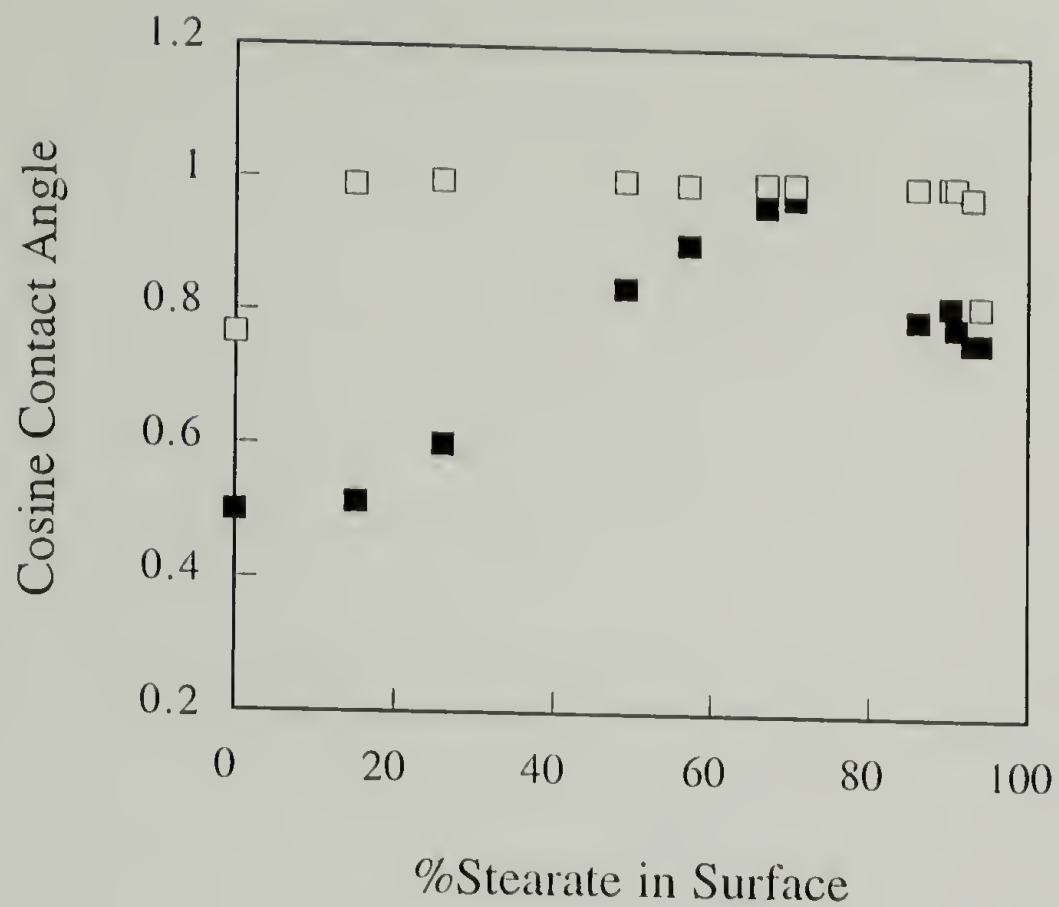
Figure 1.43. Cosine hexadecane contact angle data for PCTFE-OCOC$_{17}$H$_{35}$/-OCOC$_3$F$_7$ prepared by partial esterification: θ_A (■); θ_R (□).
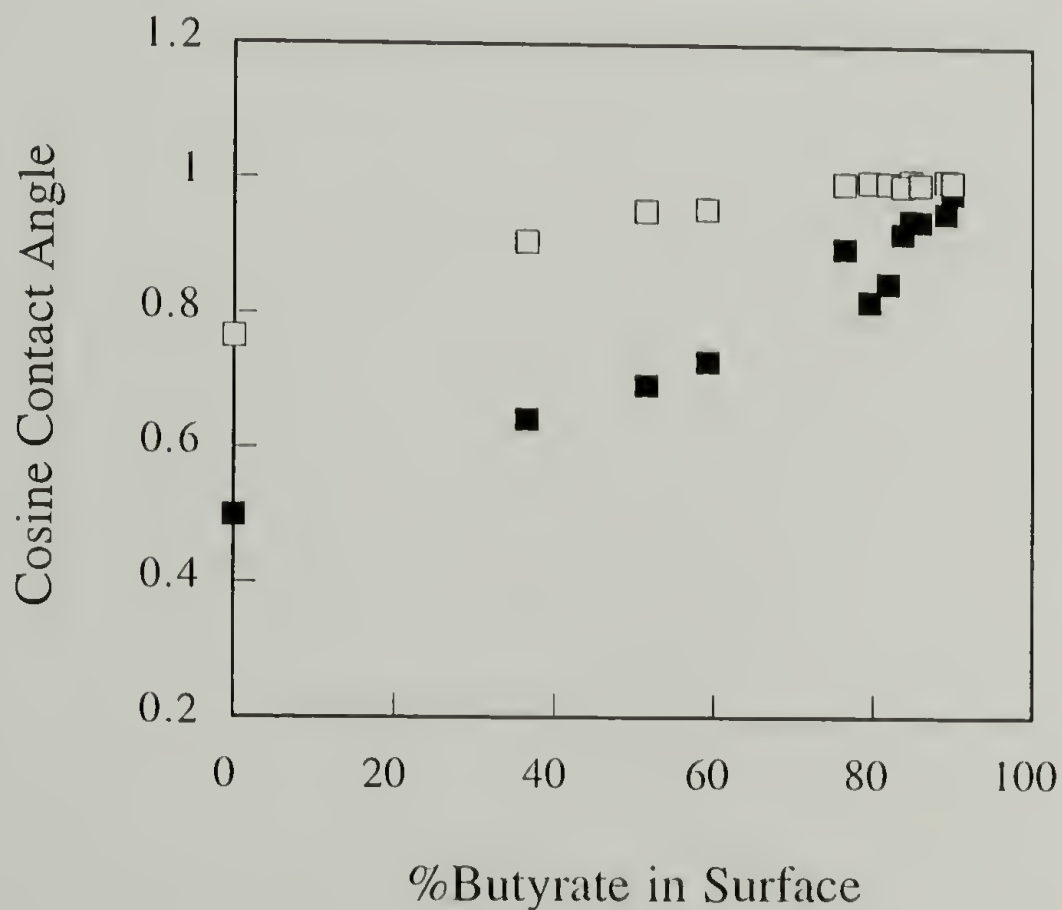
Figure 1.44. Cosine hexadecane contact angle data for PCTFE-OCOC$_3$H$_7$/-OCOC$_3$F$_7$ prepared by partial esterification: θ_A (■); θ_R (□).
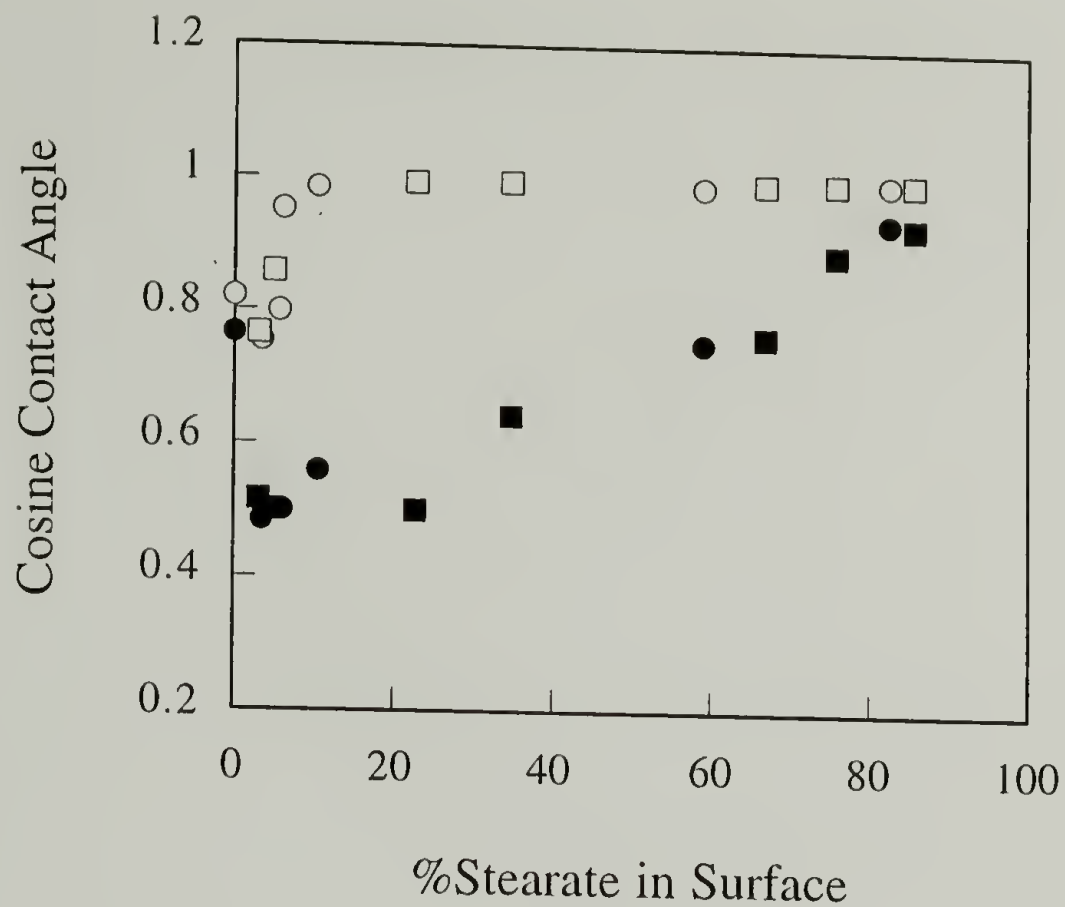
Figure 1.45. Cosine hexadecane contact angle data for PCTFE-OCOC$_{17}$H$_{35}$/-OCOC$_3$F$_7$ prepared by partial hydrolysis/methanolysis in methanol: θ_A (●); θ_R (○) and in 25:75 water:methanol solution: θ_A (■); θ_R (□).
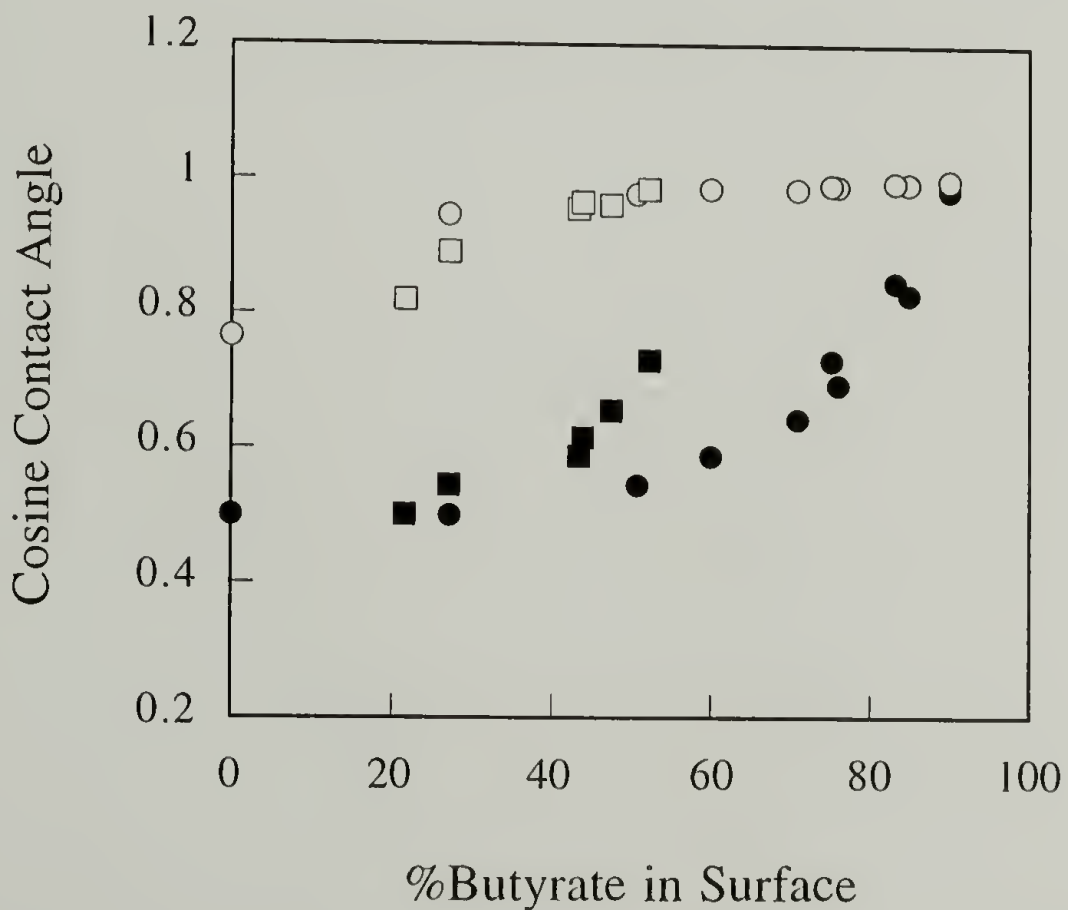
Figure 1.46. Cosine hexadecane contact angle data for PCTFE-OCOC$_3$H$_7$/-OCOC$_3$F$_7$ prepared by partial hydrolysis in aqueous solution: θ_A (●); θ_R (○) and in 75:25 water:methanol solution: θ_A (■); θ_R (□).

75:25 water:methanol as well as those from 0:100, 25:75 and 50:50 (not shown) can also be superimposed on those from Figure 1.43. This behavior indicates that these hydrolysis conditions (water:mathanol, 0:100, 25:75, 50:50, 75:25) render randomly functionalized surfaces. The $\cos\theta_A$ results for the 100:0 partial hydrolysis/re-esterification show significant deviation from the others and greater contact angle hysteresis which agree with the results from the PCTFE-OH/-OCOC$_3$F$_7$ mixed surfaces and implies that patchy mixed surfaces have been formed.

The hexadecane contact angle results of hydrocarbon ester/heptafluorobutyrate mixed surfaces prepared by competitive esterification of PCTFE-OH with acid chloride mixtures are shown in Figures 1.47 and 1.48. The gradual increase of both $\cos\theta_A$ and $\cos\theta_R$ as a function of butyrate composition indicates that the two functional groups in PCTFE-OCOC$_3$H$_7$/-OCOC$_3$F$_7$ are dispersed randomly throughout the modified surfaces. For the PCTFE-OCOC$_{17}$H$_{35}$/-OCOC$_3$F$_7$ mixed surfaces, $\cos\theta_A$ and $\cos\theta_R$ exhibit the same trends observed as the surface mixtures prepared by sequential esterification. The ordered structure of stearate esters is observed when the stearate content reaches ~70% where and the decrease of $\cos\theta_R$ was observed at higher concentration.

The reason that the hexadecane $\cos\theta_A$ and $\cos\theta_R$ values obtained from both mixed PCTFE-OCOC$_3$H$_7$/-OCOC$_3$F$_7$ and PCTFE-OCOC$_{17}$H$_{35}$/-OCOC$_3$F$_7$ surfaces prepared by competitive esterifications (Figures 1.47 and 1.48) are lower (higher θ_A/θ_R) than the ones obtained from mixed surfaces prepared by sequential esterifications (Figures 1.43 and 1.44) can be explained by the fact that the former mixed surfaces consist of thicker modified layer since they were prepared from PCTFE-OH modified at -15 °C (modified thickness ~1000 Å) while the latter set of mixed surfaces were prepared from PCTFE-OH modified at -78 °C (modified thickness ~50 Å). The slightly higher contact angle hysteresis for the mixed surfaces prepared by competitive esterifications suggests that these mixed surface with thick modified layer are relatively rougher than the mixed surfaces with a smaller depth of modification.
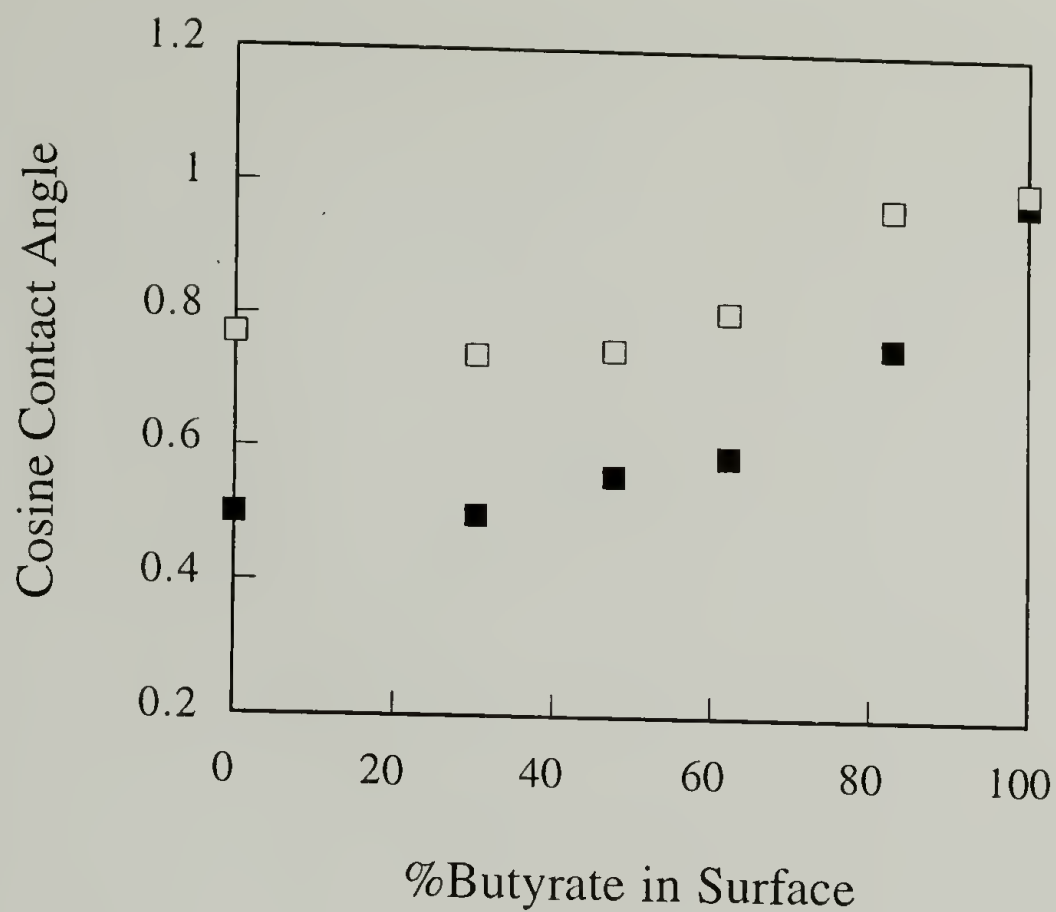
Figure 1.47. Cosine hexadecane contact angle data for PCTFE-OCOC$_3$H$_7$/-OCOC$_3$F$_7$ prepared by competitive esterification: θ_A (■); θ_R (□).
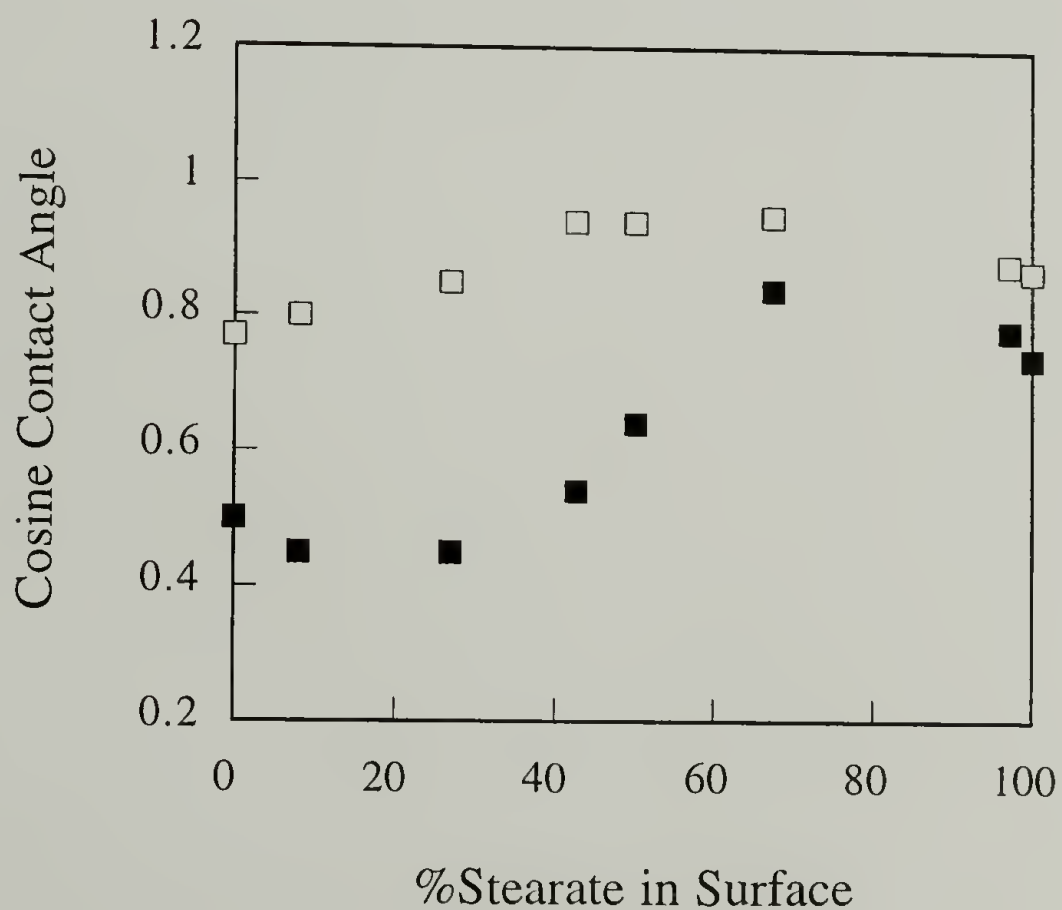
Figure 1.48. Cosine hexadecane contact angle data for PCTFE-OCOC$_{17}$H$_{35}$/-OCOC$_3$F$_7$ prepared by competitive esterification: θ_A (■); θ_R (□).

Conclusions

The results presented above indicate that the pyridine-catalyzed esterifications of PCTFE-OH with a number of acid chlorides (heptafluorobutyryl chloride (C_3F_7COCl), butyryl chloride (C_3H_7COCl) and stearoyl chloride ($C_{17}H_{35}COCl$)) are more rapid and proceed in higher yield (>90%) than the uncatalyzed esterifications. The yields for the uncatalyzed esterifications of PCTFE-OH with butyryl chloride and stearoyl chloride are 84% and 70%, respectively. The high reactivity of heptafluorobutyryl chloride towards esterification made it infeasible to prepare surface mixtures with a controlled range of composition from partially reacted PCTFE-OCOC$_3$H$_7$ and PCTFE-OCOC$_{17}$H$_{35}$. A second method to prepare surface mixtures used kinetic control of the hydrolysis of a number of PCTFE-Esters (PCTFE-OCOC$_3$F$_7$, PCTFE-OCOC$_3$H$_7$, PCTFE-OCOC$_{17}$H$_{35}$). The results indicate that the perfluorinated ester reacts much more quickly than its hydrocarbon analog due to the high electrophilicity of the carbonyl carbon. The rate of hydrolysis decreases as the length of the ester chain increases and/or as the hydrolysis solution becomes less polar (contains more methanol content than water). These two effects are the result of a decrease in the interfacial energy that allows the reagents to penetrate into the surface. Attempts to prepare mixed surfaces through competitive esterifications of PCTFE-OCOC$_3$H$_7$/-OCOC$_3$F$_7$ and PCTFE-OCOC$_{17}$H$_{35}$/-OCOC$_3$F$_7$ were successful by using very low concentrations (<1.5%) of the highly reactive heptafluorobutyryl chloride in the reaction solutions.

The method of mixed surface preparation has a profound effect on the wetting behavior of the resulting surfaces. The linear dependence of both $\cos\theta_A$ and $\cos\theta_R$ with surface composition indicates that the mixed surfaces prepared by sequential esterification and competitive esterification consist of two functional groups randomly distributed throughout the surface. Partial hydrolysis/re-esterification, on the other hand, provides patchy mixed surfaces as evidenced by the relatively high contact angle hysteresis. The formation of patchy mixed surfaces depends largely on the interfacial energy between the

71

hydrolysis solution and the ester surface. In some cases, partial hydrolysis results in surfaces with two functionalities mixed in a random fashion. The higher the interfacial energy, the greater chance that a patchy mixed surface is formed. Patchy mixed PCTFE-$OCOC_3H_7$/-OH and PCTFE-$OCOC_3H_7$/-$OCOC_3F_7$ were formed only if the hydrolysis was carried out in aqueous solution, whereas patchy mixed PCTFE-$OCOC_{17}H_{35}$/-OH and PCTFE-$OCOC_{17}H_{35}$/-$OCOC_3F_7$ could be formed when even low polarity solution was used for reaction (0:100 water:methanol).

References

(1) Oster, G.; Shibata, O. *J. Polym. Sci.* **1957**, *26*, 233.

(2) Yamamoto, F.; Yamakawa, S. *J. Polym. Sci. Polym. Chem. Ed.* **1979**, *17*, 1581.

(3) Clark, D. T.; Wilson, R. *J. Polym. Sci. Polym. Chem. Ed.* **1983**, *21*, 837.

(4) Collin, G. C. S.; Lowe, A.C.; Nicholas, D. *Eur. Polym. J.* **1973**, 9, 1173.

(5) Rossman, K. *J. Polym. Sci.* **1956**, *19*, 141.

(6) Amouroux, J.; Goldman, M.; Revoil, M. F. *J. Polym. Sci. Polym. Chem. Ed.* **1982**, *20*, 1373.

(7) Dias, A. J.; McCarthy, T. J. *Macromolecules* **1987**, *20*, 2068.

(8) Lee, K.-W.; McCarthy, T. J. *Macromolecules* **1988**, *21*, 3353.

(9) **Aclar Technical Data**, Allied-Signal Chemical Corp. Morristown, New Jersey.

(10) Bee, T. G. *Ph.D. dissertation* University of Massachusetts, **1993**.

(11) Hall, S. M.; Andrade, J. D.; Ma, S. M.; King, R. N. *J. Electron Spectrosc.* **1979**, *17*, 181.

(12) Clark, D. T.; Fok, Y. C. T.; Roberts, G. G. *J. Electron Spectrosc.* **1981**, *22*, 173.

(13) Laibinis, P. E.; Bain, C. D.; Whitesides, G. M. *J. Phys. Chem.* **1991**, *95*, 7017.

(14) Clark, D. T.; Thomas, H. R.; Shuttleworth, D. *J. Polym. Sci., Polym. Lett.* **1978**, *16*, 465.

(15) Clark, D. T.; Thomas, H. R. *J. Polym. Sci., Chem.* **1977**, *15*, 2843.

(16) Cadman, P.; Gossedge, G.; Scott, J. D. *J. Electron Spectr.* **1978**, *13*, 1.

(17)   Ashley, J. C. *IEEE Trans. Nucl. Sci.* **1980**, *NS-27*, 1454.

(18)   Harrick, N. J. *Internal Reflection Spectroscopy*, Wiley Interscience: New York, 1967.

(19)   Mirabella, F. M. Jr. *Applied Spectroscopy Reviews* **1985**, *21(1&2)*, 45.

(20)   Muller, G.; Abraham, K.; Schaldach, M. *Applied Optics* **1981**, *20(7)*, 1182.

(21)   Knutson, K.; Lyman, D. In *Surface and Interfacial Aspects of Biomedical Polymers*, Andrade, J. D., Ed., Plenum: New York, 1985; Vol.1, Chap. 6, pp 197-247.

(22)   Langmuir, I. *J. Am. Chem. Soc.* **1916**, *38*, 2221.

(23)   Young, T. (a) *Phil. Trans.* **1805**, 95, 65., (b) *Phil. Trans.* **1805**, *95*, 82.

(24)   Johnson, R. E., Jr.; Dettre, R. *Surface Colloid Sci.* **1979**, *11*, 1.

(25)   Andrade, J. D.; Smith, L. M.; Gregonis, D. E. In *Surface and Interfacial Aspects of Biomedical Polymers*, Andrade, J. D., Ed., Plenum: New York, 1985; Vol.1, Chap. 7, pp 249-292.

(26)   Johnson, R. E., Jr.; Dettre, R. H. In *Surface and Colloid Science*, Matijevic, E., Ed., Wiley-Interscience: New York, 1969.

(27)   Johnson, R. E., Jr.; Dettre, R. H. In *Contact Angle, Wettability and Adhesion*, Fowkes, F. M., Ed.; Advances in Chemistry Series No. 43; American Chemical Society: Washington, D. C., 1964.

(28)   Cassie, A. B. D. *Discuss. Faraday. Soc.* **1948**, *3*, 11.

(29)   Israelachvili, J. N.; Gee, M. L. *Langmuir* **1989**, *5*, 288.

(30)   Johnson, R. E., Jr.; Dettre, R. H. *J. Phys. Chem.* **1964**, *68*, 1744.

(31)   Dettre, R. H.; Johnson, R. E., Jr. *J. Phys. Chem.* **1965**, *69*, 1507.

(32)   Timmons, C. O.; Zisman, W. A. *J. Colloid Interface Sci.* **1966**, 165.
(33)   Langmuir, I. *Science* **1938**, *87*, 493.

(34)   Penning, J. F. M.; Bosman, B. *Colloid Polym. Sci.* **1979**, *257*, 720.

(35)   Yasuda, H.; Sharma, A. K.; Yasuda, T. *J. Polymer Sci., Phys.* **1981**, *19*, 1258.

(36)   Holmes-Farley, S. R.; Reamey, R. H.; Nuzzo, R. G.; McCarthy, T. J.; Whitesides, G. M. *Langmuir* **1987**, *3*, 799.

(37)   Cross, E. M.; McCarthy, T. J. *Macromolecules* **1990**, *23*, 3916.

(38)   Evans, S. D.; Sharma, R.; Ulman, A. *Langmuir* **1991**, *7*, 156.

(39)   Nuzzo, R. G.; Allara, D. L. *J. Am. Chem. Soc.* **1983**, *105*, 4481.

(40)   Porter, M. D.; Bright, T. B.; Allara, D. L.; Chidsey, C. E. D. *J. Am. Chem. Soc.* **1987**, *109*, 3559.

(41)   Laibinis, P. E.; Marye, A. F.; Folkers, J. P.; Whitesides, G. M. *Langmuir* **1991**, 7, 3167.

(42)   Laibinis, P. E.; Whitesides, G. M. *J. Am. Chem. Soc.* **1992**, *114*, 1990.

(43)   Laibinis, P. E.; Whitesides, G. M.; Allara, D. L.; Tao, Y. -T.; Parikh, A. N.; Nuzzo, R. G. *J. Am. Chem. Soc.* **1991**, *113*, 7152.

(44)   Tam-Chang, S. -W.; Biebuyck, H. A.; Whitesides, G. M.; Jeon, N.; Nuzzo, R. G. *Langmuir* **1995**, *11*, 4371.

(45)   Bain, C. D.; Whitesides, G. M. *Science* **1988**, *240*, 62.

(46)   Bain, C. D.; Whitesides, G. M. *J. Am. Chem. Soc.* **1988**, *110*, 3665.

(47)   Bain, C. D.; Whitesides, G. M. *J. Am. Chem. Soc.* **1988**, *110*, 6560.

(48)   Bain, C. D.; Whitesides, G. M. *Langmuir* **1989**, *5*, 1370.

(49)   Atre, S. V.; Liedberg, B.; Allara, D. L. *Langmuir* **1995**, *11*, 3882.

(50)   Troughton, E. B.; Bain, C. D.; Whitesides, G. M.; Allara, D. L.; Nuzzo, R. G.; Porter, M. D. *Langmuir* **1988**, *4*, 365.

(51)   See the calculation of surface composition in Appendix B.

(52)   Silverstein, R. M.; Bassler G. C.; Morrill, T. C. *Spectrometric Identification of Organic Compounds*, John Wiley and Sons: New York, 1981, pp 107.

(53)   Snyder, R. G.; Hsu, S. L.; Krimm, S. *Spectrochim. Acta, Part A*, **1978**, *34*, 395.

(54)   See the data tables in Appendix A for further information.

CHAPTER 2

STEPWISE POLYMER SURFACE MODIFICATION:
CHEMISTRY - LAYER-BY-LAYER DEPOSITION

Introduction

Layer-by-layer deposition of polyelectrolytes has been developed over the past several years[1-9] as a versatile method for preparing supported multilayer films. The fabrication process involves consecutive alternating adsorptions of oppositely charged polyelectrolytes which are driven by electrostatic attraction between anionic and cationic species along the polymer chains. In contrast to other conventional approaches (the Langmuir-Blodgett technique, self-assembly based on chemisorption) used for preparing multilayer thin films, no stoichiometric control is necessary to maintain surface functionality and the spontaneous adsorptions can be applied to any substrate regardless of its size, shape, topography, or topology. Not only may this technique serve as a tool for surface modification, it also offers other advantages. The process is simple, environmentally benign and potentially economical. Surface functionality can be controlled directly by choosing appropriate polyelectrolytes.

The surface modification of fluoropolymers has been a long time interest in McCarthy's group. A number of research papers describing chemical methods for introducing functionality to the surfaces of the following polymers have been published: poly(chlorotrifluoroethylene) (PCTFE),[10-14] poly(vinylidene fluoride),[14-16] poly(tetrafluoroethylene-co-hexafluoropropylene)[14,17] and poly(tetrafluoroethylene).[18] In this study, particular attention was focused on one functionalized surface, PCTFE-OH, that contains a primary alcohol attached to the fluoropolymer chain by a three-methylene spacer. This surface exhibits versatile chemistry; studies of its structure and chemistry were

75

described in considerable detail.[10] For the reason that well-controlled chemistry and structure of this functionalized surface have been developed, it was chosen as a substrate for further modification using layer-by-layer deposition. Poly(sodium styrenesulfonate) (PSS) and poly(allylamine hydrochloride) (PAH) were chosen as polyelectrolytes for deposition because this system has been most widely studied, and direct comparisons of multilayer assembly processes and resulting structures on different substrates can be made.

Layer-by-Layer Deposition Technique

The layer-by-layer deposition process, in its simplest form, involves sequentially dipping a charged substrate into dilute aqueous solutions of oppositely charged polyelectrolytes and allowing the polymers to adsorb and reverse the charge of the substrate surface. The sequential adsorptions of anionic and cationic polyelectrolytes allow the build up multilayer film structures (Scheme 2.1). The charge reversal occurs because the polyelectrolytes adsorb in excess over the surface charge. In individual adsorption steps this leads to a charged surface in contact with a solution of a polyelectrolyte with the same charge and electrostatic repulsion limits the adsorption to a single polymer monolayer. In principle, one can incorporate more than two kinds of monolayer simply by dipping in as many polyelectrolyte solutions as desired, as long as the charge is reversed from layer to layer.

The rinsing steps between deposition of each layer are strongly recommended to avoid coprecipitation. If the rinsing steps were omitted, an adhering layer of one solution would be left on the surface of the substrate. This would lead to contamination of the next dipping solution causing co-precipitation which would eventually incorporate into subsequent layers.
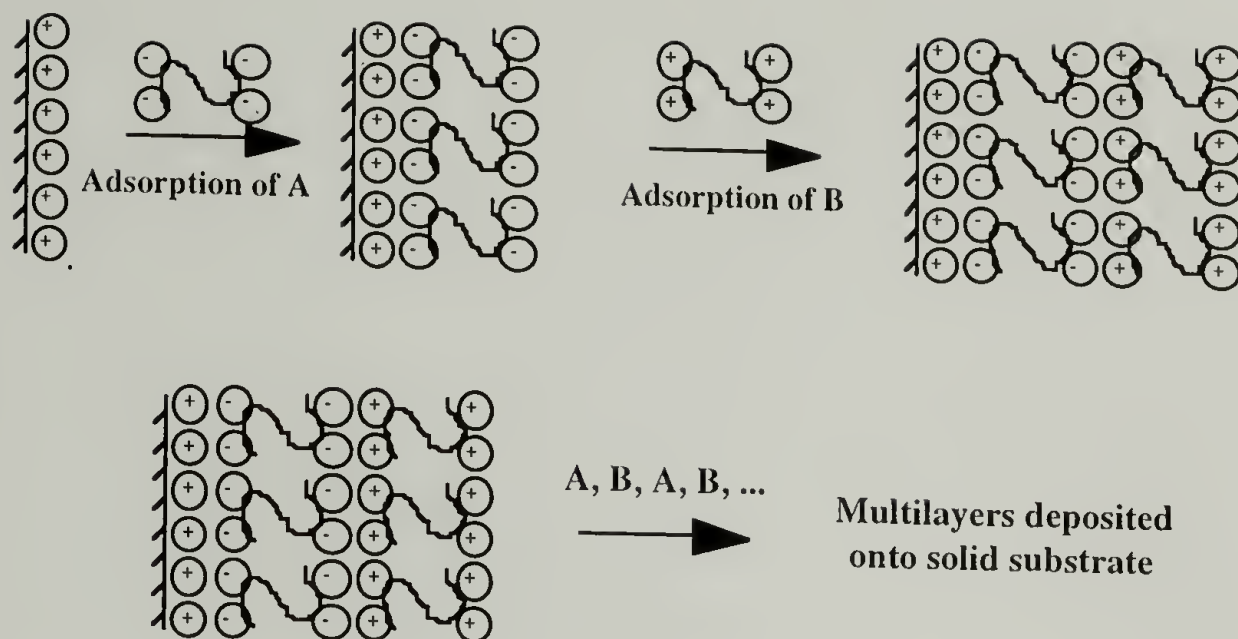
Scheme 2.1. Layer-by-layer deposition of polyelectrolytes onto positively charged substrate where A and B are anionic and cationic polyelectrolytes, respectively.

Substrates

A number of studies have revealed that various substrates with neutral or charged surfaces can been used for layer-by-layer deposition. Depending on the application, the multilayers may be fabricated on planar surfaces, latex particles or custom surfaces. Polyelectrolyte multilayers were reported to selectively grow on defined areas of a patterned surface.[9]

Inorganic substrates including fused quartz, silicon single crystals, and glass are commonly used. By cleaning the substrates with hot H_2SO_4/H_2O_2 (7:3) and then $H_2O/H_2O_2/NH_3$ (5:1:1), hydrophilic surfaces can be produced.[1] Reacting the substrates with 3-aminopropyldimethylethoxysilane results in positively charged surfaces. Glass substrates have been used in the forms of hydrophilic (cleaned), hydrophobic (vapor phase hexamethyldisilazane treatment),[3,8] positively charged (reacting with N-2-aminoethyl-3-aminopropyl-trimethoxysilane[3,8] or with boladication solution)[12] and negatively charged surfaces (plasma treatment with CH_4 and O_2).[19]

In addition to the work presented here, extensions of the layer-by-layer deposition technique to organic polymer substrates have been reported,[20,21] using it to prepare polyelectrolyte multilayer films supported on oxidized poly(4-methyl-1-pentene) (PMP-CO_2^-), virgin poly(ethylene terephthalate) (PET), hydrolyzed PET (PET-CO_2^-), and amidated PET (PET-NH_3^+). The studies were confined to poly(allylamine hydrochloride) (PAH) and poly(sodium styrenesulfonate) (PSS). It was found that the initial substrate surface chemistry defines the entire assembly process - the thickness of all the layers and the stoichiometry of the assembly (ammonium:sulfonate ratio) is predetermined by the substrate. The assembly process does not revert to a substrate-independent process after a certain number of layers is deposited.

Adsorption Systems

In principle, any polymer capable of being charged can be used for assembling layered structures based on ionic interactions. By choosing the appropriate system of polymers, one can achieve heterostructure multilayers with desired properties. The most widely used polyelectrolytes are poly(allylamine hydrochloride)[1,3,7,8,20-24] and poly(4-vinylbenzyl-(N,N-diethyl-N-methyl)-ammonium iodide,[1] to form positively charged layers and poly(styrenesulfonate),[1,3,7,8,20,21] poly(vinyl sulfate),[1,22] poly(thiophene-3-acetic acid)[3,7,8] and sulfonated polyaniline[3,7] to form negatively charged layers. The fact that water is used as a solvent allows the incorporation of several natural and modified biological materials. Some charged polypeptides have been used to create multilayers including poly(L-lysine), poly(L-glutamic acid), polyuracil and polyadenine.[25] Biomolecular layers constructed with charged DNA[23] and charged virus particles[24] have been reported. Other groups of researchers have incorporated charged globular proteins such as myoglobin, lysozyme, glucose oxidase, cytochrome C, hemoglobin, and glucose isomerase.[26-28]

An approach to reduce the layer interpenetration was attempted by the incorporation of Langmuir-Blodgett layers or polymers bearing mesogenic groups.[29-30] Incorporation of conjugated polymers such as poly(2-N-methyl pyridinium acetylene),[3,7] p-type doped polyaniline[3] and polypyrrole[3,7,8] into the multilayer heterostructures can significantly increase electronic conductivity. Light emitting diodes composed of naphthalene-containing conjugated polymers have been obtained and characterized with tunable emission.[31] Progress towards light emitting diodes was also made using poly(phenylene vinylene) in multilayer assemblies.[32] Studies of self-assembly of multilayers from photopolymerizable bolaform amphiphiles have shown that one can create more robust layered structures using a combination of ionic interaction (between layers) and covalent bonding (within layers).[6] The incorporation of polypeptide dyes[25] and semiconductor nanoparticles[33] in polyelectrolyte multilayers has been reported.

The adsorption solutions for layer-by-layer deposition are composed of polymer dissolved in a solvent (almost exclusively water). In some cases, a non-aqueous solvent or cosolvent is incorporated to increase polymer solubility. Acid or base is selectively added to adjust the pH of the adsorption solution. Ionic strength, which affects the polymer conformations and solvent properties is also adjusted and can control layer thickness.

Control of Layer Thickness

The total thickness of the deposited layers increases linearly with the number of dips and individual layer thickness. The key factors controlling the adsorption process, adsorbed polymer conformation and the individual layer thickness are described below. Some aspects of the discussion are related to polyelectrolyte adsorption theory developed by Van der Schee and Lyklema[34] which was later extended by Evers et al.[35] and Böhmer et al.[36] These theories are based on the self consistent field approaches proposed by Scheutjens and Fleer. Experimental evidence is explained along with theoretical predictions.

Surface of Substrate. The nature of substrates and their charge densities have significant effects on the conformation and the amount of adsorbing polyelectrolytes. For highly charged surfaces, the polymers appear to adsorb in the form of a flat conformation or relatively short loops with low adsorbed amount.[37] Surfaces with lower charge densities have less available charged sites that can attract the opposite charges of polymer and tend to give more extended polymer chains and thus increase the amount of adsorbed polymer.[38]

Polymer Concentration. In the case of strong ionic interaction between the polyelectrolyte and charged surface, the total amount of polymer adsorbed increases linearly with polyelectrolyte concentration (see Figure 2.1).[38] When the interaction becomes weaker because of lower charge density of the polymer and/or substrate or because of screening effects caused by added salt, the amount of adsorbed polymer increases nonlinearly. The adsorption isotherms as a result exhibit a rounded shape (lower affinity).
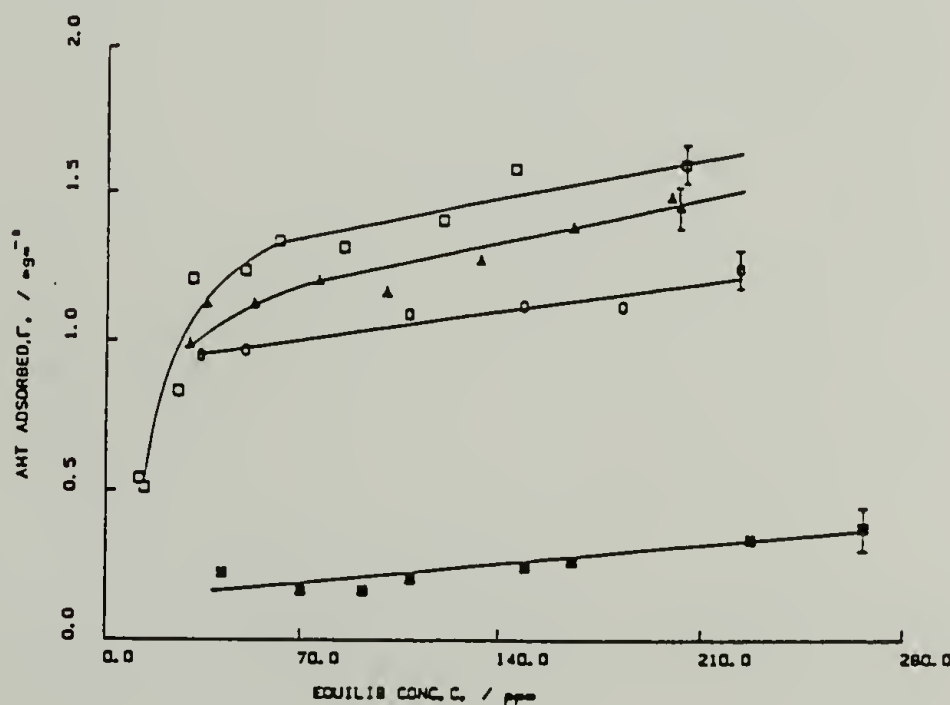
Figure 2.1. Adsorption isotherms of poly(styrenesulfonate) (M_w 780,000) adsorbed on positively charged polystyrene latex as a function of salt concentration: 1.0 M NaCl (open square), 0.5 M NaCl (triangle), 0.1 M NaCl (circle) and 0 M NaCl (filled square).[38]

Ionic Strength. The ionic strength of polyelectrolyte solutions can be adjusted by the addition of salt (e.g. KNO_3, NaCl, $MnCl_2$). The magnitude of changes in solvent properties and interactions between ionic species (inter- and intramolecular interactions of polyelectrolyte and the substrate) in the solutions are varied with the amount of salt added. The conformation of an adsorbed polyelectrolyte layer is markedly dependent on the ionic strength of the solution from which the adsorption takes place. For strong polyelectrolyte systems, polymer chains adsorb in very flat conformations (trains with few loops and tails) especially to highly charged surfaces with low adsorbed amount at low salt concentration. At higher salt concentration, intra- and interchain repulsions of segments in loops or tails are suppressed and polyelectrolytes behave essentially like neutral polymers.[38]

Increasing ionic strength is related to decreasing the solvency, and promotes more adsorption. Polymer segments tend to form more loops, tails and eventually extended chains as the adsorbed amount and layer thickness increase.[36] Lvov et al.[22] reported the nonlinear increase of layer thickness and roughness of poly(vinyl sulfate)/polyallylamine multilayers deposited on glass slides when ionic strength of solution is increased (Figure 2.2). As reported by Decher et al., the thickness of poly(styrenesulfonate)/polyallylamine layer pairs increases from 1.77 nm to 2.26 nm when NaCl concentration increases from 1.0 mol to 2.0 mol (Figure 2.3).[2]

At very high ionic strength, however, where all charges on polymer segments are completely screened, a more random coil-like conformation with a smaller radius of gyration is more favorable than the extended chain. This collapse of extended chains can actually cause a decrease in layer thickness which was observed by Cosgrove et al. on adsorption of poly(styrenesulfonate) to polystyrene latex particles.[38] The systems with weaker interactions between polyelectrolytes and surfaces (low charge density or neutral) should show a similar trend with fewer flat conformations and more loops, tails and extended chains.
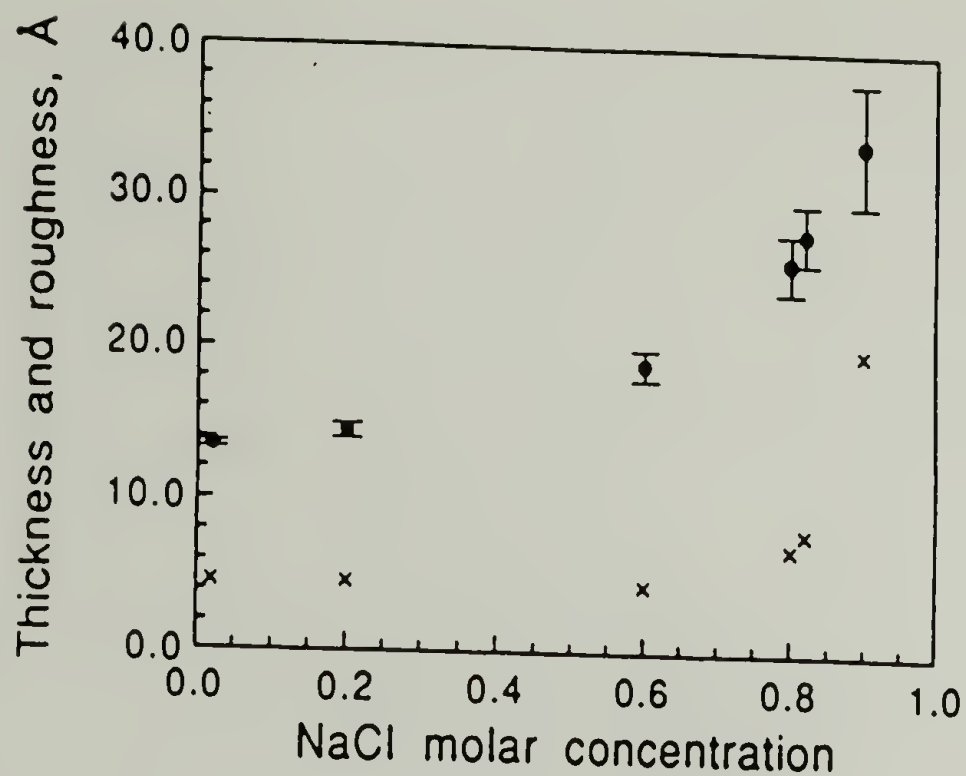
Figure 2.2. Variation of thickness (dots) and surface roughness (crosses) of poly(vinyl sulfate)/polyallylamine bilayers as a function of salt concentration.[22]
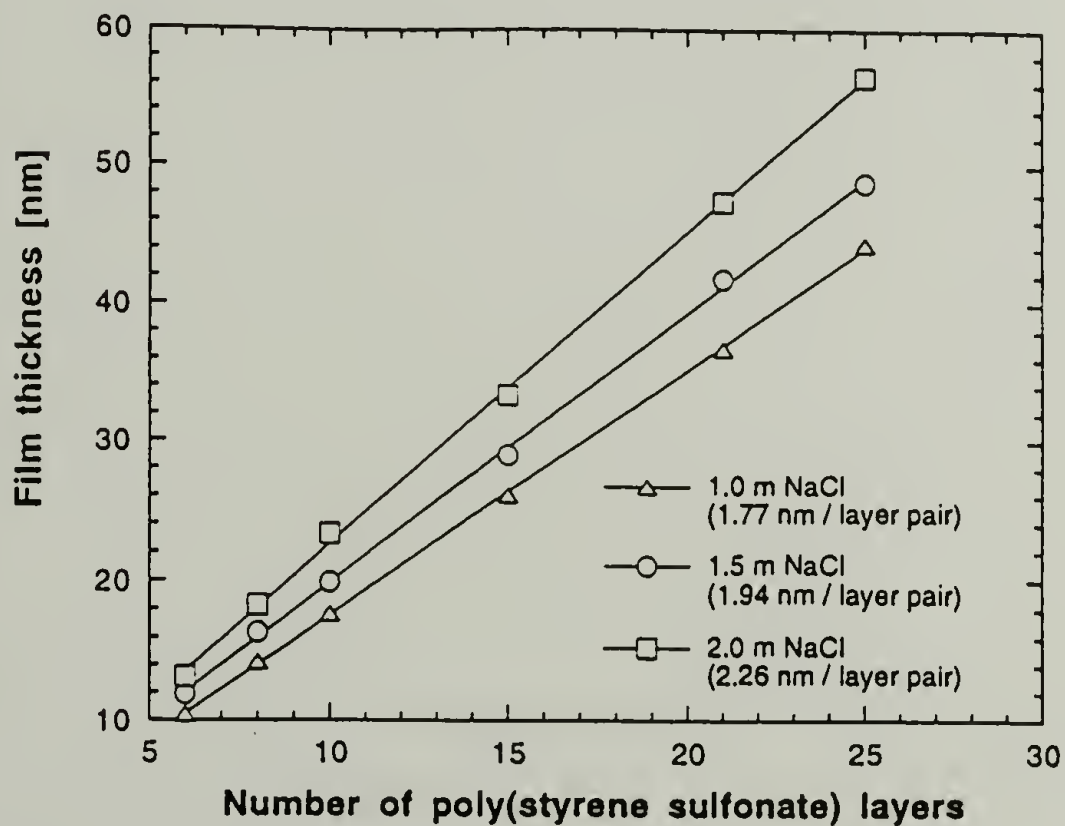
Figure 2.3. Variation of thickness increments of poly(allylamine)/poly(styrenesulfonate) multilayers as a function of NaCl concentration added in poly(styrenesulfonate) solutions.[2]

Adsorption pH. The adsorption of strong polyelectrolytes does not depend on pH. The effect of pH on the adsorbed amount is much more pronounced for weak polyelectrolytes since the charge density and degree of dissociation are varied with pH. At very low pH (lower than pK_0), polyacid chains are virtually neutral with very few charged segments. Adsorption behaviors are similar to those of neutral polymers. When the pH is increased, the adsorption to an uncharged surface decreases due to the electrostatic repulsions of charged segments opposing the accumulation of polyelectrolyte near the surface.

Different behavior is predicted for the adsorption to oppositely charged surfaces. The plot of excess adsorbed amount (the plateau values obtained from adsorption isotherms) as a function of pH (Figure 2.4) indicates that maximum adsorption takes place at about 1-1.5 unit below pK_0 for a weak polyacid.[37] This maximum adsorption is a trade-off between two opposite trends: favorable electrostatic attractions between the surface and polyelectrolyte which enhance adsorption and electrostatic repulsions between charged polymer segments which inhibit deposition.

Characterization of Multilayers

Most characterization studies have focused on the determination of layer thickness, polymer orientation, and roughness. The techniques employed are varied with the type of polymers and their specific functionalities. So far, self-assembled multilayer structures have been analyzed by small angle neutron and x-ray reflectivity,[1,19,22-24] ellipsometry,[3] profilometry,[3] UV-VIS spectroscopy,[1,3,7,8,19,22,23] and light microscopy.[39] There have been some studies of the mechanical rigidity and integrity of layered structures using surface force measurements.[6] Topological information has also been reported by studies using Atomic Force Microscopy (AFM).[6]
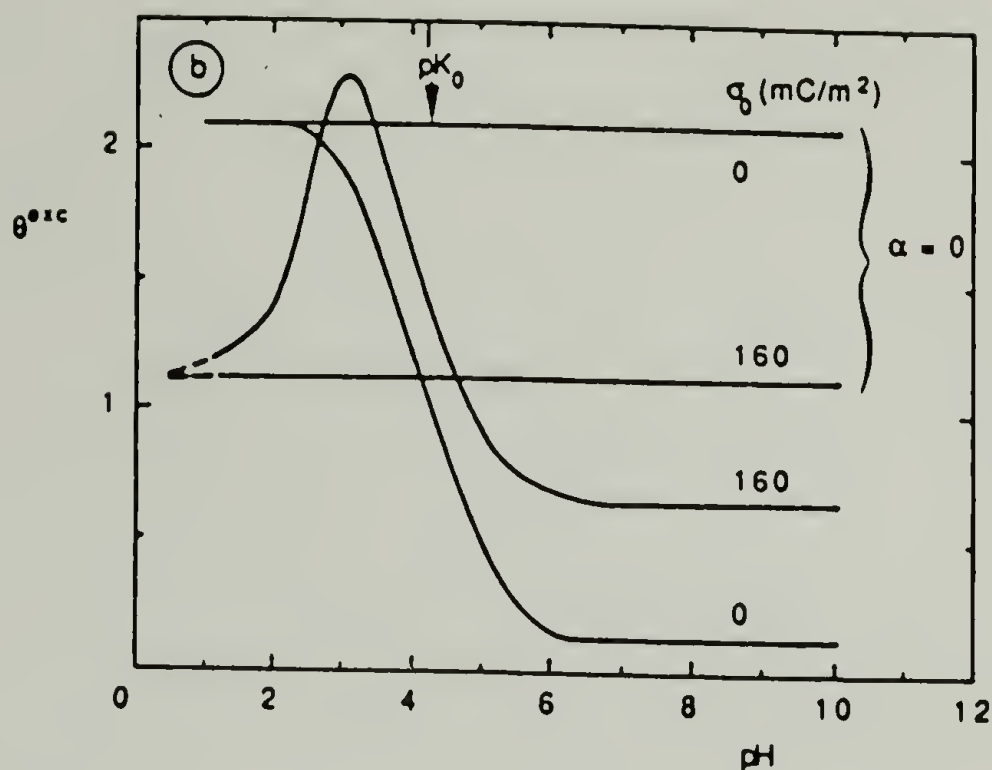
Figure 2.4. Excess adsorbed amount of a neutral polymer ($\alpha = 0$) and a weak polyelectrolyte ($pK_0 \sim 4$) adsorbed onto surfaces with different charge densities ($q = 0$ and 40 mC/m^2) as a function of pH.[37]

Experimental

General Procedures

PCTFE-OH was prepared from PCTFE film (Allied 5 mil Aclar 33C) and lithiopropyl ethyl acetaldehyde acetal as previously described at -15 °C in 50:50 THF:heptane.[10] Poly(allylamine hydrochloride) (PAH) ($M_w = 50,000 - 65,000$) and poly(sodium styrenesulfonate) (PSS) ($M_w = 70,000$) were obtained from Aldrich and used as received. Water was purified using a Millipore Milli-Q system that involves reverse osmosis, ion-exchange and filtration steps. Solution pH for adsorption studies was adjusted with either HCl or NaOH solution using a Fisher 825MP pH meter. X-ray photoelectron spectra (XPS) were obtained using a Perkin-Elmer Physical Electronics 5100 spectrometer with Mg K$_\alpha$ excitation (15.0 kV, 400 W). Spectra were recorded at two

different take-off angles, 15° and 75° between the plane of the sample surface and the entrance lens of the detector optics. Atomic concentration data were determined using sensitivity factors obtained from samples of known composition: C_{1s}, 0.232; O_{1s}, 0.628; $F1s$, 1.000; N_{1s}, 0.420; S_{2p}, 0.540. Contact angle measurements were made with a Ramé-Hart telescopic goniometer and a Gilmont syringe with a 24-gauge flat-tipped needle. Water (purified as described above) was used as the probe fluid. Dynamic advancing (θ_A) and receding angles (θ_R) were recorded while the probe fluid was added to and withdrawn from the drop, respectively. Peel tests were performed manually with an angle of 180° between the delaminated film surface and tape (3M #810).

Polyelectrolyte Depositions

Adsorptions were carried out at room temperature from unstirred polyelectrolyte solutions freshly prepared prior to use. The alternating layers were formed by sequentially dipping the PCTFE-OH substrates into 0.02 M PAH (167 mg/ 120 ml Milli-Q water) and 0.02 M PSS solutions (360 mg/ 120 ml Milli-Q water) for generally 20 min. Substrates were rinsed with three 150 mL aliquots of water between each dipping and after the final adsorption. PAH and PSS solutions were adjusted to the desired pH using HCl and NaOH aqueous solutions. The ionic strength of solutions was changed by the addition of $MnCl_2$. After the desired number of layers was deposited, the PCTFE-OH - supported multilayer assemblies were dried at room temperature under reduced pressure (0.01 mm, room temperature, >24 h) before analysis. These conditions were determined to be optimum based on a series of experiments described below.

Results and Discussion

Substrate Preparation

The substrate used for all of the experiments described in this chapter was 5-mil poly(chlorotrifluoroethylene) (PCTFE) film that had been chemically modified to incorporate alcohol functionality in its surface region (PCTFE-OH). This modification chemistry has been reported[10,12,14] and is reviewed in Chapter 1. The conditions (50:50 THF:heptane, -15 °C) were chosen to yield a surface containing a modified thickness of ~1000 Å.

First Layer Adsorptions

The general conditions for all polyelectrolyte adsorptions described here were modeled after those reported by Decher[1,2] for inorganic substrates modified by silanation to contain ammonium ions. A series of initial experiments was carried out to assess the tendencies of PAH and PSS to adsorb to PCTFE-OH from aqueous solution. As no charge exists on PCTFE-OH, the adsorption has to be driven by forces that are much weaker than electrostatic attraction: hydrogen bonding and interfacial free energy decreases. It was determined that PAH adsorbs under a variety of conditions and that PSS adsorbs only from solutions of high ionic strength (0.2 M $MnCl_2$) as indicated by the data in Table 2.1. It was decided that PAH would be used as the polyelectrolyte for the first layer adsorptions.

Figure 2.5 shows the kinetics of adsorption of PAH to PCTFE-OH as monitored by XPS and contact angle. The PAH concentration was 0.02 M (based on repeat units, 1.4 mg/mL) and pH was adjusted to 4.0. XPS indicates that the adsorption is fast, reaching a final state in 5 min or less. The term "final state" and not "equilibrium" is used because these adsorptions are irreversible; the PAH does not desorb upon rinsing with large amounts of water at pH 4. The receding contact angle decreases initially and then increases

86

Table 2.1. XPS atomic composition data for PSS adsorption onto PCTFE-OH at pH 4.

Atomic Composition (%)	PSS adsorption without MnCl$_2$ added		PSS adsorption with 0.2 M MnCl$_2$ added	
	15° take-off angle data	75° take-off angle data	15° take-off angle data	75° take-off angle data
C	69.04	66.85	69.16	68.14
O	16.11	16.78	15.09	16.53
F	14.75	16.28	14.83	14.67
S	0.1	0.09	0.92	0.65

gradually over the first 30 min of adsorption and then levels at $\theta_R = 27°$. The advancing contact angle decreases during this 30 min and levels at $\theta_A = 61°$. Initial contact angles for PCTFE-OH are $\theta_A / \theta_R = 69°/25°$.

Several comments concerning this data are in order: The adsorption involves a charged polyelectrolyte and a neutral surface, thus the surface becomes charged during adsorption and at some point in the process (5 min or less as assessed by XPS), polyelectrolyte chains are repelled by the surface and further adsorption does not occur. The adsorption is fast relative to other neutral (and charged) substrates previously studied.[10] Presumably, the hydrogen bonding interactions between ammonium ions and alcohols are strong. The wetting behavior of the isolated supported monolayers indicates that changes in the adsorbed polyelectrolyte structure continue after the adsorption is complete.
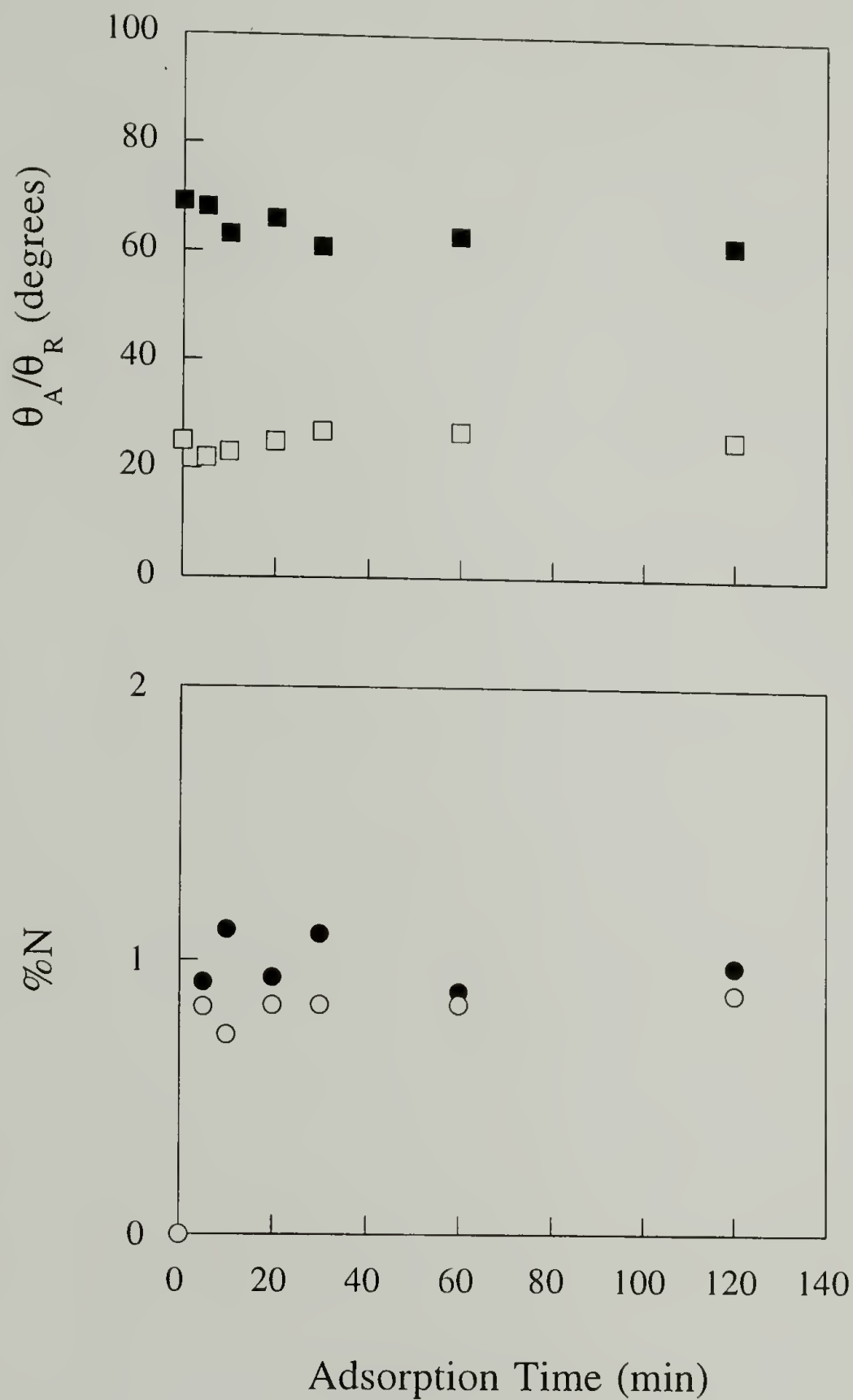
Figure 2.5. Kinetics of adsorption of PAH (0.02 M) to PCTFE-OH at pH 4. Nitrogen atomic concentration was determined using XPS at two take-off angles, 15° (●) and 75° (○). Advancing (■) and receding (□) contact angles were determined using water as the probe fluid.

The XPS data indicate that the nitrogen atomic concentration is ~1% and this value can be used to estimate the concentration of allylamine repeat units in the XPS sampling region of PCTFE-OH. The repeat unit structure of PCTFE-OH contains 1 fluorine atom, thus the N:F ratio is indicative of the PAH:PCTFE-OH repeat unit ratios. This indicates that approximately 1 PAH repeat unit is present per 12 PCTFE-OH repeat units in the 15° take-off angle sampling depth and that ~1 PAH repeat unit is present per 16 PCTFE-OH repeat units in the 75° take-off angle sampling region. The 15° and 75° take-off angle sampling regions are the outermost ~10 Å and ~40 Å, respectively; the attenuation of substrate photoelectron signals due to the adsorbed layers is discussed below in quantitative terms. The absence of a strong take-off angle dependence in this data and, particularly, all of the data in Figure 2.5 suggest that the adsorbed PAH chains penetrate (at least) the outer few tens of angstroms of PCTFE-OH and may be more accurately described as "absorbed" chains. Based on these results, an adsorption time of 30 min was chosen for the first layer in the multilayer adsorption studies.

The effect of pH on the adsorption of PAH to PCTFE-OH was assessed by carrying out 30 min adsorptions as a function of the pH of the PAH (0.02 M) solution. Figure 2.6 shows XPS atomic concentration (nitrogen) and contact angle data for a range of solution pH values. The PCTFE-OH structure should not be pH sensitive over this range, but PAH has a reported pKa of ~10.6 [40,41] and its degree of protonation should be pH dependent. At low pH values, all of the PAH repeat units are protonated and the low adsorbance (nitrogen content) is due to charge-charge repulsion of ammonium ions. There is a very gradual rise in adsorbance from pH 2 to pH 7 and a steeper rise from pH 7 to pH 11 as PAH becomes increasingly deprotonated and both charge-charge repulsion and polyelectrolyte solubility are diminished. Water contact angle data showed a slight dependence on the pH with θ_A increasing and θ_R decreasing with increasing pH. Note that a take-off angle dependence on nitrogen content is observed at pH values other than 4 and
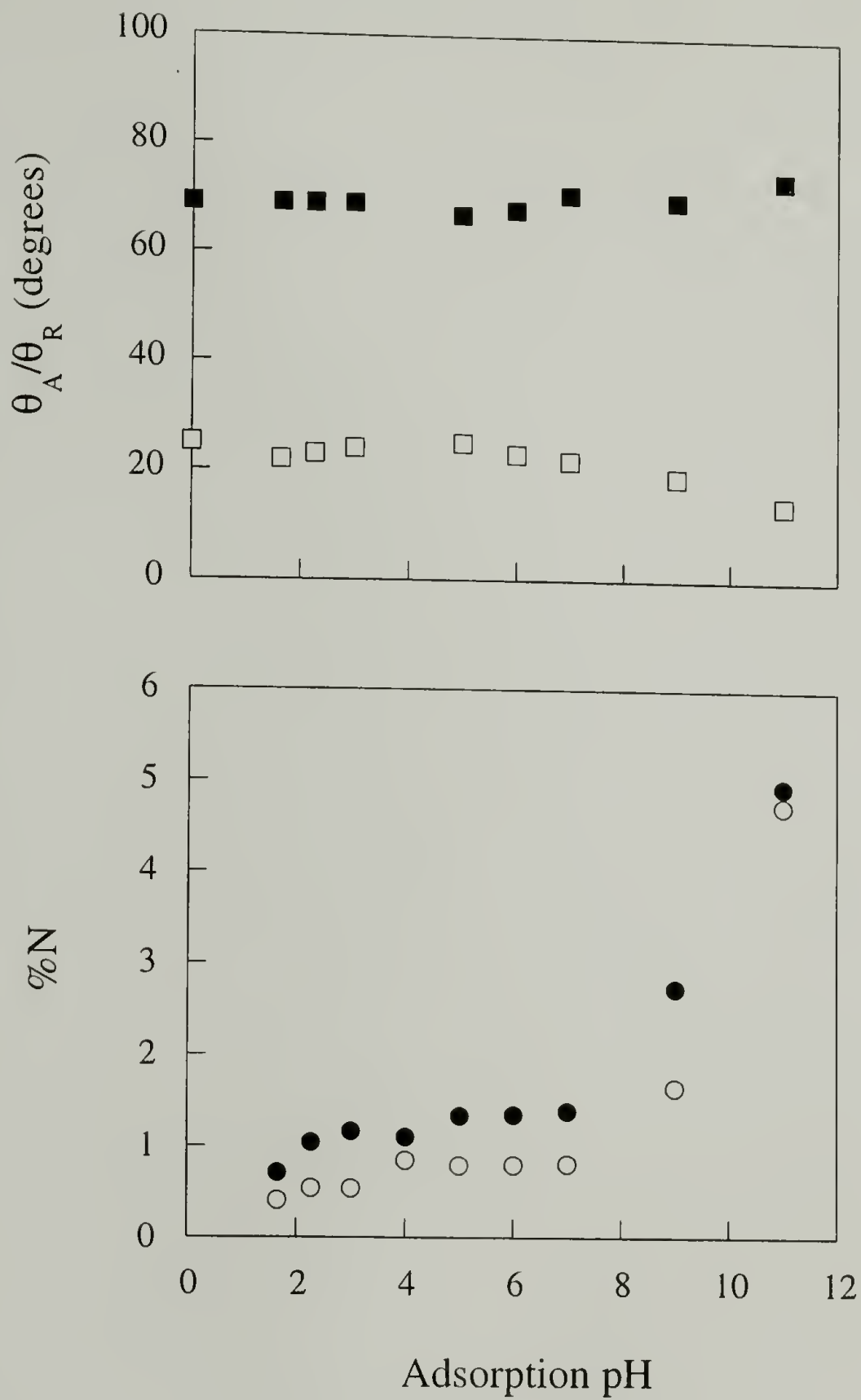
Figure 2.6. Effect of pH on the adsorption of PAH (0.02 M) to PCTFE-OH. Nitrogen atomic concentration was determined using XPS at two take-off angles, 15° (●) and 75° (○). Advancing (■) and receding (□) contact angles were determined using water as the probe fluid.

11. These first layer adsorption experiments were confined to these pH values and the slight take-off angle dependence was consistent (see data in Figures 2.5 and 2.14).

A second type of first layer substrate (PCTFE-OH-PAH) for multilayer formation, with a higher charge density and thicker adsorbed PAH layer, was devised from this pH dependence study: PAH was adsorbed to PCTFE-OH at pH 11 and then immersed in pH 4 solution to desorb any weakly attached polyelectrolyte that might desorb and reprecipitate as a polyelectrolyte complex in the subsequent adsorption of an oppositely charged polyelectrolyte. The kinetics for desorption were monitored by XPS and contact angle analysis (Figure 2.7). PCTFE-OH-PAH samples prepared at pH 11 (30 min adsorptions) were immersed in pH 4 water from 5-60 min. The desorption was rapid as indicated by XPS; nitrogen concentration decreased from ~5% to ~3.5% over the first 10 minutes and leveled at this value. Water contact angles did not change upon desorption and remained at $\theta_A/\theta_R = 70°/14°$. This surface exhibits a higher contact angle hysteresis than the one prepared by adsorption at pH 4 ($\theta_A/\theta_R = 61°/27°$) suggesting that this surface may be rougher and/or more chemically heterogeneous. Surfaces of this type that were used to prepare multilayers were prepared by adsorption at pH 11 for 30 min followed by desorption at pH 4 for 20 min. These surfaces were more concentrated in ammonium ions by a factor of ~3.5 over those prepared by adsorption at pH 4.

The effects of PAH concentration (Figure 2.8) and solution ionic strength (Figure 2.9) were also assessed for the first PAH layer adsorption. Adsorbance (as assessed by nitrogen content of the PCTFE-OH - supported first layer) is essentially independent of PAH concentration from 0.005 to 0.2 M (indicating a high affinity concentration isotherm) and independent of $MnCl_2$ concentration from 0 to 1.5 M.
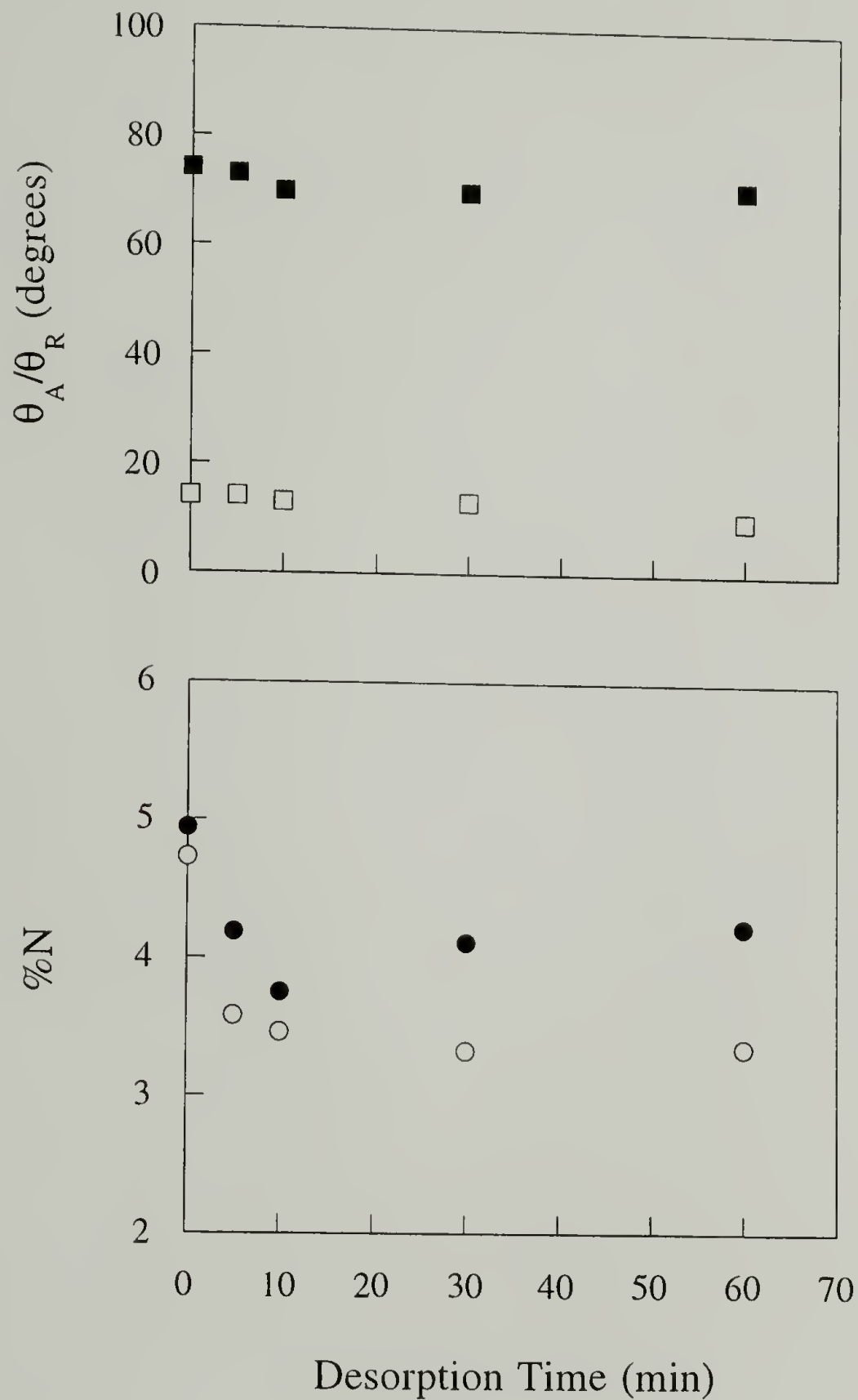
Figure 2.7. Kinetics of desorption of PAH adsorbed at pH 11(0.02 M) to PCTFE-OH and treated in water at pH 4. Nitrogen atomic concentration was determined using XPS at two take-off angles, 15° (●) and 75° (○). Advancing (■) and receding (□) contact angles were determined using water as the probe fluid.
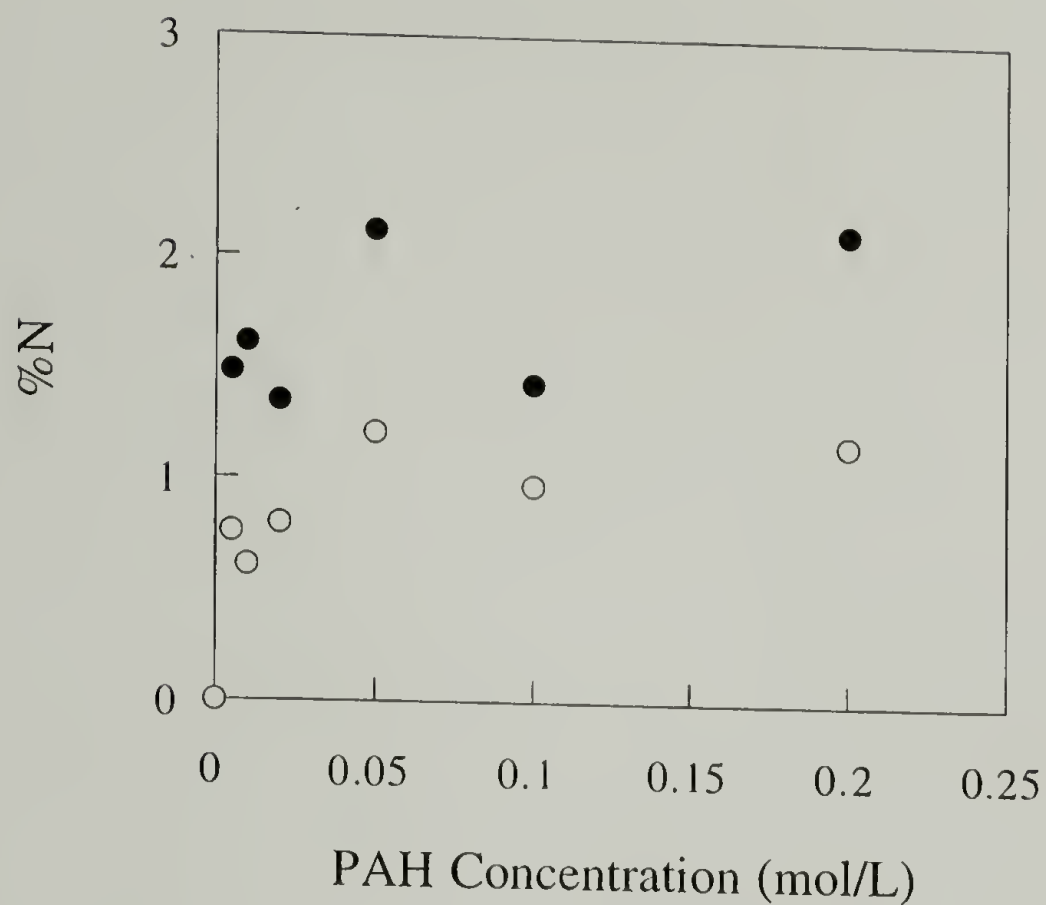
Figure 2.8. Adsorption isotherm of PAH (0.02 M) to PCTFE-OH at pH 6. Nitrogen atomic concentration was determined using XPS at two take-off angles, 15° (●) and 75° (○).
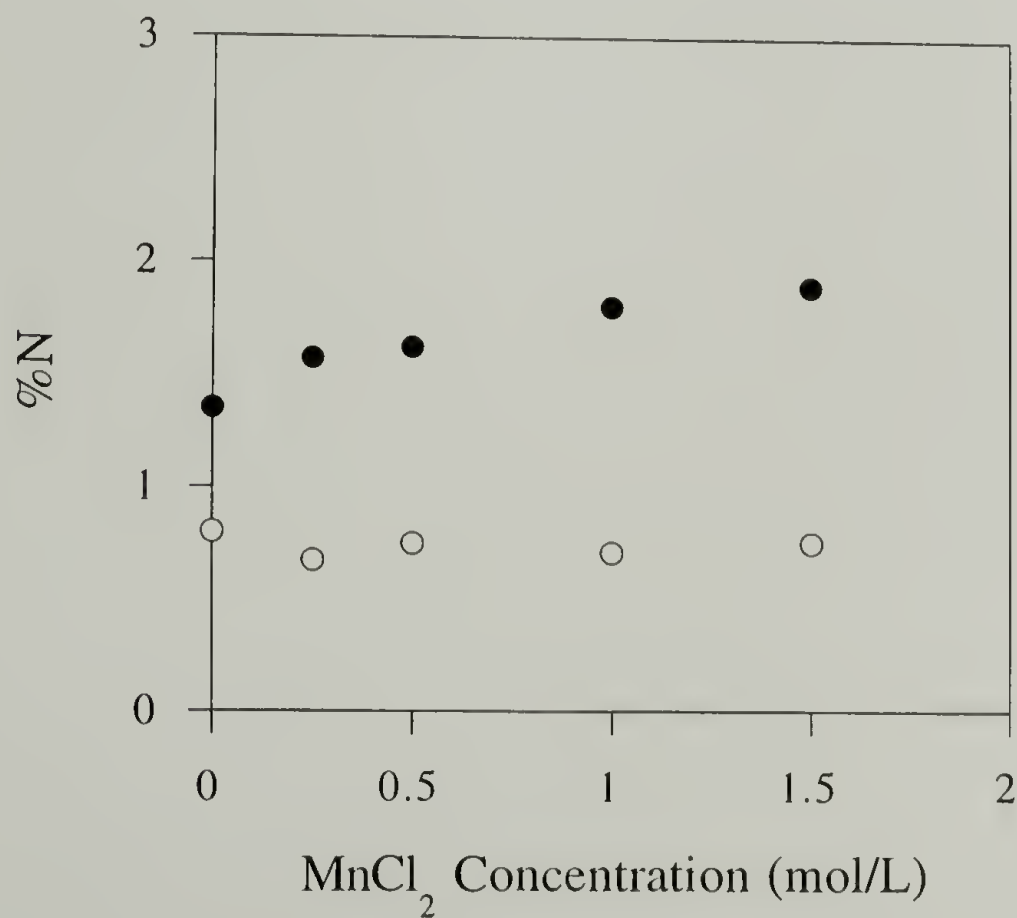
Figure 2.9. Effect of $MnCl_2$ concentration on the adsorption of PAH (0.02 M) to PCTFE-OH. Nitrogen atomic concentration was determined using XPS at two take-off angles, 15° (●) and 75° (○).

Second Layer Adsorptions

The adsorption of poly(sodium styrenesulfonate) (PSS) to PCTFE-OH-PAH (prepared by adsorption of 0.02 M PAH from pH 4 solution for 30 min) was studied with regard to kinetics and solution ionic strength. Figure 2.10 describes the kinetics by plotting the XPS sulfur:nitrogen atomic ratio and contact angle data as a function of adsorption time. The data indicate that adsorption is complete within 20 min. The receding water contact angle decreases during the first 20 min of adsorption to 18° (from $\theta_R = 27°$ for PCTFE-OH-PAH) and remains constant at that value. The advancing contact angle remains unchanged.

The absence of an XPS take-off angle dependence indicates that the PSS (second) layer is not stratified over the PAH (first) layer, but that ammonium and sulfonate ions are dispersed to the same extent throughout the XPS sampling depth (outermost ~40 Å) of the sample. What is not apparent from this ratioed data is that both the PSS and the PAH become stratified in the XPS sampling region during the second layer adsorption. Both nitrogen and sulfur atomic concentrations are take-off angle - dependent (the data is presented in Figures 2.14 and 2.15), indicating that both polyelectrolytes are more concentrated near the surface than in the subsurface XPS sampling region. The first PAH layer thus restructures during the adsorption of PSS and the formation of the PAH-PSS polyelectrolyte complex. The S:N ratio of ~0.6 indicates that the surface should have a net positive charge at pH 4, but apparently this is not the case: the adsorption of PSS ceases as indicated by the data in Figure 2.10 and PAH (the third layer) adsorbs to this surface suggesting that it functions as a negatively charged or neutral surface. This can be explained by the fact that using XPS data (obtained at high vacuum) to analyze the structure or predict the behavior of surfaces in contact with liquids may lead to erroneous conclusions. The S:N ratio (which is also the sulfonate to ammonium ion ratio) of ~0.6 also predicts that chloride should be present in significant concentration; this is not the case at high vacuum.
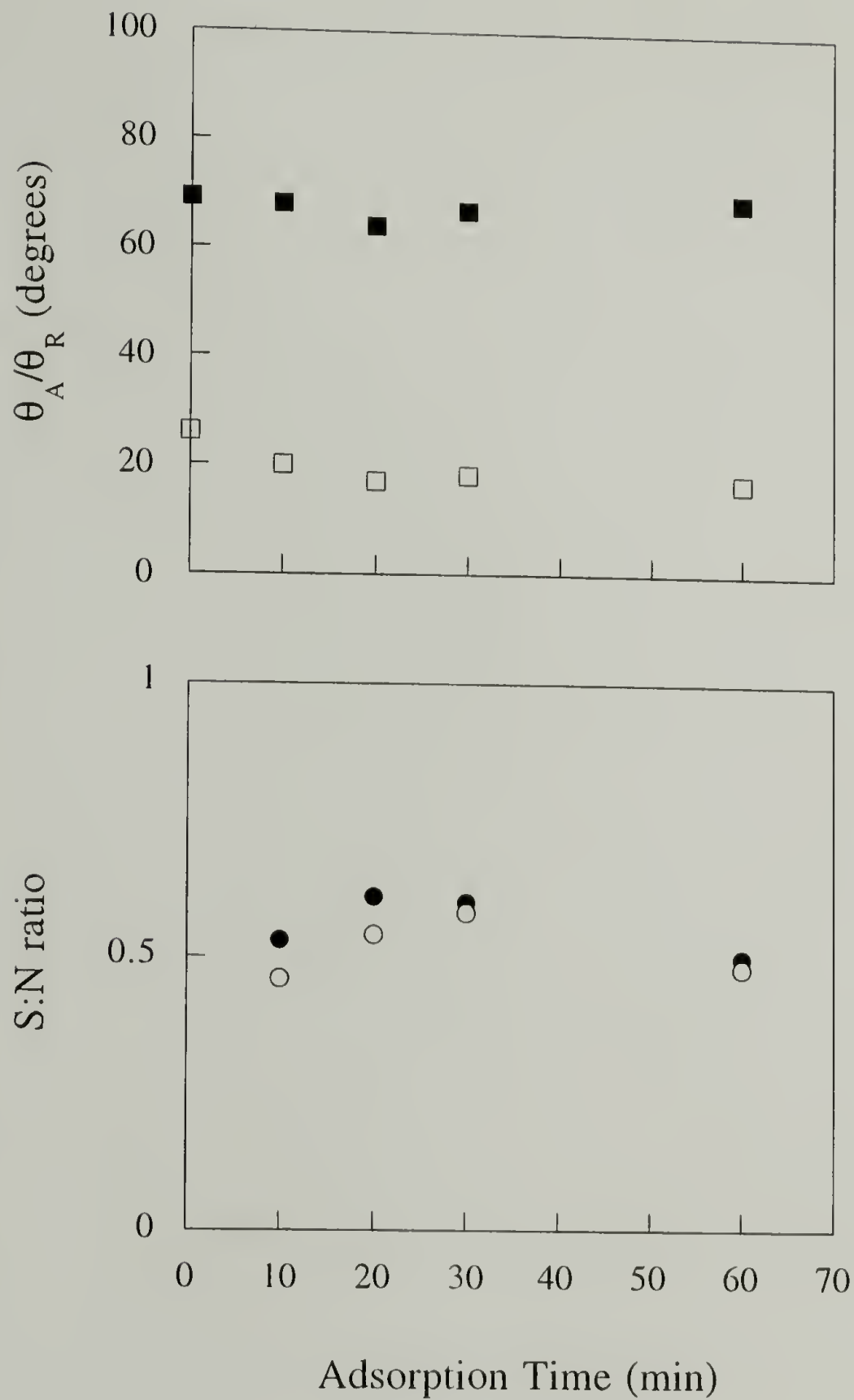
Figure 2.10. Kinetics of adsorption of PSS (0.02 M) to PCTFE-OH-PAH at pH 4. Sulfur : nitrogen atomic ratios were determined using XPS at two take-off angles, 15° (●) and 75° (O). Advancing (■) and receding (□) contact angles were determined using water as the probe fluid.

The effect of solution ionic strength for the second layer adsorption was studied by adding $MnCl_2$ to the PSS solution (0.02 M, pH 4) in concentrations ranging from 0.1-1.5 M. The adsorbed amount of PSS increases significantly (indicated by the increase of sulfur composition in Figure 2.11) at all $MnCl_2$ concentrations studied. Both sulfur content and contact angle data (θ_A/θ_R) reached their plateau values above 0.2 M. The XPS data of these two-layer assemblies show pronounced take-off angle dependence as well, indicating that a thicker PSS layer is stratified above the PCTFE-OH-PAH substrate. S:N ratios of 2.8 and 1.8 are observed at 15° and 75° take-off angles for a sample prepared with 1.0 M $MnCl_2$ (see Figure 2.12).

Multilayer Assembly

From these initial experiments, three protocols were chosen for multilayer assembly. In Protocol 1, PAH and PSS were deposited at pH 4 without $MnCl_2$ added. In Protocol 2, the first PAH layer was adsorbed at pH 11, treated with water at pH 4 and subsequent PSS and PAH layers were deposited at pH 4 without $MnCl_2$ added. In Protocol 3, the first PAH layer was adsorbed as in Protocol 2 and subsequent PSS and PAH layers were deposited at pH 4 with 0.2 M $MnCl_2$ added to the PSS adsorption solutions. Polyelectrolyte concentrations were held at 0.02 M and all adsorptions were carried out for 20 min except the first PAH layer adsorptions. The first layer adsorptions for Protocols 2 and 3 were carried out for 30 min followed by 20 min treatments with water at pH 4 to desorb weakly bound PAH. The polyelectrolytes were adsorbed in the same sequence for each protocol beginning with PAH as the first layer so in all cases multilayer assemblies with an even number of layers contain PSS as the top (outermost) layer and odd number-of-layer multilayers have PAH as the outermost layer.

The principal analytical tool used in analyzing the multilayer structures was XPS. A survey spectrum of a 22-layer film on PCTFE-OH prepared using Protocol 1 is shown in Figure 2.13. All of the features of interest are present in this spectrum. The intensities of
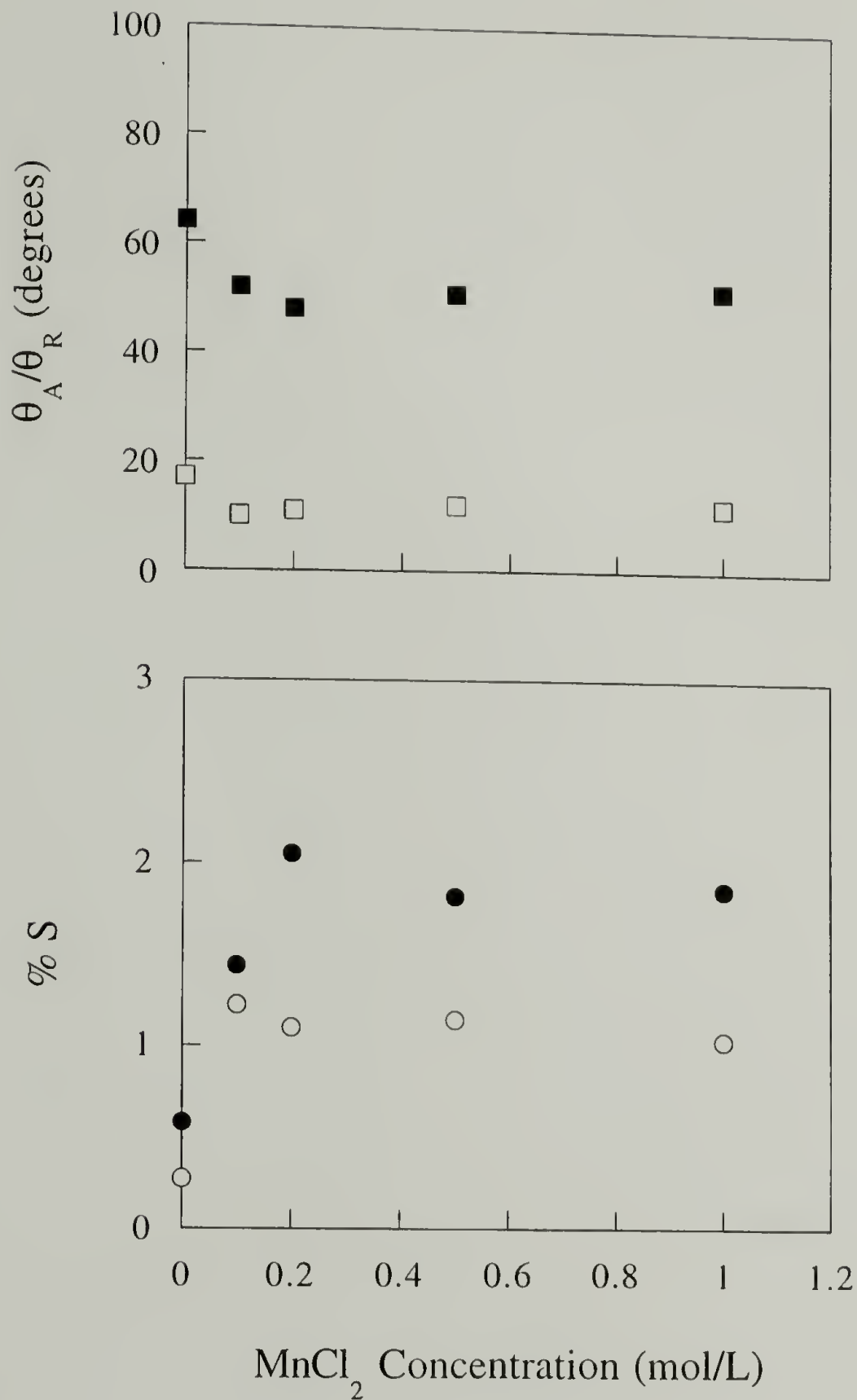
Figure 2.11. Effect of $MnCl_2$ concentration on the adsorption of PSS (0.02 M) to PCTFE-OH-PAH. Sulfur atomic concentration was determined using XPS at two take-off angles, 15° (●) and 75° (○). Advancing (■) and receding (□) contact angles were determined using water as the probe fluid.
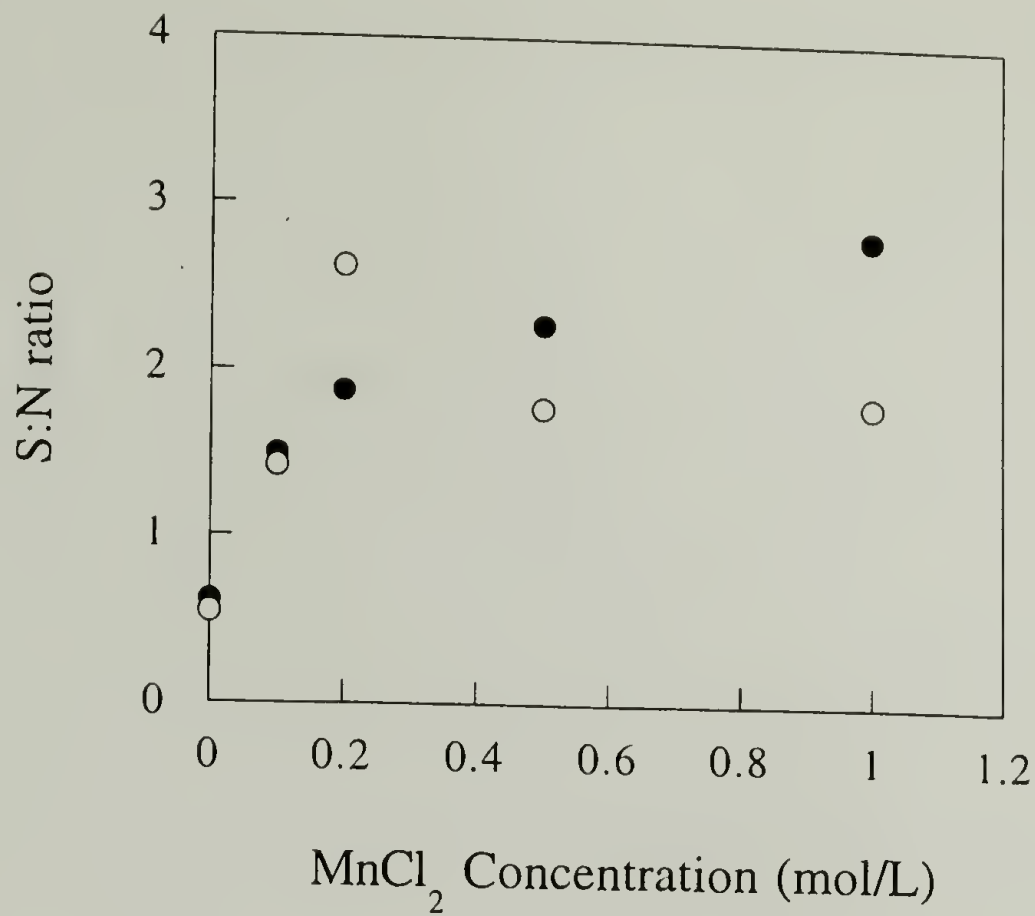
Figure 2.12. Effect of MnCl$_2$ concentration on the adsorption of PSS (0.02 M) to PCTFE-OH-PAH. Sulfur : nitrogen atomic ratios were determined using XPS at two take-off angles, 15° (●) and 75° (○).
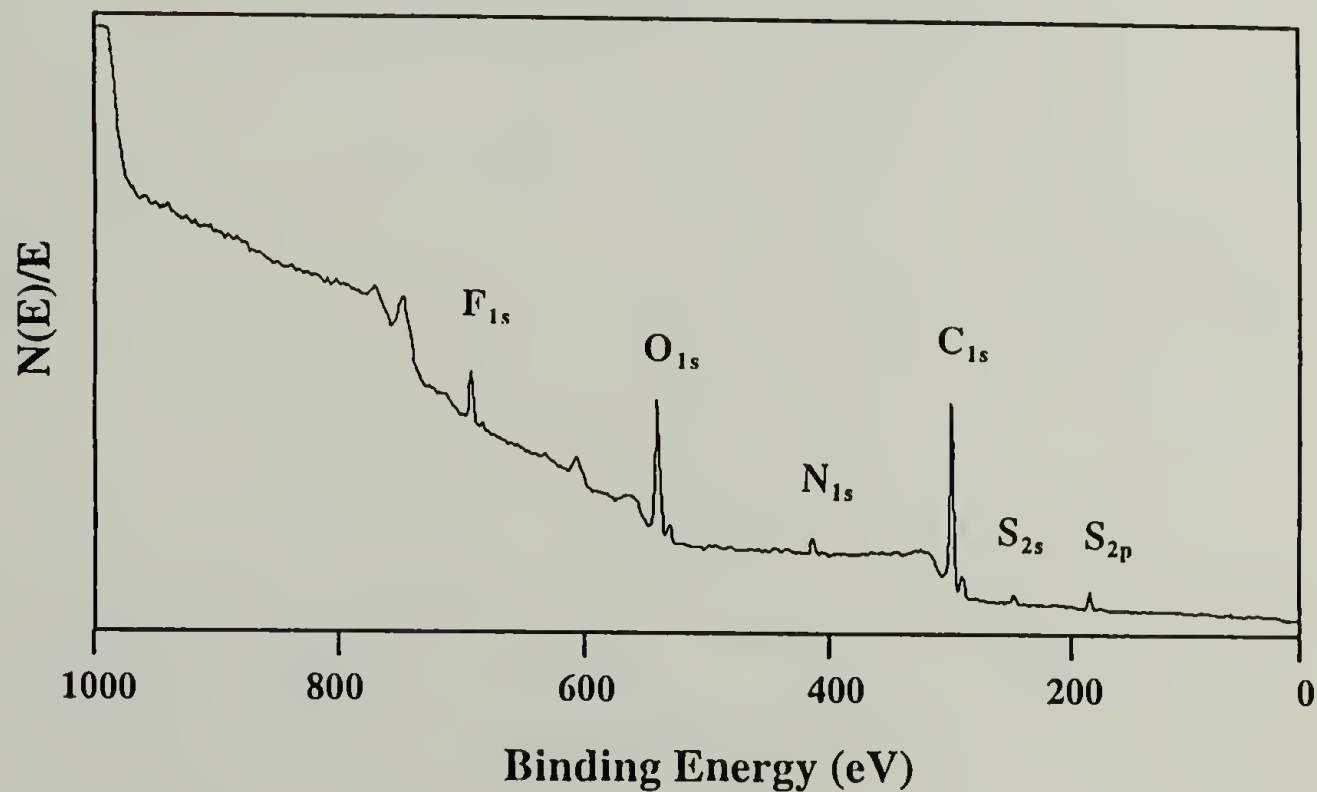
Figure 2.13. Survey XPS spectrum of a 22-layer polyelectrolyte film supported on PCTFE-OH prepared using Protocol 1.

the N_{1s} (404 eV), and S_{2p} (169 eV) photoelectron lines can be used to assess the relative concentrations of PAH and PSS and degree of stratification (layer segregation) in the multilayers. The F_{1s} photoelectron line is due entirely to the PCTFE-OH substrate; this peak decreases in intensity and eventually disappears as more layers are deposited. The thickness of the multilayer assemblies and individual layers can be estimated from the decrease in intensity of this substrate peak.

<u>Protocol 1</u>. As PAH and PSS polyelectrolytes are sequentially adsorbed to PCTFE-OH, photoelectron spectra of isolated samples show that nitrogen and sulfur atomic concentration gradually increase and fluorine concentration gradually decreases, implying that PAH/PSS multilayer assemblies are being built up and are covering the fluorine-containing substrate. As discussed above, the absence of a take-off angle dependence in the N:S ratio of a two-layer sample (Figure 2.10) suggests that the layers are not individually stratified and that the two polyelectrolytes are distributed uniformly (with respect to one another) within the outer few tens of angstroms of PCTFE-OH. Based on this data they cannot be considered layers. Spectra of samples that have undergone more sequential adsorptions do provide evidence for layer formation and some degree of stratification of the layers. These layers are extremely thin, however (less than 1 Å average thickness - discussed below) and not close-packed so they are forced to interdigitate to fill space. Figures 2.14 and 2.15 (Protocol 1) show plots of nitrogen and sulfur concentration as a function of the number of layers in the multilayer film for a series of samples prepared. The increasing take-off angle dependence with number of layers indicates that the polyelectrolytes are concentrated in the outermost regions of the samples and must be adsorbing to the surface as opposed to being absorbed by the water-swollen PCTFE-OH layer, as was the case for the first two layers.

Nitrogen:sulfur atomic ratio data for the same series of multilayers are shown in Figure 2.16 (Protocol 1). There are four important points concerning this data: One, there

is a pronounced odd-even trend at low layer numbers that decreases in amplitude with increasing number of layers adsorbed. The large changes are due to the fact that an additional PSS or PAH layer significantly affects the multilayer assembly composition. The high ratios at low layer numbers are the result of the relatively large amount of PAH that adsorbs in the first adsorption. Two, the ratios level after ~6 layers for 15° take-off angle data and ~10 layers for 75° take-off angle data indicating that the composition is not greatly affected by the addition of one more PAH or PSS layer after this point; the stoichiometry of the assembly process (ammonium ion:sulfonate ion ratio) can be determined using this information. The 15° data converge on a N:S ratio of ~1.2 and the 75° data converge on a N:S ratio of ~1.5. These two values suggest ammonium ion:sulfonate ion ratios of 6:5 and 3:2, respectively. The 75° take-off angle data are presumably a better reflection of the stoichiometry (3 ammoniums per 2 sulfonates). This discrepency is expected to be due to the greater mean free path of the S_{2p} photoelectrons compared with the N_{1s} photoelectrons - this should bias the N:S ratios low, particularly at the 15° take-off angle. Three, The odd-even trend persists even at high layer numbers, with the nitrogen content relatively high when PAH is the last layer adsorbed and relatively low when PSS is the top layer. The trend is more apparent in the more surface-selective 15° data. This indicates that some degree of stratification occurs in the assembly. Four, the odd-even trends at higher layer numbers indicating stratification, as well as the take-off angle dependence of the data indicate that adsorption to a reasonably rigid interface is occurring after a few layers have more "absorbed into" rather than adsorbed to the polymer surface.

Figure 2.17 (Protocol 1) shows the fluorine atomic composition data versus number of layers for the same series of PAH/PSS multilayer assemblies supported on PCTFE-OH. The fluorine concentration decreases continually indicating that the polyelectrolyte overlayer increases in thickness with increasing number of layers. Estimates of the thickness of individual polyelectrolyte layers are discussed below.
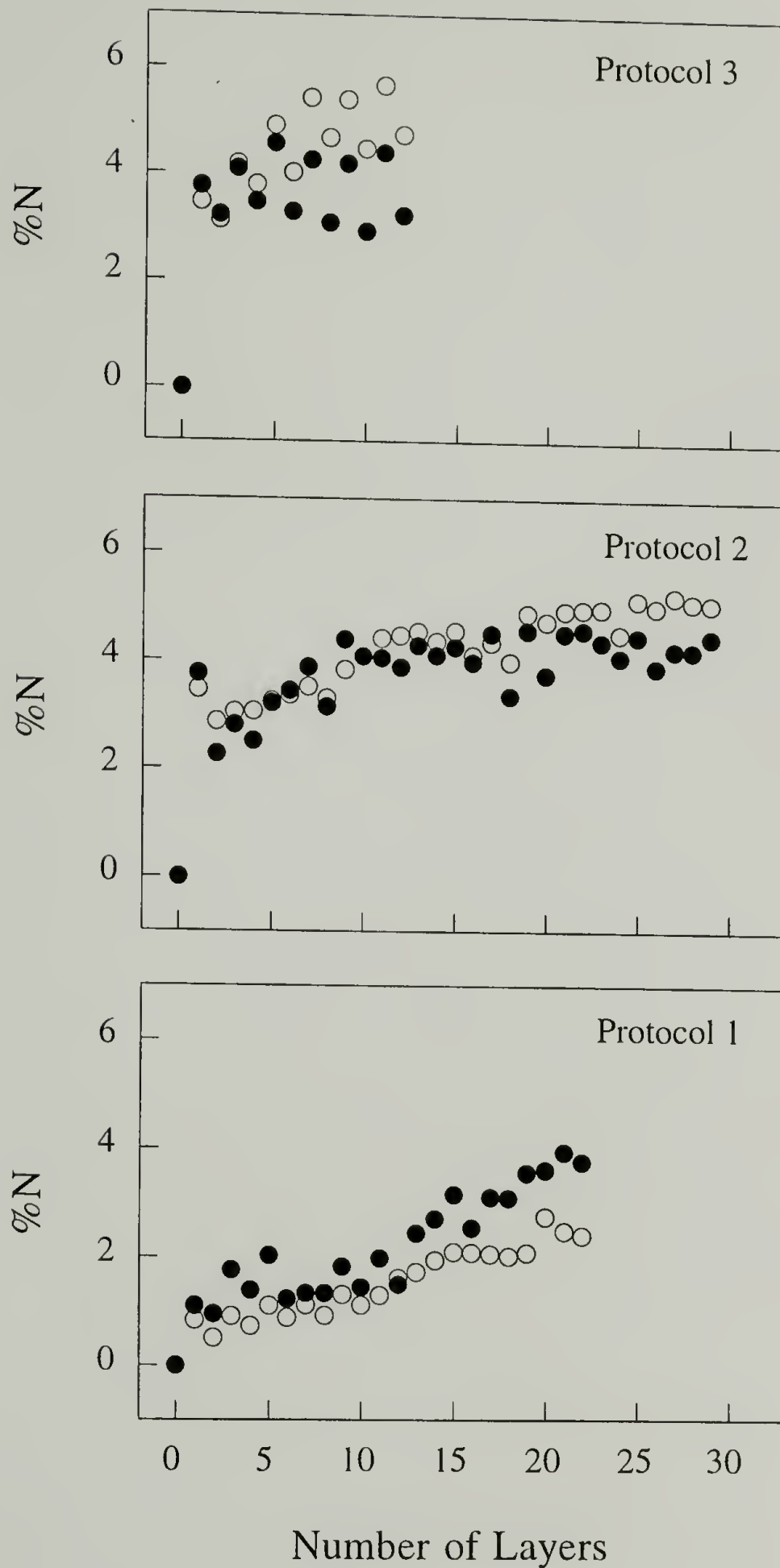
Figure 2.14. Nitrogen atomic concentrations determined at 15° (●) and 75° (○) take-off angles as a function of the number of layers in the multilayer film.
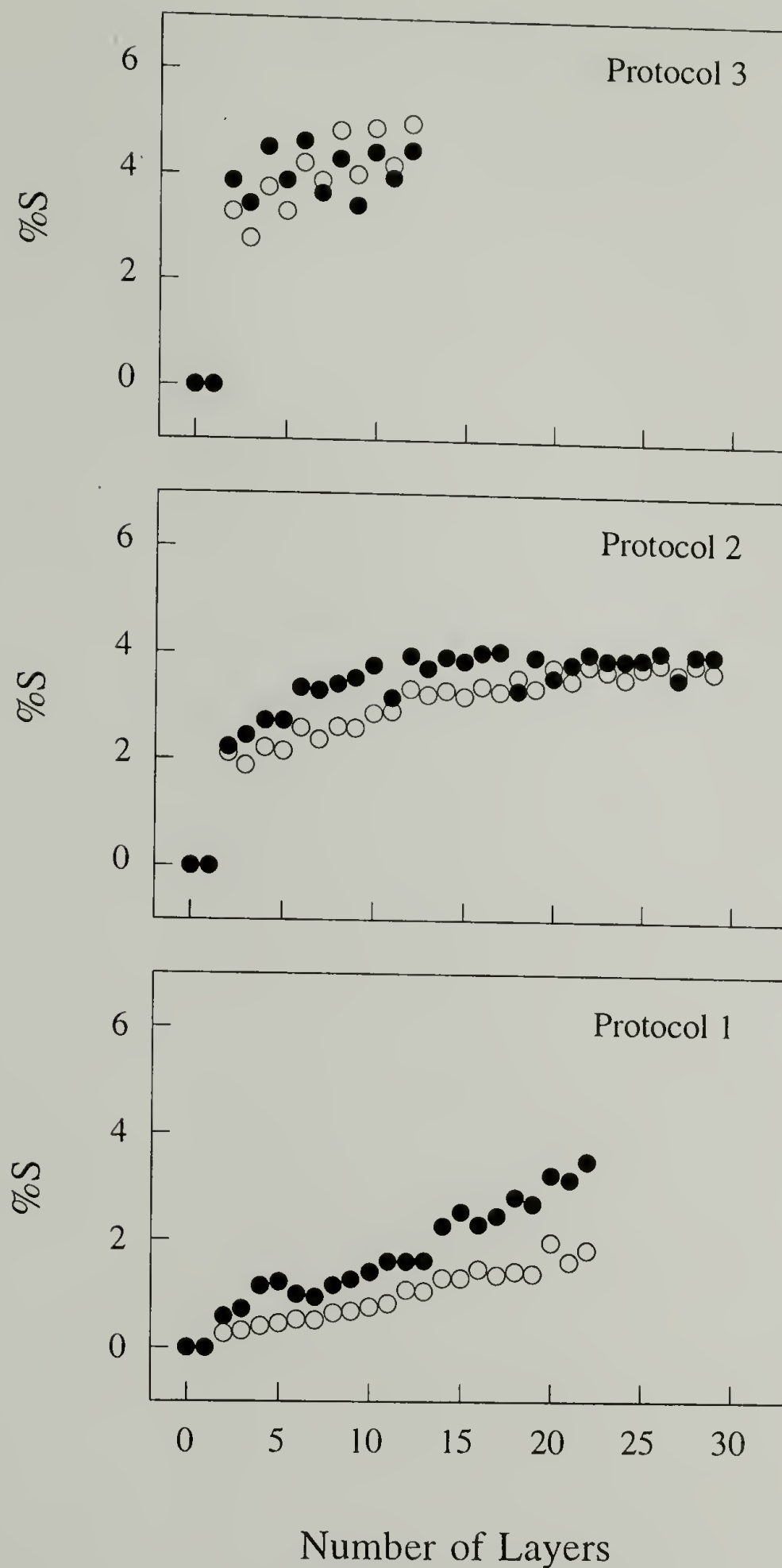
Figure 2.15. Sulfur atomic concentrations determined at 15° (●) and 75° (○) take-off angles as a function of the number of layers in the multilayer film.
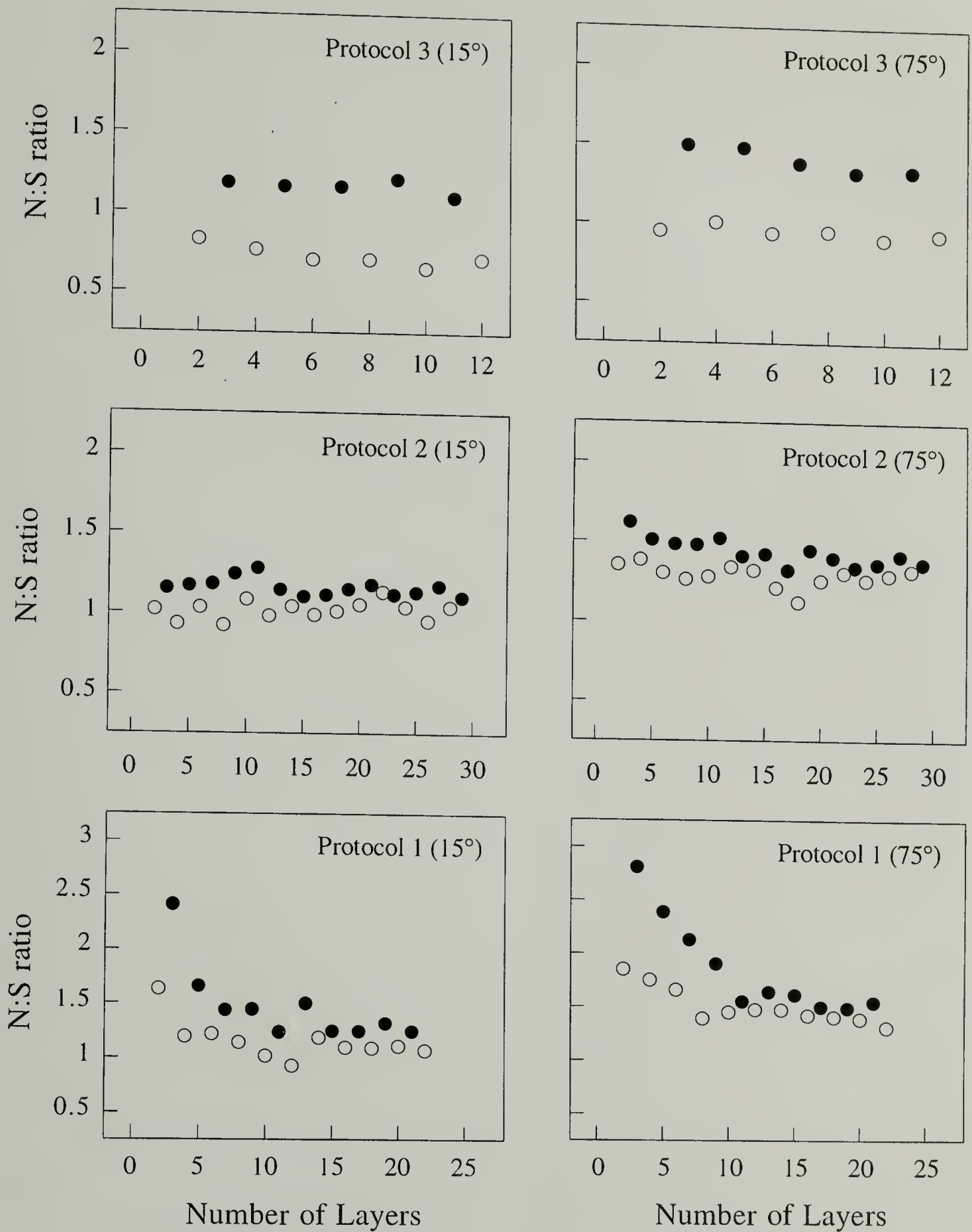
Figure 2.16. Nitrogen:sulfur atomic ratio data versus the number of layers for the 3 series of PAH/PSS multilayer assemblies: odd number of layers (●), even number of layers (O).
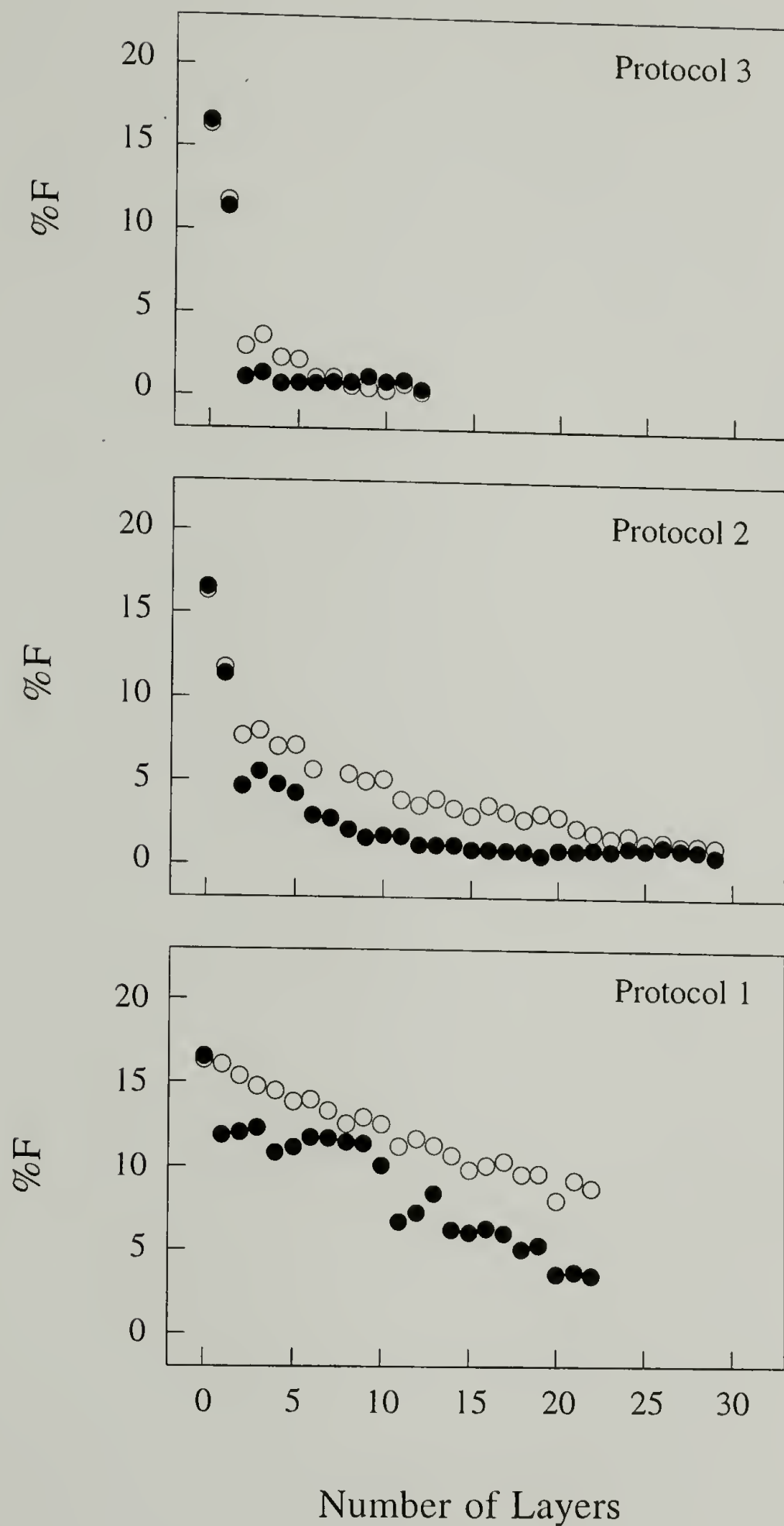
Figure 2.17. Fluorine atomic concentrations determined at 15° (●) and 75° (○) take-off angles as a function of the number of layers in the multilayer film.

The intensity of the fluorine signal at 75° take-off angle is attenuated only by ~40% after greater than 20 layers have been adsorbed implying that the layers are extremely thin. Considerable scatter in the 15° take-off angle data and variable take-off angle dependence are observed. Some degree of scatter in the data is expected due to the fact that separate samples prepared by multistep procedures were used for analysis of each thickness (number of layers) multilayer (samples were not used after analysis as substrates for further depositions). This degree of scatter, however, is greater than what was observed in other systems, including data presented below. This, coupled with the fact that similar scatter is not observed in the 75° data for this series, suggests that the conversion from an absorption into the 1000 Å-thick PCTFE-OH layer to an adsorption to a more rigid interface is gradual and occurs at different points in the multilayer assembly process in different individual experiments. In retrospect, this suggests that a reconstruction of the multilayer, similar to what was observed by receding contact angle changes in the first layer adsorption, may be occurring subsequent to the polyelectrolyte adsorption step. No experiments were carried out to address this issue. The consistency of take-off angle dependence for multilayer assemblies with 14 layers or more is observed. Scatter in the receding contact angle data (Figure 2.18, Protocol 1) reflect the scatter in the 15° take-off angle data. The contact angle data is included for comparison with data presented below; there is not an observable odd-even effect in the advancing contact angle data for samples prepared using Protocol 1.

Protocols 2 and 3. The same series of experiments and analyses were carried out using Protocols 2 and 3 and data analogous to that presented for Protocol 1 is presented in Figures 2.14 - 2.18 for these conditions. Both of these protocols involve using a different procedure for adsorption of the first PAH layer that yields a surface that is more concentrated in ammonium ions. In Protocol 2, subsequent layers are adsorbed in identical fashion as those using Protocol 1; in Protocol 3, $MnCl_2$ is added to the PSS adsorption solutions. These variations give rise to differences in multilayer assembly structure.

The XPS data (nitrogen, sulfur and fluorine concentrations) in Figures 2.14, 2.15 and 2.17 for samples prepared using Protocol 2 indicate that the composition of the region of the samples assessed by XPS reaches a plateau after a sufficient number of layers has been adsorbed to form a multilayer assembly that is thick enough to effectively attenuate photoelectrons originating in the substrate. This occurs after ~9 layers have been deposited for the 15° take-off angle data and after ~25 layers for the 75° data. This is in contrast to the data for Protocol 1, which does not reach plateau values, and this contrast indicates that the multilayer assemblies prepared using Protocol 2 are thicker. This increased thickness is due, in large part, to the first two layers although the subsequent layers are thicker than those prepared using Protocol 1. This can be seen most clearly in the fluorine composition data that decreases sharply after the first two layers have been adsorbed and more gradually with subsequent layers. This disparity in thickness can also be inferred from the nitrogen:sulfur ratios (Figure 2.16). A relatively thick second (PSS) layer is indicated by the depression of the N:S ratio after the second layer is adsorbed (compare with Protocol 1). N:S ratios of 1.0 and 1.35 are observed for 15° and 75° take-off angle data compared with 1.7 and 1.9 for Protocol 1. The first layer in Protocol 2 samples contains approximately three times the density of ammonium ions as that for Protocol 1, thus the second layer in protocol 2 samples is greater than three times thicker than the second layer in Protocol 1 samples. That the subsequent (third and higher) layers are not as thick as the first two (their thickness is discussed in quantitative terms below) is also indicated by the N:S ratio data. The amplitude of the odd-even effect is approximately the same as that for Protocol 1. The increased surface charge (higher ammonium ion density) on Protocol 2 first layers induces a greater adsorption of PSS, but the resulting increased surface sulfonate group concentration does not enhance the adsorption of the third layer. The layer-by-layer deposition process reverts to one very similar to that of Protocol 1. The stoichiometry of the assembly processes (ammonium ion:sulfonate ion ratio) is indistinguishable with N:S ratios of ~1.2 and ~1.5 for 15° and 75° take-off angle data,

respectively. Water contact angle data are consistent with this analysis (Figure 2.18, Protocol 2). The receding contact angle data converge to the same value as that of Protocol 1 samples ($\theta_R = 10°$), but this value is reached with fewer layers adsorbed.

The corresponding data for samples assembled with $MnCl_2$ added to the PSS adsorption solutions (Protocol 3, Figures 2.14 - 2.18) indicate that much thicker layers are formed under these conditions. The atomic concentration data reach plateau values at a fewer number of layers. The N:S ratios for a 2-layer sample are 0.8 and 0.95 (15° and 75° take-off angle data) indicating that sulfonate ions are present in excess of ammonium ions. The increased surface anion concentration increases the adsorbance of the third (PAH) layer and this enhancement propagates to higher layer numbers. The increased layer thickness is indicated by the amplitude of the odd-even effect in the N:S ratio (Figure 2.16). It is much higher than in the cases of Protocols 1 and 2 and indicates that the layers are quite rigorously stratified. The layers are thick enough to cause an odd-even effect in the advancing water contact angle as well (Figure 2.18). Samples prepared using Protocols 1 and 2 do not display this effect presumably because the technique samples two (or more) of the thinner layers. The stoichiometry of assembly for Protocol 3 differs from Protocols 1 and 2 with ammonium ion:sulfonate ion ratios of ~1.0 and ~1.2 for 15° and 75° take-off angle data, respectively.

Estimates of Layer Thicknesses

The thicknesses of the multilayer assemblies and the average thickness of individual layers were estimated from the XPS data. The F_{1s} peak intensity should decrease exponentially with the buildup of layers and the data (Figure 2.17) qualitatively fit the predicted decrease. Knowing the mean free path of the F_{1s} photoelectron in the multilayer assemblies, ones should be able to estimate the average thickness. A mean free path of ~20 Å has been calculated for Mg K_α - excited Si_{2p} electrons in PAH/PSS multilayer assemblies supported on silicon wafers using XPS (75° take-off angle) and X-ray
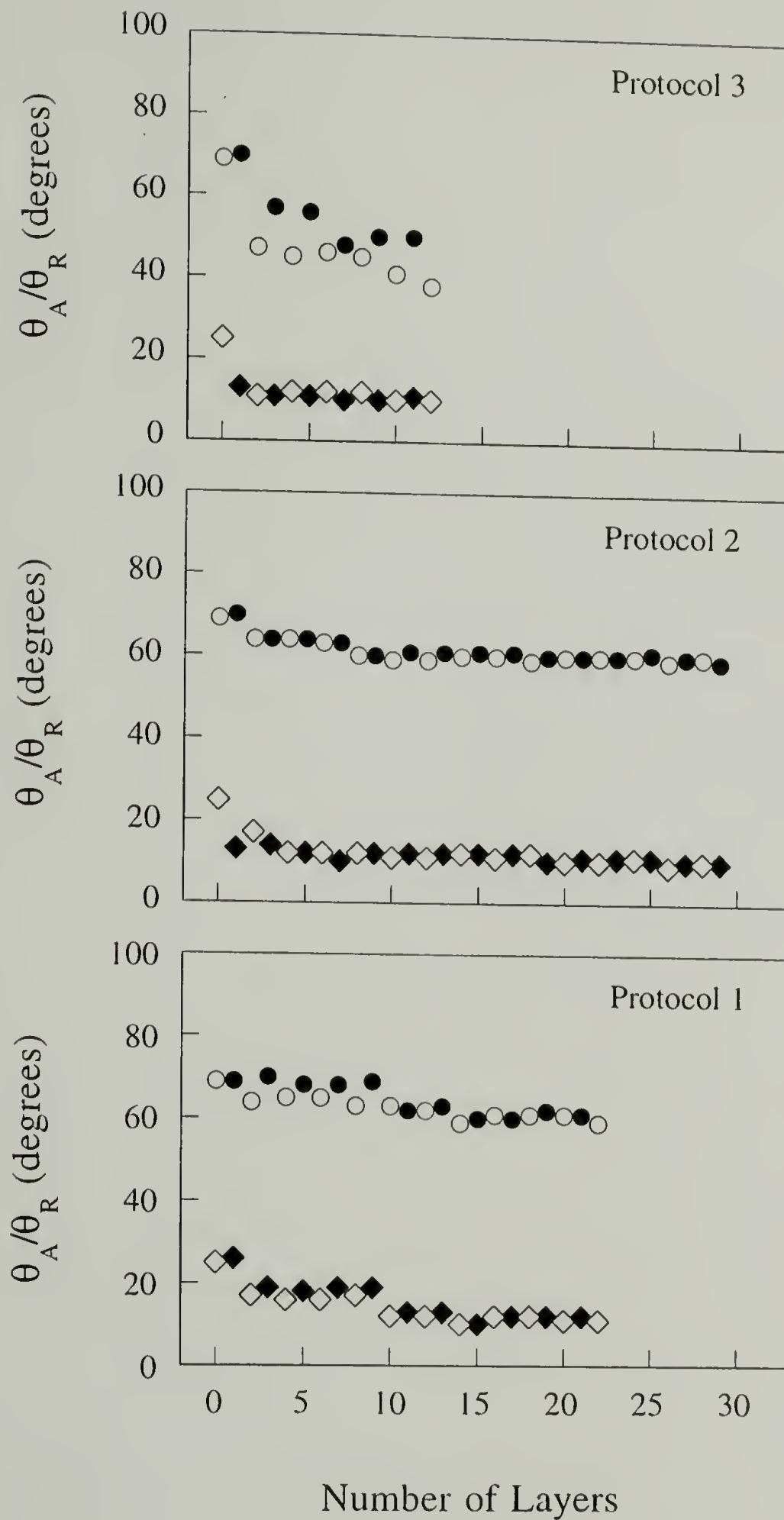
Figure 2.18. Advancing (●, ○) and receding (◆, ◇) contact angle data for each of the three series of samples: closed and open symbols indicate an odd and even number of layers, respectively.

reflectivity data.[11] Based on this value, a mean free path of 11.5 Å for the F_{1s} photoelectron has been calculated and is used below to estimate layer thicknesses.

The attenuation of photoelectron intensity in solids as a function of sampling depth is expressed in Equation 1.5. The expression indicates that 95% of detected photoelectrons originate in the outermost $3\lambda\sin\theta$. As a result, the F_{1s} peak should be attenuated to 5% of its original intensity when the multilayer thickness is $3\lambda\sin\theta$. The equation also indicates that the spectra recorded at 15° takeoff angle contains the composition of the outermost ~27% of the region analyzed at 75° takeoff angle. According to the expression, it should take approximately 4 times as many layers to attenuate the 75° fluorine signal to the same extent that the 15° signal is attenuated (at the thickness $3\lambda\sin\theta$: 0.78λ for 15° and 2.90λ for 75°). The data however do not agree with this prediction since only twice as many layers are required. This inconsistency can be explained as the effect of angular dependence of mean free paths of electrons in the layered materials. This behavior is also observed in the small dependence on take-off angle of nitrogen and sulfur composition (Figures 2.14 - 2.15).

Equation 1.5 can be rearranged by substituting t with nz where n is the number of layers and z is the average thickness of the individual layers. The rearranged form is expressed as Equation 2.1.

$$-\ln(N/N_0)\sin\theta \quad = \quad nz/\lambda \qquad\qquad (2.1)$$

For this expression here, N is the atomic concentration of fluorine (data from Figure 2.17), N_0 is the fluorine concentration of the substrate (PCTFE-OH), θ is the take-off angle, n is the number of layers, z is the average thickness of the individual layers and λ is the F_{1s} photoelectron mean free path. In Figure 2.19 are plots of $-\ln(N/N_0)\sin\theta$ as a function of number of layers for the series of samples prepared using each protocol. The slopes of the lines indicate the average layer thickness divided by the photoelectron mean free paths.
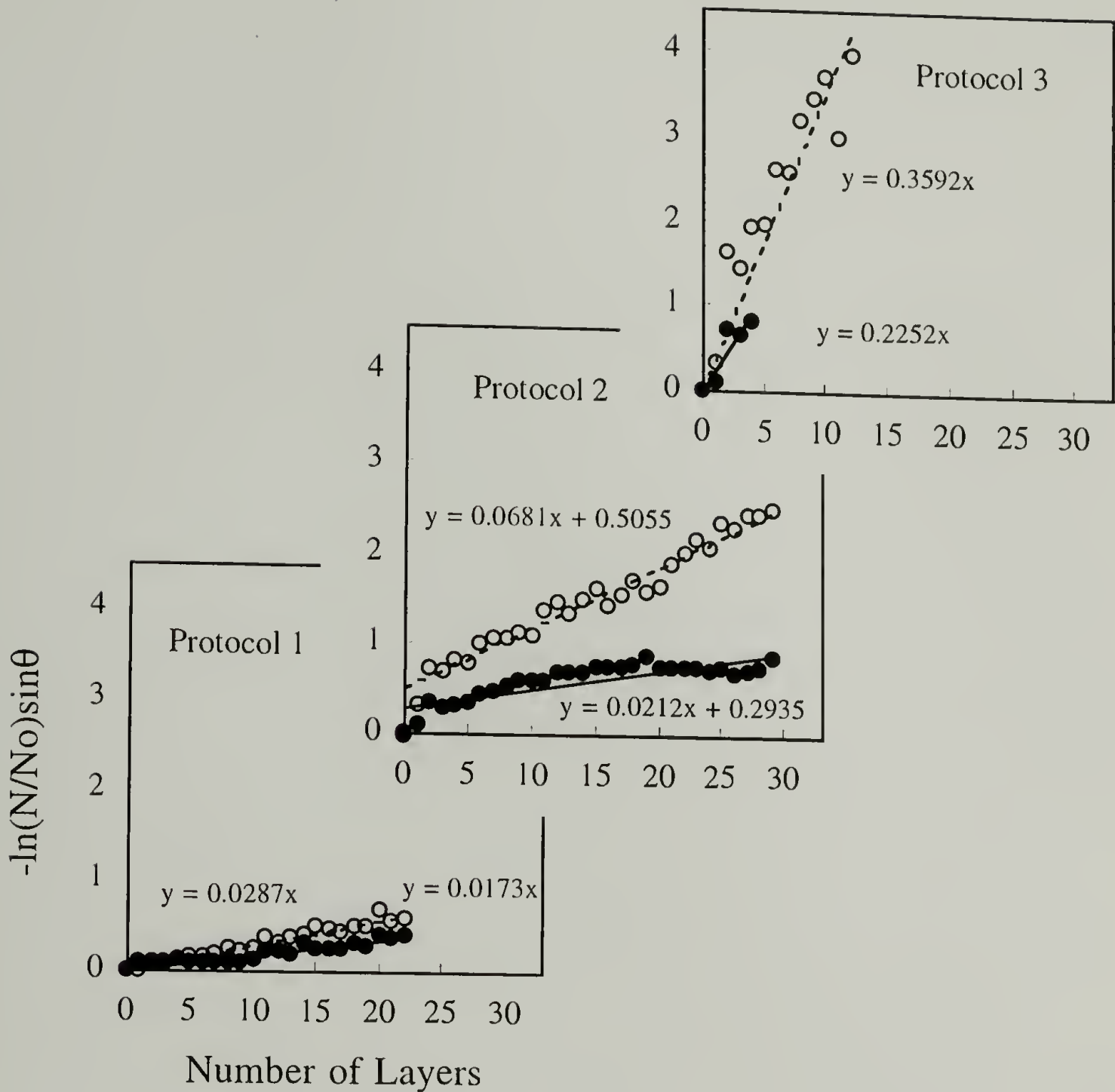
Figure 2.19. Plots of $-\ln(N/N_o)\sin\theta$ vs. number of layers in the multilayer film for the 3 series of PAH/PSS multilayer assemblies. The slopes of the lines indicate the ratio of the average layer thickness to the F_{1s} photoelectron mean free path. The closed (●) and open (O) circles are data recorded at 15° and 75° take-off angles, respectively.

The fact that the 15° and 75° data yield different slopes indicates that the electron mean free path depends on take-off angle. This issue has been previously discussed[20] and it is not unexpected for an anisotropic system with thin stratified layers. Using a mean free path of 11.5 Å, the average layer thicknesses calculated from the 75° data are 0.3 Å, 0.8 Å and 4.1 Å for Protocols 1, 2 and 3, respectively. The least squares analysis that was used to determine the slopes included the origin for Protocols 1 and 3. As Protocol 2 causes the first two layers to be exceptionally thick, the origin and the first point were not included in the slope determination for Protocol 2. Note that these values are only estimates based on the assumption that the mean free paths are the same as that determined for the silicon-supported multilayer films.

Notwithstanding the assumption made in determining these thicknesses, the data indicate extraordinarily thin individual layers and the concept of stratified polymer monolayers of sub-angstrom thickness is counterintuitive and warrants additional comment. Close-packed monolayers of poly(allylammonium) and poly(styrenesulfonate) would have thicknesses of ~6 Å and ~9 Å, assuming a density of 1.0. The sub-angstrom thick monolayers must be far from close-packed with chain segments occupying only ~10% of the available surface area. It is believed, however, based on gas permeability measurements,[21] that the multilayer assemblies are quite dense and thus the chains must be interdigitated.

Mechanical Properties of Multilayer Assemblies

Peel tests using pressure-sensitive adhesive tape (3M #810) were performed in order to determine the locus of failure in PCTFE-OH/multilayer assembly/adhesive tape composites. Peel tests on samples prepared by all three protocols with both odd and even numbers of layers were performed: 39 and 40 layers for Protocol 1, 29 and 30 layers for Protocol 2, 11 and 12 layers for Protocol 3. The tape was applied and peeled from the samples and XPS spectra (15° take-off angle) of both surfaces were compared with spectra

obtained before the adhesive joint was formed (Table 2.2). The adhesive on the tape contains only carbon and oxygen and the supported polyelectrolyte multilayer samples contain nitrogen and sulfur (each present in ~4 atom % -see Figures 2.14 and 2.15), so the analysis should be straight-forward.

In all cases small amounts of sulfur and nitrogen (less that 0.5 atom %) were transferred to the tape upon peeling, indicating some cohesive failure in the multilayer assemblies; sulfur and nitrogen content in the supported multilayer assemblies remained high. Except for one case (Protocol 1, 40 layers), the carbon concentration in the supported multilayer assembly increased (by 2-4 %) indicating that some cohesive failure in the adhesive also occurs. These results indicate that the mechanical strength of the multilayer assemblies is approximately equal to the cohesive strength of the adhesive of the pressure sensitive tape (not very strong) and that failure occurs very near to (within a few angstroms of) the adhesive/multilayer assembly interface. That the adhesive strength between the multilayers and the PCTFE-OH substrate is stronger than this value is also indicated.

Conclusions

Poly(chlorotrifluoroethylene) film, chemically modified to contain alcohol functionality (PCTFE-OH) (a neutral surface), supports the layer-by-layer assembly of polyelectrolytes (PAH and PSS) when PAH is adsorbed as the first layer. The adsorbance of the first PAH layer can be controlled using pH, hence the ammonium ion concentration of the first layer (charge density) can be controlled. Three different sets of conditions were used to prepare multilayer assemblies: Protocols 1 and 2 differ by the charge density of the first layer. Protocol 3 differs from Protocol 2 in that $MnCl_2$ was added to the PSS adsorption solutions. The thickness of the individual layers in the assemblies depends both on the charge density of the first layer and the ionic strength of the PSS adsorption solution. The stoichiometry of the assembly process (ammonium:sulfonate ratio) also

112

Table 2.2. XPS atomic composition data (15° take-off angle) for peel tests of PAH/PSS multilayer assemblies using Protocols 1, 2 and 3 using pressure sensitive adhesive tape (3M #810).

Sample Surface	Atomic Composition (%)				
	C	O	F	N	S
Adhesive Tape	83.64	16.36	-	-	-
PCTFE-OH	67.95	17.66	14.39	-	-
alcohol surface (peeled off tape)	76.98	14.19	8.83	-	-
Tape (peeled off alcohol surface)	84.60	15.32	0.08	-	-
Protocol 1: 39 layers (PAH surface)	72.02	17.86	1.71	4.52	3.89
PAH surface (peeled off tape)	76.40	14.76	0.79	4.04	4.00
Tape (peeled off PAH surface)	84.79	14.52	0.16	0.34	0.18
40 layers (PSS surface)	71.93	18.89	1.45	3.95	3.78
PSS surface (peeled off tape)	71.88	21.00	1.36	2.63	3.13
Tape (peeled off PSS surface)	85.58	14.47	0.07	0.08	0.00
Protocol 2: 29 layers (PAH surface)	75.09	15.43	0.95	4.64	3.89
PAH surface (peeled off tape)	78.19	13.42	0.29	4.14	3.96
Tape (peeled off PAH surface)	84.21	14.47	0.20	0.49	0.24
30 layers (PSS surface)	70.61	20.41	1.45	3.73	3.80
PSS surface (peeled off tape)	72.46	19.57	1.34	3.19	3.44
Tape (peeled off PSS surface)	84.77	14.90	0.02	0.30	0.01
Protocol 3: 11 layers (PAH surface)	74.00	16.59	1.01	4.42	3.98
PAH surface (peeled off tape)	74.52	18.87	0.98	2.58	3.05
Tape (peeled off PAH surface)	83.61	16.00	0.10	0.10	0.19
12 layers (PSS surface)	74.34	17.47	0.42	3.26	4.51
PSS surface (peeled off tape)	78.02	14.83	0.29	2.63	4.24
Tape (peeled off PSS surface)	84.87	14.29	0.16	0.40	0.29

depends on the ionic strength of the PSS adsorption solution. The average individual layer thicknesses for Protocols 1, 2 and 3, respectively, are 0.3, 0.8 and 4.1 Å thick, as assessed by XPS. Although the layers are extremely thin, XPS data (and contact angle data for Protocol 3) indicate that the layers are stratified. Peel tests indicate that the multilayer assemblies on PCTFE-OH exhibit poorer mechanical integrity than those on other substrates (PMP-CO_2^-, PET-CO_2^- and PET-NH_3^+).[20,21]

References

(1)   Decher, G.; Hong, J. D.; Schmitt, J. *Thin Solid Films* **1992**, *210/211*, 831.

(2)   Decher, G. "Multilayer Films (Polyelectrolytes)" in "Polymeric Materials Encyclopedia: Synthesis, Properties, and Applications;" Salamone, J.C., Ed., vol. 6, CRC Press, Inc.: Boca Raton, 1996, 4540.

(3)   Cheung, J. H.; Fou, A. C.; Rubner, M. F. *Thin Solid Films* **1994**, *244*, 985.

(4)   Bell, C. M.; Arendt, M. F.; Gomez, L.; Schmehl, R. H.; Mallouk, T. E. *J. Am. Chem. Soc.* **1994**, *116*, 8374.

(5)   Kleinfeld, E. R.; Ferguson, G. S. *Science* **1994**, *265*, 370.

(6)   Mao, G.; Tsao, Y.; Tirrell, M.; Davis, H. T. *Langmuir* **1993**, *9*, 3461.

(7)   Ferreira, M.; Rubner, M. F. *Macromolecules* **1995**, *28*, 7107.
(8)   Fou, A. C.; Rubner, M. F. *Macromolecules* **1995**, *28*, 7115.

(9)   Hammond, P. T.; Whitesides, G. M. *Macromolecules* **1995**, *28*, 7569.

(10)   Lee, K. -W.; McCarthy, T. J. *Macromolecules* **1988**, *21*, 2318.

(11)   Dias, A. J.; McCarthy, T. J. *Macromolecules* **1985**, *18*, 1826.

(12)   Dias, A. J.; McCarthy, T. J. *Macromolecules* **1987**, *20*, 2068.

(13)   Bee, T. G.; McCarthy, T. J. *Macromolecules* **1992**, *25*, 2093.

(14)   Shoichet, M. S.; McCarthy, T. J. *Macromolecules* **1991**, *24*, 982.

(15)   Dias, A. J.; McCarthy, T. J. *Macromolecules* **1984**, *17*, 2529.

(16)   Brennan, J. V.; McCarthy, T. J. *Polym. Prepr. (Am. Chem. Soc. Div. Polym. Chem.)* **1989**, *30(2)*, 152.

(17)   Bening, R. C.; McCarthy, T. J. *Macromolecules* **1990**, *23*, 2648.

(18)   Costello, C. A.; McCarthy, T. J. *Macromolecules* **1987**, *20*, 2819.

(19)   Lvov, Y.; Haas, H.; Decher, G.; Möhwald, H. *J. Phys. Chem.* **1993**, *97*, 12835.

(20)   Chen, W.; McCarthy, T. J. *Macromolecules* **1997**, *30*, 78.

(21)   Leväsalmi, J. -M.; McCarthy, T. J. *Macromolecules* **1997**, *30*, 1752.

(22)   Lvov, Y.; Decher, G.; Möhwald, H. *Langmuir* **1993**, *9*, 481.

(23)   Lvov, Y.; Decher, G.; Sukhorukov, G. *Macromolecules* **1993**, *26*, 5396.

(24)   Lvov, Y.; Haas, H.; Decher, G.; Möhwald, H. *Langmuir* **1994**, *10*, 4232.

(25)   Cooper, T. M; Campbell, A. L.; Crane, R. L. *Langmuir* **1995**, *11*, 2713.

(26)   Keller, S. W.; Kim, H. -N.; Mallouk, T. E. *J. Am. Chem. Soc.* **1994**, *116*, 8817.

(27)   Lvov, Y.; Ariga, K.; Kunitake, T. *Chem. Lett.* **1994**, 2323.

(28)   Kong, W.; Zhang, X; Gao, M. L.; Zhou, H.; Zhang, X.; Li, W.; Shen, J. C.
        J. Chem. Soc., Chem. Commun. **1994**, 1297.

(29)   Lvov, Y.; Essler, F.; Decher, G. *J. Phys. Chem.* **1993**, *97*, 13773.

(30)   Gao, M.; Kong, X.; Zhang, X.; Shen, J. *Thin Solid Films* **1994**, *244*, 815.

(31)   Hong, H.; Davidov, D.; Avny, Y.; Chayet, H.; Faraggi, E. Z.; Neumann, R.
        Adv. Mater. **1995**, *7*, 846.

(32)   Fou, A. C.; Ontisuka, O.; Ferreira, M.; Rubner, M. F.; Hsieh, B. R.
        Mat. Res. Soc. Symp. Proc. **1995**, *369*, 575.

(33)   Kotov, N. A.; Dekany, I.; Fendler, J. H. *J. Phys. Chem.* **1995**, *99*, 13065.

(34)   Van der Schee, H. A.; Lyklema, J. *J. Phys. Chem.* **1984**, *88*, 6661.

(35)   Evers, O. A.; Fleer, G. J.; Scheutjens, J. M. H. M.; Lyklema
        J. Colloid Interface Sci. **1986**, *111(2)*, 446.

(36)   Böhmer, M. R.; Evers, O. A.; Scheutjens, J. M. H. M. *Macromolecules* **1990**,
        23, 2288.

(37)   BlaakMeer, J.; Böhmer, M. R.; Cohen Stuart, M. A.; Fleer, G. J. *Macromolecules*
        1990, *23*, 2301.

(38)   Cosgrove, T.; Obey, T. M.; Vincent, B. *J. Colloid Interface Sci.* **1986**, *111(2)*,
        1986.

(39)   Stockton, W. B.; Rubner, M. F. *Polymer Prepr.*
        (Am. Chem. Soc. Div. Polym. Chem.) **1994**, *35*, 319.

(40)   Arnett, E. M. *Prog. Phys. Org. Chem.* **1963**, *1*, 223.

(41) Brown, H. C.; McDaniel, D. H.; Hflinger, O. In *Determination of Organic Structures by Physical Methods*; Braude, E. A., Nachod, F. C., Eds; Academic Press: New York, 1955; p 567.

CHAPTER 3

RATIONAL CONTROL OF HETEROGENEOUS (GAS-SOLID)
POLYMER SURFACE MODIFICATION

Introduction

Considerable effort has been focused on controlling the surface selectivity of polymer modification reactions so that thin (<100 Å) layers of reactive functionality can be introduced to relatively thick film samples. These modified film samples are amenable to surface - property correlations that can be used to control (and understand) macroscopic surface properties. Surface-selective modification reactions with varying degrees of selectivity have been developed and reported for poly(chlorotrifluoroethylene),[1-3] poly(vinylidene fluoride),[3-5] polypropylene,[6] poly(tetrafluoroethylene-co-hexafluoropropylene),[3,7] poly(ether ether ketone)[8] and poly(ethylene terephthalate).[9] These modification procedures involve reactions at an interface between the solid polymer film and a solution that does not swell the polymer.

The heterogeneous (gas-solid) photochlorination of polymers is also of interest from the perspective that under certain conditions, the reaction is inherently surface-selective. Studies of photochlorination of polyethylene[10] and poly(4-methyl-1-pentene)[11] have been previously reported. The products, chlorinated polyethylene and chlorinated poly(4-methyl-1-pentene), are less permeable to gases (including chlorine) than the virgin polymers, so that under conditions in which chlorination is more rapid than permeation of chlorine into the polymer, a barrier layer of chlorinated polymer forms at the surface and slows bulk chlorination.

In the research studies reported here, heterogeneous (gas-solid) chlorination of poly(trifluoroethylene) (PF_3E) has been investigated (Scheme 3.1). It is conceivable that

117

the product, poly(chlorotrifluoroethylene) (PCTFE) that is a particularly good gas barrier, should lead to much greater surface selectivity than was observed for polyethylene[10] and poly(4-methyl-1-pentene).[11] Since PF$_3$E is completely soluble in several solvents (e.g. THF and methanol) and can be conveniently cast as a film or coating, it may serve as a practical precursor to PCTFE (or other fluoropolymers) for surface or coating applications. In addition to the chlorination studies, the gas fluorination of PF$_3$E has been studied to some extent in collaboration with the Fluorine Division of Air Products.
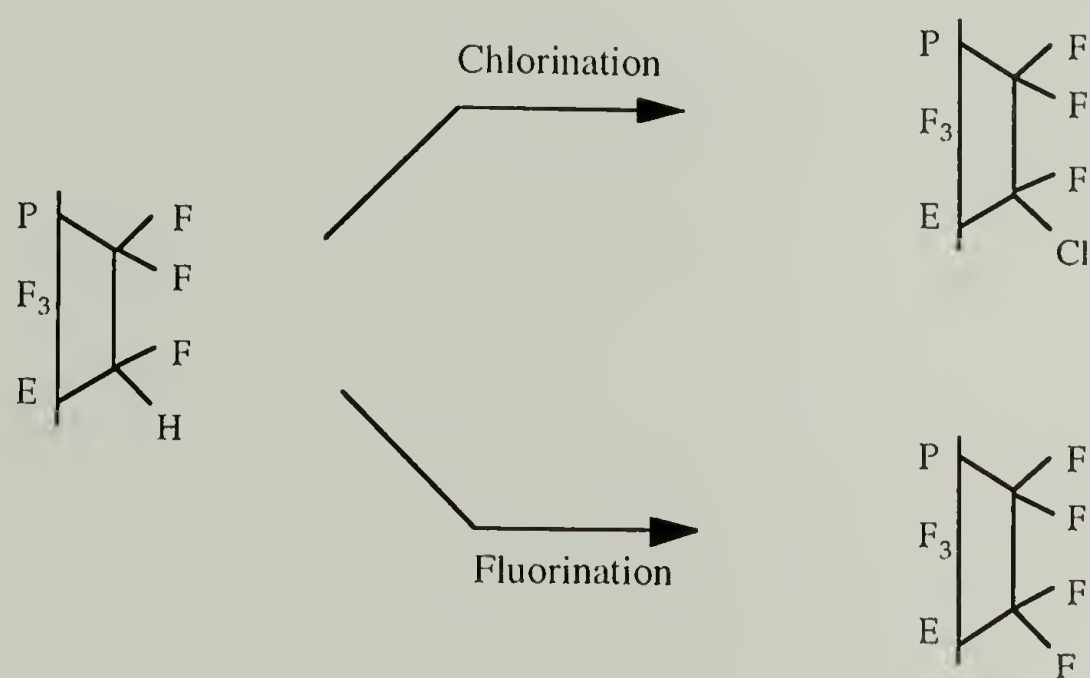
Scheme 3.1. Heterogeneous (gas-solid) surface modification of poly(trifluoroethylene).

Poly(trifluoroethylene)

Polytrifluoroethylene (PF$_3$E), one of the least studied fluoropolymers has recently gained more attention since it was discovered that copolymers of trifluoroethylene and vinylidene fluoride display piezoelectric, pyroelectric and ferroelectric properties over a wide range of composition.[12-14] This has stimulated a number of investigations involving the synthesis, properties, structure and morphology of this polymer.

Synthesis of Poly(trifluoroethylene)

Direct polymerizations (bulk or emulsion polymerization) of trifluoroethylene form polymers with significant regioirregular defects as a result of head-to-head and tail-to-tail addition of monomeric units during the free radical process. Cais et al. have proposed a synthetic route that yields isoregic PF_3E using reductive dechlorination or debromination of the precursor polymers, poly(bromotrifluoroethylene) or poly(chlorotrifluoroethylene).[15] ^{19}F NMR analysis indicates that the polymer products obtained are essentially isoregic with practically 100 % head-to-tail addition and free of reversed monomeric units within the polymer chain. Poly(trifluoroethylene) used in the studies was synthesized by the reductive dechlorination of poly(chlorotrifluoroethylene) (see Scheme 3.2). The reaction was conducted in tetrahydrofuran (THF) at 65 °C using azo(bisisobutyronitrile) (AIBN) as the initiator and tributyltin hydride (Bu_3SnH) as the reducing agent.
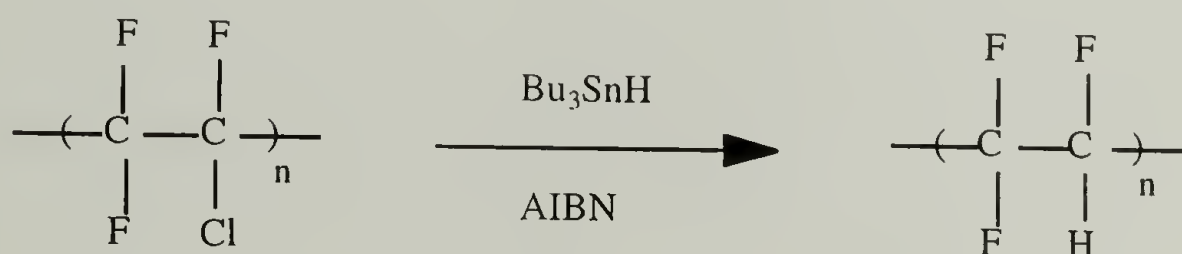
Scheme 3.2. Reductive dechlorination of poly(chlorotrifluoroethylene).

Physical Properties of Poly(trifluoroethylene)

The melting behavior of PF_3E reflects its thermal history, polydispersity and molecular weight. Essentially isoregic polymer with fairly high molecular weight and low polydispersity displays a sharp single endotherm ranging from 175 - 185 °C depending on crystallization temperature.[15] The glass transition temperature has been reported as 30 - 40 °C as determined by differential thermal analysis.[16] Even though this polymer is essentially atactic, the polymer chains are able to crystallize. The structure and morphology of PF_3E

have been investigated using X-ray and electron diffraction. The results indicate that variations in degree of isoregicity from 86 % to 98 % have no significant effect on the crystalline structure of polymer.[17] X-ray diffraction data reflect hexagonal packing of polymer chains. A diffuse meridional reflection observed at 2.29 Å, however, indicates a disordered conformation presumably caused by an irregular succession of TG, TG and TT groups. This distorted behavior also explains the large cross-sectional area of the polymer chains and their packing in a hexagonal lattice (a = 5.61 Å). Electron diffraction demonstrates an unusual single crystal structure with circular, lobed or cellulated habits.[17]

Surface Halogenation of Polymers

Gas-phase halogenations have been utilized as modification methods to improve surface properties of polymer films such as adhesion, wettability, gas permeation and barrier properties. A number of studies have been reported on polyethylene,[10,18-20] poly(4-methyl-1-pentene),[11,21] polystyrene,[19,22] polycarbonate,[22] polysulfone,[23] poly(methyl methacrylate)[22] and polystyrene/polybutadiene block copolymers.[24] Gas chlorination and fluorination are most commonly and used industrially due to their high rates of reaction. The halogenations are typical radical chain reactions; the kinetics are thus significantly effected by the reactivity of halogen radicals (fluorine > chlorine > bromine > iodine). The rates of bromination and iodination are found to be orders of magnitude slower than that of chlorination.[20]

Chlorination

Extensive studies of gas phase chlorination of polyethylene[10] and poly(4-methyl-1-pentene)[11] indicate that one can independently and simultaneously control the depth and density of chlorination of polymer surfaces by manipulating chlorination conditions: chlorine gas pressure, light intensity and exposure time.

Figures 3.1 and 3.2 show the results of gas chlorination of poly(4-methyl-1-pentene) (PMP) as a function of chlorine pressure for 2 min using ambient light and high-intensity UV light as light sources, respectively. The Cl/C ratio data indicate that the extent of chlorination (density of chlorine atoms on the polymer chain) is independent of pressure at chlorine pressures above 50 mm for ambient light conditions and at all pressures studied under UV light source. The mass increases, however, are highly dependent on chlorine pressure. A nonlinear pressure dependence of mass gain of samples chlorinated under UV light source suggests that a sufficient high chlorine content in the modified surface region exhibits barrier properties to chlorine gas. The dependence of mass uptake and the independence of XPS Cl/C ratio on chlorine pressure allow control of the thickness of the modified layer at a constant chlorine content.

The photointensity controls the rate of formation of chlorine radicals that initiate radical chain chlorination and thus the concentration of radical species in the film region that chlorine has diffused to during reaction. The higher the photointensity, the higher the probability that chlorine molecules diffusing into the film will react with polymer chain radicals rather than diffuse deeper into the film sample. Studies of the effect of light source intensity used for chlorination of PMP are illustrated in Figures 3.3 and 3.4. Compositions level at Cl/C ratios of 0.6, 0.8 and 1.1 for ambient, medium-intensity UV and high-intensity UV light, respectively. The data indicate that the chlorination in the dark is slower and has not leveled. Samples continue to gain mass with longer reaction times under all photointensity conditions, indicating that good gas barrier properties toward chlorine are not achieved under any conditions and reactions proceed deep into the bulk of the film. The differences in mass uptake rate, however, suggest that barrier properties are improved with increasing photointensity.
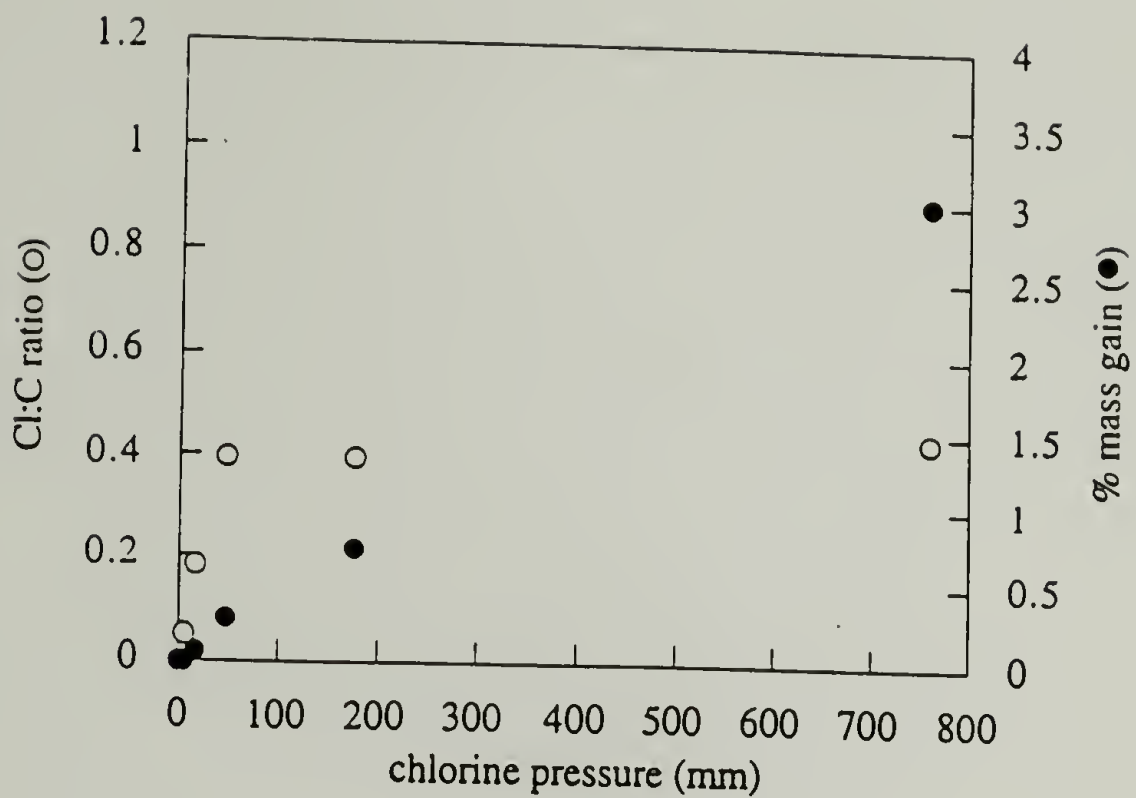
Figure 3.1. XPS and gravimetric data of chlorinated PMP using ambient light for 2 min.
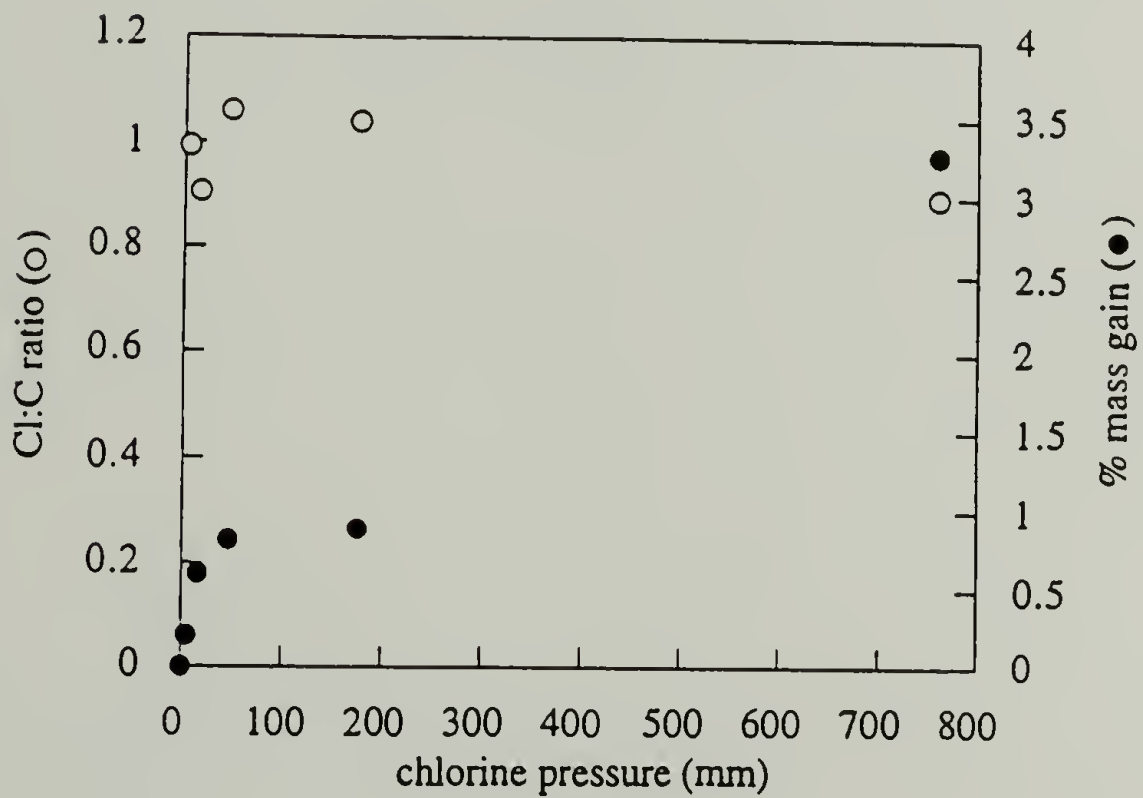
Figure 3.2. XPS and gravimetric data of chlorinated PMP using high-intensity UV light for 2 min.
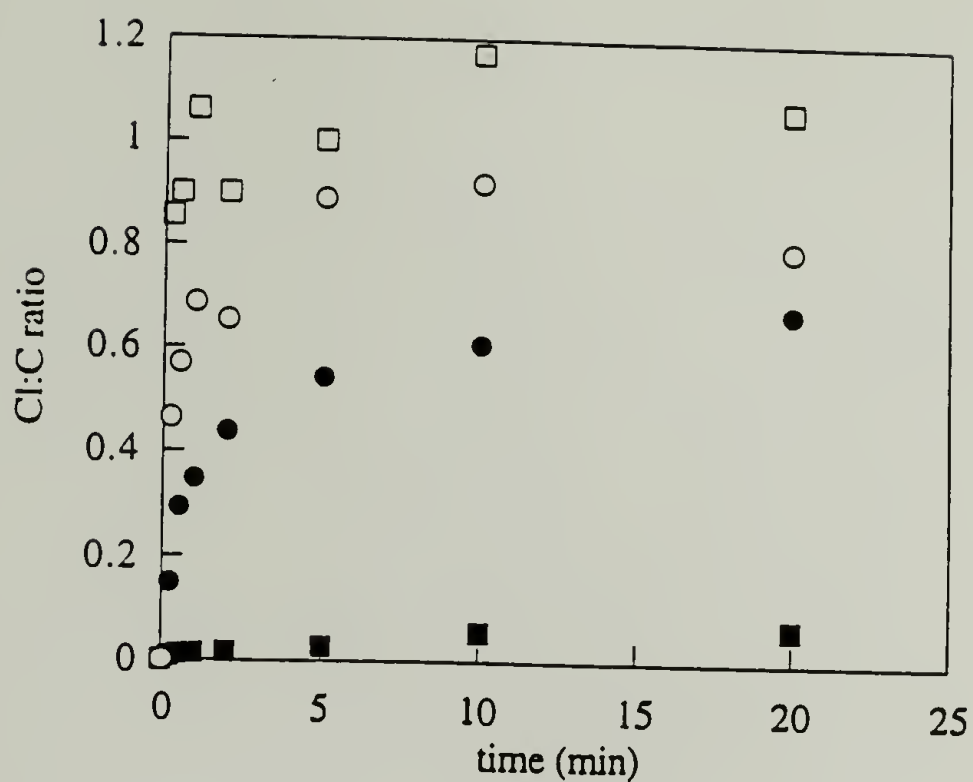
Figure 3.3. XPS data for chlorinated PMP using 1 atm chlorine pressure in the dark (■), in ambient light (●), in medium-intensity UV light (○) and in high-intensity UV light (□).
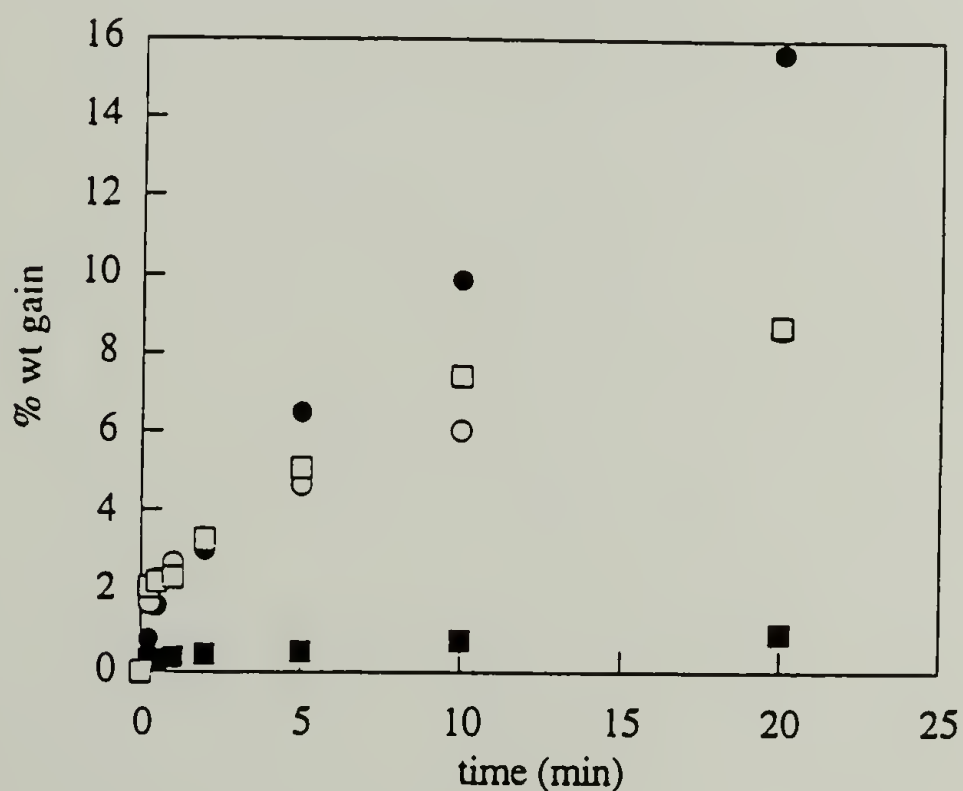
Figure 3.4. Gravimetric data for chlorinated PMP using 1 atm chlorine pressure in the dark (■), in ambient light (●), in medium-intensity UV light (○) and in high-intensity UV light (□).

The results obtained from chlorination of polyethylene demonstrate similar effects of chlorine gas pressure, light intensity and reaction time on the density and the depth of modification.[10] Greater light intensity increases the rate of chlorination and, as a result, the rate of diffusion of chlorine gas is decreased. The data also suggest that chlorination in the presence of light is more surface selective due to a decreased rate of chlorine diffusion through a highly chlorinated product. The gas permeability data for highly and deeply chlorinated PMP shows a significant decrease in gas permeability and improved selectivities (Tables 3.1 and 3.2).[11]

Table 3.1. Gas permeability data of highly and deeply chlorinated PMP compared to virgin PMP.

Sample	Permeability (10^{-9} cm^3(STP) cm/cm^2 ·s ·cmHg			
	Nitrogen (N_2)	Oxygen (O_2)	Carbon Dioxide (CO_2)	Hydrogen (H_2)
PMP	1.3	5.4	11.5	22.0
Chlorinated PMP	0.12	0.90	2.3	11.8

Table 3.2. Gas selectivity data of highly and deeply chlorinated PMP.

Sample	O_2/N_2	H_2/N_2	CO_2/N_2	CO_2/O_2	H_2/O_2	H_2/CO_2
PMP	4.1	16.5	8.6	2.1	4.1	1.9
Chlorinated PMP	7.3	95.9	18.9	2.6	13.1	5.1

<u>Fluorination</u>

Fluorination of hydrocarbon polymers originally became of interest since it is an inexpensive route to modify the properties of readily fabricated hydrocarbon polymers to resemble especially those of poly(tetrafluoroethylene) (PTFE). Extensive studies have been done on polyethylene to improve the barrier properties, adhesion and wettability. The permeability and selectivity of poly(4-methyl-1-pentene)[21] and polysulfone membranes[23] have been significantly improved by surface fluorination.

Fluorine reacts exothermically and rapidly with hydrocarbon polymers. In general, the direct gas fluorination of polymer surfaces is begun with a low concentration of fluorine gas (2 - 5 % diluted in an inert gas i.e. nitrogen, helium, or argon) to minimize the localization of released energy that may cause the structural degradation of polymer. The effect of diluting gas has been investigated.[25] Once the fluorination takes place, the progression of fluorination becomes increasingly difficult because the electron cloud of the fluorine substituent deactivates the adjacent hydrogen atoms and provides steric hindrance. For this reason, the fluorine gas concentration is then increased to maintain a practical reaction rate. Degradation and cross-linking have been observed with some reactions of polymers using high concentrations of fluorine gas. Polymer fluorination carried out in a plasma has been described as an alternative to overcome the deactivation problems.[26] The increased rate of fluorination was explained by the formation of several active species of fluorine, diluting gas, and the polymer surface itself.

The deactivation effect has been confirmed by studies of fluorination of poly(vinyl fluoride) and poly(vinylidene fluoride) using 10% F_2/N_2 (Figure 3.5). Sanderson et al. have shown that poly(vinyl fluoride) gained mass during fluorination with a very low rate of reaction, but no mass gain was observed for poly(vinylidene fluoride) under the same conditions.[25]
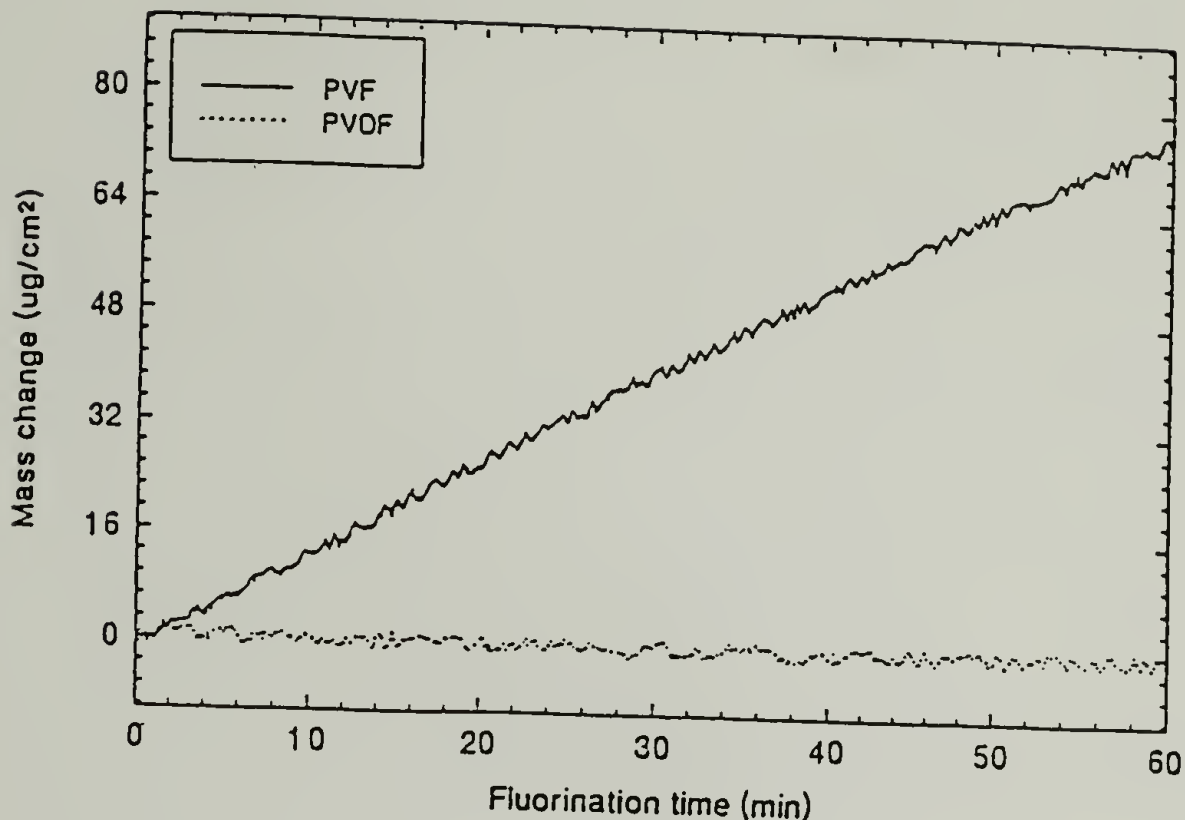
Figure 3.5. Fluorination of poly(vinyl fluoride) (PVF) and poly(vinylidene fluoride) (PVDF) at 50 °C in a thermobalance with 10% F_2/N_2.[25]

Adsorption of Polymers

Adsorption of polymers at interfaces is very important to many technologies [27-30] including coating, lubrication, adhesion and colloid stabilization. Theoretical and experimental work has been reviewed extensively on the adsorption of homopolymers and copolymers.[31,32] A typical polymer adsorption system consists of polymer, solvent and substrate. There are three types of interaction governing the adsorption of polymer to a surface: the polymer segment-surface interaction, the solvent-surface interaction and the polymer segment-solvent interaction. The difference between the polymer segment-surface interaction and the polymer segment-solvent interaction (Flory-Huggins χ parameter) is defined as the exchange free energy (χ_s). It is the energy needed for a polymer segment to adsorb to the surface by replacing a solvent molecule on the surface with a polymer segment. The adsorption, which is a thermodynamic process requiring a negative free energy change, can take place if the loss of configurational entropy upon adsorption is

compensated by the gain of enthalpy due to multiple polymer segment-surface interactions. In other words, the exchange free energy has to exceed a critical value (a critical exchange free energy, χ_{sc}) for the adsorption to occur. The polymer chains normally adsorb to the surface in the form of trains, loops and tails. The distribution of trains, loops and tails varies with polymer concentration and molecular weight.

The most widely accepted homopolymer adsorption theory that has been shown to agree well with experimental results was developed by Scheutjens and Fleer.[33,34] Based on a lattice model, the partition function for a mixture of polymer chains and solvent molecules is determined by assuming random mixing within the adsorption layer (the mean-field approximation). The probability of each possible polymer chain conformation (trains, loops and tails) can be generated. Scheutjens and Fleer's theory can predict the amount of adsorption, polymer segment distributions and the structure of the adsorbed polymer. This theory is, however, valid only in the dilute regime or in poor solvent conditions.

Polymer adsorption tendencies from good solvents are predicted by the scaling argument presented by de Gennes.[35] The correlations between polymer segments (self-avoidancy of segments) is taken into consideration. The uniform self-consistent potential that is assumed in Scheutjens and Fleer's theory cannot account for the swelling of polymer chains in good solvents or the overlapped polymer segments in concentrated polymer solutions. The scaling theory has been experimentally verified by a number of polymer adsorption studies.

Both theoretical and experimental studies have indicated that homopolymer adsorption can be enhanced by increasing the surface affinity (increasing the polymer segment-surface interaction) and/or decreasing solvent quality (decreasing polymer segment-solvent interaction).

Adsorption of Poly(trifluoroethylene)

The adsorption of polymer from solution was chosen as a way to fabricate very thin coatings of poly(trifluoroethylene) on Si wafer substrates. Since the polymer chains do not contain any specific functionality that can facilitate the adsorption to the surface, two approaches were proposed to promote the adsorption: (1) the addition of non-solvent or poor solvent to the polymer solution (dissolved in good solvent) to adjust the solvent quality and to increase the amount of adsorbed polymer, (2) the incorporation of polar functionality to the polymer backbone. Attempts to introduce polar functional groups to poly(trifluoroethylene) by radical grafting reactions of maleic anhydride (MAH) were carried out.

Maleation

Free radical grafting reactions of maleic anhydride are commonly used to introduce polar functional groups to commercial polymers such as polyethylene,[36-40] polypropylene,[41-43] ethylene-propylene copolymer,[44] polystyrene[45] and styrene-(ethylene-butylene)-styrene block copolymer.[46] Studies indicate significant improvement of interfacial adhesion[47] and compatibility.[48,49] Grafting reactions have been investigated in solution,[38,39,46] in the melt[39] and in the solid state.[37,43] The reaction carried out in the melt is a diffusion controlled process which is limited by high melt viscosity and results in crosslinked products with low grafting efficiency.[46] The addition of additives such as dimethylformamide (DMF) was suggested to eliminate the crosslinking problem.[39,40,43] Another drawback of grafting in the polymer melt is degradation, since the reaction has to proceed at a temperature higher than the melting point of the polymer. The maleic anhydride grafting in solution is more feasible, since the reaction can be carried out at lower temperatures with minimum crosslinking and degradation.

For a typical grafting reaction, the reaction proceeds via chain transfer to polymer chains. The termination step can be either disproportionation or coupling (which leads to

128

crosslinking). The extent of grafting, graft density and modified polymer structure are influenced by the grafting method as well as the grafting conditions. The effects of monomer concentration, initiator concentration, reaction time, reaction temperature and solvent on the percentage of grafting have been extensively investigated in several systems.

As reported by Sathe et al.,[41] the percentage of grafting onto polypropylene increases initially as a function of initiator concentration due to the increased amount of radical formed via initiator decomposition which leads to an increase in chain transfer and grafting. The increase is offset at higher initiator concentration by an increase in termination rate causing a maximum in grafting yield at an intermediate initiator concentration. A similar trend was observed on the effect of reaction temperature on the percentage of grafting. Higher temperature increases the rate of decomposition of initiator. The increase in radical concentration as well as the radical mobility can increase the percentage of grafting. Too high chain and radical mobility may also increase the probability of chain termination and decrease the grafting process. Studies of the effect of maleic anhydride concentration on grafting yield for polypropylene indicate that the grafting extent is more strongly influenced by the number of radical sites on polymer chains than the amount of maleic anhydride.[41] The yield of grafting remains unchanged after a sufficient amount of monomer has been consumed. No maleic anhydride homopolymer has been detected despite the excess amount of maleic anhydride monomer. This is due to the fact that the grafting process is more favorable than homopolymerization. In the absence of polymer, homopolymerization of maleic anhydride can take place as reported by Gaylord et al.[39] The percentage of grafting usually increases with time until all the radicals formed are consumed.[41] As evidenced by liquid chromatographic analysis of maleic anhydride grafted onto a styrene-(ethylene-butylene)-styrene triblock copolymer, a solvent (xylene in this case) that undergoes radical chain transfer can significantly reduce the rate and efficiency of grafting.[46]

Recently, radical grafting of maleic anhydride onto linear low density polyethylene (LLDPE) and poly(4-methyl-1-pentene) (PMP) in supercritical carbon dioxide (SC-CO$_2$) medium have been reported.[50] Maleic anhydride and a radical initiator are first infused into the polymers using SC-CO$_2$ and the reaction is subsequently thermally initiated. These modification reactions take advantage of the unique properties of supercritical fluid solvents - high diffusivity, zero surface tension and ease of removal. Maleated LLDPE and PMP (2 - 3 % maleation) prepared by this method contain a significantly higher number of anhydride groups than commercial maleated samples (<1% maleation) as analyzed by transmission infrared spectroscopy and elemental analysis. Analysis of maleated PMP by attenuated total reflectance spectroscopy (ATR IR) revealed that the maleation was a bulk modification with no surface selectivity.

Experimental

General Procedures

Poly(chlorotrifluoroethylene) (PCTFE) powder (3M Kel-F 81) was obtained from 3M and used as received without further purification. Azo(bisisobutyronitrile) (AIBN) from Aldrich was recrystallized from methanol prior to use. Tributyltin hydride (Bu$_3$SnH) was purchased from Aldrich and used as received. Tetrahydrofuran (Aldrich) was distilled under nitrogen from sodium/benzophenone. Heptane and hexane (both Fisher) were used as received for polymer purification. Chlorine gas (Aldrich, 99.5+ %) was used as received. Toluene (Fisher) was distilled under nitrogen from calcium hydride. Surface chlorinations were run on both sides of the film, controlling reaction time and light intensity (ambient light and a high-intensity UV light source (UVP Inc., Black-Ray B-100A, 6000 μW/cm^2 at 365 nm). Silica gel thin layer chromatography plates (TLC plates), purchased as Silica Gel 60A (K6F) from Whatman, were cut to size (3.0 x 6.5 cm) and conditioned in an oven (150 - 200 °C) overnight prior to use. Si wafers (1" diameter, 500 - 550 μm

thick, orientation <100>, resistivity of 70 - 130 ohm-cm, doped N/ND), purchased from International Wafer Service, were cleaned in 30 % H_2O_2 (30 % H_2O_2/H_2O) /H_2SO_4 for 30 min, rinsed thoroughly with water and dried under vacuum (0.01 mm, 24 h). Maleic anhydride, purchased from Fisher, was recrystallized from chloroform. Benzoyl peroxide (Aldrich) was recrystallized from chloroform/methanol. Carbon dioxide (Coleman grade) was purchased from Merriam Graves and used as received. X-ray photoelectron spectra (XPS) were obtained with a Perkin Elmer-Physical Electronics 5100 with Al K_α excitation (400 W, 15.0 kV). Spectra were recorded at two different take-off angles, 15° and 75° between the plane of the sample surface and the entrance lens of the detector optics. Atomic composition data were determined using sensitivity factors obtained from samples of known composition: F_{1s}, 1.000; C_{1s}, 0.201; O_{1s}, 0.522; Cl_{2p}, 0.580; Si_{2p}, 0.220. Attenuated total reflectance infrared (ATR IR) spectra were recorded using an IBM 38 FTIR at 4 cm^{-1} resolution with a 10 x 5 x 1 mm germanium internal reflection element (45°). Gravimetric measurements were made with a Sartorius 1612MP8-1 analytical balance. Dynamic advancing (θ_A) and receding (θ_R) contact angles were measured with a Rame'-Hart telescopic goniometer and a Gilmont syringe with a 24-gauge flat-tipped needle as the probe fluid was added to and withdrawn from the drop, respectively. Probe fluids used were water and hexadecane.

Synthesis of Poly(trifluoroethylene)

To a nitrogen-purged round-bottomed flask containing PCTFE powder (6.0 g, 51 mmol, M_n ~750,000) and a teflon-coated magnetic stir bar, Bu_3SnH (22 g, 76 mmol) in 112 ml THF solution was added followed by AIBN (1.2 g, 7.3 mmol) dissolved in 30 ml THF. The reaction mixture was then refluxed in an oil bath at 65 °C and stirred for 24 h. Additional AIBN (1.2 g) in THF (30 ml) was added after the reaction had proceeded for 12 h. The polymer was purified by precipitation 3 times using 150 ml THF/600 ml cold

hexane (in dry ice) and was extracted with heptane in a Soxhlet extractor for 24 h. The polymer was dried in a vacuum oven (0.01 mm, 75 °C, >24 h).

Preparation of Poly(trifluoroethylene) Films

Polymer films were cast from 4 % w/v of PF_3E in THF solution in a Petri dish (14 cm i.d.). The dish was covered with aluminum foil (with holes) to let the solvent slowly evaporate at room temperature overnight. The film was transferred from the dish by introducing water at the edge of the film. The water helps the film float from the bottom of the dish and it is easily peeled off. The film was laid on a square-shaped glass frame which allows both sides of the film to dry without touching to any surfaces in a vacuum oven (0.01 mm, 75 °C, >24 h).

Chlorination

All chlorination reactions were carried out in a secondary manifold connected to a vacuum manifold (Figure 3.6). Reactions under atmospheric chlorine pressure were carried out in the dark, using ambient light or a high-intensity UV light source which was placed at the base of an aluminum foil funnel below the sample container. For reactions that were run in the dark, the manifold was wrapped with a thick, black cloth. The sample vessel containing the tared samples, chlorine reservoir and secondary manifold were evacuated and refilled with nitrogen several times before each reaction. Chlorine gas (5 psig) was introduced after the last evacuation. The overpressure of chlorine gas in the manifold was depressurized through a bubbler to allow the pressure inside to equilibrate with the outside pressure. The reaction was stopped by evacuating the system and replacing the unreacted chlorine and product HCl with nitrogen. Samples were dried/degassed under vacuum (0.01 mm, room temperature, >24 h).

to vacuum/nitrogen

sample container

chlorine reservoir

water trap

chlorine gas tank
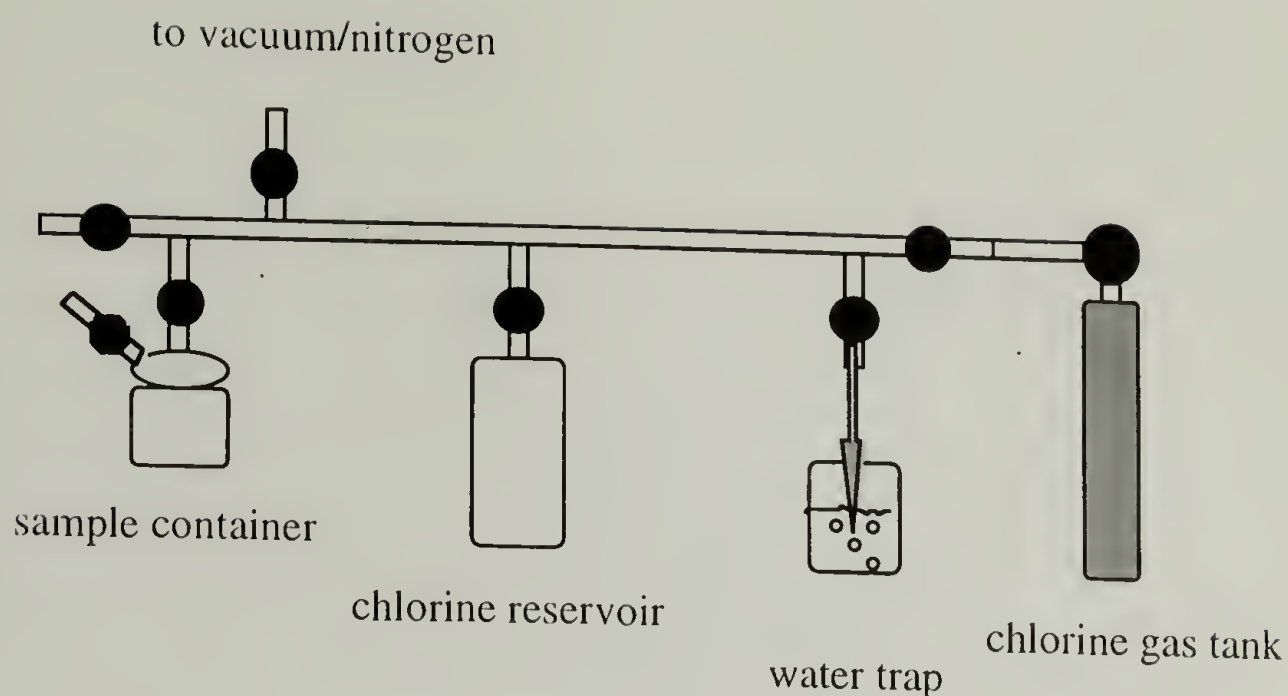
Figure 3.6. A secondary manifold used for gas chlorination.

Gas Permeation Measurements

Gas permeation studies were run one gas at a time with hydrogen and nitrogen at 40 °C with an upstream pressure of 6 atm (3.5 atm for hydrogen) and a downstream pressure of 0 atm. After reaching a steady-state flux of gas, a pressure increase of 0.50 mm in a known volume on the downstream side was timed. A home-built pressure/vacuum manifold (Figure 3.7) was built around a Millipore 25 mm membrane cartridge (25 mm diameter) and a Celesco DP 31 differential pressure transducer. The rate of gas permeation for PF_3E and chlorinated PF_3E were calculated as previously described.[51]

Maleation of Poly(trifluoroethylene) in Supercritical Carbon Dioxide

A PF_3E sample (0.4 g, 4.9 mmol) was placed in a stainless steel, high pressure vessel that was machined from hexagonal stock (4" long x 7/16" i.d.) and fitted with a 5000 psi Omega pressure gauge and needle valve on one end and a NPT plug on the other end. Maleic anhydride (MAH) (0.2 g, 2.0 mmol) and benzoyl peroxide (BPO) (0.08 g, 0.3 mmol) were also added into the vessel which was then put in an ethylene glycol/water bath (60 °C) before it was filled with approximately 5.8 g of carbon dioxide (2500 psi).

133

The reactants were allowed to soak at 60 °C for 4 h before transferring the vessel to a silicone oil bath (125 °C) for 4 h. The vessel was quenched in cold, running water immediately after removal from the high temperature bath. The carbon dioxide was released in the hood.
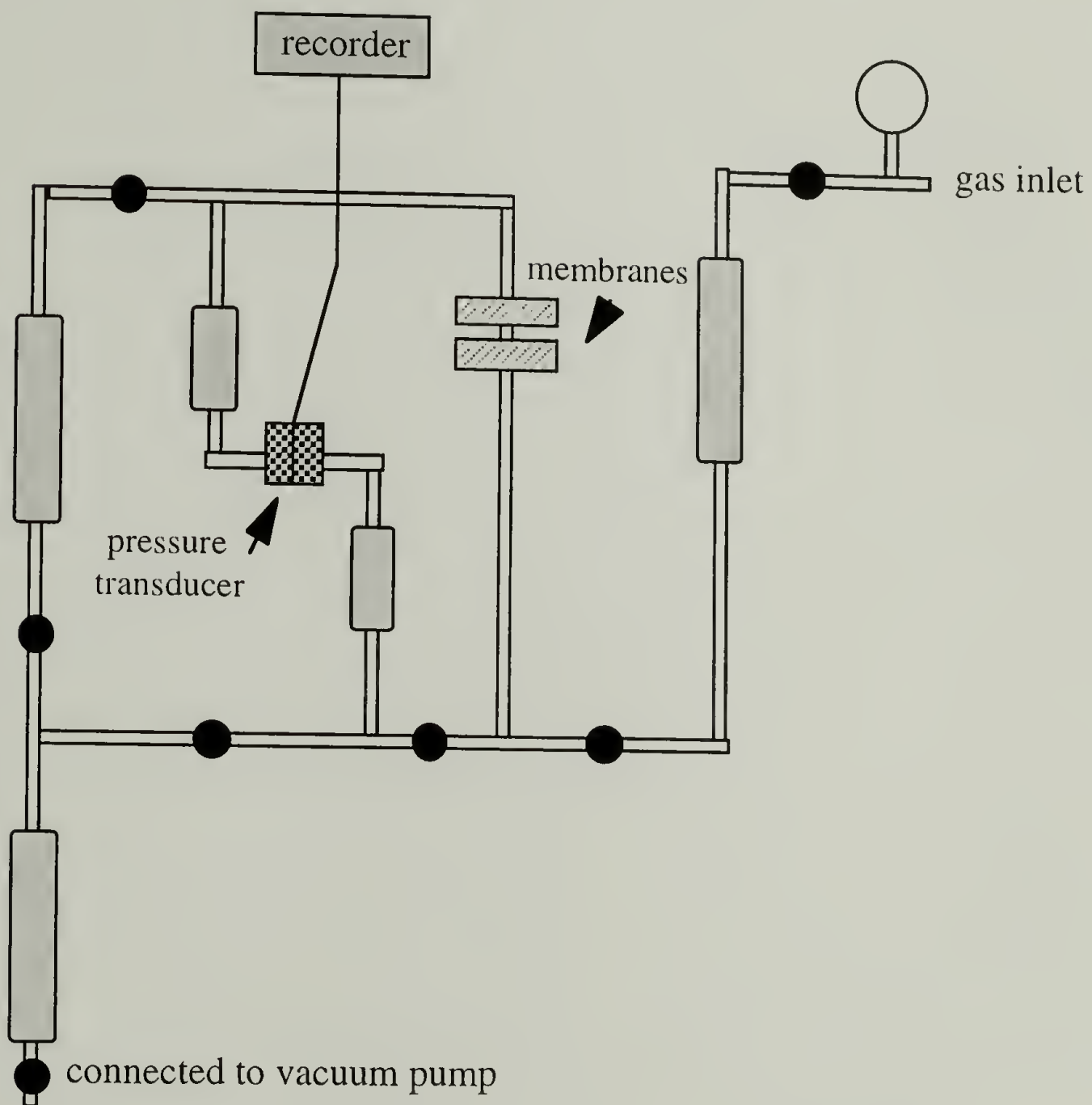
Figure 3.7. Gas permeation apparatus.

Adsorption Studies of Poly(trifluoroethylene)

Thin Layer Chromatography (TLC). TLC was carried out by applying 30 µl of polymer solution (5 mg/ml) as a circular spot of diameter 2-3 mm using a 10 µl microsyringe. The spots were 1.5 cm from the bottom of the plate. Elution was carried out in a filter-paper-lined TLC tank filled to 0.5 cm depth with eluent. The TLC plates were equilibrated for 5 min in the tank before elution. The solvent front was allowed to proceed 5 cm from the level of the spots. The TLC plates were air-dried in the hood for 15 min after elution and then developed under iodine vapor for 15 - 30 min. The results were viewed as dark spots in a fluorescent background under a UV lamp ($\lambda = 254$ nm). R_f values are reported in the standard way where R_f = elution distance of sample/elution distance of eluent.

Adsorption of Poly(trifluoroethylene) and Maleated Poly(trifluoroethylene). To a nitrogen-purged, jacketed Schlenk tube containing cleaned Si wafers, 50 ml of a polymer solution (1.0 - 3.0 mg/ml) dissolved in THF or THF:toluene mixture (25:75, 50:50, 75:25 v/v) was selected. Polymer solutions in THF:toluene mixtures were made by the addition of the desired amount of toluene to a homogeneous solution of polymer in THF. All adsorptions were carried out at 25 °C (temperature was adjusted using a circulator connected to the jacketed Schlenk tube). After the desired adsorption time, the solution was removed and the Si wafers were washed (3 x 50 ml) with the same solvent mixtures (THF or THF:toluene mixtures) used for adsorption. The Si wafers were then dried (0.01 mm, room temperature, >24 h).

Results and Discussion

Synthesis and Characterization of Poly(trifluoroethylene)

The synthesis of PF_3E was carried out by the reductive dechlorination of poly(chlorotrifluoroethylene) (Scheme 3.2). This radical reaction was conducted in tetrahydrofuran at 65 °C employing azo(bisisobutyronitrile) as the radical initiator and tributyltin hydride as the reducing agent. An excess molar ratio (50-100 %) of tributyltin hydride which is the hydrogen atom source was used to assure complete dechlorination. This can be confirmed by the absence of the 950 cm^{-1} absorbance assigned to the C-Cl vibration in the infrared spectrum (Figure 3.8). These conditions render a yield of approximately 80-85 %. Polymer films prepared by solution casting from 4% w/v of PF_3E/THF solution have a thickness of about 40 μm. The films are transparent, colorless, flexible and easily drawable. The stoichiometry of PF_3E product deduced from quantitative XPS (75° take-off angle) is C_2F_3 (C = 39.20%, F = 60.54%, O ~ 0.20%, Cl ~ 0% and Sn ~ 0%). This indicates complete dechlorination and the complete removal of residual tin compounds (Bu_3SnCl and unreacted Bu_3SnH) (See XPS survey spectum in Figure 3.9). The C_{1s} region of the XPS spectrum of PF_3E consists of two peaks. The lower binding energy peak corresponds to the carbons bound to one hydrogen and one fluorine and the other peak is assigned to carbons bound to two fluorines.

The cast PF_3E film exhibits contact angles (θ_A/θ_R) of 96°/73° (water) and 25°/11° (hexadecane). Gel permeation chromatography (GPC) analysis yields weight average molecular weight (M_w) of approximately 750,000 with a polydispersity of 1.5. Melting temperature (T_m) of the polymer was analyzed by differential scanning calorimetry (DSC, using a 10 °C/min heating rate, under nitrogen in the range of room temperature to 250 °C). The result in Figure 3.10 indicates a melting temperature of ~179 °C. The glass transition temperature (T_g), which was expected to be in the range of 30-50 °C was not observed by DSC analysis.

136

Wavenumbers
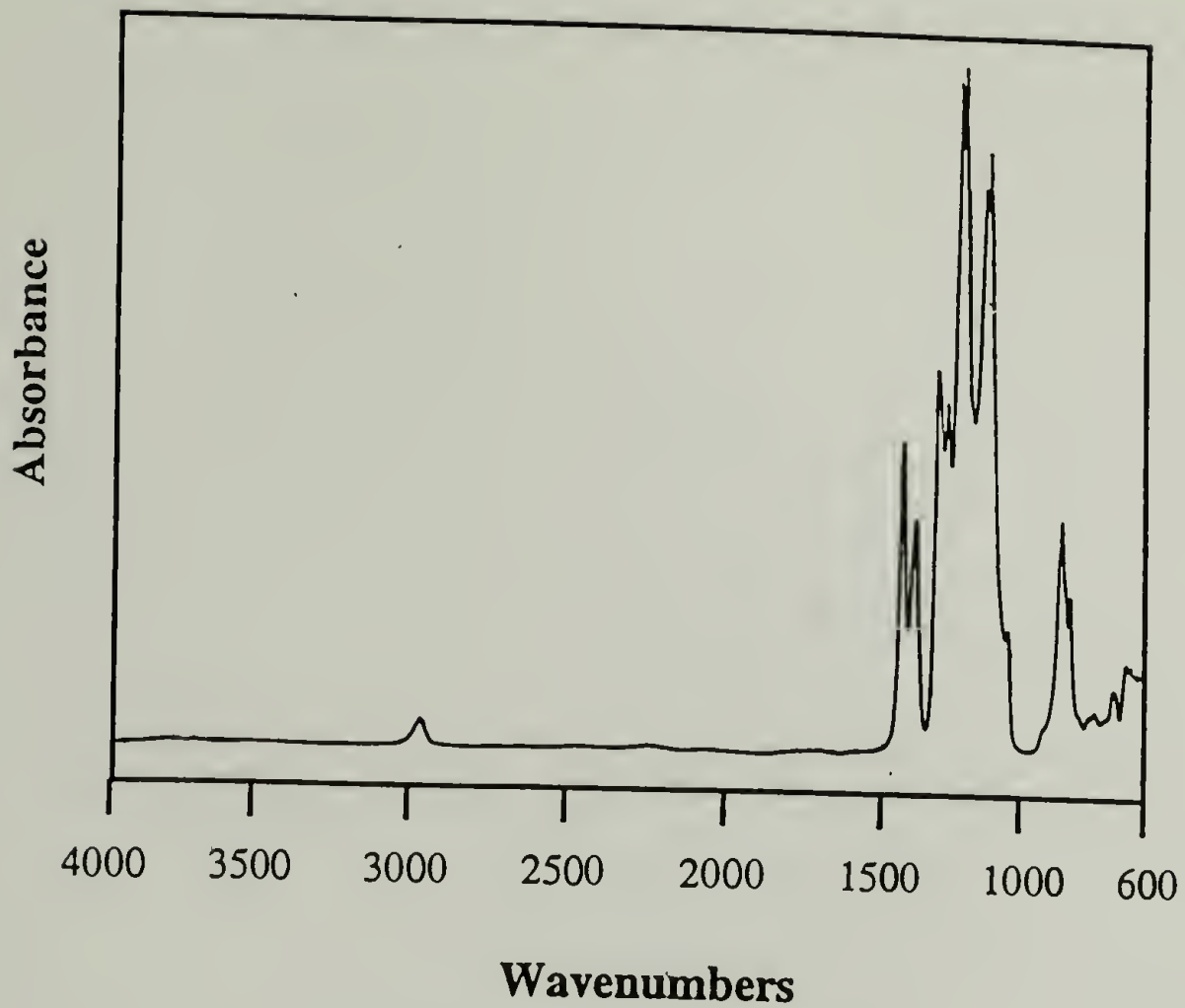
Figure 3.8. Infrared spectrum of poly(trifluoroethylene).

Binding Energy (eV)
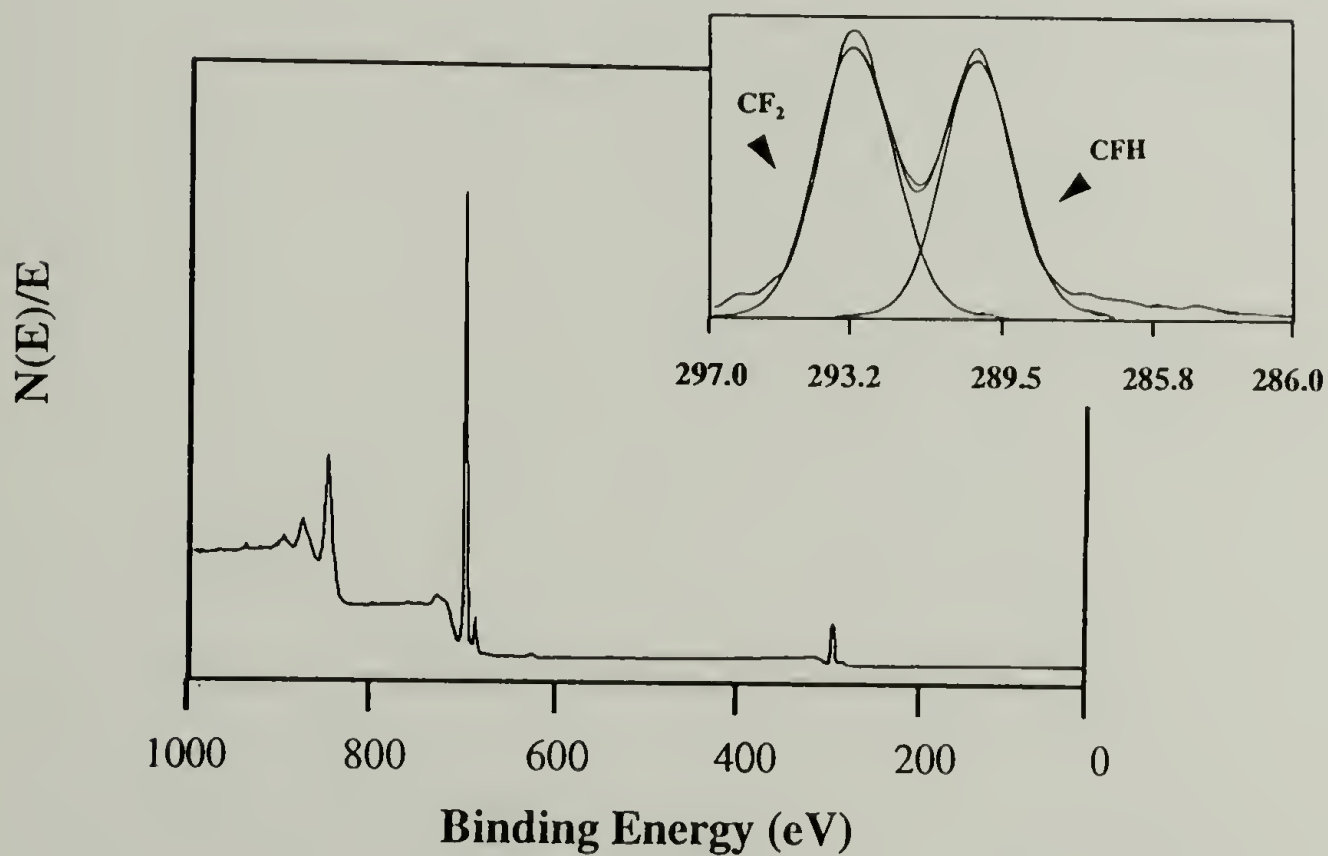
Figure 3.9. XPS survey and C_{1s} spectra of PF_3E film analyzed using 75° take-off angle.

PF$_3$E is thermally stable up to 350 °C, as indicated by thermal gravimetric analysis (TGA, 20 °C/min heating rate). Figure 3.11 indicates that only 0.1 % weight loss occurs when the temperature is raised from 250 °C to 350 °C.

The degree of crystallinity of PF$_3$E was estimated using an analysis of wide angle X-ray scattering (WAXS) data. Scattering intensity as a function of scattering angle (2θ) for PF$_3$E is displayed in Figure 3.12. Cu K$_\alpha$ (λ = 1.5418 Å) radiation with a Ni filter was used. The degree of crystallinity can be estimated from Equation 3.1:

$$\text{Degree of Crystallinity} \quad = \quad \int I_{crystalline} \, (s^2) \, ds / \int I_{total} \, (s^2) \, ds \qquad (3.1)$$

where s = 1/d = 2sinθ/λ and s and d are the scattering factor and the crystalline spacing, respectively. To obtain the degree of crystallinity of PF$_3$E, the data in Figure 3.12 was replotted into the curve as shown in Figure 3.13. The ratio between the area under the curve above the baseline ($\int I_{crystalline} \cdot s^2 \, ds$) and the total area under the curve ($\int I_{total} \cdot s^2 \, ds$) yields ~45% crystallinity. An identical diffraction pattern was obtained from the film sample rotated 90° from the original alignment indicaing that there are no specific orientations induced in the polymer film during the fabrication process.

Chlorination of Poly(trifluoroethylene)

Two series of photochlorination reactions were carried out at atmospheric chlorine pressure using ambient light and high-intensity UV light source. Kinetics of chlorination was studied by XPS as shown in Figure 3.14. The slow increase of Cl/C ratio with exposure time using ambient light indicates that the chlorination proceeds very slowly with low yield (only 3% Cl after 100 min reaction). The chlorination using a high-intensity UV light occurs faster and results in a more densely chlorinated modified layer. Under these conditions, the Cl/C ratio reaches a limiting value of ~0.45 (PCTFE exhibits a Cl/C ratio of 0.5) after 10 min of chlorination (Figure 3.14). This indicates that there is approximately

138
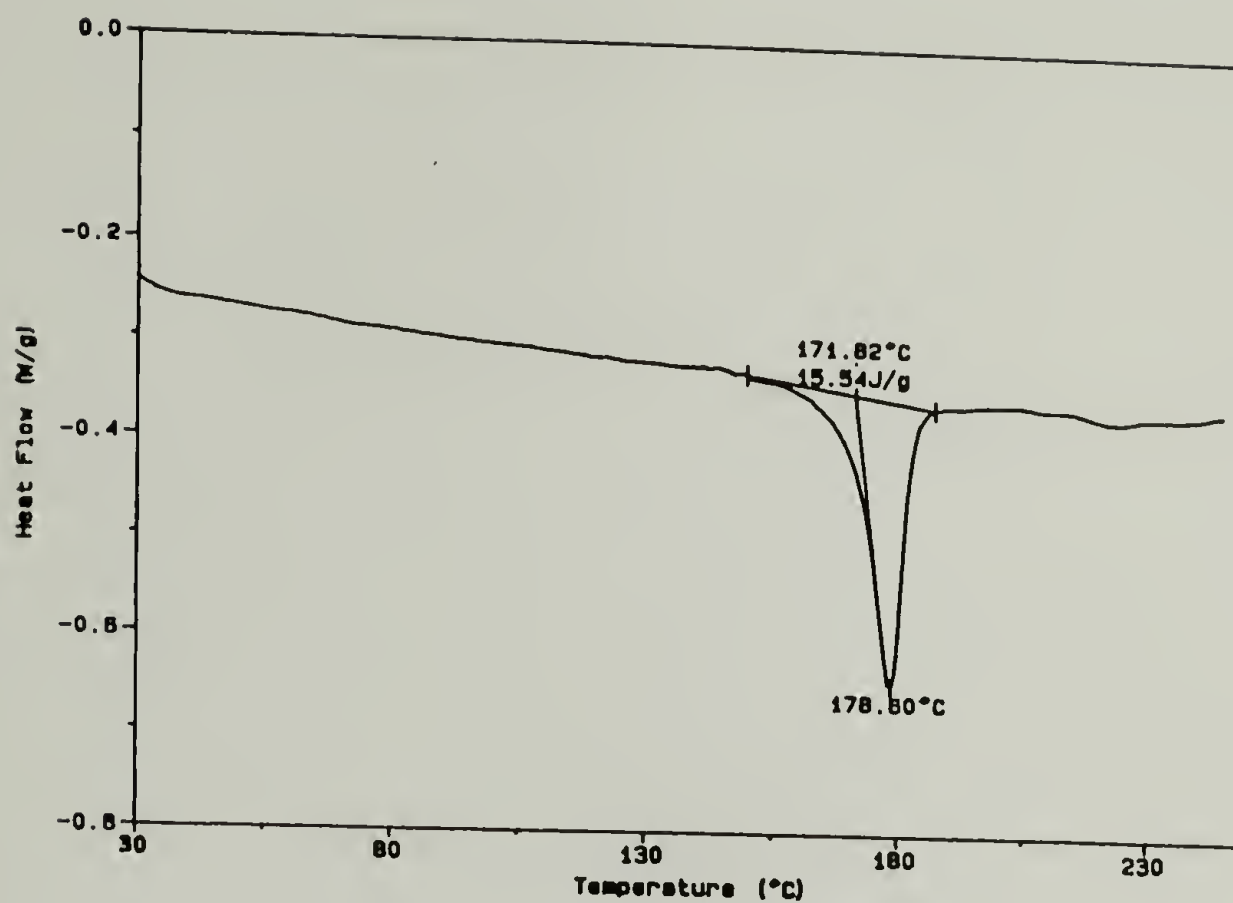
Figure 3.10. Differential scanning calorimetry profile of poly(trifluoroethylene).
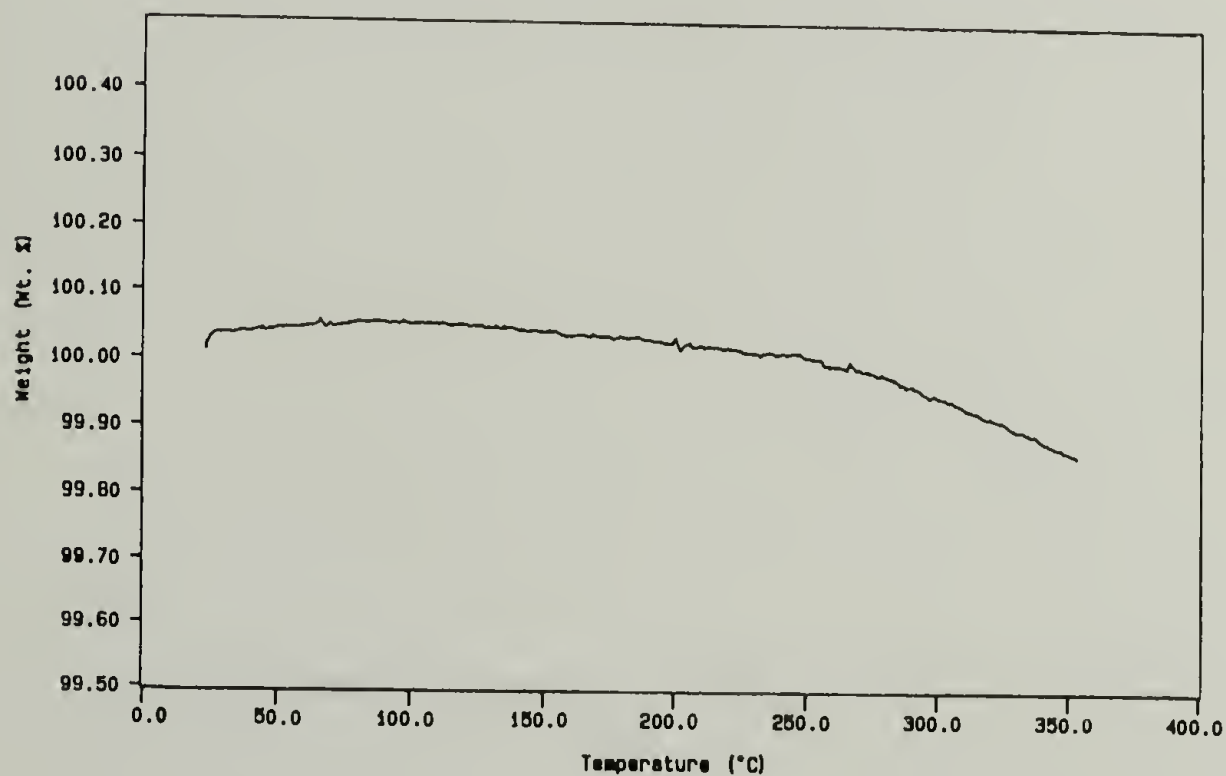
Figure 3.11. Thermal gravimetric analysis data of poly(trifluoroethylene).
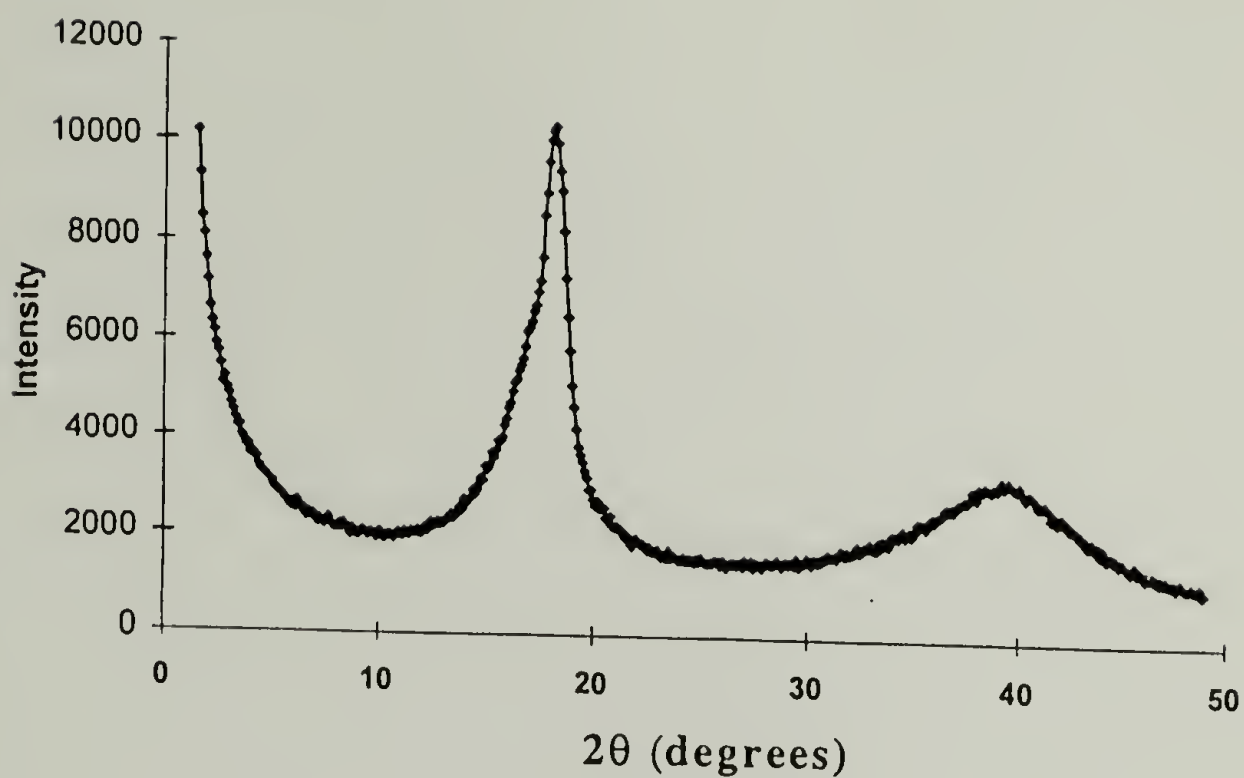
Figure 3.12. Plot of diffraction intensity (I) as a function of scattering angle (2θ) obtained from WAXS analysis of PF_3E film.
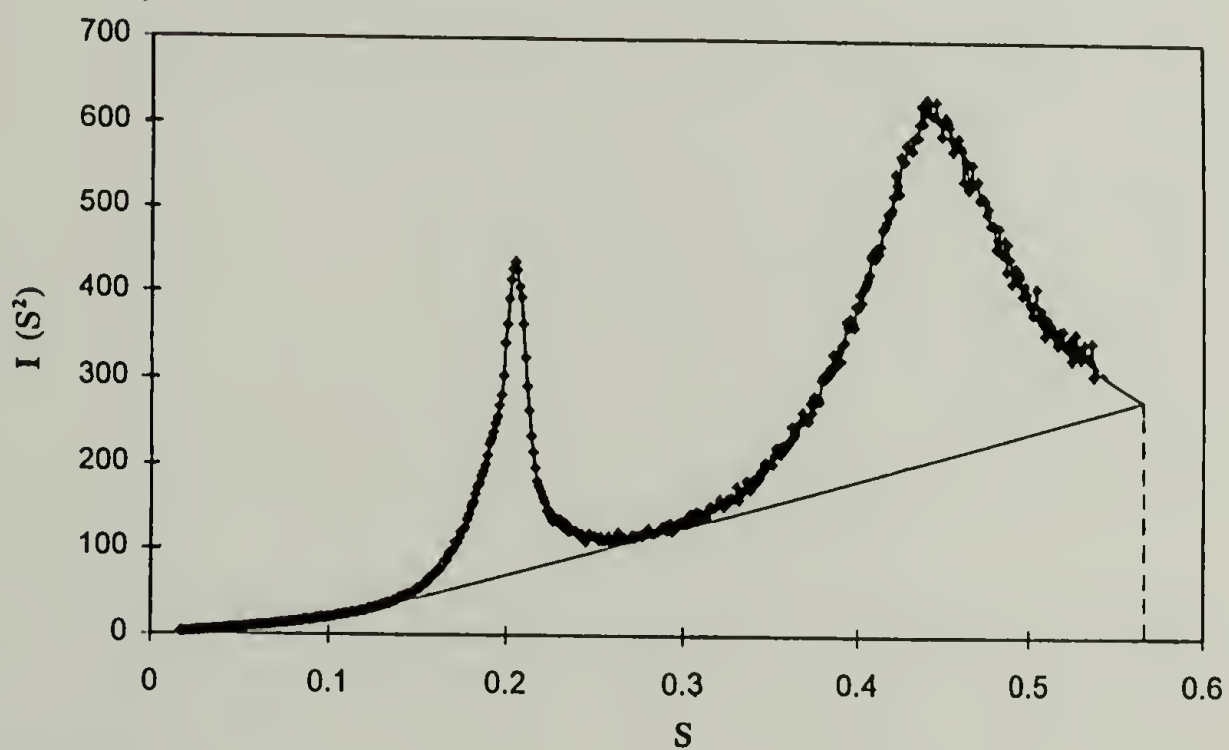
Figure 3.13. Plot of I (s^2) as a function of scattering factor (s) calculated from the plot in Figure 3.12 using $\lambda = 1.5418$ Å.

1 chlorine per repeat unit of PF_3E and the similarity between data recorded at 15° and 75° take-off angles indicates that there is little or no surface selectivity in the XPS sampling region (within the outer ~40 Å) and that the chlorination proceeds throughout the XPS sampling depth. Figure 3.15 shows XPS survey and C_{1s} region spectra for a PF_3E film chlorinated using the UV light for 150 min. The C_{1s} peak appears as a broad spectrum which is a combination of carbons from CF_2 and $CFCl$. Variable small amounts (1-2 %)[52] of oxygen are observed in product films (seen in Figure 3.15); this is attributed to termination of the radical chain reaction by adventitious oxygen. The chlorinations were also attempted in the dark without using any light source. There was no significant amount of chlorine (< 0.1%) detected by XPS analysis of PF_3E chlorinated in the dark after 20 min of exposure time. These results demonstrate a significant effect of photointensity on the extent of chlorination. The photointensity influences the rate of chlorine radical formation that initiates radical chain chlorination and the concentration of radical species in the polymer film.

ATR IR spectra for PF_3E samples photochlorinated using a UV light are shown in Figure 3.16. The C-Cl stretching band (1000-900 cm⁻¹) of chlorinated PF_3E increases in intensity with longer reaction time up until ~100 min reaction after which time no further increase in intensity is observed. C-H bending (1400-1350 cm⁻¹) was observed in all samples indicating that the ATR IR sampling depth (~1 μm) was not completely reacted. Comparison of transmission IR with ATR IR spectra indicates that the chlorination of PF_3E is surface selective. ATR IR spectra exhibit stronger C-Cl stretching bands than those in transmission spectra (Figure 3.17) for samples chlorinated for the same period of time. Kinetics determined using transmission IR indicate that the reaction stops after ~100 min. Transmission spectra of 100 min and 150 min chlorinated samples are superimposable.

The absorbance due to C-Cl stretching normalized to the absorbance of C-F stretching (1200-1100 cm⁻¹) are plotted as a function of reaction time for chlorinated samples analyzed by both ATR IR and transmission IR (shown in Figure 3.18). The ratios
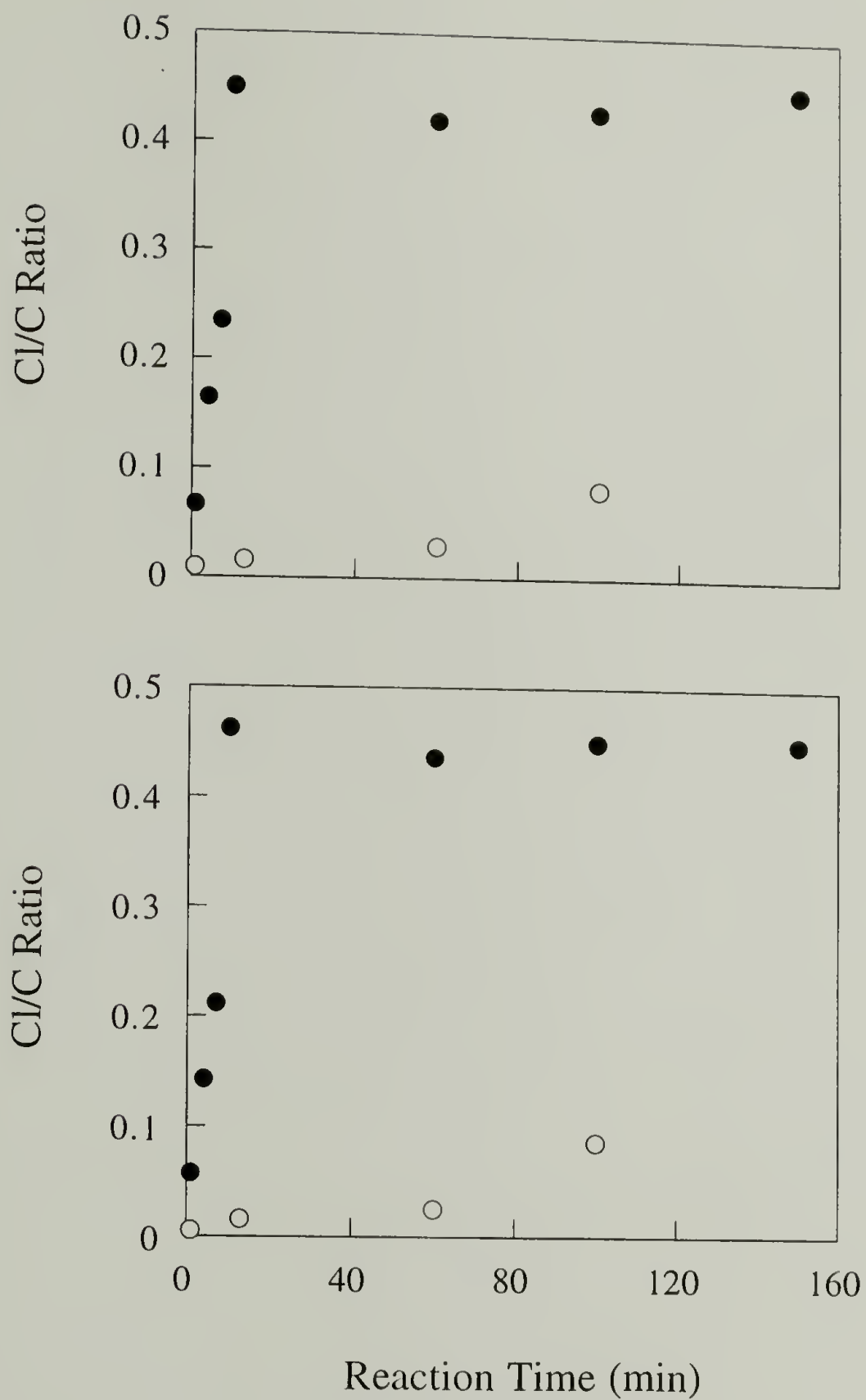
Figure 3.14. XPS Cl/C ratio of chlorinated PF_3E using ambient light (O) and high-intensity UV light (●) obtained from 15° take-off angle data (top), 75° take-off angle data (bottom).
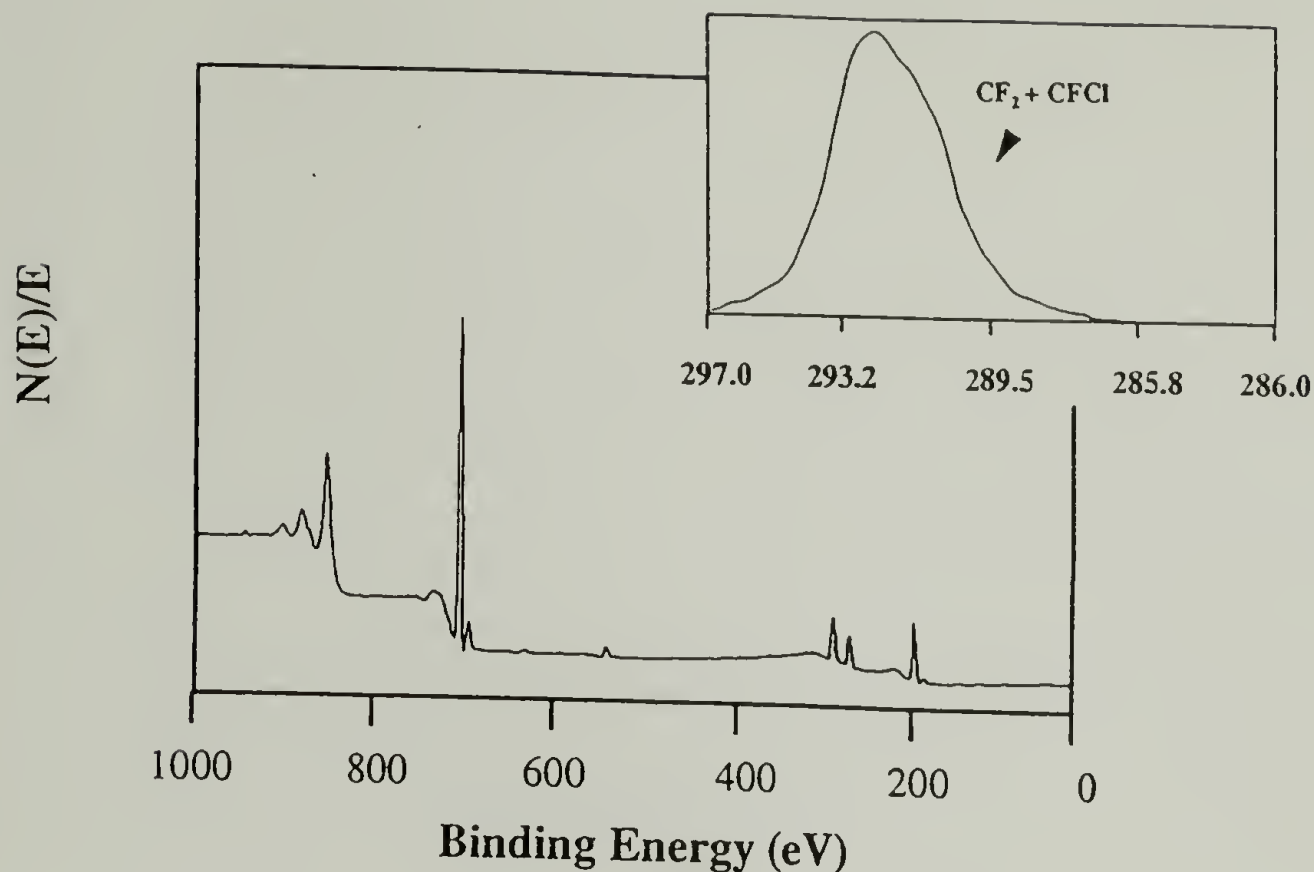
Figure 3.15. XPS survey and C_{1s} spectra of PF_3E film chlorinated for 150 min using UV light source analyzed using 75° take-off angle.

The absorbance due to C-Cl stretching normalized to the absorbance of C-F stretching ($1200\text{-}1100$ cm^{-1}) are plotted as a function of reaction time for chlorinated samples analyzed by both ATR IR and transmission IR (shown in Figure 3.18). The ratios obtained from ATR IR and transmission IR reach their plateau values after 100 min reaction time. This suggests that under these reaction conditions, a barrier layer of chlorinated PF_3E (PCTFE) is formed and inhibits permeation of chlorine gas to greater depth. The better barrier properties of chlorinated PF_3E compared to PF_3E can be quantified by gas permeation and results of these experiments are shown in Table 3.3. The permeability of nitrogen and hydrogen gases through the films were measured at 40 °C (higher than T_g of PF_3E).

There is no clear trend of gravimetric data as a function of extent of chlorination. The mass increase varies in the range of 1-3 %.[52] Despite the inconsistent mass increase of
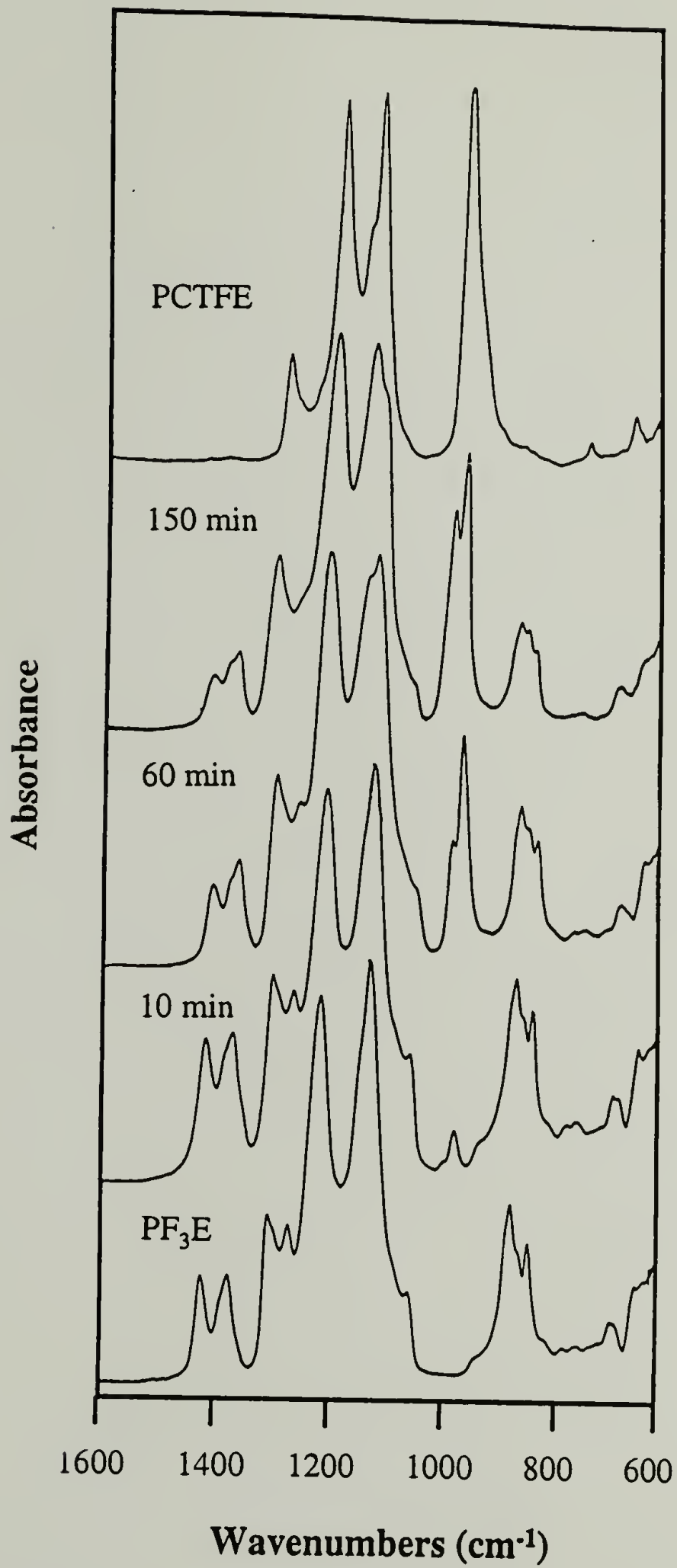
Figure 3.16. ATR IR spectra of chlorinated PF_3E prepared by using high-intensity UV light.

144
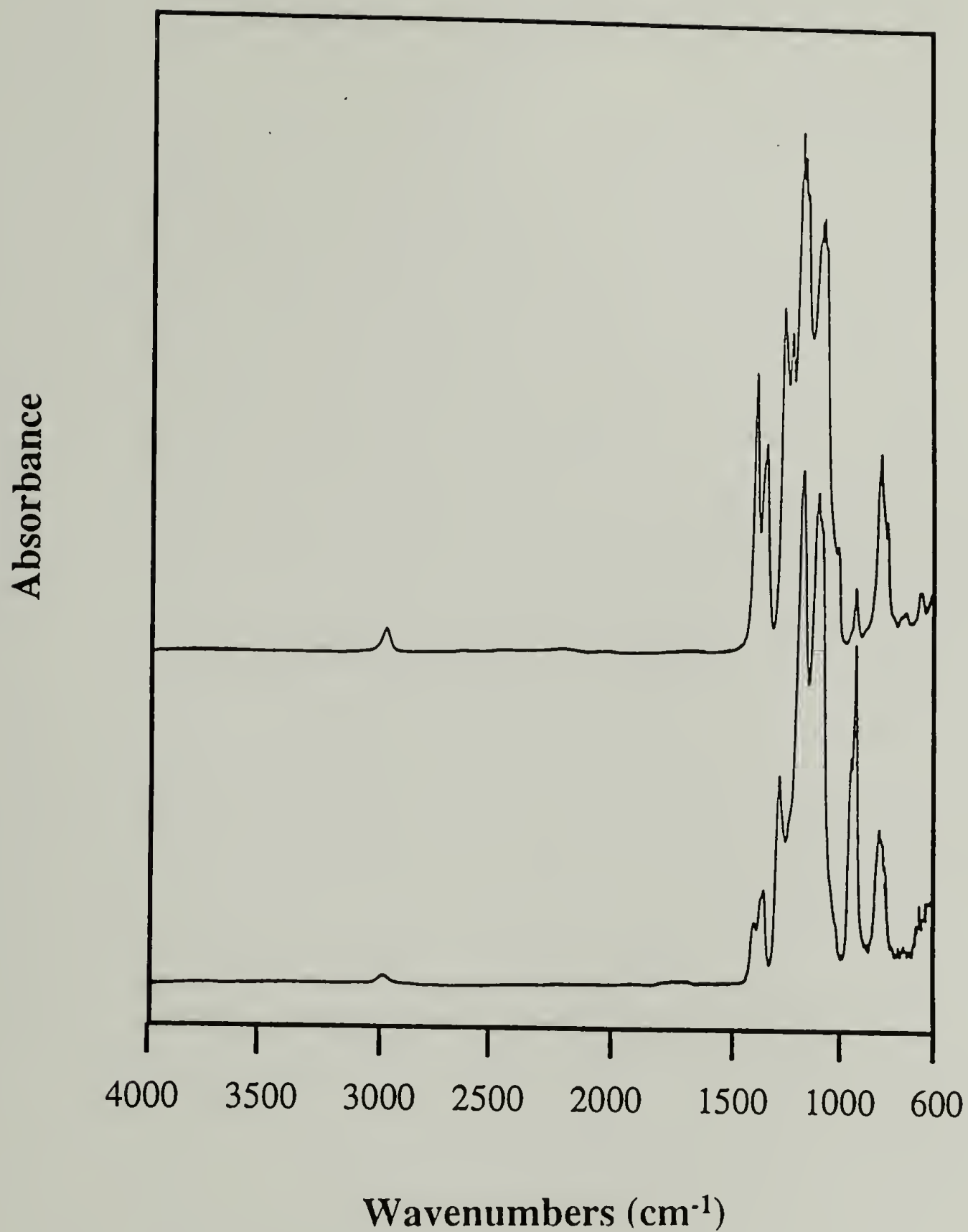
Figure 3.17. Transmission (top) and ATR IR (bottom) spectra of chlorinated PF$_3$E prepared by using high-intensity UV light for 100 min.
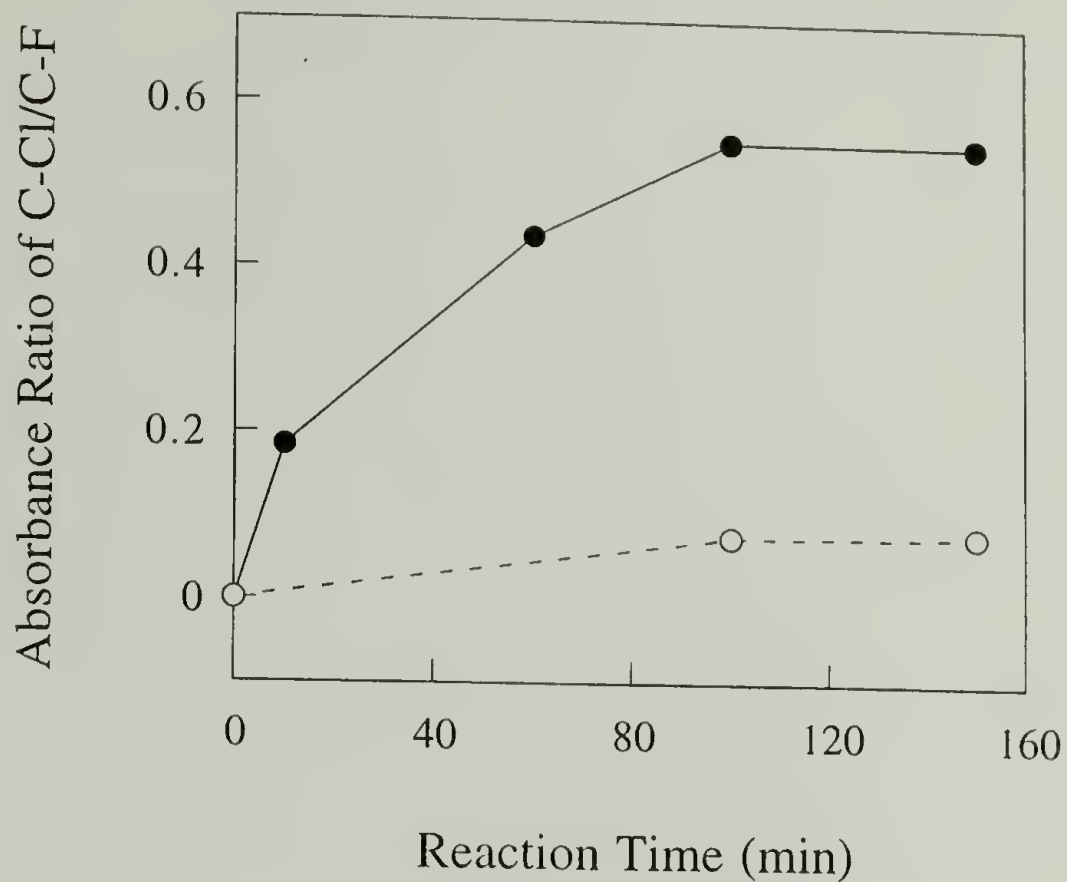
Figure 3.18. C-Cl/C-F absorbance ratio from ATR IR (●) and transmission IR (○) of chlorinated PF$_3$E prepared using high-intensity UV light as a function of reaction time.

Table 3.3. Gas permeability data of PF$_3$E and 100 min chlorinated PF$_3$E.

Sample	Permeability $(10^{-9}$ cm^3(STP) cm/cm^2 ·s ·cmHg)		Selectivity of H$_2$/N$_2$
	Nitrogen (N$_2$)	Hydrogen (H$_2$)	
PF$_3$E	4.2 x 10^{-2}	1.3	30.9
100 min chlorinated PF$_3$E	9.2 x 10^{-3}	0.6	65.2

146

chlorinated PF_3E, these data are in marked contrast to the results observed for polyethylene[10] and poly(4-methyl-1-pentene);[11] significant mass changes (2-16 %) were observed for these less surface-selective chlorinations. The relatively low gas permeability of PF_3E is another factor that renders high surface selectivity of chlorination. At 40 °C, PF_3E is 30 times less permeable to nitrogen gas than is poly(4-methyl-1-pentene) (See Table 3.1). The hexadecane contact angle (θ_A/θ_R) decreases from 25°/11° for PF_3E to 9°/2° for 150 min chlorinated PF_3E which is close to the 8°/2° values for PCTFE. This implies that chlorinated PF_3E film has surface properties similar to PCTFE.

Fluorination of Poly(trifluoroethylene)

Gas fluorination studies were carried out in collaboration with the Fluorine Division of Air Products. The fluorine concentration used for fluorination was 5% fluorine gas diluted in nitrogen gas. The reaction time was varied from 15 to 300 min. Kinetics of fluorination was studied using XPS (Figure 3.19). XPS F/C ratios of ~2 were obtained for all fluorinated PF_3E samples indicating that the reaction proceeds rapidly and reaches the XPS sampling depth (40 Å) within the first 15-30 min of reaction. These conditions render complete fluorination of the surface as indicated by the stoichiometry (C_2F_4).[52] There is no surface selectivity in the XPS region as shown by the similarity of F/C ratio data obtained at 15° and 75° take-off angles.[52] The gravimetric data displayed in Figure 3.20 indicate the apparent tendency for mass increase at longer reaction times, unlike the chlorination. The rate of mass increase, however, appears to slow after 120 min of reaction. Mass gain increases from 0.1% at 60 min to 0.3% at 120 min and to 0.5% at 300 min. This implies that the fluorinated layer becomes a better barrier as more polymer is fluorinated.

The 15 min fluorinated film showed a slight weight loss which is in the order of error.[52] All fluorinated films remain transparent (no appearance of crystalline domains). Interestingly, the fluorinated films become non-stick (do not stick to the glass wall of
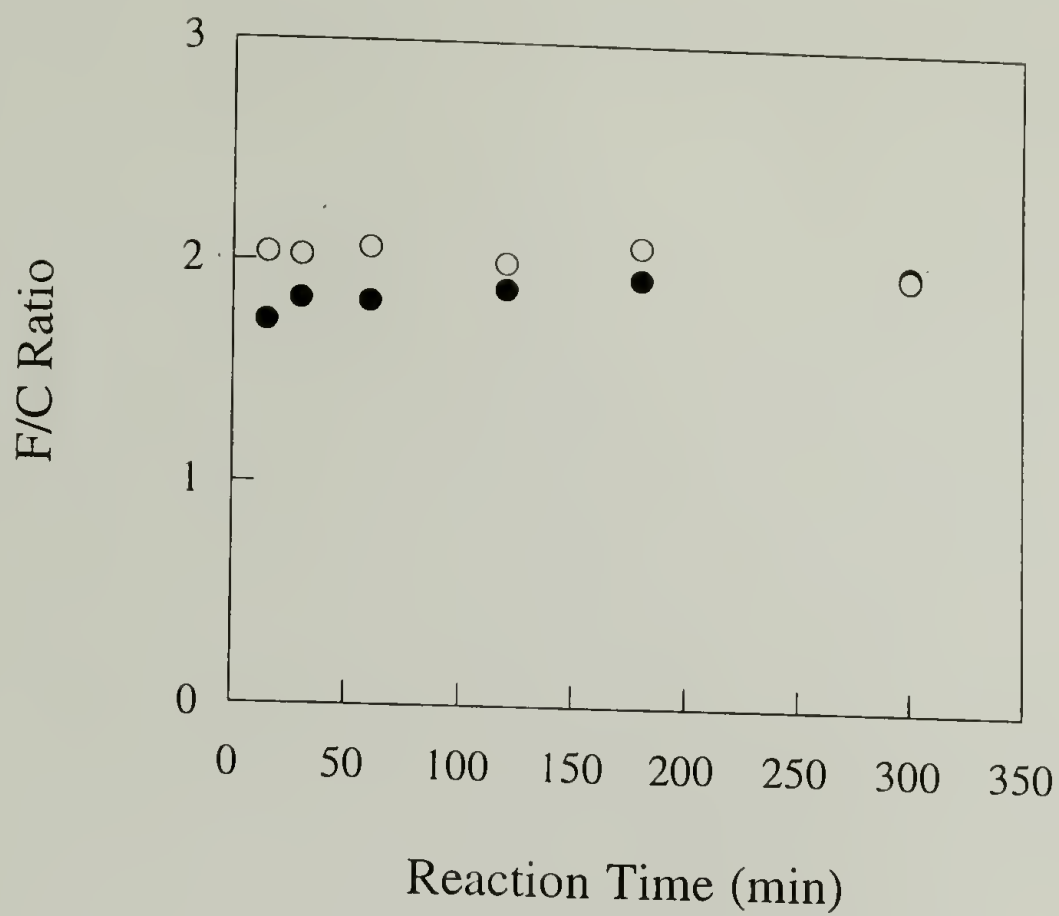
Figure 3.19. XPS F/C ratio of fluorinated PF_3E using 5% F_2/N_2; 15° take-off angle (●), 75° take-off angle (O).
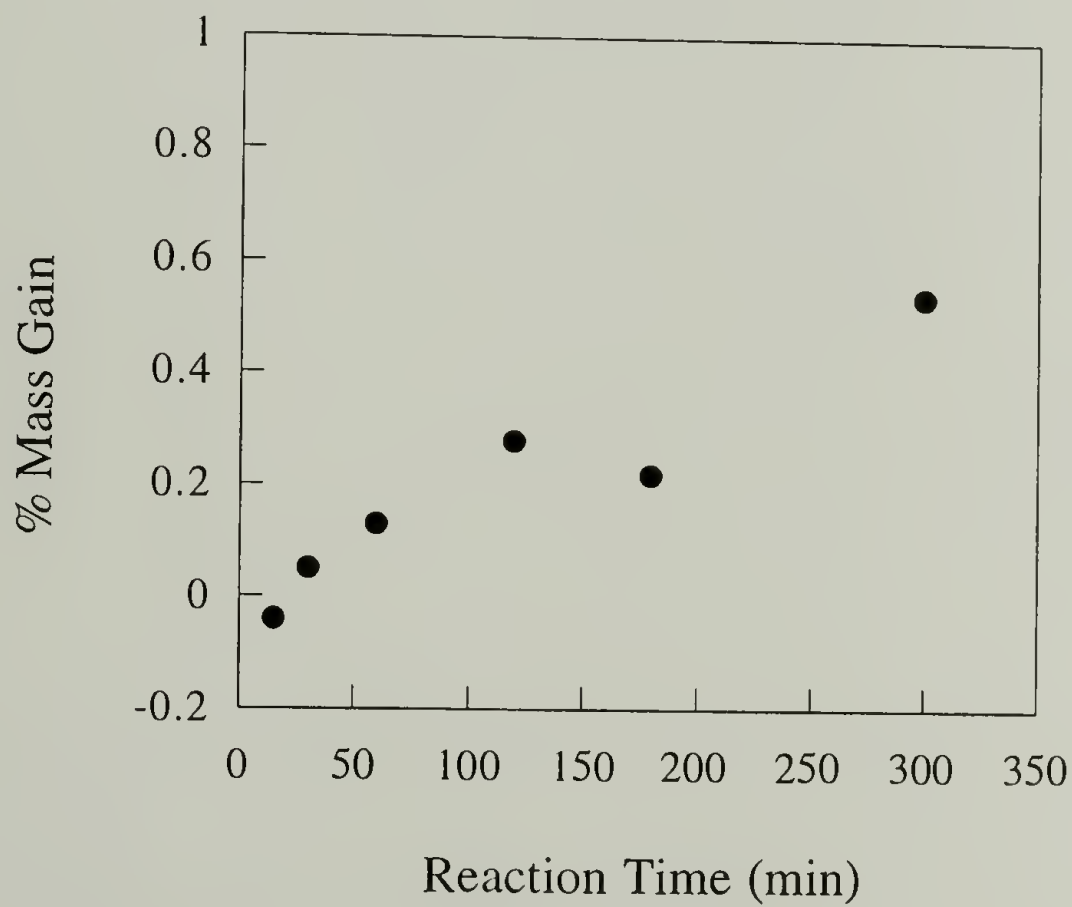
Figure 3.20. Gravimetric data for PF_3E fluorinated using 5% F_2/N_2.

sample vials) which represents a characteristic of PTFE. The 300 min fluorinated PF_3E exhibited hexadecane contact angles (θ_A/θ_R) of 43°/23° similar to those of PTFE (42°/25°).

Maleation of Poly(trifluoroethylene)

Several experiments were attempted using AIBN as an initiator for radical grafting reactions of maleic anhydride (MAH) to PF_3E in homogeneous solutions of THF. The reactions were carried out at 65°C and were not successful. The ratio of MAH to PF_3E was varied from 0.25:1 to 1:1 (AIBN:MAH = 1:2). There was no carbonyl functionality detected in the products as analyzed by infrared spectroscopy. It is possible that AIBN may not be reactive enough for this grafting reaction to take place. Benzoyl peroxide (BPO) is a more commonly used initiator for grafting reactions and may be a better initiator. Since PF_3E is only soluble in some solvents such as THF and methanol which have low boiling points (45-50 °C), the reaction temperature to be used for maleation is then limited. The half-life of benzoyl peroxide at 60 °C is about 100 h. Using BPO as an initiator for grafting reaction of MAH in homogeneous THF solution at 65 °C seems to be impractical under atmospheric pressure. Reactions under higher pressure in THF medium were not attempted.

PF_3E is a fluoropolymer that can be effectively plasticized by $SC-CO_2$. The polymer swells tremendously after soaking at 125 °C (5000 psi) for 1 h. Another reaction procedure that was attempted and seems to be promising was running the maleation in $SC-CO_2$ (Scheme 3.3). The reaction was carried out in a high pressure vessel that allows the reaction to proceed at higher temperature (125 °C) using the more reactive initiator, BPO. The reaction vessel containing PF_3E, MAH, BPO and CO_2 was soaked at 60 °C for 4 h to allow the reagents to infuse into the polymer. The reaction was then thermally initiated by soaking the vessel at 125 °C for 1 h (half-life of BPO is 30 min at 125 °C). At this point the pressure of CO_2 raised to 5000 psi. The vessel was quenched in cold running water and the CO_2 was released.

149
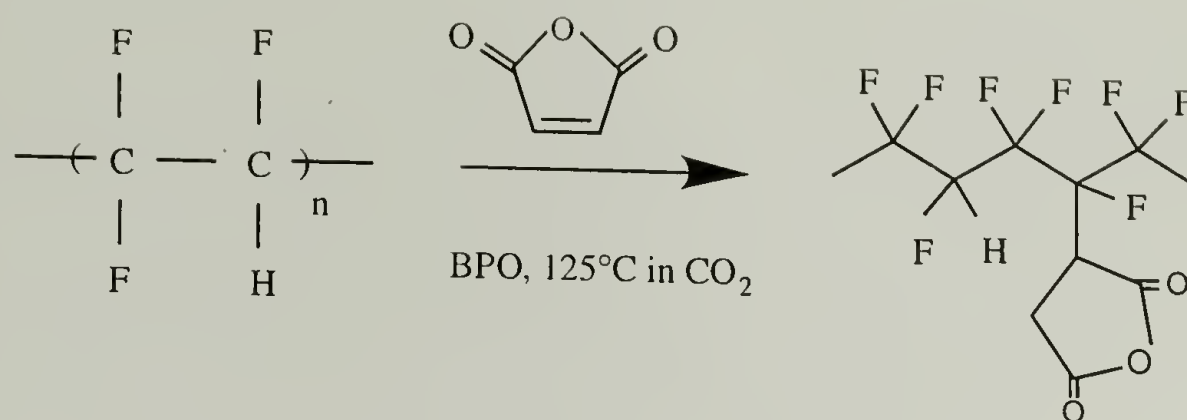
Scheme 3.3. Maleation of PF_3E in $SC-CO_2$.

The optimized purification procedure of the product involves precipitation 4 times in THF/water. Since MAH is soluble in water, the precipitation in water helped remove the unreacted MAH from the product. It is apparent that the brownish color of the product as well as the solvent mixture (THF mixed with water) remaining after the precipitation becomes lighter as the precipitation is repeated. After dissolutions and precipitations, the color of the product remains unchanged (slight brown) and the solvent mixture becomes colorless. A polymer film was cast and dried in a vacuum oven at 75 °C for two days. The drying step under vacuum at high temperature is also expected to assist the removal of unreacted MAH. Figure 3.21 shows that after drying, the ratio of the intensities of the carbonyl peak at 1787 cm^{-1} (symmetric stretching of carbonyl from the grafted anhydride) to that at 1718 cm^{-1} (maleic anhydride) becomes higher and remains consistent after 2 days of drying. Note that the small peak at 1661 cm^{-1} is due to the PF_3E itself. The IR spectrum of the purified maleated poly(trifluoroethylene) (PF_3E-g-MAH) is shown in Figure 3.22. An O-H stretching band was not observed above 3000 cm^{-1} implying that hydrolyzed monomers (both unreacted and grafted monomer) do not exist in the product. The off-scale substrate peak (C-F stretching) intensity compared to that of the carbonyl stretching indicates that the product contains a very small percent of grafted MAH. The PF_3E-g-MAH

product obtained with its polar functionality is, however, expected to adsorb to inorganic substrates more effectively than PF_3E.

A one-step reaction combining reductive dechlorination with maleation of PCTFE was also attempted. Two different ratios of MAH : PCTFE were chosen. Both sets of experiments were carried out under the same conditions used for the synthesis of PF_3E (described in experimental section) except MAH was also added at the beginning of reaction. Even though the ratio of 0.1:1 MAH:PCTFE yields a product with a slight brown color (purified PF_3E is clear), characterization by XPS and infrared spectroscopy indicate that no maleation has occurred.
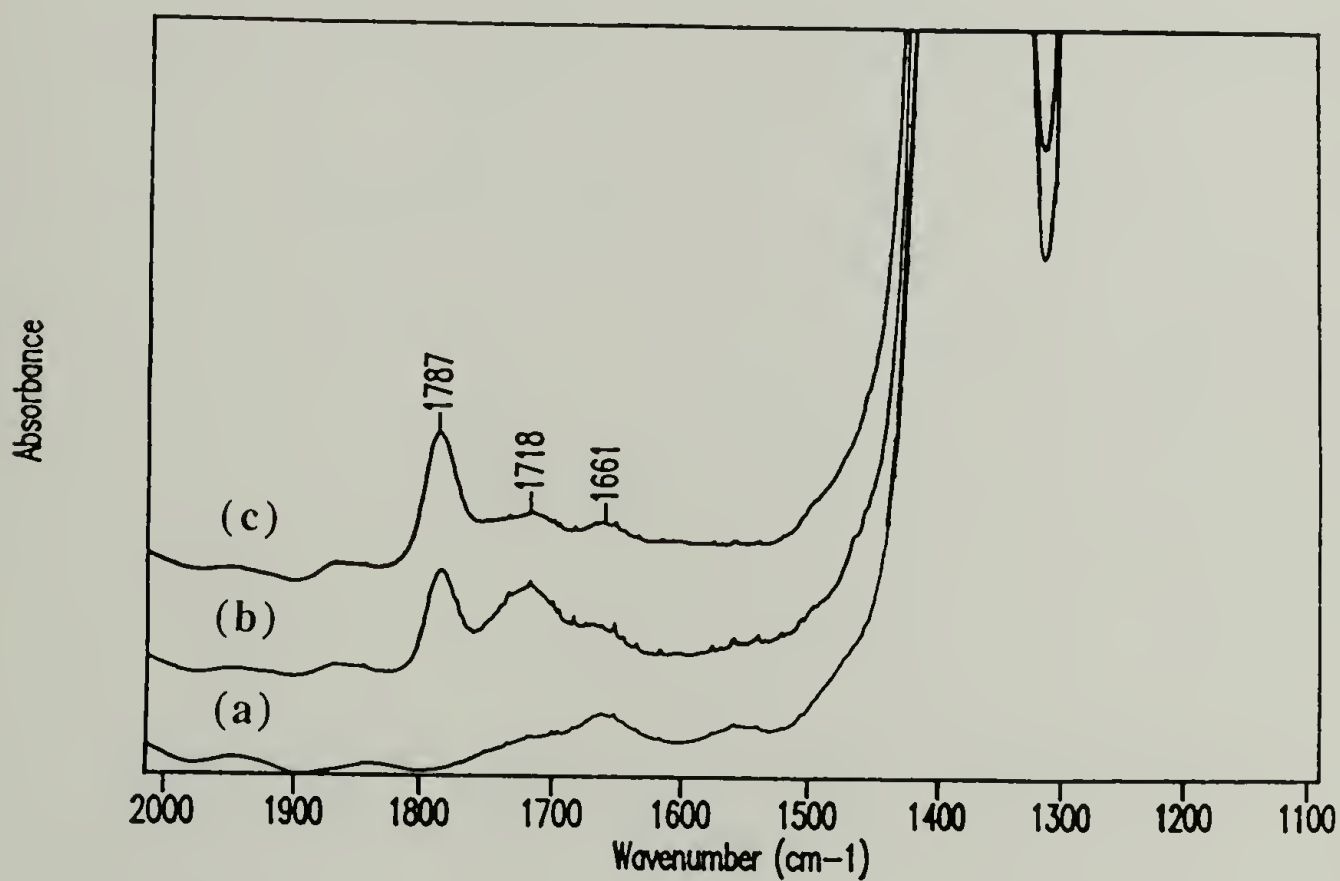
Figure 3.21. Transmission IR spectra of (a) PF_3E (b) PF_3E-g-MAH (after precipitation) (c) PF_3E-g-MAH (after drying).
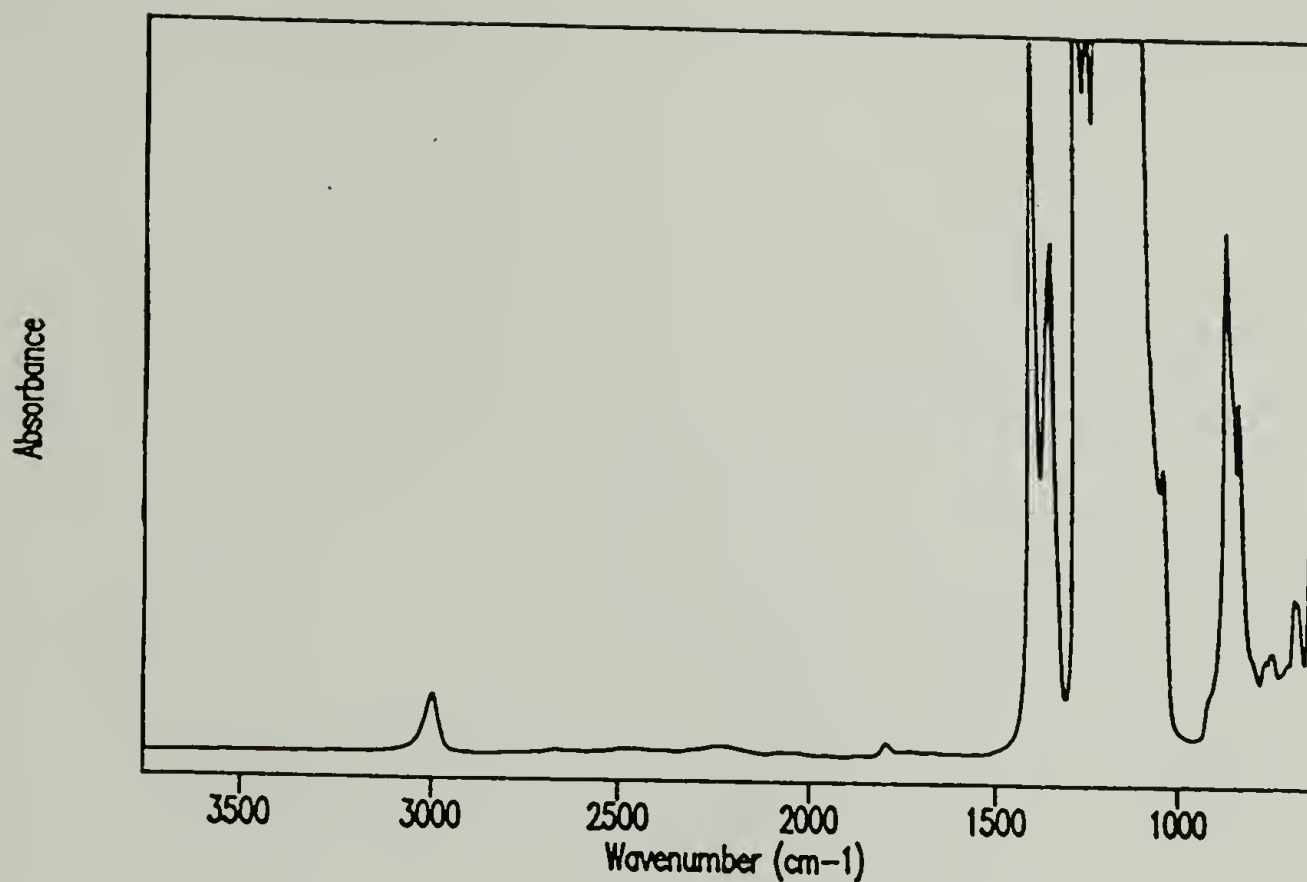
Figure 3.22. Transmission IR spectrum of purified PF$_3$E-g-MAH.

A larger amount of MAH was used in a second set of reaction (MAH:PCTFE = 1:3) for the reason that there may not have been a sufficient concentration of MAH to compete with the reductive dechlorination in the first set of experiments. It turns out that the reduction of MAH by Bu$_3$SnH dominates both the dechlorination and the maleation due to the overadded MAH. The solution remained inhomogeneous with PCTFE powder dispersed in a dark red solution, the color which is caused by the reduced MAH.

Adsorption of PF$_3$E and Maleated PF$_3$E

Prior to the adsorption experiments, general solubility tests and thin layer chromatography (TLC) of PF$_3$E were performed (results in Table 3.4). The adsorption studies from pure solvents and solvent mixtures were carried out using cleaned Si wafers as substrates. PF$_3$E is soluble only in solvents with high polarity (acetone, methanol and THF) but not soluble in solvents with medium (chloroform, dichloromethane) or low

polarity (toluene, benzene). The TLC results are consistent with the solubility tests. R_f values are close to 1.0 in the cases when polar solvents were used as eluents. These results suggest that one hydrogen atom in a repeat unit surrounded by five electronegative fluorines may be electropositive and capable of forming hydrogen bonding with such high polar solvents leading to solubility. THF and toluene were selected for adsorption studies as a solvent and a non-solvent, respectively. The TLC results of PF_3E eluted with solvent mixtures of THF:toluene of various compositions are shown in Figure 3.23. This indicates that the adsorption of PF_3E can be varied as a function of solvent quality (solvent composition). The better the solvent quality is, the less the tendency for polymer to adsorb.

Table 3.4. Solubility tests and TLC results of PF_3E.

Solvent	Solubility (room temperature)	R_f
Toluene	insoluble	0.04
Benzene	insoluble	0.04
Chloroform	insoluble	0.10
Dichloromethane	insoluble	0.17
Acetone	soluble	0.92
Methanol	soluble	0.92
Tetrahydrofuran (THF)	soluble	1.00

These data are supported by the results obtained from adsorption of PF_3E onto Si wafers from THF solution and solutions of THF:toluene mixtures (25:75, 50:50 and 75:25) (See Figure 3.23). The adsorption studies were carried out from 2.0 mg/ml PF_3E solutions for 24 h at 25 °C. The XPS data in Figure 3.24 show a significant increase in the amount of polymer adsorbed from 25:75 THF:toluene solution. The take-off angle dependent data and the appearance of a Si signal indicate that the thickness of adsorbed polymer in all cases does not reach the XPS sampling depth. Water contact angle data (Figure 3.25) exhibit an increase in contact angle hysteresis at higher toluene composition suggesting that the adsorbed layer becomes rougher as more polymer is adsorbed. Note that a clean Si wafer exhibits θ_A/θ_R (water) of 30°/15° and θ_A/θ_R (hexadecane) of 7°/0°.
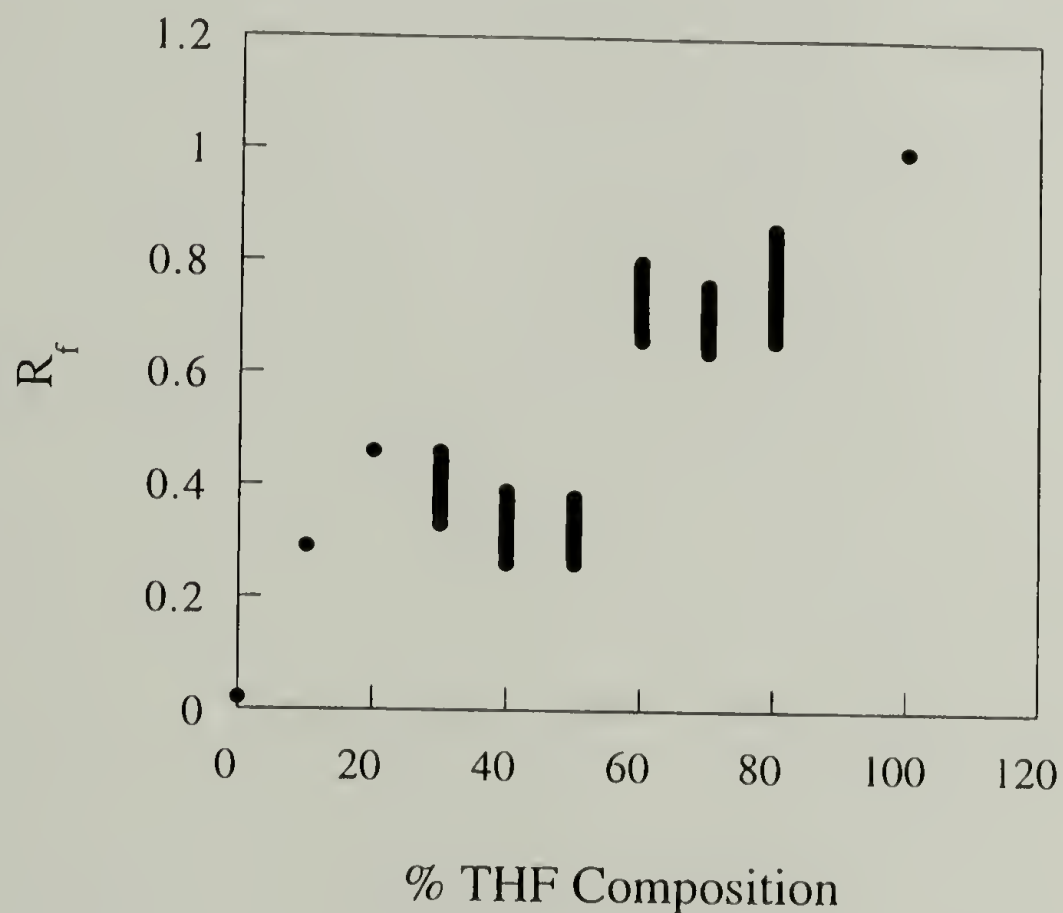
Figure 3.23. TLC results of PF_3E eluted from THF:toluene mixtures.
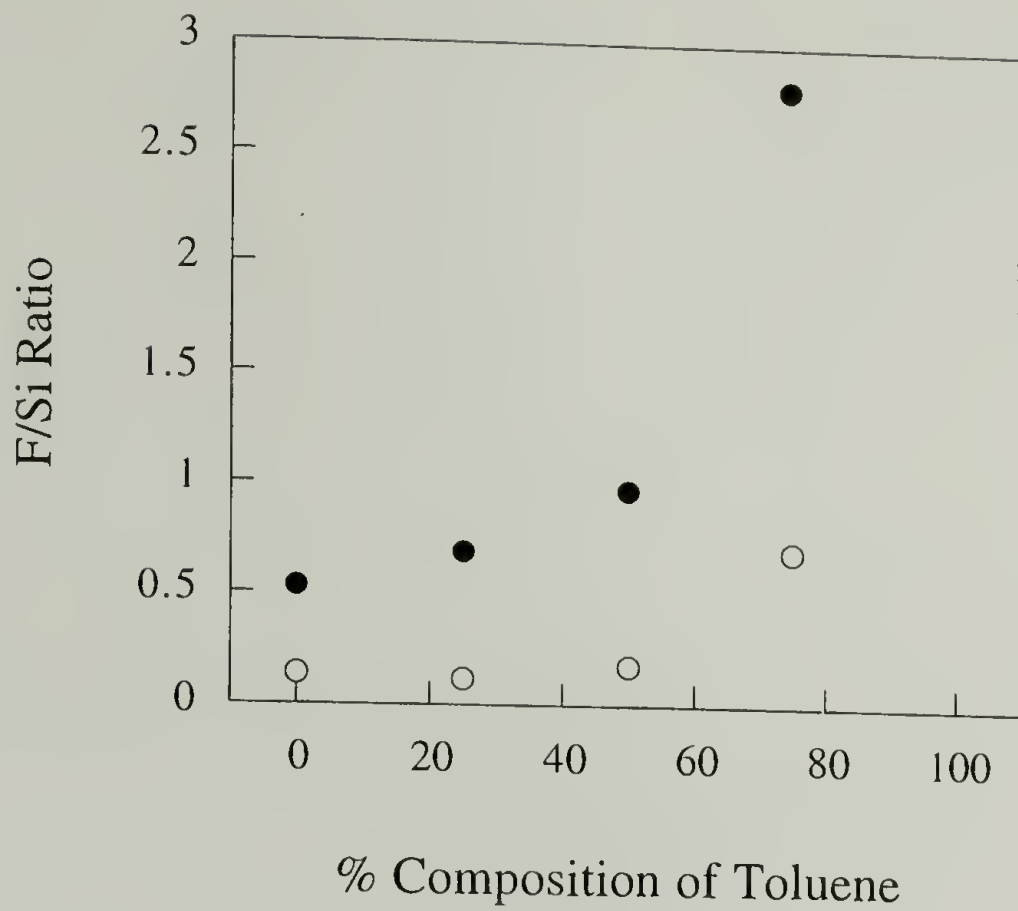
Figure 3.24. XPS F/Si ratio of adsorbed PF_3E on Si wafers as a function of solvent composition; 15° take-off angle (●), 75° take-off angle (○).
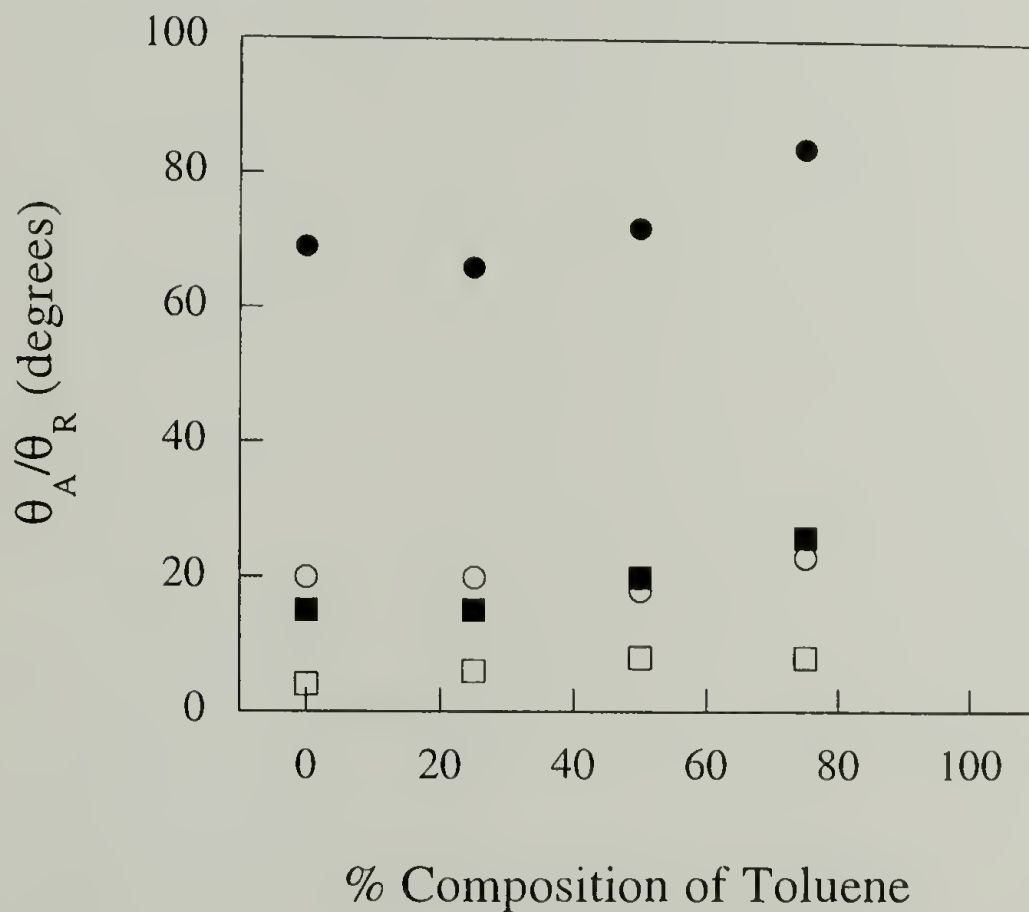
Figure 3.25. Water contact angle (θ_A (●),θ_R (○)) and hexadecane contact angle (θ_A (■),θ_R (□)) data for Si wafers with adsorbed PF_3E as a function of solvent composition.

The surface roughness of the adsorbed PF_3E films was analyzed using Atomic Force Microscopy (AFM) in the tapping mode. The AFM micrographs are shown in Figures 3.26 - 3.29. The Si wafer substrate has a relatively smooth surface with root mean square (rms) roughness of 0.17 nm (Figure 3.25). As the amount of adsorbed polymer is increased with the increasing toluene content of the polymer solution, the surface roughness increases as indicated in Table 3.5.

Table 3.5. Root mean square (rms) roughness data of a Si wafer and Si wafers with adsorbed PF_3E analyzed by AFM.

Sample	Root mean square (rms) roughness (nm)
Si wafer	0.17
PF_3E adsorbed from THF solution	0.63
PF_3E adsorbed from 50:50 THF:toluene solution	1.54
PF_3E adsorbed from 25:75 THF:toluene solution	6.94
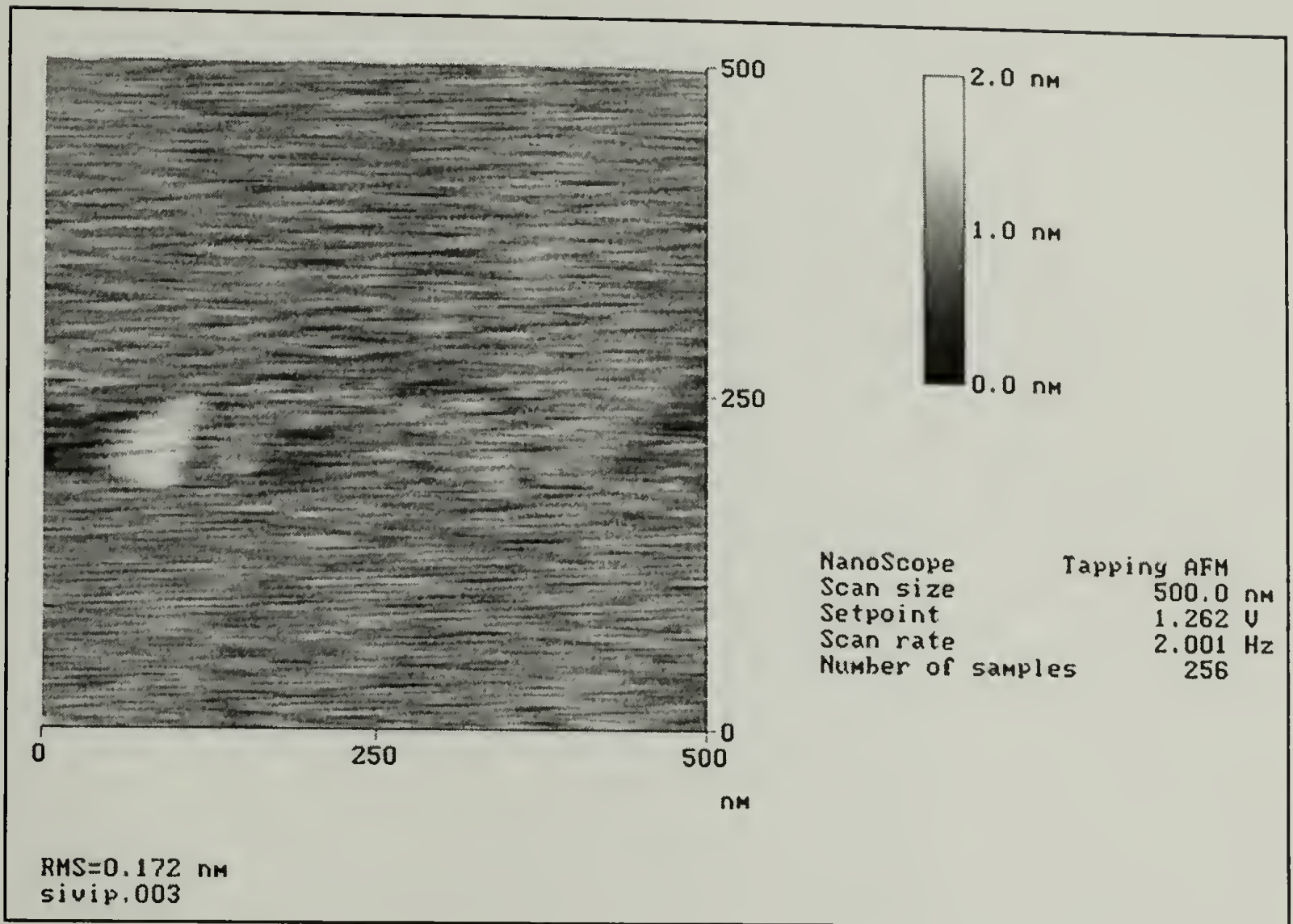
Figure 3.26. AFM micrograph of a clean Si wafer.
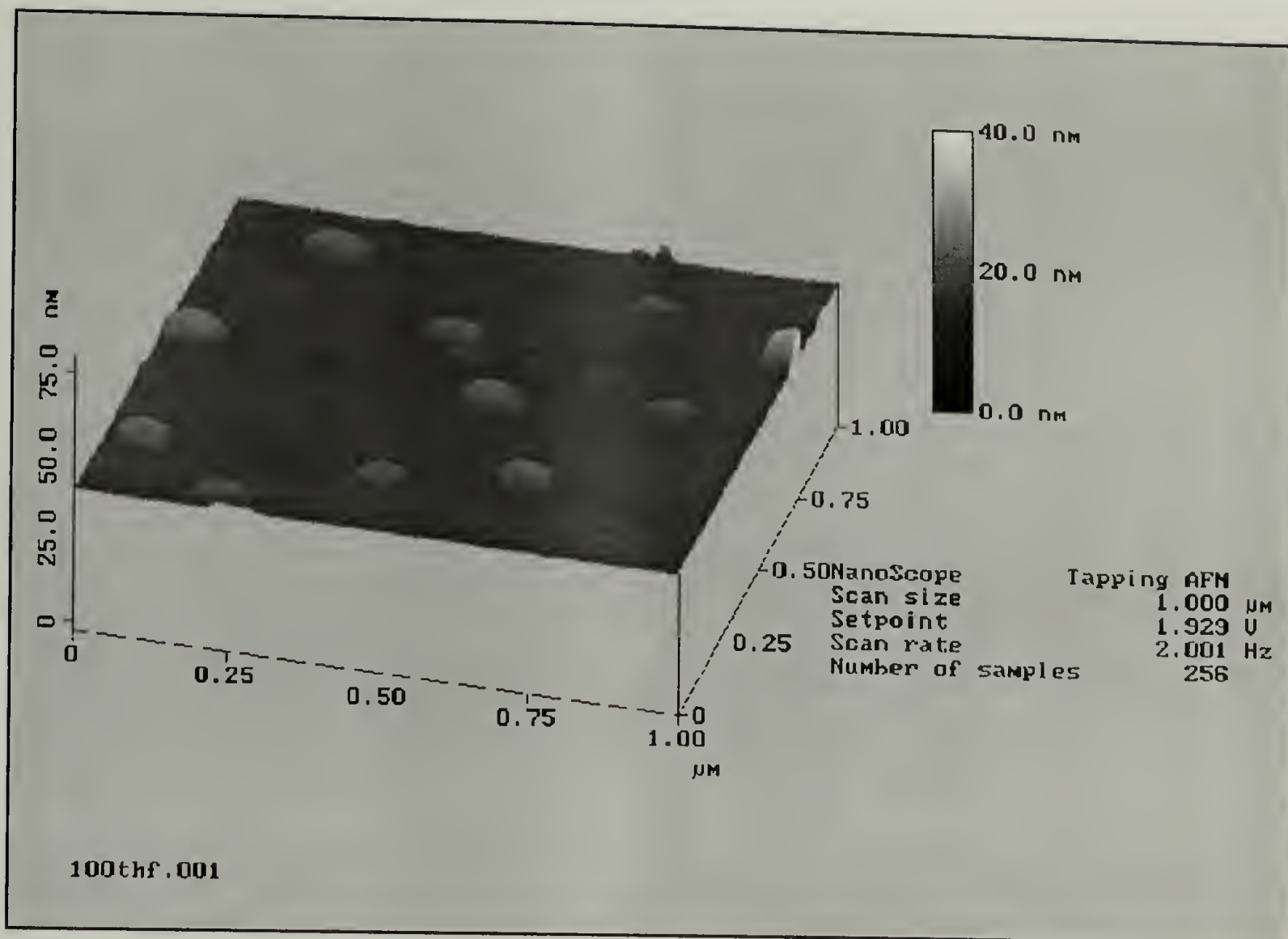
Figure 3.27. AFM micrograph of a Si wafer with adsorbed PF$_3$E from THF solution.
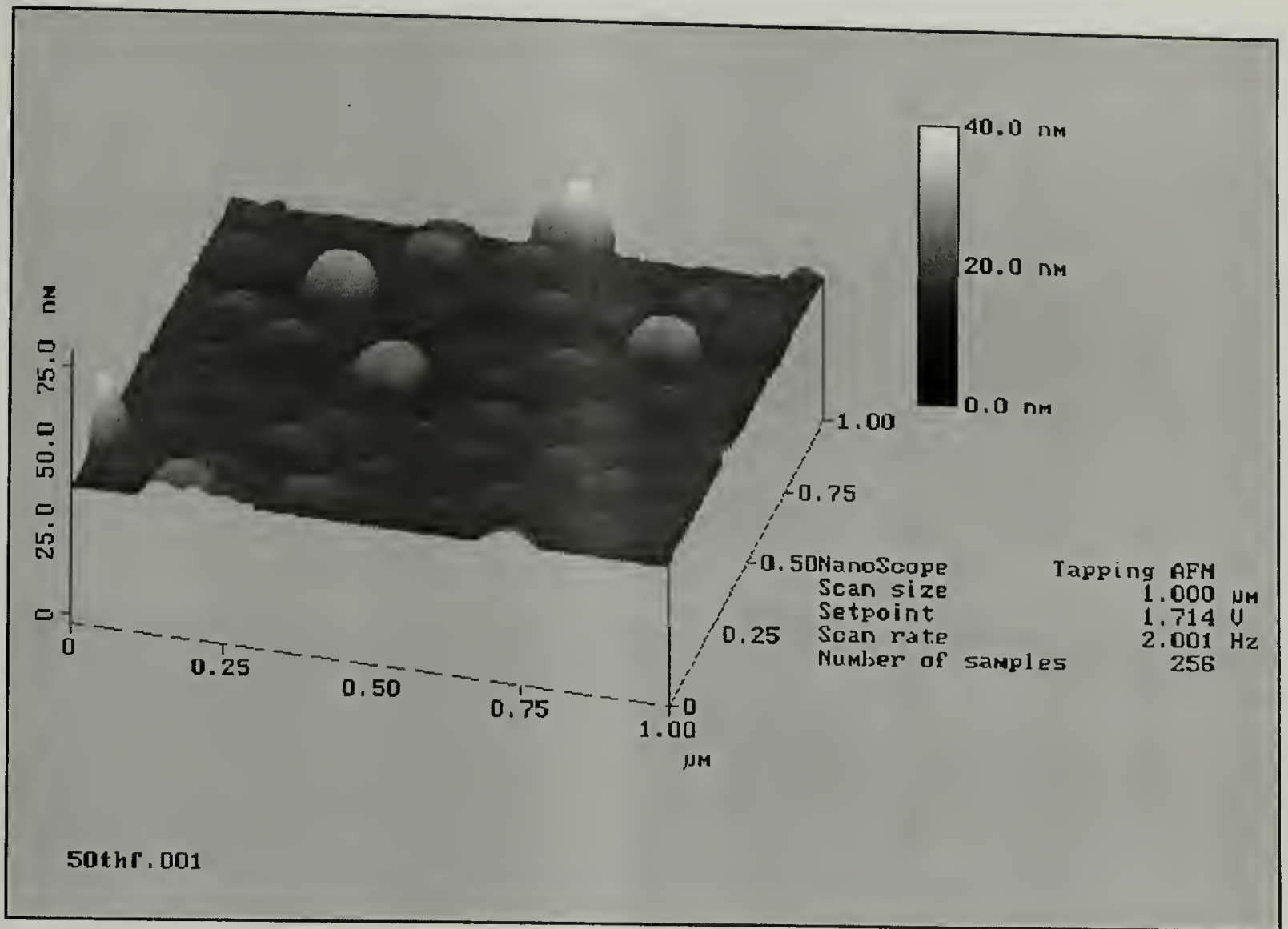
Figure 3.28. AFM micrograph of a Si wafer with adsorbed PF$_3$E from 50:50 THF:toluene solution.
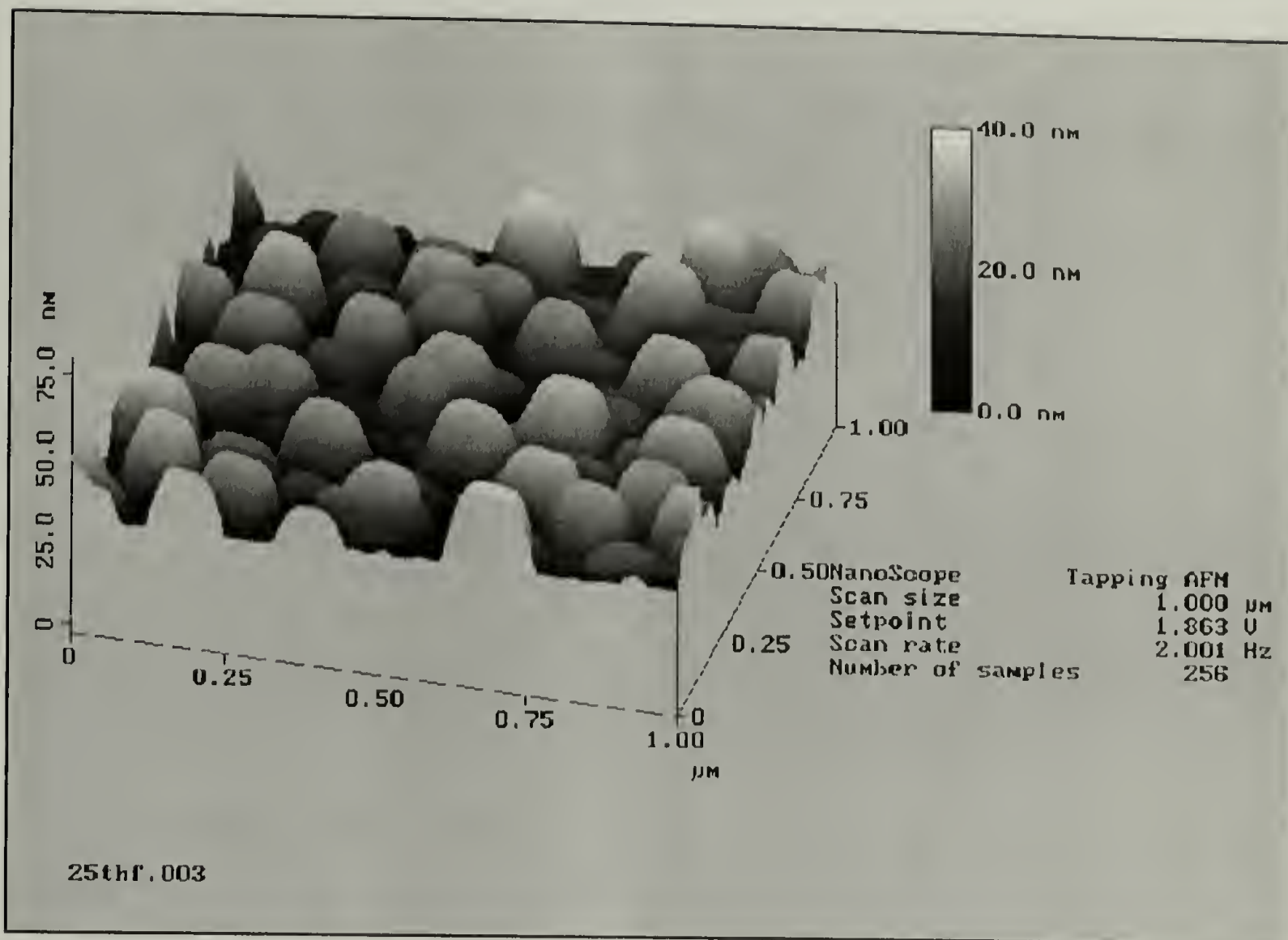
Figure 3.29. AFM micrograph of a Si wafer with adsorbed PF_3E from 25:75 THF:toluene solution.

The adsorption isotherms (Figure 3.30) and adsorption kinetics (Figure 3.31) of PF$_3$E from THF solution and 50:50 THF:toluene solutions were also investigated. The extent of adsorption was followed by XPS F/Si ratio. Adsorption of PF$_3$E from THF solution reaches its maximum extent at lower concentration with a lower amount of polymer adsorbed compared with the adsorption from 50:50 THF:toluene solution as displayed in Figure 3.30. The adsorption kinetics (shown in Figure 3.31) indicate that the adsorption from THF is rapid (reaching the final state within 1 h), while it takes much longer (24 h) for adsorption from 50:50 THF:toluene mixture to reach its final state. These results suggest that the adsorption from THF:toluene mixtures (driven by induced phase separation) requires a longer period of time to complete and this allows more polymer to adsorb than occurs in the adsorption from THF solution, which is driven by a decrease in interfacial energy.

Two sets of adsorption studies were carried out for PF$_3$E-g-MAH; one from THF solution, the other from a 50:50 THF:toluene solution. Both experiments were done using 2.0 mg/ml PF$_3$E for 24 h at 25 °C. The surface analytical data for the adsorbed polymers on Si wafers are shown in Table 3.6. The F/Si ratio data indicate that the amount of adsorption of PF$_3$E-g-MAH is higher than the amount of PF$_3$E adsorbed from the same solvent composition. A significant decrease of contact angle of adsorbed PF$_3$E-g-MAH from 50:50 THF:toluene solution reflects the higher polarity of PF$_3$E-g-MAH compared with PF$_3$E. Surface roughness data analyzed by AFM imply that the adsorbed PF$_3$E-g-MAH surfaces are smoother than the adsorbed PF$_3$E surface with a similar amount of adsorption. PF$_3$E-g-MAH adsorbed from THF solution exhibits an XPS F/Si ratio (15° take-off angle) of 1.10 and a rms roughness of 0.85 nm while PF$_3$E adsorbed from 50:50 THF:toluene solution shows XPS F/Si ratio (15° take-off angle) of 0.97 and a rms roughness of 1.54 nm. As shown in Figure 3.32, the topography of the surface of PF$_3$E-g-MAH adsorbed from THF solution is, however, different from what was observed from the surface of PF$_3$E adsorbed from 50:50 THF:toluene solution (Figure 3.28) implying

161
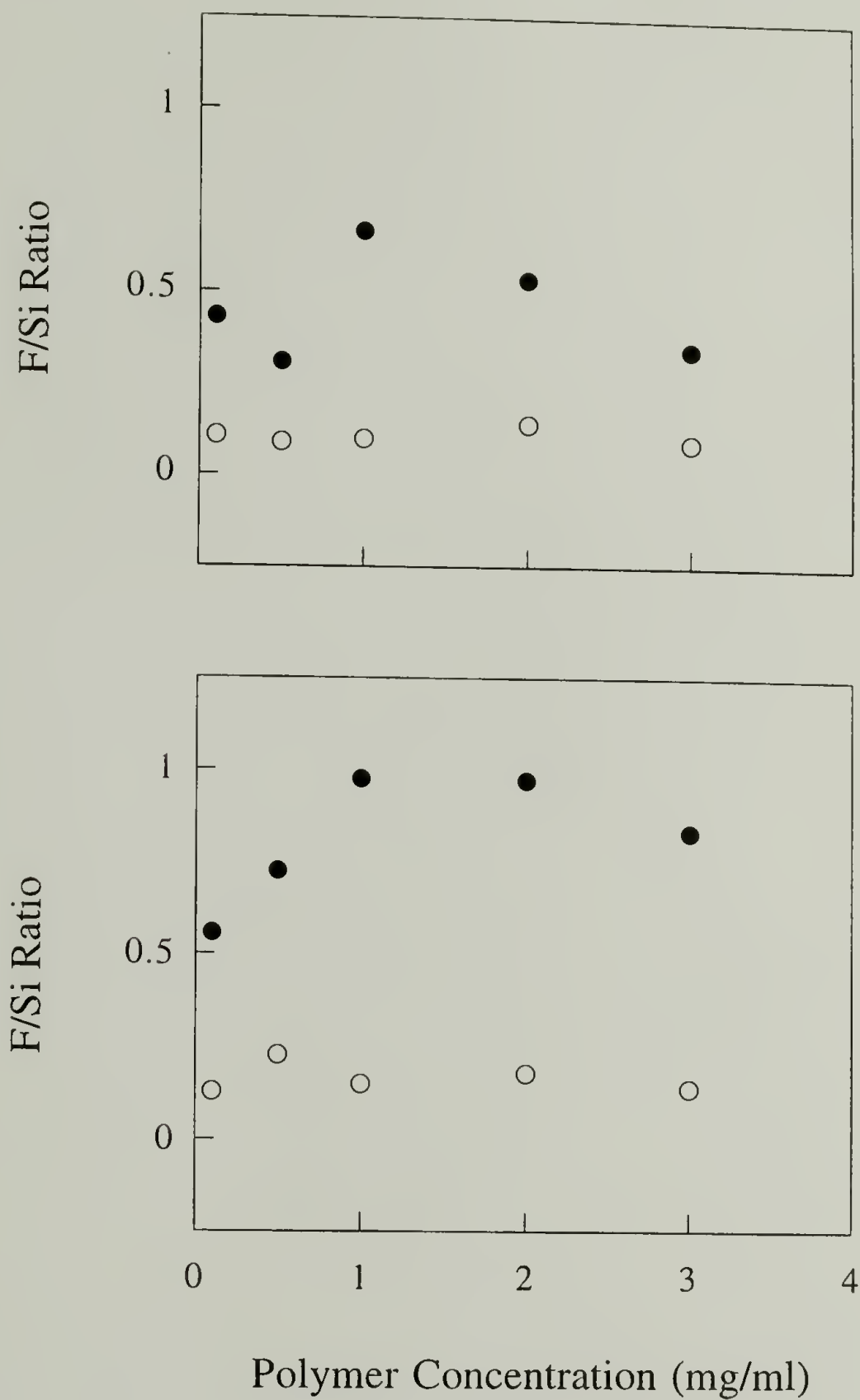
Figure 3.30. XPS F/Si ratio of Si wafers with adsorbed PF$_3$E from THF solution (top) and from 50:50 THF:toluene solution (bottom) as a function of polymer concentration; 15° take-off angle (●), 75° take-off angle (○).

162
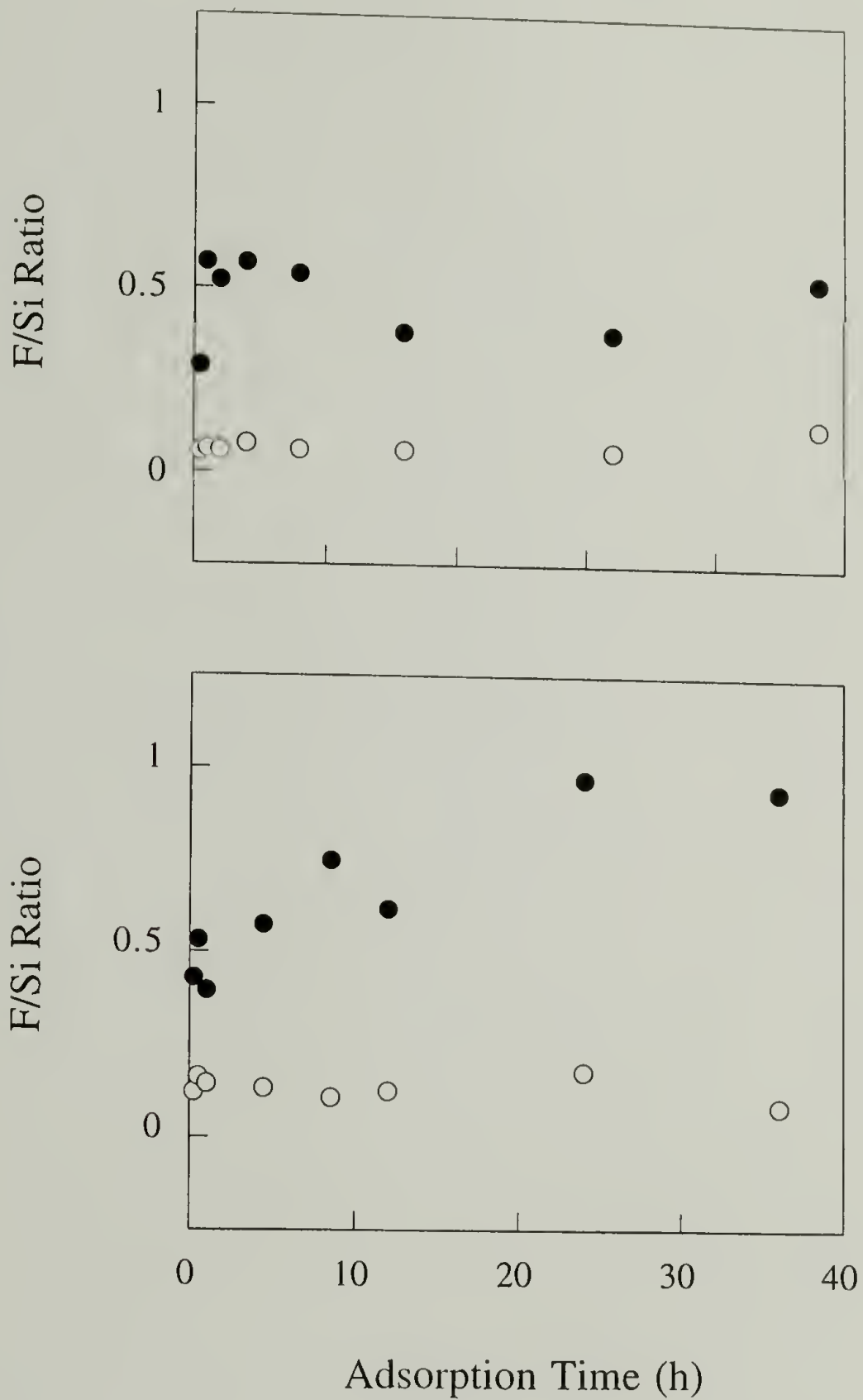
Figure 3.31. XPS F/Si ratio of Si wafers with adsorbed PF$_3$E from THF solution (top) and from 50:50 THF:toluene solution (bottom) as a function of adsorption time; 15° take-off angle (●), 75° take-off angle (O).

Table 3.6. Comparison of the results obtained from surface analysis of adsorbed PF_3E and adsorbed PF_3E-g-MAH on Si wafers from various solvent compositions.

Sample	Solvent Composition	XPS F/Si (15°/75°)	Water Contact Angle (θ_A/θ_R)	rms Roughness (nm)
PF_3E	THF	0.54/0.14	69°/20°	0.63
	50:50 (THF:toluene)	0.97/0.18	72°/18°	1.54
	25 : 75 (THF:toluene)	2.81/0.70	84°/23°	6.94
PF_3E-g-MAH	THF	1.10/0.21	66°/14° .	0.85
	50:50 (THF:toluene)	1.50/0.31	48°/15°	1.20

differences in the adsorption process. The addition of toluene also increases the adsorption of PF_3E-g-MAH but not to the great extent as the case of PF_3E. An AFM micrograph of PF_3E-g-MAH adsorbed from 50:50 THF:toluene solution is displayed in Figure 3.33.

Chlorination of PF_3E adsorbed onto Si wafers

To obtain a thin film coating of chlorinated PF_3E, a Si wafer with PF_3E adsorbed from 50:50 THF:toluene solution (2.0 mg/ml, 24 h) was chlorinated under high-intensity UV light for 100 min. The XPS atomic concentration data analyzed from both 15° and 75° take-off angles indicate that the F:Cl ratios (Table 3.7) are ~2:1 as opposed to what was expected from complete chlorination of PF_3E (F:Cl ratio is 3:1 for PCTFE). Due to the fact that the amount of PF_3E adsorbed is very low, the surface of Si wafer with its high surface energy is covered not only by the polymer but also by other hydrocarbon contaminants as
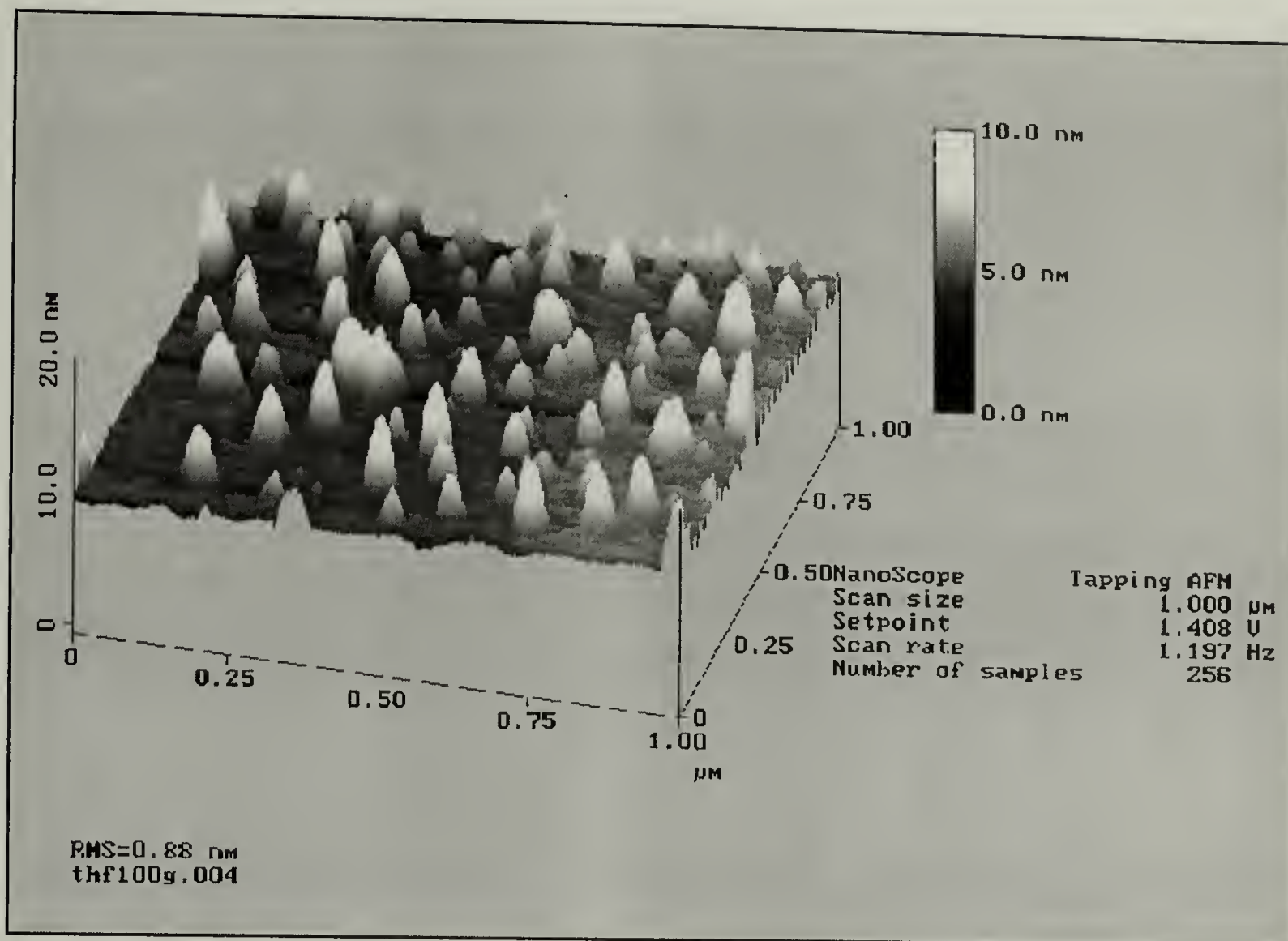
Figure 3.32. AFM micrograph of a Si wafer with adsorbed PF₃E-g-MAH from THF
solution.
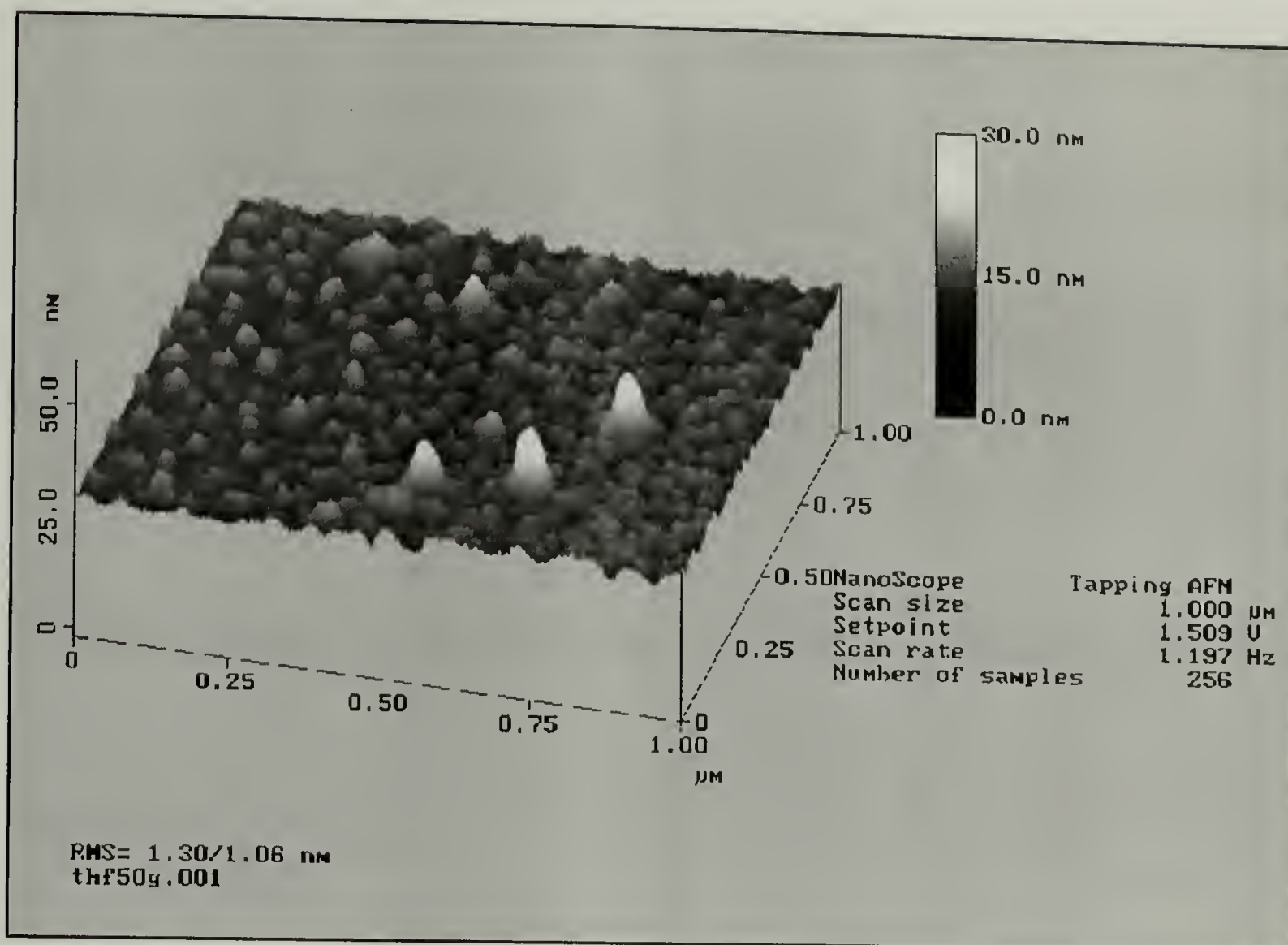
Figure 3.33. AFM micrograph of a Si wafer with adsorbed PF$_3$E-g-MAH from 50:50 THF:toluene solution.

indicated in C_{1s} region (Figure 3.34) by the extra broad peak on the low binding energy side of the two peaks of PF_3E (see Figure 3.9). The additional chlorine could be from reaction with those contaminants. The C_{1s} region of chlorinated adsorbed PF_3E is displayed in Figure 3.35. As expected, the relative ratios of peak area are altered after chlorination (see Table 3.8). The one broad peak with the low binding energy assigned to hydrocarbon contaminants becomes two separated peaks which could be the result of combination of monochlorinated and dichlorinated hydrocarbons. The ratio of the peak area between the band at 295.0 eV and 292.6 ev (previously assigned to CF_2 and CFH of PF_3E, respectively) is changed from ~1:1 to ~2:3. From this data, it can be assumed that the chlorination of adsorbed thin films of PF_3E can be accomplished using the controlled conditions that have been investigated for the bulk film. The data interpretation can be quite complicated depending on the substrates used.

Table 3.7. XPS atomic composition data for Si wafers with adsorbed PF_3E from 50:50 THF:toluene solution before and after chlorination using high-intensity UV light for 100 min.

Sample	θ_T (degrees)	Atomic Composition (%)				
		C	O	F	Si	Cl
Before Chlorination	15	32.16	36.76	15.31	15.77	-
	75	15.22	34.99	7.51	42.27	-
After Chlorination	15	34.58	25.85	18.71	10.37	10.50
	75	16.49	39.33	9.25	29.53	5.41
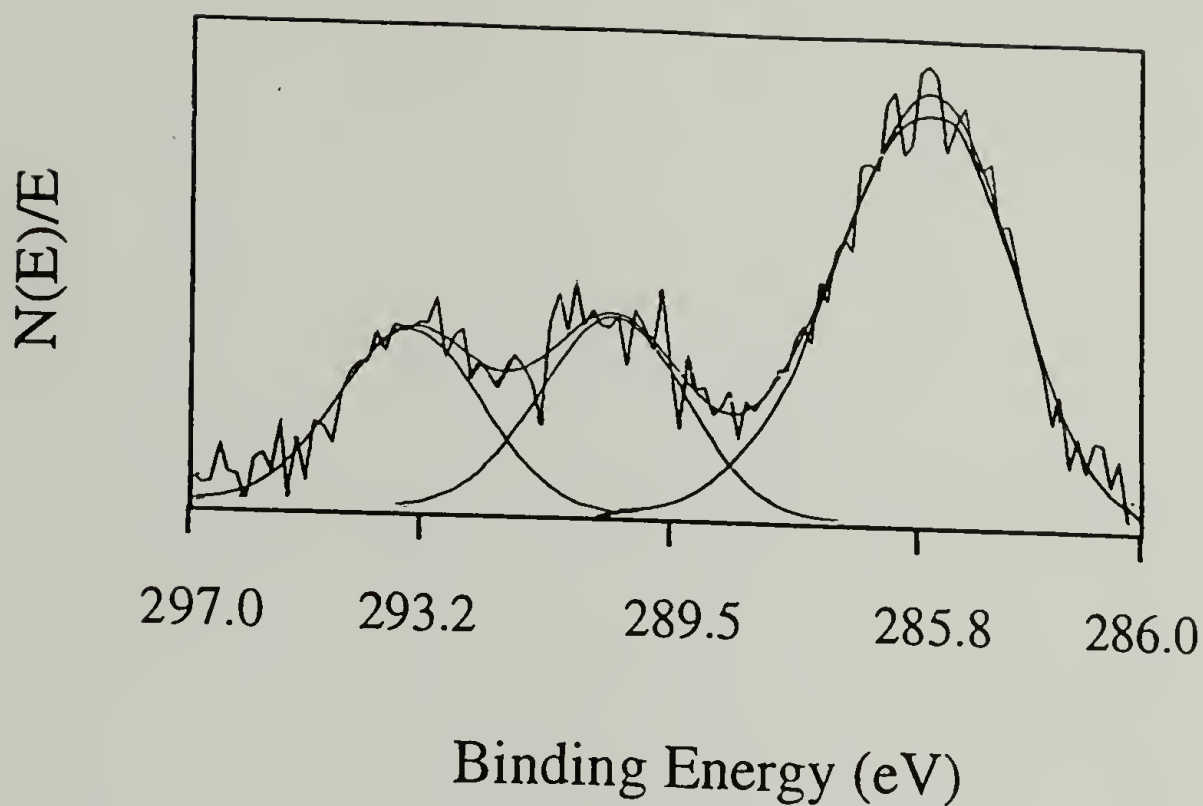
Figure 3.34. C_{1s} region (75° takeoff angle) of a Si wafer with PF_3E adsorbed from 50:50 THF:toluene solution.
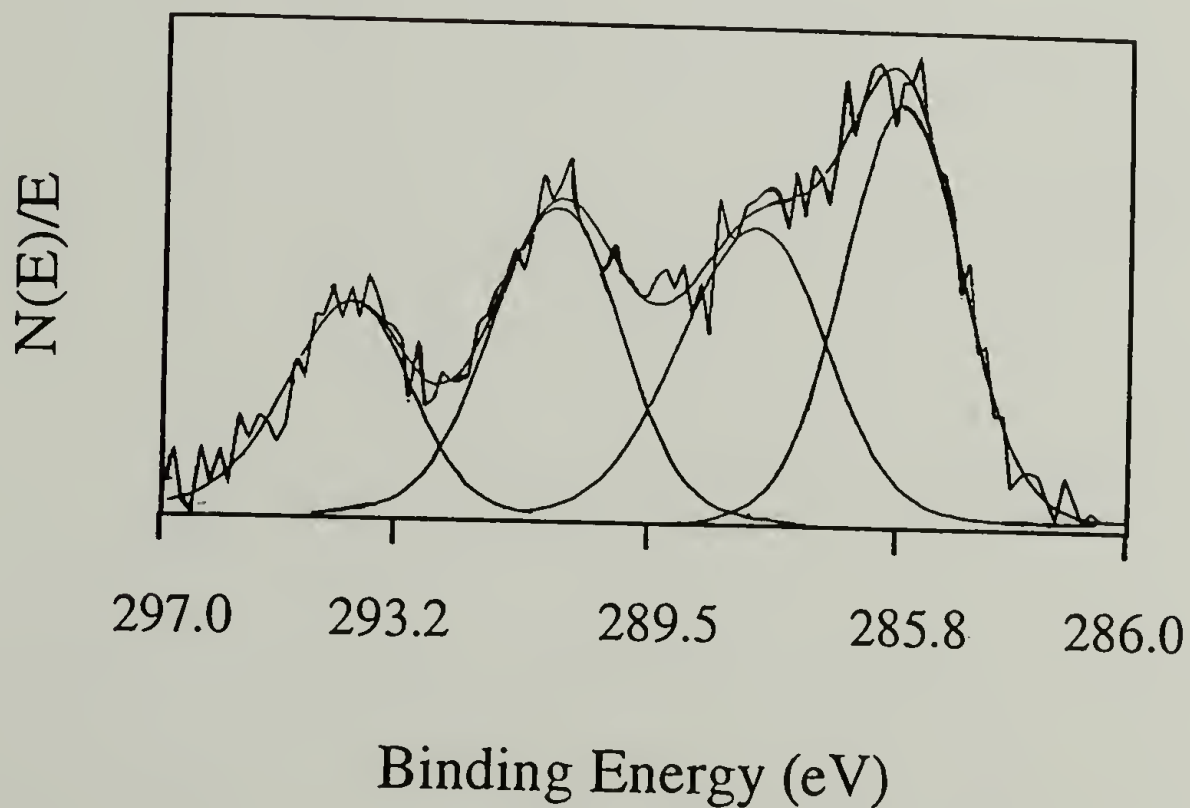
Figure 3.35. C_{1s} region (75° takeoff angle) of a Si wafer with PF_3E adsorbed from 50:50 THF:toluene solution after chlorination under high-intensity UV light for 100 min.

Table 3.8. Curve fitting data of XPS C_{1s} region for PF_3E adsorbed on Si wafers before and after chlorination.

Peak Position (eV)	Total Peak Area (%)	
	PF_3E adsorbed on a Si wafer (before chlorination)	PF_3E adsorbed on a Si wafer (after chlorination)
295.0	19.31	16.00
292.6	21.90	24.48
290.4	-	27.33
288.6	58.78	32.20

Conclusions and Suggestions for Future Work

It has been demonstrated that the extent of chlorination of PF_3E can be adjusted by controlling reaction time and light intensity. Heterogeneous (gas-solid) chlorination of PF_3E is a surface-selective reaction. The chlorinated PF_3E layer behaves as a good barrier to chlorine gas and can efficiently stop the bulk chlorination. The fluorination data done in collaboration with Air Products indicates that the fluorinated PF_3E exhibits similar surface properties to PTFE. Fluorination under the chosen condition is, however, not surface-selective. More detailed investigations are suggested in order to achieve a product with controllable extent of fluorination which could be varied as a function of fluorine gas concentration or the identity of the diluting gas.

A maleic anhydride grafting reaction to PF_3E was successfully carried out in SC-CO_2 medium using benzoyl peroxide as an initiator. Despite the low grafting density (not calculated), the amount of polymer adsorption was significantly increased due to the increase in polarity of polymer. Further studies of the grafting density and the grafting

yield of maleation in SC-CO$_2$ medium as a function of experimental variables (i.e. initiator concentration, ratio of initiator to PF$_3$E, CO$_2$ density, reaction temperature) are recommended. The PF$_3$E-g-MAH products with various grafting extent, thus different polarity will be very beneficial for coating applications.

The amount of PF$_3$E adsorbed can also be controlled by the change in solvent quality by varying the solvent composition of THF:toluene mixtures. The surface roughness of substrates with adsorbed polymer is higher as more polymer is deposited. The adsorbed PF$_3$E-g-MAH offers a smoother surface with a similar amount of adsorption and different topography. The investigation of gas chlorination of PF$_3$E thin film coated on Si wafer has confirmed that the chlorination can be applied to the supported-film system.

References

(1)   Lee, K., -W.; McCarthy, T. J. *Macromolecules* **1988**, *21*, 2318.

(2)   Bee, T. G.; McCarthy, T. J. *Macromolecules* **1992**, *25*, 2093.

(3)   Shoichet, M. S.; McCarthy, T. J. *Macromolecules* **1991**, *24*, 982.

(4)   Dias, A. J.; McCarthy, T. J. *Macromolecules* **1984**, *17*, 2529.

(5)   Brennan, J. V.; McCarthy, T. J. *Polym. Prep. (Am. Chem. Soc. Div. Polym. Chem.)* **1989**, *30(2)*, 152.

(6)   Lee, K. -W.; McCarthy, T. J. *Macromolecules* **1988**, *2*, 309.

(7)   Bening, R. C.; McCarthy, T. J. *Macromolecules* **1990**, *23*, 2648.

(8)   Franchina, N. L.; McCarthy, T. J. *Macromolecules* **1991**, *24*, 3045.

(9)   Chen, W.; McCarthy, T. J. *Polym. Prep. (Am. Chem. Soc. Div. Polym. Chem.)* **1996**, *37(1)*, 457.

(10)   Cross, E. M.; McCarthy, T. J. *Macromolecules* **1992**, *25*, 2603.

(11)   Leväsalmi, J. -M.; McCarthy, T. J. *Macromolecules* **1995**, *28*, 1733.

(12)   Yamada, T. K., Kitayama, T. J. *J. Appl. Phys.* **1981**, *52*, 6859.

(13)   Lovinger, A., J.; Davis, G. T.; Furukawa, T.; Broadhurst, M. G. *Macromolecules* **1982**, *15*, 323, 329.

(14)   Wang, H.; Zhang, Q. M.; Cross, L. E.; Sykes, A. O. *J. Appl. Phys.* **1993**, *74*, 3394.

(15)   Cais, R. E.; Kometani, J. M. *Macromolecules* **1984**, *17*, 1932.

(16)   Yagi, T. *Polymer J.* **1979**, *11*, 711.

(17)   Lovinger, A. J.; Cais, R. E. *Macromolecules* **1984**, *17*, 1939.

(18)   Schonhorn, H.; Hansen, R. H. *J. Appl. Polym. Sci.* **1968**, *12*, 1231.

(19)   Nakagawa, T.; Yamada, S. *J. Appl. Polym. Sci.* **1972**, *16*, 1997.

(20)   Elman, J. F.; Gerenser, L. J.; Goppert-Berarducci, K. E.; Pochan, J. M. *Macromolecules* **1990**, *23*, 3922.

(21)   Mohr, J. M.; Paul, D. R.; Taru, Y.; Mlsna, T. E.; Lagow, R. J. *J. Membr. Sci.* **1991**, *55*, 149.

(22)   Shimada, J.; Hoshino, M. *J. Appl. Polym. Sci.* **1975**, *19*, 1439.

(23)   Mohr, J. M.; Paul, D. R.; Pinnau, I.; Koros, W. J. *J. Membr. Sci.* **1991**, *56*, 77.

(24)   Csernica, J.; Rein, H.; Baddour, R. F.; Cohen, R. E. *Macromolecules* **1991**, *24*, 3612.

(25)   Sanderson, R. D.; du Toit, F. J.; Carstens, P. A. B.; Wagner, J. B. *Thermal Analysis* **1994**, *41*, 563.

(26)   Anand, M.; Cohen, R. E.; Baddour, R. F. *Polymer* **1981**, *22*, 361.

(27)   Napper, D. *Polymeric Stabilization of Colloidal Dispersions*; Academic Press: London, **1983**.

(28)   Dorinson, A.; Ludima, K. C. *Mechanism and Chemistry in Lubrication*; Elsevier Applied Science Publishers: Amsterdum, 1985.

(29)   Mittal, K. L., Ed.; *Adhesion Aspects of Polymeric Coatings.*; Plenum Press: New York, 1983.

(30)   Tadras, T. F. In *Polymer Colloids* ; Corner, T.; Buscall, R., Eds.; Elsevier Applied Science Publishers: New York, 1984.

(31)   Cohen Stuart, M. A.; Cosgrove, T.; Vincent, B. *Adv. Colloid Interface Sci.* **1986**, *24*, 143.

(32)   Fleer, G. J.; Lyklema, J. In *Adsorptions from Solution at the Solid/Liquid Interface*; Chapter 4; Parfitt, G. D.; Rochester, C. H., Eds.; Academic Press: New York, 1983.

(33)   Scheutjens, J. M. H. M.; Fleer, G. J. *J. Phys. Chem.* **1980**, *84*, 178.

(34)   Scheutjens, J. M. H. M.; Fleer, G. J. *J. Phys. Chem.* **1979**, *83*, 1619.

(35)   de Gennes, P. G. *Macromolecules* **1982**, *15*, 492.

(36)   Gaylord, N. G.; Mehta, R.; Mohan, D. R.; Kumar, V. *J. Appl. Polym. Sci.*
        1992, *44*, 1941.

(37)   Gabara, W.; Porejko, S. *J. Polym. Sci. (A-1)* **1967**, *5*, 1547.

(38)   Porejko, S.; Gabara, W.; Kulesza *J. Polym. Sci. (A-1)* **1967**, *5*, 1563.

(39)   Gaylord, N. G.; Mehta, R.; Deshpande, A. B. In *New Advances in Polyolefins*,
        Chung, T. C., Ed.; Plemum Press: New York, 1993; p 115.

(40)   Samay, G.; Nagy, T.; White, J. L. *J. Appl. Polym. Sci.* **1995**, *56*, 1423.

(41)   Sathe, S. N.; Rao, G. S. S.; Devi, S. *J. Appl. Polym. Sci.* **1994**, *53*, 239.

(42)   Roover, B. D.; Sclavons, M.; Carlier, V.; Devaux, J.; Legras, R.; Momtaz, A.
        J. Appl. Polym. Sci. **1987**, *33*, 2549.

(43)   Borsig, E.; Hrckova, H., L. *J. M. S.-Pure Appl. Chem.* **1994**, *10*, 1447.

(44)   Gaylord, N. G.; Mehta, M.; Mehta, R. *J. Appl. Polym. Sci.* **1987**, *33*, 2549.

(45)   Mitsuaki, N.; Masuasu, A. *J. Chem. Soc. Jpn.* **1970**, *70*, 1432.

(46)   Wu, C. -J.; Chen, C. -Y.; Woo, E.; Kuo, J. -F. *J. Polym. Sci. Polym. Chem.Ed.*
        1993, *31*, 3405.

(47)   Cimmino, S.; Mancarella, C.; Martuscelli, E.; Palumbo, R.; Ragosta, G. *Polym.
        Eng. Sci.* **1984**, *24*, 48.

(48)   Xanthas, M. *Polym. Eng. Sci.* **1988**, *28*, 1392.

(49)   Gaylord, N. G. *J. Macromol. Sci. Chem.* **1989**, *A26*, 1211.

(50)   Hayes, H. J.; McCarthy, T. J. *Polym. Prep.*
        (Am. Chem. Soc. Div. Polym. Chem.) **1997**, 38(2), in press.

(51)   Leväsalmi, J. -M. *Ph.D. Dissertation*, 1997.

(52)   See the data tables in Appendix D for more information.

172

APPENDIX A

DATA TABLES FOR CHAPTER 1

Table A.1. XPS atomic composition and water contact angle (θ_A/θ_R) data for the reaction of PCTFE-OH (initially modified at -78 °C) with C_3F_7COCl using pyridine as catalyst and XPS atomic composition and hexadecane (HD) contact angle data after labelling with C_3H_7COCl.

Time (min)	θ_T degrees	Atomic Composition (%) before Labelling				θ_A/θ_R (water) degrees	Atomic Composition (%) after Labelling				θ_A/θ_R (HD) degrees
		C	F	O	Cl		C	F	O	Cl	
0	15	68.4	18.8	11.2	1.6	67/17	71.9	12.3	15.0	0.8	10/0
	75	61.4	22.8	10.9	4.8		70.7	13.3	14.8	1.1	
3	15	45.5	44.9	9.3	0.3	106/64	46.4	43.6	9.8	0.2	58/37
	75	49.2	40.1	9.6	1.2		50.5	38.8	9.9	0.8	
7	15	44.1	46.3	9.3	0.3	106/69	45.6	44.6	9.2	0.6	59/40
	75	48.0	41.5	9.0	1.5		47.8	41.2	8.6	2.4	
15	15	44.0	46.1	9.7	0.3	108/67	43.9	46.3	8.8	1.0	59/40
	75	47.5	41.9	9.4	1.3		46.6	42.2	8.8	2.4	

Table A.2. XPS atomic composition and water contact angle (θ_A/θ_R) data for the reaction of PCTFE-OH (initially modified at -78 °C) with C_3H_7COCl using pyridine as catalyst and XPS atomic composition and hexadecane (HD) contact angle data after labelling with C_3F_7COCl.

Time (min)	θ_T degrees	Atomic Composition (%) before Labelling				θ_A/θ_R (water) degrees	Atomic Composition (%) after Labelling				θ_A/θ_R (HD) degrees
		C	F	O	Cl		C	F	O	Cl	
0	15	68.4	18.8	11.2	1.6	67/17	44.0	46.1	9.7	0.3	60/40
	75	61.4	22.8	10.9	4.8		47.5	41.9	9.4	1.3	
3	15	69.8	15.4	13.6	1.2	78/40	61.2	23.8	13.7	1.3	35/8
	75	64.6	18.9	12.4	4.1		61.1	22.6	12.9	3.4	
7	15	70.7	13.8	14.4	1.1	83/45	66.6	18.4	14.1	0.9	26/6
	75	67.1	16.3	13.5	3.2		62.4	20.7	12.9	4.0	
15	15	71.4	13.1	14.3	1.3	86/49	67.0	17.2	14.3	1.6	23/7
	75	66.0	17.5	13.1	3.4		65.5	18.2	13.3	3.1	
30	15	72.0	13.0	14.3	1.0	88/52	69.2	16.5	13.3	1.0	20/6
	75	66.8	16.7	12.8	3.7		65.7	17.2	13.6	3.5	
60	15	71.9	12.6	14.3	1.2	87/53	69.8	14.3	14.9	1.0	18/0
	75	65.7	17.4	13.7	3.3		67.4	16.0	13.6	3.1	
120	15	72.2	11.9	15.0	0.9	89/54	70.7	14.3	13.5	1.5	11/3
	75	69.6	14.2	13.7	2.6		67.7	15.7	12.7	3.0	

Table A.3. XPS atomic composition and water contact angle (θ_A/θ_R) data for the reaction of PCTFE-OH (initially modified at -78 °C) with $C_{17}H_{35}COCl$ using pyridine as catalyst and XPS atomic composition and hexadecane (HD) contact angle data after labelling with C_3F_7COCl.

Time (min)	θ_T degrees	Atomic Composition (%) before Labelling				θ_A/θ_R (water) degrees	Atomic Composition (%) after Labelling				θ_A/θ_R (HD) degrees
		C	F	O	Cl		C	F	O	Cl	
0	15	68.4	18.8	11.2	1.6	67/17	44.0	46.1	9.7	0.95	60/40
	75	61.4	22.8	10.9	4.8		47.5	41.9	9.4	1.13	
3	15	90.3	4.2	5.0	0.6	104/74	83.4	10.4	5.5	8.01	44/24
	75	84.8	7.2	7.2	0.7		80.2	11.6	7.4	6.91	
7	15	93.0	3.0	3.5	0.6	108/88	83.6	9.9	5.7	8.44	37/3
	75	86.4	6.0	6.9	0.7		82.5	9.5	7.1	8.68	
15	15	92.8	2.7	3.9	0.5	108/91	86.3	7.7	5.3	11.2	35/0
	75	85.3	6.4	7.6	0.8		83.8	8.3	7.4	10.1	
30	15	92.9	2.9	3.9	0.3	108/90	88.4	5.9	5.1	15.0	38/2
	75	85.5	6.8	7.0	0.8		83.5	8.0	7.6	10.4	
60	15	92.4	3.1	4.0	0.5	108/90	89.3	5.7	4.1	15.7	40/10
	75	86.5	6.2	6.8	0.6		84.7	7.5	7.0	11.3	
120	15	92.8	3.0	3.8	0.4	109/91	90.9	4.4	4.2	20.7	40/35
	75	86.4	6.4	6.5	0.7		85.1	7.2	7.0	11.8	

Table A.4. XPS atomic composition and water contact angle (θ_A/θ_R) data for the reaction of PCTFE-OH (initially modified at -78 °C) with C_3F_7COCl without catalyst and XPS atomic composition and hexadecane (HD) contact angle data after labelling with C_3H_7COCl.

Time (min)	θ_r degrees	Atomic Composition (%) before Labelling				θ_A/θ_R (water) degrees	Atomic Composition (%) after Labelling				θ_A/θ_R (HD) degrees
		C	F	O	Cl		C	F	O	Cl	
0	15	68.4	18.8	11.2	1.6	67/17	71.9	12.3	15.0	0.8	10/0
	75	61.4	22.8	10.9	4.8		70.7	13.3	14.8	1.1	
15	15	43.6	46.2	9.8	0.5	106/63	44.7	46.8	8.3	0.3	61/28
	75	47.7	41.2	9.9	1.3		48.9	39.8	10.9	0.4	
30	15	43.5	47.1	9.2	0.2	108/66	43.4	45.7	10.7	0.2	60/40
	75	47.7	41.4	9.8	1.2		47.4	41.7	10.0	0.9	
60	15	45.6	44.9	9.1	0.4	108/67	43.7	45.9	10.1	0.3	61/41
	75	47.2	42.1	9.3	1.4		46.7	41.1	9.9	0.7	

Table A.5. XPS atomic composition and water contact angle (θ_A/θ_R) data for the reaction of PCTFE-OH (initially modified at -78 °C) with C_3H_7COCl without catalyst and XPS atomic composition and hexadecane (HD) contact angle data after labelling with C_3F_7COCl.

Time (h)	θ_T degrees	Atomic Composition (%) before Labelling				θ_A/θ_R (water) degrees	Atomic Composition (%) after Labelling				θ_A/θ_R (HD) degrees
		C	F	O	Cl		C	F	O	Cl	
0	15	68.4	18.8	11.2	1.6	67/17	44.0	46.1	9.7	0.3	60/40
	75	61.4	22.8	10.9	4.8		47.5	41.9	9.4	1.3	
1	15	66.8	18.4	13.4	1.4	79/31	51.8	37.7	10.0	0.5	50/25
	75	65.7	19.0	13.0	2.3		54.3	33.9	11.0	0.9	
2	15	67.9	17.8	12.9	1.4	82/33	53.3	35.6	10.4	0.7	46/18
	75	66.9	17.7	13.1	2.3		57.4	29.6	11.5	1.5	
4	15	66.5	18.6	13.8	1.2	80/40	56.3	30.7	11.5	1.6	43/17
	75	65.1	18.3	14.2	2.5		58.7	26.9	11.9	2.5	
8	15	70.0	14.5	14.3	1.3	85/43	59.2	27.6	12.6	0.6	35/4
	75	68.4	15.8	14.2	1.7		65.1	20.6	12.9	1.4	
12	15	70.3	14.2	14.4	1.1	90/46	62.6	23.4	13.0	1.0	32/5
	75	68.6	15.9	14.2	1.3		65.9	19.2	13.6	1.3	
24	15	68.7	16.0	14.0	1.3	94/46	64.4	21.3	13.3	1.0	20/0
	75	67.2	17.1	14.3	1.5		66.6	18.0	14.2	1.2	

Table A.6. XPS atomic composition, water and hexadecane (HD) contact angle (θ_A/θ_R) data for the reaction of PCTFE-OH (initially modified at -78 °C) with $C_{17}H_{35}COCl$ without catalyst and XPS atomic composition and hexadecane (HD) contact angle data after labelling with C_3F_7COCl.

Time (h)	θ_T degrees	Atomic Composition (%) before Labelling				θ_A/θ_R (water), (HD) degrees	Atomic Composition (%) after Labelling				θ_A/θ_R (HD) degrees
		C	F	O	Cl		C	F	O	Cl	
0	15	68.4	8.8	11.2	1.6	67/17	44.0	46.1	9.7	0.95	60/40
	75	61.4	22.8	10.9	4.8	, 18/6	47.5	41.9	9.4	1.13	
1	15	71.1	17.3	10.3	1.3	80/19	51.6	39.3	8.6	1.31	59/8
	75	71.3	15.1	10.9	2.7	, 11/0	54.7	35.0	9.0	1.56	
2	15	78.4	12.5	7.9	1.2	98/27	55.6	35.2	8.7	1.58	53/4
	75	74.4	13.3	9.7	2.6	, 20/4	59.5	30.2	8.7	1.97	
4	15	88.7	6.0	4.8	0.5	104/56,	60.7	30.3	8.5	2.00	33/0
	75	82.4	8.8	8.0	0.9	27/17	69.4	21.5	8.5	3.23	
8	15	90.4	4.7	4.4	0.6	105/75,	66.8	24.2	8.3	2.76	25/5
	75	82.6	8.2	8.1	1.1	34/25	72.1	18.6	8.4	3.88	
12	15	90.4	5.1	3.9	0.7	108/84,	74.9	16.5	8.0	4.54	15/0
	75	83.6	7.9	7.4	1.1	42/34	75.3	15.2	8.5	4.95	
24	15	91.6	4.5	3.5	0.4	111/91,	75.7	16.5	7.0	4.59	12/0
	75	84.2	7.8	7.3	0.8	41/35	77.3	14.2	7.7	5.44	

Table A.7. XPS atomic composition and water contact angle (θ_A/θ_R) data for the methanolysis of PCTFE-OCOC$_3$F$_7$ (initially modified at -78 °C) in 0:100 water:methanol solution and XPS atomic composition and hexadecane (HD) contact angle data after labelling with C$_3$H$_7$COCl.

Time (min)	θ_T degrees	Atomic Composition (%) before Labelling				θ_A/θ_R (water) degrees	Atomic Composition (%) after Labelling				θ_A/θ_R (HD) degrees
		C	F	O	Cl		C	F	O	Cl	
0	15	44.0	46.1	9.7	0.3	108/67	43.9	46.3	8.8	1.0	60/40
	75	47.5	41.9	9.4	1.3		46.6	42.2	8.8	2.4	
15	15	64.9	21.4	12.2	1.6	70/21	68.0	15.4	14.7	1.9	14/5
	75	62.6	21.9	11.5	4.6		67.2	16.9	13.1	2.9	
30	15	63.0	20.5	14.5	2.1	71/20	66.8	14.9	15.2	3.1	15/4
	75	61.6	21.1	12.7	4.6		64.3	18.6	13.1	4.0	
60	15	63.3	19.5	15.1	2.1	69/19	69.5	13.0	15.8	1.7	12/3
	75	61.2	21.3	12.6	5.0		67.5	15.6	14.5	2.5	
120	15	63.7	20.5	13.8	2.0	71/18	65.0	16.4	15.6	3.0	11/3
	75	59.9	21.6	12.7	5.8		62.4	19.2	13.8	4.7	

Table A.8. XPS atomic composition and water contact angle (θ_A/θ_R) data for the hydrolysis of PCTFE-OCOC$_3$F$_7$ (initially modified at -78 °C) in 25:75 water:methanol solution and XPS atomic composition and hexadecane (HD) contact angle data after labelling with C$_3$H$_7$COCl.

Time (min)	θ_T degrees	Atomic Composition (%) before Labelling				θ_A/θ_R (water) degrees	Atomic Composition (%) after Labelling				θ_A/θ_R (HD) degrees
		C	F	O	Cl		C	F	O	Cl	
0	15	44.0	46.1	9.7	0.3	108/67	43.9	46.3	8.8	1.0	60/40
	75	47.5	41.9	9.4	1.3		46.6	42.2	8.8	2.4	
15	15	64.5	21.5	12.2	1.8	70/20	70.0	12.1	16.6	1.4	10/5
	75	61.5	22.7	11.4	4.5		69.0	14.4	14.8	1.8	
30	15	64.2	19.3	14.0	2.5	72/19	67.9	15.6	14.2	2.2	12/3
	75	58.0	24.2	10.5	7.3		64.9	17.9	13.4	3.7	
60	15	64.6	21.5	11.8	2.1	70/21	66.8	16.4	14.2	2.7	11/0
	75	60.0	23.8	10.8	5.4		65.8	17.8	12.4	3.9	
120	15	61.4	21.2	14.0	3.3	73/19	69.7	13.6	15.0	1.7	12/5
	75	55.4	26.5	11.0	7.1		66.5	16.2	14.5	2.8	

Table A.9. XPS atomic composition and water contact angle (θ_A/θ_R) data for the hydrolysis of PCTFE-OCOC$_3$F$_7$ (initially modified at -78 °C) in 50:50 water:methanol solution and XPS atomic composition and hexadecane (HD) contact angle data after labelling with C$_3$H$_7$COCl.

Time (min)	θ_T degrees	Atomic Composition (%) before Labelling				θ_A/θ_R (water) degrees	Atomic Composition (%) after Labelling				θ_A/θ_R (HD) degrees
		C	F	O	Cl		C	F	O	Cl	
0	15	44.0	46.1	9.7	0.3	108/67	43.9	46.3	8.8	1.0	60/40
	75	47.5	41.9	9.4	1.3		46.6	42.2	8.8	2.4	
15	15	63.9	22.2	11.8	2.1	72/21	72.6	11.9	13.9	1.6	9/0
	75	59.0	24.6	10.7	5.7		67.5	16.0	13.5	3.1	
30	15	62.0	23.0	12.8	2.2	71/21	67.9	15.6	14.4	2.1	14/1
	75	59.9	23.1	11.4	5.6		66.0	17.5	13.6	2.9	
60	15	59.8	23.9	14.4	2.0	66/14	67.5	15.3	14.8	2.4	14/4
	75	59.2	23.2	12.6	5.0		65.4	16.9	14.4	3.3	
120	15	62.2	20.1	15.1	2.5	71/13	71.4	12.0	15.4	1.2	14/0
	75	56.6	24.2	12.8	6.4		70.0	13.7	14.8	1.4	

Table A.10. XPS atomic composition and water contact angle (θ_A/θ_R) data for the hydrolysis of PCTFE-OCOC$_3$F$_7$ (initially modified at -78 °C) in 75:25 water:methanol solution and XPS atomic composition and hexadecane (HD) contact angle data after labelling with C$_3$H$_7$COCl.

Time (min)	θ_T degrees	Atomic Composition (%) before Labelling				θ_A/θ_R (water) degrees	Atomic Composition (%) after Labelling				θ_A/θ_R (HD) degrees
		C	F	O	Cl		C	F	O	Cl	
0	15	44.0	46.1	9.7	0.3	108/67	43.9	46.3	8.8	1.0	60/40
	75	47.5	41.9	9.4	1.3		46.6	42.2	8.8	2.4	
15	15	66.4	18.9	13.4	1.3	74/27	63.2	15.6	20.2	1.0	23/9
	75	63.3	21.1	12.2	3.4		66.1	16.4	15.7	1.7	
30	15	64.6	22.7	10.9	1.7	72/21	71.0	11.4	16.8	0.8	14/6
	75	61.1	23.0	11.4	4.6		71.3	12.3	15.9	0.5	
60	15	62.6	23.7	11.0	2.7	72/18	64.3	20.9	11.5	3.3	13/0
	75	57.4	26.7	9.9	6.0		58.8	24.7	8.22	5.9	
120	15	60.2	25.6	10.5	3.8	66/15	67.5	12.0	18.2	2.4	14/4
	75	58.8	25.3	10.4	5.5		61.1	20.2	13.8	4.9	

Table A.11. XPS atomic composition and water contact angle (θ_A/θ_R) data for the hydrolysis of PCTFE-OCOC$_3$F$_7$ (initially modified at -78 °C) in 100:0 water:methanol solution and XPS atomic composition and hexadecane (HD) contact angle data after labelling with C$_3$H$_7$COCl.

Time (min)	θ_T degrees	Atomic Composition (%) before Labelling				θ_A/θ_R (water) degrees	Atomic Composition (%) after Labelling				θ_A/θ_R (HD) degrees
		C	F	O	Cl		C	F	O	Cl	
0	15	44.0	46.1	9.7	0.3	108/67	43.9	46.3	8.8	1.0	60/40
	75	47.5	41.9	9.4	1.3		46.6	42.2	8.8	2.4	
15	15	63.5	23.2	10.9	2.5	74/26	64.5	19.3	14.3	1.8	24/12
	75	57.8	25.7	11.7	4.8		65.7	17.8	14.3	2.3	
30	15	66.0	18.7	13.3	2.0	68/18	67.5	15.3	15.4	1.7	19/6
	75	64.3	19.8	12.6	3.4		68.2	14.6	15.4	1.8	
60	15	66.8	19.5	11.9	1.7	65/15	66.9	15.3	15.2	2.6	12/4
	75	61.1	22.6	11.8	4.5		69.3	14.2	14.5	2.0	
120	15	65.7	19.2	12.7	2.4	65/16	65.0	17.4	14.6	3.0	10/0
	75	60.0	23.3	11.4	5.3		63.4	18.0	14.5	4.1	

Table A.12. XPS atomic composition and water contact angle (θ_A/θ_R) data for the hydrolysis of PCTFE-OCOC$_3$F$_7$ (initially modified at -78 °C) in 100:0 water:methanol solution for 15 min as a function of temperature and XPS atomic composition and hexadecane (HD) contact angle data after labelling with C$_3$H$_7$COCl.

Temp. (°C)	θ_T degrees	Atomic Composition (%) before Labelling				θ_A/θ_R (water) degrees	Atomic Composition (%) after Labelling				θ_A/θ_R (HD) degrees
		C	F	O	Cl		C	F	O	Cl	
Control	15	44.0	46.1	9.7	0.3	108/67	43.9	46.3	8.8	1.0	60/40
	75	47.5	41.9	9.4	1.3		46.6	42.2	8.8	2.4	
30	15	49.4	39.0	11.2	0.5	99/36	52.3	36.5	11.0	0.3	48/15
	75	54.1	33.0	11.9	1.0		57.0	30.1	11.2	1.6	
60	15	53.9	34.0	10.9	1.2	90/31	53.7	32.2	13.0	1.2	44/12
	75	55.3	31.1	10.6	3.1		60.0	25.2	12.6	2.3	
90	15	61.1	25.4	12.4	1.0	84/27	65.3	18.0	15.3	1.4	26/11
	75	62.2	22.8	12.6	2.4		68.1	14.9	15.7	1.3	
105	15	63.5	23.2	10.9	2.5	74/26	64.5	19.3	14.3	1.8	24/12
	75	57.8	25.7	11.7	4.8		65.7	17.8	14.3	2.3	

Table A.13. XPS atomic composition and water contact angle (θ_A/θ_R) data for the methanolysis of PCTFE-OCOC$_3$H$_7$ (initially modified at -78 °C) in 0:100 water:methanol solution and XPS atomic composition and hexadecane (HD) contact angle data after labelling with C$_3$F$_7$COCl.

Time (min)	θ_T degrees	Atomic Composition (%) before Labelling				θ_A/θ_R (water) degrees	Atomic Composition (%) after Labelling				θ_A/θ_R (HD) degrees
		C	F	O	Cl		C	F	O	Cl	
0	15	71.9	12.3	15.0	0.8	89/54	70.7	14.3	13.5	1.5	10/0
	75	70.7	13.3	14.8	1.1		67.7	15.7	12.7	3.0	
15	15	67.1	18.3	13.1	1.6	71/25	49.2	40.1	9.5	1.2	56/28
	75	63.5	20.5	11.7	4.3		48.8	39.0	9.8	2.5	
30	15	67.1	19.1	12.5	1.2	62/19	47.4	42.4	9.8	0.4	57/36
	75	63.7	20.1	12.3	4.0		49.5	38.9	10.0	1.7	
60	15	66.6	20.1	12.1	1.2	73/18	47.3	42.3	9.9	0.6	59/38
	75	65.2	19.2	12.9	2.8		50.0	39.0	9.7	1.3	
120	15	65.6	18.9	13.2	2.3	75/20	45.3	44.6	9.4	0.7	60/41
	75	62.0	21.1	11.5	5.4		49.3	39.0	9.5	2.2	

Table A.14. XPS atomic composition and water contact angle (θ_A/θ_R) data for the hydrolysis of PCTFE-OCOC$_3$H$_7$ (initially modified at -78 °C) in 25:75 water:methanol solution and XPS atomic composition and hexadecane (HD) contact angle data after labelling with C$_3$F$_7$COCl.

Time (min)	θ_T degrees	Atomic Composition (%) before Labelling				θ_A/θ_R (water) degrees	Atomic Composition (%) after Labelling				θ_A/θ_R (HD) degrees
		C	F	O	Cl		C	F	O	Cl	
0	15	71.9	12.3	15.0	0.8	89/54	70.7	14.3	13.5	1.5	10/0
	75	70.7	13.3	14.8	1.1		67.7	15.7	12.7	3.0	
15	15	67.2	18.2	12.4	2.3	77/29	48.9	40.1	10.3	0.6	56/22
	75	64.3	20.2	12.2	3.4		51.1	36.9	10.8	1.3	
30	15	65.7	20.9	11.4	2.0	64/16	45.7	43.9	8.7	1.7	59/35
	75	61.6	21.8	11.6	5.0		49.0	38.7	8.7	3.6	
60	15	65.8	16.9	15.7	1.7	72/17	46.9	42.8	9.5	0.8	58/37
	75	65.1	18.5	13.7	2.8		50.2	38.6	9.8	1.5	
120	15	64.2	18.0	16.0	1.7	73/19	46.4	43.5	9.8	0.3	60/39
	75	61.0	21.0	13.0	5.0		49.9	39.3	9.7	1.1	

Table A.15. XPS atomic composition and water contact angle (θ_A/θ_R) data for the hydrolysis of PCTFE-OCOC$_3$H$_7$ (initially modified at -78 °C) in 50:50 water:methanol solution and XPS atomic composition and hexadecane (HD) contact angle data after labelling with C$_3$F$_7$COCl.

Time (min)	θ_T degrees	Atomic Composition (%) before Labelling				θ_A/θ_R (water) degrees	Atomic Composition (%) after Labelling				θ_A/θ_R (HD) degrees
		C	F	O	Cl		C	F	O	Cl	
0	15	71.9	12.3	15.0	0.8	89/54	70.7	14.3	13.5	1.5	10/0
	75	70.7	13.3	14.8	1.1		67.7	15.7	12.7	3.0	
15	15	67.4	17.7	13.1	1.9	80/29	48.9	40.9	9.0	1.3	54/23
	75	63.5	20.2	11.8	4.5		48.8	39.5	9.0	2.8	
30	15	65.2	19.4	14.3	1.1	72/19	48.5	41.1	9.5	0.9	57/25
	75	62.2	21.2	13.5	3.1		50.3	38.9	9.7	1.7	
60	15	63.2	21.7	13.3	1.8	64/19	48.3	40.9	10.1	0.8	58/31
	75	61.5	21.7	12.7	4.1		50.2	37.2	10.8	1.9	
120	15	62.9	18.6	16.1	2.4	68/20	47.8	41.4	10.1	0.6	59/31
	75	61.2	20.0	14.4	4.4		50.0	37.5	10.0	2.4	

Table A.16. XPS atomic composition and water contact angle (θ_A/θ_R) data for the hydrolysis of PCTFE-OCOC$_3$H$_7$ (initially modified at -78 °C) in 75:25 water:methanol solution and XPS atomic composition and hexadecane (HD) contact angle data after labelling with C$_3$F$_7$COCl.

Time (h)	θ_T degrees	Atomic Composition (%) before Labelling				θ_A/θ_R (water) degrees	Atomic Composition (%) after Labelling				θ_A/θ_R (HD) degrees
		C	F	O	Cl		C	F	O	Cl	
0	15	71.9	12.3	15.0	0.8	89/54	70.7	14.3	13.5	1.5	10/0
	75	70.7	13.3	14.8	1.1		67.7	15.7	12.7	3.0	
0.25	15	71.2	13.4	14.7	0.8	82/39	53.4	31.9	13.9	0.8	43/10
	75	67.4	16.2	14.4	2.0		57.1	29.1	12.9	0.8	
0.5	15	70.7	14.4	13.8	1.1	81/33	54.4	34.3	10.7	0.6	49/16
	75	67.6	16.7	13.3	2.5		56.5	30.8	11.3	1.5	
1	15	68.3	16.8	13.3	1.6	80/27	51.6	37.6	10.2	0.6	52/15
	75	65.1	18.7	12.8	3.5		55.8	31.8	11.0	1.5	
2	15	67.5	18.0	12.5	2.0	76/26	51.0	36.8	11.4	0.8	54/17
	75	64.5	20.0	12.1	3.5		55.0	31.7	11.5	1.8	
5	15	67.3	18.3	13.2	1.3	73/25	48.4	41.3	9.6	0.7	57/27
	75	64.3	19.5	12.6	3.7		51.6	35.9	9.8	2.7	
10	15	66.2	19.7	13.4	0.7	70/17	46.7	42.5	10.3	0.7	60/35
	75	63.4	21.3	13.8	1.5		50.5	37.1	10.9	1.5	

Table A.17. XPS atomic composition and water contact angle (θ_A/θ_R) data for the hydrolysis of PCTFE-OCOC$_3$H$_7$ (initially modified at -78 °C) in 100:0 water:methanol solution and XPS atomic composition and hexadecane (HD) contact angle data after labelling with C$_3$F$_7$COCl.

Time (h)	θ_T degrees	Atomic Composition (%) before Labelling				θ_A/θ_R (water) degrees	Atomic Composition (%) after Labelling				θ_A/θ_R (HD) degrees
		C	F	O	Cl		C	F	O	Cl	
0	15	71.9	12.3	15.0	0.8	89/54	70.7	14.3	13.5	1.5	10/0
	75	70.7	13.3	14.8	1.1		67.7	15.7	12.7	3.0	
0.25	15	70.4	13.3	15.3	1.0	88/39	61.2	23.5	14.5	0.9	32/5
	75	70.0	13.9	14.7	1.5		65.2	18.4	15.2	1.2	
0.5	15	70.2	13.9	14.7	1.3	87/35	60.1	24.3	14.8	0.8	34/6
	75	70.1	13.7	15.0	1.3		66.1	17.8	14.9	1.2	
1	15	71.7	12.1	15.6	0.6	87/28	56.7	28.3	13.7	1.3	43/7
	75	70.1	13.9	14.9	1.1		62.8	21.4	14.2	1.6	
2	15	71.0	12.3	16.1	0.6	87/25	55.1	29.0	14.8	1.1	46/8
	75	70.7	13.1	15.4	0.8		62.2	20.9	15.1	1.8	
5	15	70.5	13.2	15.1	1.2	83/14	54.9	29.5	14.3	1.3	50/10
	75	69.4	14.1	15.0	1.5		61.0	22.7	14.6	1.7	
10	15	68.6	14.6	15.3	1.5	82/15	52.0	33.4	12.5	2.1	54/10
	75	68.3	15.3	14.0	2.4		57.8	26.1	12.9	3.2	
15	15	69.8	15.4	14.0	0.8	80/15	50.7	38.0	11.1	1.1	57/12
	75	67.2	17.2	13.9	1.7		56.8	29.6	11.7	2.6	
24	15	66.8	19.0	13.5	0.7	70/16	46.8	42.3	10.4	0.7	60/19
	75	63.31	21.5	13.7	1.5		51.5	36.1	10.9	1.5	

Table A.18. XPS atomic composition and water contact angle (θ_A/θ_R) data for the methanolysis of PCTFE-OCOC$_{17}$H$_{35}$ (initially modified at -78 °C) in 0:100 water:methanol solution and XPS atomic composition and hexadecane (HD) contact angle data after labelling with C$_3$F$_7$COCl.

Time (h)	θ_T degrees	Atomic Composition (%) before Labelling				θ_A/θ_R (water) degrees	Atomic Composition (%) after Labelling				θ_A/θ_R (HD) degrees
		C	F	O	Cl		C	F	O	Cl	
0	15	92.8	2.7	3.9	0.5	108/90	90.9	4.4	4.2	0.6	40/35
	75	85.3	6.4	7.6	0.8		85.1	7.2	7.0	0.8	
0.5	15	90.0	4.9	4.4	0.6	107/87	81.9	11.3	6.2	0.6	20/3
	75	83.4	7.9	7.5	1.2		81.2	10.5	7.8	0.6	
1	15	88.0	5.8	5.4	0.8	103/57	68.5	23.3	7.0	1.2	41/8
	75	82.5	8.6	7.7	1.3		72.9	17.9	8.0	1.2	
1.5	15	77.3	13.0	8.3	1.5	99/28	49.5	42.3	7.6	0.7	56/10
	75	72.0	15.7	10.0	2.4		52.4	37.1	8.6	1.9	
2	15	73.3	15.7	9.5	1.5	86/24	45.9	44.0	9.0	1.0	60/18
	75	66.1	18.5	11.0	4.5		49.9	38.9	9.6	1.5	
2.5	15	60.3	25.0	11.2	3.5	69/18	45.8	44.5	9.0	0.7	60/37
	75	59.2	24.9	10.7	5.3		49.6	39.2	9.5	1.7	
3	15	62.4	23.4	11.6	2.7	70/16	45.0	45.3	8.5	1.1	61/41
	75	60.2	24.0	10.9	5.0		48.6	40.1	9.4	2.0	

Table A.19. XPS atomic composition and water contact angle (θ_A/θ_R) data for the hydrolysis of PCTFE-OCOC$_{17}$H$_{35}$ (initially modified at -78 °C) in 25:75 water:methanol solution and XPS atomic composition and hexadecane (HD) contact angle data after labelling with C$_3$F$_7$COCl.

Time (h)	θ_T degrees	Atomic Composition (%) before Labelling				θ_A/θ_R (water) degrees	Atomic Composition (%) after Labelling				θ_A/θ_R (HD) degrees
		C	F	O	Cl		C	F	O	Cl	
0	15	92.8	2.7	3.9	0.5	108/90	90.9	4.4	4.2	0.6	40/35
	75	85.3	6.4	7.6	0.8		85.1	7.2	7.0	0.8	
0.5	15	91.8	3.4	4.2	0.6	108/89	81.3	11.3	6.9	0.5	21/3
	75	85.6	6.4	7.1	0.9		82.5	9.6	7.4	0.5	
1	15	91.0	4.4	3.8	0.8	108/73	72.5	18.1	8.8	0.7	27/3
	75	85.2	6.9	7.0	0.9		78.8	12.5	7.8	0.9	
2	15	91.6	4.2	3.6	0.6	108/61	69.2	21.4	8.7	0.7	40/5
	75	84.5	7.2	7.4	0.9		76.1	15.4	7.9	0.6	
6	15	82.5	9.6	7.0	0.9	101/33	59.5	31.2	8.7	0.6	50/5
	75	80.0	9.7	9.5	0.8		62.9	26.5	9.5	1.1	
12	15	80.6	11.1	7.3	1.0	98/20	53.1	36.2	9.9	0.9	60/7
	75	79.3	11.2	8.4	1.1		58.0	31.4	9.6	1.1	
18	15	60.5	26.6	11.1	1.8	70/15	46.8	42.1	9.7	1.5	60/31
	75	63.0	21.1	12.2	3.6		49.2	39.3	10.2	1.3	
24	15	58.3	28.3	11.0	2.4	67/16	43.6	45.1	9.8	1.5	59/40
	75	57.3	27.7	10.8	4.2		47.8	39.8	10.1	2.3	

Table A.20. XPS atomic composition and hexadecane (HD) contact angle (θ_A/θ_R) data for the reaction of PCTFE-OH (modified at -15 °C) with the acid chloride mixture of C_3H_7COCl and C_3F_7COCl.

Mole% of C_3F_7COCl	θ_T degrees	Atomic Composition (%)				θ_A/θ_R (HD) degrees
		C	F	O	Cl	
Control PCTFE-OH	15	69.32	16.52	14.05	0.11	5/0
	75	69.40	16.32	14.03	0.26	
0 (PCTFE-OCOC$_3$H$_7$)	15	76.55	7.71	15.64	0.09	10/0
	75	74.70	9.38	15.69	0.23	
0.5	15	61.51	25.93	12.30	0.26	41/14
	75	67.13	19.09	13.20	0.58	
1.0	15	60.21	31.25	8.17	0.37	54/36
	75	62.28	27.16	9.45	1.11	
1.2	15	50.59	39.09	10.12	0.20	56/41
	75	57.90	31.41	10.08	0.60	
1.3	15	47.92	42.29	9.69	0.09	60/42
	75	53.55	35.92	10.23	0.31	
100 (PCTFE-OCOC$_3$F$_7$)	15	47.79	42.86	9.29	0.06	60/40
	75	52.26	38.31	9.23	0.20	

Table A.21. XPS atomic composition and hexadecane (HD) contact angle (θ_A/θ_R) data for the reaction of PCTFE-OH (modified at -15°C) with the acid chloride mixture of $C_{17}H_{35}COCl$ and C_3F_7COCl.

Mole% of C_3F_7COCl	θ_T degrees	Atomic Composition (%)				θ_A/θ_R (HD) degrees
		C	F	O	Cl	
Control	15	69.32	16.52	14.05	0.11	5/0
PCTFE-OH	75	69.40	16.32	14.03	0.26	
0	15	93.69	2.09	4.22	0.00	42/35
(PCTFE-	75	88.40	4.46	7.09	0.06	
OCOC$_{17}$H$_{35}$)						
0.25	15	87.53	2.47	9.89	0.12	39/29
	75	83.67	6.18	9.80	0.35	
0.4	15	70.41	20.24	9.09	0.26	33/19
	75	74.28	14.87	10.68	0.18	
0.5	15	65.31	25.28	9.33	0.08	50/20
	75	68.45	20.67	10.68	0.20	
0.6	15	54.78	33.97	10.95	0.30	57/20
	75	65.45	23.27	11.10	0.18	
0.8	15	50.32	38.47	11.08	0.13	63/32
	75	59.08	29.43	11.27	0.22	
1.0	15	46.40	43.44	9.99	0.17	63/37
	75	50.99	38.00	10.73	0.27	
100	15	47.79	42.86	9.29	0.06	60/40
(PCTFE-	75	52.26	38.31	9.23	0.20	
OCOC$_3$F$_7$)						

CALCULATION OF % COMPOSITION OF SURFACE MIXTURES

A composition of hydrocarbon ester/fluorocarbon mixed surface (Figure B.1) was calculated based on the structure of alcohol-functionalized poly(chlorotrifluoroethylene) (PCTFE-OH) containing 4 alcohol-functionalized repeat units and one unfunctionalized unsaturation unit in every 5 repeat units (Figure 1.1). The PCTFE-OH/-OCOC$_3$H$_7$, PCTFE-OCOC$_{17}$H$_{35}$ samples were labelled with heptafluorobutyryl chloride (C$_3$F$_7$COCl) resulting PCTFE-OCOC$_3$H$_7$/-OCOC$_3$F$_7$ and PCTFE-OCOC$_{17}$H$_{35}$/-OCOC$_3$F$_7$, respectively. The PCTFE-OH/-OCOC$_3$F$_7$ samples were labelled with butyryl chloride (C$_3$H$_7$COCl) resulting in PCTFE-OCOC$_3$H$_7$/-OCOC$_3$F$_7$.
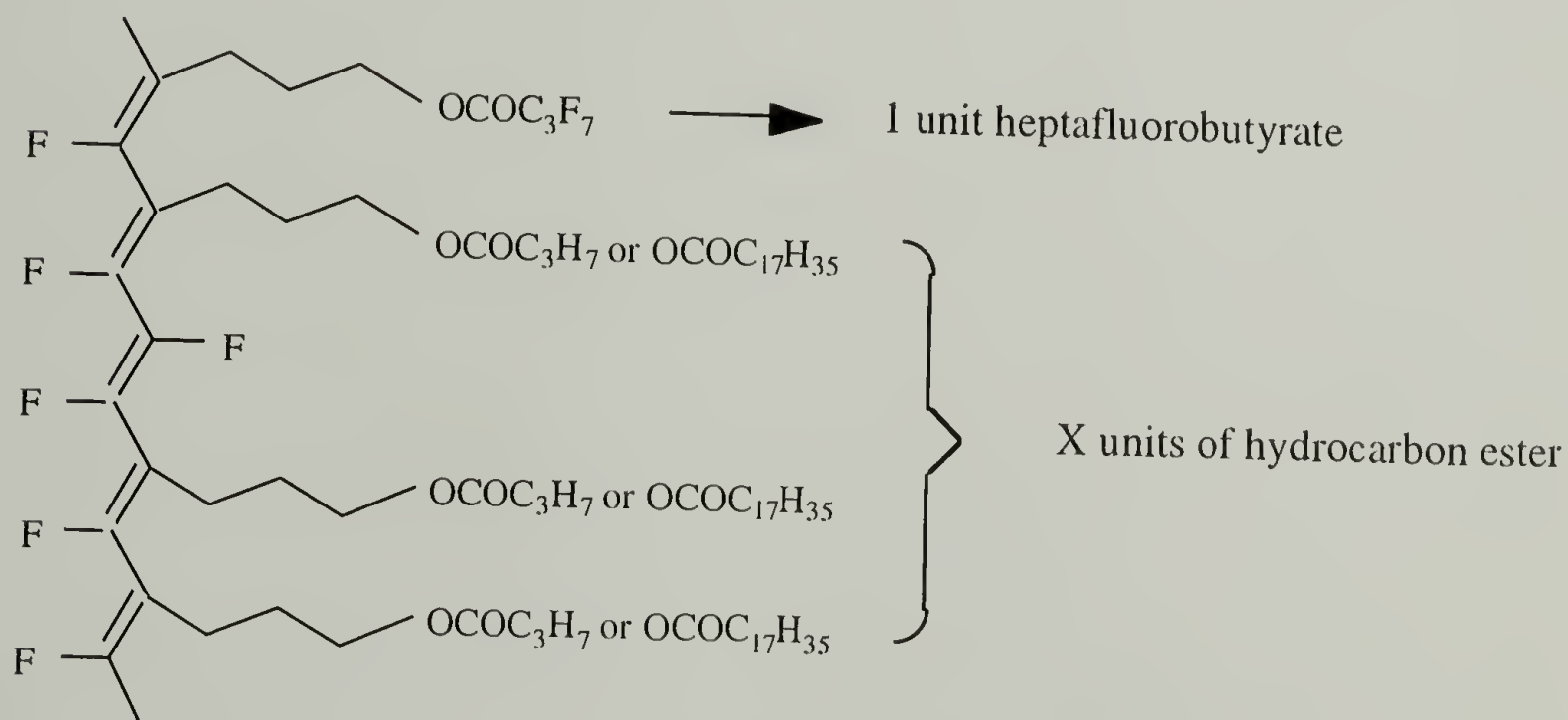
Figure B.1. Structure of hydrocarbon ester/heptafluorobutyrate mixed surface.

For PCTFE-OCOC$_3$H$_7$/OCOC$_3$F$_7$ mixed surface, carbon/fluorine ratio is equal to:

Heptafluorobutyrate unit

Butyrate unit

Every 8 carbons on backbone
contain 2 carbons from an unsaturation unit

$$\frac{C}{F} = \frac{9 + 9X + 2(2X + 2)/8}{8 + X + 2(X + 1)/4}$$ (B.1)

Butyrate unit

Heptafluorobutyrate unit

Every 4 fluorines on backbone
contain 2 fluorines from an unsaturation unit

A number of butyrate units ($X_{butyrate}$) in a PCTFE-OCOC$_3$H$_7$/-OCOC$_3$F$_7$ mixed surface can be calculated from:

$$X_{butyrate} = \frac{8.5(C/F) - 9.5}{9.5 - 1.5(C/F)}$$ (B.2)

For PCTFE-OCOC$_{17}$H$_{35}$/-OCOC$_3$F$_7$ mixed surface, carbon:fluorine ratio is equal to:

$$\frac{C}{F} = \frac{9 + 23X + 2(2X + 2)/8}{8 + X + 2(X + 1)/4}$$ (B.3)

A number of stearate units ($X_{stearate}$) in a PCTFE-OCOC$_{17}$H$_{35}$/-OCOC$_3$F$_7$ mixed surface can be calculated from:

$$X_{stearate} = \frac{8.5(C/F) - 9.5}{23.5 - 1.5(C/F)}$$ (B.4)

191

For a hydrocarbon ester/heptafluorobutyrate mixed surface which is composed of 1 heptafluorobutyrate unit and X hydrocarbon ester units, % composition of hydrocarbon ester can be calculated from:

$$\text{\% Composition of Hydrocarbon Ester} = X/(X+1) \times 100\% \qquad \text{(B.5)}$$

Note that this calculation assumes that all hydroxyl groups are converted into ester functional groups (hydrocarbon esters or fluorocarbon esters).

DATA TABLES FOR CHAPTER 2

Table C.1. XPS atomic composition and water contact angle (θ_A/θ_R) data for kinetics studies of PAH first layer adsorption to PCTFE-OH at pH 4.

Time (min)	θ_T (degrees)	Atomic Composition (%)					θ_A/θ_R (degrees)
		C	O	F	Cl	N	
0	15	73.63	15.16	11.15	0.06	-	69/25
	75	73.60	15.27	11.00	0.13	-	
5	15	73.56	15.25	9.97	0.29	0.92	68/22
	75	72.64	15.80	10.43	0.30	0.83	
10	15	75.22	14.97	8.39	0.32	1.11	63/23
	75	74.11	15.09	9.78	0.30	0.73	
20	15	75.79	15.40	7.46	0.41	0.94	66/25
	75	73.36	16.02	9.39	0.40	0.84	
30	15	77.50	14.82	6.24	0.34	1.10	61/27
	75	76.03	15.06	7.73	0.34	0.84	
60	15	73.82	15.07	9.93	0.29	0.89	63/27
	75	72.64	15.30	10.96	0.26	0.84	
120	15	75.89	14.04	8.76	0.33	0.98	62/26
	75	73.28	14.69	10.87	0.28	0.88	

Table C.2. XPS atomic composition and water contact angle (θ_A/θ_R) data for pH dependent adsorption studies of PAH first layer to PCTFE-OH.

pH	θ_T (degrees)	Atomic Composition (%)					θ_A/θ_R (degrees)
		C	O	F	Cl	N	
1.7	15	69.78	13.68	15.67	0.16	0.71	69/22
	75	70.22	14.45	14.81	0.11	0.41	
2.3	15	68.14	13.36	17.25	0.21	1.04	69/23
	75	69.79	13.48	16.03	0.16	0.54	
3.0	15	68.32	13.42	16.81	0.28	1.17	69/24
	75	69.93	14.10	15.23	0.21	0.53	
5.0	15	69.42	15.26	13.59	0.40	1.33	67/25
	75	69.24	15.05	14.59	0.32	0.79	
6.0	15	70.54	14.37	13.32	0.45	1.35	68/23
	75	70.43	14.28	14.15	0.34	0.80	
7.0	15	70.98	14.60	12.49	0.54	1.39	71/22
	75	70.62	14.43	13.78	0.37	0.81	
9.0	15	70.44	13.76	12.02	1.04	2.73	70/19
	75	70.79	14.14	12.51	0.92	1.65	
11.0	15	75.97	11.35	4.14	3.59	4.94	74/14
	75	72.17	11.63	7.94	3.53	4.73	

Table C.3. XPS atomic composition and water contact angle (θ_A/θ_R) data for adsorption studies of PAH first layer to PCTFE-OH at pH 6 as a function of PAH concentration.

[PAH] (mol/L)	θ_T (degrees)	Atomic Composition (%)					θ_A/θ_R (degrees)
		C	O	F	Cl	N	
0.00	15	69.32	14.05	16.52	0.11	-	
	75	69.40	14.03	16.32	0.26	-	69/25
0.005	15	70.45	14.79	12.79	0.49	1.48	
	75	70.03	14.24	14.79	0.18	0.76	66/25
0.01	15	73.80	14.04	10.12	0.43	1.61	
	75	71.74	13.96	13.46	0.23	0.61	67/23
0.02	15	70.54	14.37	13.32	0.45	1.35	
	75	70.43	14.28	14.15	0.34	0.80	68/23
0.05	15	74.41	13.75	8.95	0.77	2.12	
	75	71.45	14.36	12.46	0.52	1.21	69/18
0.10	15	71.97	15.67	10.07	0.87	1.43	
	75	71.15	14.80	12.65	0.43	0.97	70/18
0.20	15	72.04	11.41	12.90	1.51	2.13	
	75	71.82	12.80	13.56	0.65	1.17	72/15

Table C.4. XPS atomic composition and water contact angle (θ_A/θ_R) data for ionic strength dependent adsorption studies of PAH first layer to PCTFE-OH at pH 6 as a function of MnCl$_2$ concentration.

MnCl$_2$ (mol/L)	θ_T (degrees)	Atomic Composition (%)						θ_A/θ_R (degrees)
		C	O	F	Cl	N	Mn	
0	15	70.54	14.37	13.32	0.45	1.35	-	68/23
	75	70.43	14.28	14.15	0.34	0.80	-	
0.25	15	69.08	13.42	15.13	0.30	1.57	0.50	64/25
	75	69.55	14.16	14.67	0.25	0.67	0.70	
0.50	15	69.64	15.11	12.43	0.43	1.62	0.78	66/24
	75	69.32	14.50	14.57	0.23	0.75	0.63	
1.00	15	67.75	16.47	11.77	1.22	1.80	0.99	72/25
	75	69.36	15.15	13.82	0.40	0.71	0.57	
1.50	15	68.91	12.18	15.10	0.78	1.89	1.15	69/24
	75	68.50	14.87	14.76	0.34	0.75	0.78	

Table C.5. XPS atomic composition and water contact angle (θ_A/θ_R) data for kinetics studies of desorption of PAH adsorbed to PCTFE-OH at pH 11 and treated with water at pH 4.

Time (min)	θ_T (degrees)	Atomic Composition (%)					θ_A/θ_R (degrees)
		C	O	F	Cl	N	
0	15	75.97	11.35	4.14	3.59	4.94	74/14
	75	72.17	11.63	7.94	3.53	4.73	
5	15	72.84	11.66	9.27	2.04	4.19	73/14
	75	69.72	13.89	10.99	1.83	3.58	
10	15	66.46	16.40	11.39	2.00	3.75	70/13
	75	69.44	13.39	11.71	2.00	3.46	
30	15	70.63	13.42	10.68	1.16	4.11	70/13
	75	67.96	16.72	11.07	0.96	3.28	
60	15	71.97	14.13	8.13	1.54	4.23	71/10
	75	69.24	16.57	9.82	1.02	3.35	

Table C.6. XPS atomic composition and water contact angle (θ_A/θ_R) data for kinetics studies of PSS adsorption to PCTFE-OH-PAH at pH 4.

Time (min)	θ_T (degrees)	Atomic Composition (%)[a]					θ_A/θ_R (degrees)
		C	O	F	N	S	
0	15	69.65	17.45	11.86	1.04	-	69/26
	75	69.81	13.67	16.06	0.47	-	
10	15	65.58	20.02	12.85	1.01	0.54	68/20
	75	68.34	13.92	16.85	0.61	0.28	
20	15	69.94	16.50	12.03	0.95	0.58	64/17
	75	69.42	14.44	15.37	0.50	0.27	
30	15	71.24	17.93	9.14	1.05	0.63	67/18
	75	69.77	14.31	15.27	0.41	0.24	
60	15	70.99	15.41	11.55	1.37	0.69	69/17
	75	68.84	14.47	15.80	0.61	0.29	

a - Atomic composition of chlorine was neglected in analysis.

Table C.7. XPS atomic composition and water contact angle (θ_A/θ_R) data for ionic strength dependent adsorption studies of PSS to PCTFE-OH-PAH at pH 4 as a function of $MnCl_2$ concentration.

[$MnCl_2$] (mol/L)	θ_T (degrees)	Atomic Composition (%)[b]					θ_A/θ_R (degrees)
		C	O	F	N	S	
0	15	69.94	16.50	12.03	0.95	0.58	64/17
	75	69.42	14.44	15.37	0.50	0.27	
0.1	15	72.69	21.46	3.45	0.96	1.44	52/10
	75	73.32	17.42	7.27	0.86	1.12	
0.2	15	72.92	19.17	4.77	1.09	2.05	48/11
	75	72.23	15.97	10.29	0.42	1.10	
0.5	15	71.40	20.58	5.41	0.80	1.82	51/12
	75	71.58	15.86	10.78	0.64	1.14	
1.0	15	71.71	20.49	5.28	0.66	1.86	52/12
	75	71.68	15.78	10.94	0.57	1.03	

b - Atomic composition of chlorine and manganese were neglected in analysis.

Table C.8. XPS atomic composition and water contact angle (θ_A/θ_R) data for the series of PAH/PSS multilayer assemblies using Protocol 1.

Number of Layers	θ_r (degrees)	Atomic Composition (%)[a]					θ_A/θ_R (degrees)
		C	O	F	N	S	
0	15	69.32	14.05	16.52	-	-	69/25
	75	69.40	14.03	16.32			
1 (PAH)	15	69.65	17.45	11.86	1.04	-	69/26
	75	69.81	13.67	16.06	0.47		
2 (PSS)	15	69.94	16.50	12.03	0.95	0.58	64/17
	75	69.42	14.44	15.37	0.50	0.27	
3 (PAH)	15	68.51	16.72	12.28	1.76	0.73	70/19
	75	69.40	14.62	14.75	0.90	0.32	
4 (PSS)	15	71.04	15.61	10.80	1.39	1.16	65/16
	75	70.67	13.71	14.48	0.72	0.41	
5 (PAH)	15	71.23	14.40	11.12	2.03	1.22	68/18
	75	70.66	13.95	13.83	1.10	0.46	
6 (PSS)	15	70.17	15.89	11.73	1.22	1.00	65/16
	75	70.28	14.33	13.98	0.88	0.53	
7 (PAH)	15	70.94	15.09	11.68	1.34	0.95	68/19
	75	70.70	14.34	13.32	1.11	0.52	
8 (PSS)	15	72.10	13.92	11.47	1.34	1.17	63/17
	75	71.29	14.60	12.54	0.92	0.66	
9 (PAH)	15	69.45	16.13	11.35	1.82	1.26	69/19
	75	70.40	14.69	12.92	1.30	0.68	
10 (PSS)	15	71.30	15.77	10.07	1.45	1.42	63/12
	75	70.87	14.72	12.53	1.12	0.77	
11 (PAH)	15	69.84	19.86	6.70	1.99	1.61	62/13
	75	72.45	14.23	11.20	1.29	0.83	
12 (PSS)	15	68.24	21.39	7.26	1.50	1.61	62/12
	75	70.65	14.99	11.67	1.61	1.09	
13 (PAH)	15	69.77	17.77	8.38	2.45	1.63	63/13
	75	71.54	14.45	11.23	1.73	1.05	
14 (PSS)	15	70.87	17.95	6.19	2.71	2.28	59/10
	75	71.23	14.85	10.66	1.94	1.31	
15 (PAH)	15	72.16	16.07	6.05	3.17	2.54	60/10
	75	72.40	14.40	9.79	2.10	1.30	
16 (PSS)	15	70.77	18.08	6.30	2.54	2.31	61/12
	75	71.32	15.06	10.06	2.09	1.47	

Table C.8, continued

Number of Layers	θ_T (degrees)	Atomic Composition (%)[a]					θ_A/θ_R (degrees)
		C	O	F	N	S	
17	15	70.27	18.17	5.98	3.10	2.48	
(PAH)	75	71.56	14.70	10.33	2.05	1.36	60/12
18	15	71.87	17.15	5.06	3.09	2.82	
(PSS)	75	72.39	14.58	9.57	2.02	1.43	61/12
19	15	70.68	17.78	5.30	3.55	2.69	
(PAH)	75	71.97	14.98	9.58	2.08	1.39	62/12
20	15	71.97	17.60	3.58	3.61	3.24	
(PSS)	75	72.05	15.21	8.01	2.75	1.98	61/11
21	15	71.04	18.19	3.68	3.94	3.15	
(PAH)	75	71.45	15.24	9.22	2.49	1.61	61/12
22	15	71.12	18.17	3.45	3.76	3.50	
(PSS)	75	71.57	15.48	8.72	2.40	1.83	59/11

a - Atomic composition of chlorine was neglected in analysis.

Table C.9. XPS atomic composition and water contact angle (θ_A/θ_R) data for the series of PAH/PSS multilayer assemblies using Protocol 2.

Number of Layers	θ_T (degrees)	Atomic Composition (%)[a]					θ_A/θ_R (degrees)
		C	O	F	N	S	
0	15	69.32	14.05	16.52	-	-	69/25
	75	69.40	14.03	16.32			
1	15	66.46	16.40	11.39	3.75	-	70/13
(PAH)	75	69.44	13.39	11.71	3.46		
2	15	67.66	23.20	4.66	2.27	2.22	64/17
(PSS)	75	71.35	16.05	7.63	2.86	2.11	
3	15	70.25	18.99	5.52	2.81	2.44	64/14
(PAH)	75	72.33	14.82	7.94	3.04	1.88	
4	15	69.91	20.10	4.76	2.52	2.71	64/12
(PSS)	75	71.64	16.11	6.98	3.06	2.21	
5	15	70.45	19.36	4.24	3.21	2.74	64/12
(PAH)	75	71.98	15.55	7.06	3.25	2.15	
6	15	69.89	20.40	2.92	3.45	3.34	63/12
(PSS)	75	72.29	16.10	5.65	3.37	2.58	
7	15	69.72	20.38	2.73	3.88	3.29	63/10
(PAH)	75	72.91	15.93	5.28	3.52	2.37	
8	15	70.93	20.43	2.07	3.15	3.42	60/12
(PSS)	75	72.31	16.38	5.40	3.30	2.61	
9	15	72.35	18.12	1.61	4.39	3.53	60/12
(PAH)	75	72.90	15.75	4.94	3.83	2.58	
10	15	70.64	19.74	1.75	4.09	3.78	59/11
(PSS)	75	70.63	17.76	5.09	3.67	2.86	
11	15	73.88	17.21	1.68	4.06	3.17	61/12
(PAH)	75	73.47	15.33	3.88	4.42	2.90	
12	15	73.70	17.30	1.16	3.89	3.96	59/11
(PSS)	75	72.93	15.74	3.54	4.47	3.33	
13	15	76.26	14.54	1.18	4.29	3.73	61/12
(PAH)	75	72.60	15.67	3.97	4.54	3.22	
14	15	76.11	14.68	1.16	4.11	3.94	60/12
(PSS)	75	72.59	16.36	3.39	4.37	3.30	
15	15	75.38	15.58	0.92	4.26	3.86	61/12
(PAH)	75	72.57	16.70	2.97	4.56	3.20	
16	15	76.64	14.41	0.93	3.99	4.03	60/11
(PSS)	75	72.83	16.05	3.62	4.11	3.39	

Table C.9, continued

Number of Layers	θ_T (degrees)	Atomic Composition (%)[a]					θ_A/θ_R (degrees)
		C	O	F	N	S	
17	15	75.60	14.95	0.88	4.52	4.05	61/12
(PAH)	75	73.71	15.47	3.19	4.35	3.29	
18	15	73.29	19.17	0.84	3.37	3.32	59/12
(PSS)	75	73.10	16.61	2.72	4.00	3.56	
19	15	74.65	16.26	0.55	4.57	3.96	60/10
(PAH)	75	73.29	15.33	3.14	4.88	3.36	
20	15	74.30	17.47	0.90	3.77	3.57	60/10
(PSS)	75	72.28	16.30	2.92	4.74	3.76	
21	15	74.30	16.45	0.89	4.52	3.83	60/11
(PAH)	75	72.31	16.98	2.26	4.94	3.52	
22	15	74.98	15.48	0.94	4.57	4.03	60/10
(PSS)	75	72.14	17.11	1.97	4.98	3.80	
23	15	74.62	16.19	0.89	4.38	3.92	60/11
(PAH)	75	73.16	16.47	1.66	4.99	3.71	
24	15	74.06	16.85	1.09	4.08	3.92	60/11
(PSS)	75	72.45	17.64	1.84	4.51	3.57	
25	15	74.34	16.32	0.94	4.47	3.94	61/11
(PAH)	75	73.10	16.57	1.38	5.16	3.78	
26	15	73.78	17.05	1.19	3.90	4.09	59/9
(PSS)	75	72.58	16.81	1.46	5.01	3.87	
27	15	74.56	16.66	0.99	4.22	3.58	60/10
(PAH)	75	73.37	16.50	1.24	5.22	3.68	
28	15	72.49	18.33	0.93	4.21	4.03	60/10
(PSS)	75	72.74	17.03	1.26	5.11	3.86	
29	15	72.53	18.38	0.60	4.47	4.03	59/10
(PAH)	75	73.19	16.81	1.18	5.09	3.72	

a - Atomic composition of chlorine was neglected in analysis.

Table C.10. XPS atomic composition and water contact angle (θ_A/θ_R) data for the series of PAH/PSS multilayer assemblies using Protocol 3.

Number of Layers	θ_T (degrees)	Atomic Composition (%)[b]					θ_A/θ_R (degrees)
		C	O	F	N	S	
0	15	69.32	14.05	16.52	-	-	
	75	69.40	14.03	16.32			69/25
1	15	66.46	16.40	11.39	3.75		
(PAH)	75	69.44	13.39	11.71	3.46	-	70/13
2	15	72.47	19.32	1.10	3.22	3.88	
(PSS)	75	73.10	17.53	2.97	3.13	2.28	47/11
3	15	75.82	15.34	1.28	4.10	3.45	
(PAH)	75	72.27	17.12	3.66	4.17	2.78	57/11
4	15	74.50	16.80	0.70	3.48	4.53	
(PSS)	75	71.53	18.67	2.24	3.80	3.75	45/12
5	15	74.98	15.79	0.75	4.57	3.91	
(PAH)	75	72.61	17.02	2.17	4.90	3.30	56/11
6	15	74.19	17.13	0.72	3.30	4.66	
(PSS)	75	72.48	18.15	1.10	4.02	4.24	46/12
7	15	71.56	19.69	0.81	4.28	3.67	
(PAH)	75	73.04	16.50	1.12	5.44	3.91	48/10
8	15	73.49	18.26	0.84	3.08	4.33	
(PSS)	75	71.55	18.31	0.59	4.68	4.87	45/12
9	15	72.11	19.10	1.16	4.19	3.44	
(PAH)	75	72.24	15.89	0.46	5.39	4.03	50/10
10	15	71.93	19.81	0.85	2.95	4.47	
(PSS)	75	71.56	18.67	0.35	4.49	4.92	41/10
11	15	74.00	16.59	1.01	4.42	3.98	
(PAH)	75	73.02	16.37	0.73	5.67	4.21	50/11
12	15	74.34	17.47	0.42	3.26	4.51	
(PSS)	75	71.54	18.43	0.27	4.75	5.05	38/10

b - Atomic composition of chlorine and manganese were neglected in analysis.

Table C.11. $-\ln(N/N_0)\sin\theta$ data for the series of PAH/PSS multilayer assemblies using Protocols 1, 2 and 3.

Number of Layers	$-\ln(N/N_0)\sin\theta$					
	Protocol 1		Protocol 2		Protocol 3	
	15 degree	75 degree	15 degree	75 degree	15 degree	75 degree
0	0	0	0	0	0	0
1	0.0858	0.0155	0.0965	0.2961	0.0962	0.3206
2	0.0821	0.0579	0.3279	0.7098	0.7012	1.6458
3	0.0768	0.0977	0.2840	0.6713	0.6620	1.4440
4	0.1100	0.1155	0.3224	0.7958	0.8182	1.9182
5	0.1024	0.1599	0.3523	0.7848	0.8003	1.9489
6	0.0886	0.1495	0.4488	1.0000	0.8109	2.6052
7	0.0897	0.1962	0.4663	1.0654	0.7804	2.5878
8	0.0944	0.2545	0.5379	1.0437	0.7710	3.2069
9	0.0972	0.2257	0.6029	1.1297	0.6875	3.4473
10	0.1281	0.2553	0.5814	1.1008	0.7679	3.7113
11	0.2336	0.3636	0.5919	1.3630	0.7233	3.0012
12	0.2128	0.3239	0.6878	1.4516	0.9504	3.9620
13	0.1757	0.3611	0.6833	1.3409	-	-
14	0.3027	0.4114	0.6878	1.4934	-	-
15	0.2560	0.4936	0.7478	1.6212	-	-
16	0.2495	0.4673	0.7450	1.4300	-	-
17	0.2630	0.4418	0.7593	1.5522	-	-
18	0.3062	0.5156	0.7713	1.7061	-	-
19	0.2942	0.5146	0.8809	1.5674	-	-
20	0.3958	0.6874	0.7535	1.6376	-	-
21	0.3887	0.5516	0.7563	1.8851	-	-
22	0.4054	0.6054	0.7422	2.0177	-	-
23	-	-	0.7563	2.1831	-	-
24	-	-	0.7039	2.0837	-	-
25	-	-	0.7422	2.3616	-	-
26	-	-	0.6812	2.3071	-	-
27	-	-	0.7288	2.4649	-	-
28	-	-	0.7450	2.4494	-	-
29	-	-	0.8584	2.5128	-	-

APPENDIX D

DATA TABLES FOR CHAPTER 3

Table D.1. XPS atomic composition for kinetics studies of chlorination of PF_3E films in the dark.

Time (min)	θ_T (degrees)	Atomic Composition (%)			
		C	O	F	Cl
PF_3E	15	39.76	1.07	59.17	0.00
	75	39.20	0.20	60.54	0.06
2.5	15	39.22	0.61	60.11	0.06
	75	38.21	0.51	61.25	0.03
5.0	15	39.05	1.22	59.17	0.02
	75	39.13	0.29	60.54	0.04
10	15	38.69	1.40	59.86	0.04
	75	39.65	0.40	59.92	0.03
20	15	39.03	0.83	60.13	0.01
	75	39.30	0.35	60.34	0.01

Table D.2. XPS atomic composition for kinetics studies of chlorination of PF$_3$E films using ambient light.

Time (min)	θ_T (degrees)	Atomic Composition (%)			
		C	O	F	Cl
PF$_3$E	15	39.76	1.07	59.17	0.00
	75	39.20	0.20	60.54	0.06
1	15	39.82	0.63	59.18	0.37
	75	38.87	0.28	60.65	0.21
13	15	39.69	0.52	59.16	0.63
	75	38.58	0.70	60.10	0.62
60	15	39.52	0.84	59.33	1.15
	75	38.71	0.53	59.79	0.97
100	15	38.86	1.40	56.54	3.20
	75	38.32	1.22	57.16	3.30

Table D.3. XPS atomic composition for kinetics studies of chlorination of PF$_3$E films using high-intensity UV light.

Time (min)	θ_T (degrees)	Atomic Composition (%)			
		C	O	F	Cl
PF$_3$E	15	39.76	1.07	59.17	0.00
	75	39.20	0.20	60.54	0.06
1	15	37.92	0.84	58.71	2.53
	75	39.07	0.80	57.85	2.28
4	15	37.74	2.00	54.05	6.21
	75	38.37	1.85	54.31	5.47
7	15	36.51	2.63	52.29	8.58
	75	36.78	1.89	53.54	7.79
10	15	33.86	1.74	49.16	15.24
	75	35.19	1.58	46.98	16.25
60	15	34.38	0.61	50.59	14.42
	75	33.79	0.88	50.60	14.73
100	15	33.56	1.82	50.14	14.48
	75	32.70	1.64	50.94	14.71
150	15	33.84	1.78	49.13	15.25
	75	33.07	1.66	50.38	14.89

Table D.4. Hexadecane contact angle (θ_A/θ_R) data for PCTFE, PF_3E and PF_3E chlorinated films using high-intensity UV light.

Sample	θ_A/θ_R (degrees)
PF_3E	25/11
1 min chlorinated PF_3E	24/6
10 min chlorinated PF_3E	10/3
100 min chlorinated PF_3E	9/2
150 min chlorinated PF_3E	9/2
PCTFE	8/2

Table D.5. Absorbance data obtained from transmission and ATR IR analysis of PF_3E films chlorinated using high-intensity UV light as a function of rection time.

Time (min)	Absorbance from Transmission Spectrum			Absorbance from ATR IR Spectrum		
	C-Cl	C-F[a]	C-Cl/C-F	C-Cl[b]	C-F[a]	C-Cl/C-F
10	-	-	-	0.16	0.85	0.19
60	-	-	-	0.27	0.62	0.44
100	0.46	3.1	0.15	0.28	0.51	0.55
150	0.44	2.7	0.16	0.34	0.62	0.56

a - The absorbance of C-F band is calculated from (Absorbance @ 1100 cm^{-1} + Absorbance @ 1186 cm^{-1})/2.

b - The absorbance of C-Cl band is calculated from (Absorbance @ 953 cm^{-1} + Absorbance @ 972 cm^{-1})/2.

Table D.6. Gravimetric data for PF_3E films chlorinated using high-intensity UV light as a function of reaction time.

Reaction Time (min)	Sample Number	Weight before Chlorination (± 0.01 mg)	Weight after Chlorination (± 0.01 mg)	Mass Gain (%)
1	1	30.40	31.58	3.74
	2	19.84	20.98	2.14
10	1	28.50	28.69	0.67
	2	33.23	33.55	0.96
100	1	38.12	38.81	1.57
	2	26.34	27.20	3.26
	3	28.04	29.07	3.67
	4	31.20	31.51	1.00
150	1	30.70	31.97	4.14
	2	53.03	54.01	1.85
	3	35.55	36.02	1.32
	4	40.90	41.81	2.22

Table D.7. Gas permeation data for PF_3E and PF_3E chlorinated films using high-intensity UV light for 100 min.

Sample	Hydrogen			Nitrogen		
	Pressure[c]	Time (sec)	Permeability[d]	Pressure[c]	Time (sec)	Permeability[d]
PF_3E	0.50	402	0.6	0.50	8373	4.2×10^{-2}
chlorinated PF_3E	0.50	880	1.3	0.20	16126	9.2×10^{-3}

c - Pressure (psi) read by transducer at the end of each measurements (start timing at 0 psi).

d - 10^{-9} cm^3(STP) cm/$cm^2 \cdot$ s $\cdot$cmHg

Table D.8. XPS atomic composition and hexadecane (θ_A/θ_R) contact angle data for kinetics studies of fluorination of PF$_3$E films using 5% F$_2$/N$_2$.

Time (min)	θ_T (degrees)	Atomic Composition (%)			θ_A/θ_R (degrees)
		C	O	F	
PF$_3$E	15	39.76	1.08	59.17	25/11
	75	39.20	0.20	60.54	
15	15	35.71	2.54	61.75	44/21
	75	32.69	0.80	66.51	
30	15	33.84	4.17	62.00	42/23
	75	32.76	0.93	66.31	
60	15	34.49	2.68	62.83	42/22
	75	32.41	0.70	66.89	
120	15	33.91	2.21	63.89	40/22
	75	33.06	0.76	66.17	
180	15	33.15	2.41	64.44	42/21
	75	32.24	0.60	67.16	
300	15	32.57	2.62	64.81	43/23
	75	33.24	1.23	65.52	

Table D.9. Gravimetric data for kinetics studies of fluorination of PF$_3$E films using 5% F$_2$/N$_2$ as a function of reaction time.

Reaction Time (min)	Weight before Fluorination (Ò 0.01 mg)	Weight after Fluorination (Ò 0.01 mg)	Mass gain (%)
15	56.37	56.35	-
30	36.78	36.80	0.05
60	55.20	55.27	0.13
120	45.55	45.68	0.28
180	45.90	46.00	0.22
300	43.93	44.17	0.54

Table D.10. Thin layer chromatography data for PF$_3$E eluted from THF:toluene mixtures (elution distance of eluent = 5.0 cm).

THF:toluene Mixture (v/v)	Elution Distance of Sample (cm)	R$_f$
0:100	0	0
10:90	1.45	0.29
20:80	2.30	0.46
30:70	1.65 - 2.30	0.33 - 0.46
40:60	1.30 - 1.95	0.26 - 0.39
50:50	1.30 - 1.90	0.26 - 0.38
60:40	3.30 - 4.00	0.66 - 0.80
70:30	3.20 - 3.80	0.64 - 0.76
80:20	3.30 - 4.30	0.66 - 0.86
100:0	5.00	1.00

Table D.11. XPS atomic composition and water and hexadecane (HD) contact angle (θ_A/θ_R) data for adsorption studies of PF$_3$E onto Si wafers as a function of THF:toluene composition.

THF:toluene	θ_T (degrees)	Atomic Composition (%)				θ_A/θ_R (water) (degrees)	θ_A/θ_R (HD) (degrees)
		C	O	F	Si		
Si wafer	15	33.82	46.90	-	19.28	30/15	7/0
	75	10.99	48.71	-	40.30		
100:0	15	35.48	38.80	8.98	16.75	69/20	15/4
	75	14.64	38.12	5.70	41.53		
75:25	15	34.17	40.17	10.45	15.21	66/20	15/6
	75	14.52	37.49	5.12	42.88		
50:50	15	32.16	36.76	15.31	15.77	72/18	20/8
	75	15.22	34.99	7.51	42.27		
25:75	15	33.82	24.03	31.08	11.07	84/23	26/8
	75	18.82	33.16	19.81	28.21		

Table D.12. XPS atomic composition and water contact angle (θ_A/θ_R) data for kinetics studies of PF$_3$E adsorption onto Si wafers from THF solution.

Time (h)	θ_T (degrees)	Atomic Composition (%)				θ_A/θ_R (degrees)
		C	O	F	Si	
0	15	33.82	46.90	-	19.28	30/15
	75	10.99	48.71	-	40.30	
0.25	15	32.47	43.68	5.33	18.53	44/18
	75	13.98	40.13	2.43	43.46	
0.50	15	42.95	37.12	7.24	12.69	43/16
	75	20.43	39.29	2.47	37.81	
1	15	34.10	42.63	8.00	15.27	49/20
	75	13.00	39.27	2.73	45.01	
2	15	32.21	43.09	8.98	15.72	48/23
	75	14.25	38.74	3.43	43.58	
4	15	34.51	44.13	7.48	13.88	59/21
	75	14.96	38.86	2.74	43.44	
8	15	32.01	45.05	6.37	16.57	68/22
	75	13.79	39.92	2.74	43.55	
16	15	33.98	41.15	6.93	17.95	-
	75	12.70	38.09	2.98	46.23	
24	15	35.48	38.80	8.98	16.75	69/20
	75	14.64	38.12	5.70	41.53	

Table D.13. XPS atomic composition and water contact angle (θ_A/θ_R) data for kinetics studies of PF$_3$E adsorption onto Si wafers from 50:50 THF:toluene solution.

Time (h)	θ_T (degrees)	Atomic Composition (%)				θ_A/θ_R (degrees)
		C	O	F	Si	
0	15	33.82	46.90	-	19.28	30/15
	75	10.99	48.71	-	40.30	
0.25	15	36.21	39.48	7.31	17.01	39/12
	75	13.91	44.48	4.51	37.10	
0.5	15	31.41	41.65	9.34	17.60	44/15
	75	12.80	44.52	5.99	36.69	
1	15	35.71	39.93	6.91	17.45	50/16
	75	13.06	45.50	5.24	36.20	
4	15	36.62	36.31	9.88	17.19	60/23
	75	14.76	37.18	5.68	42.37	
8	15	33.62	45.81	8.80	11.77	64/18
	75	13.61	38.57	4.58	43.23	
12	15	33.34	38.98	10.57	17.12	68/20
	75	13.93	36.99	5.48	43.60	
24	15	32.16	36.76	15.31	15.77	72/18
	75	15.22	34.99	7.51	42.27	
36	15	35.45	39.18	12.30	13.06	69/20
	75	15.28	37.65	5.53	41.54	

Table D.14. XPS atomic composition and water contact angle (θ_A/θ_R) data for adsorption studies of PF$_3$E onto Si wafers from THF solution as a function of polymer concentration.

Concentration (mg/ml)	θ_T (degrees)	Atomic Composition (%)				θ_A/θ_R (degrees)
		C	O	F	Si	
0	15	33.82	46.90	-	19.28	30/15
	75	10.99	48.71	-	40.30	
0.1	15	31.87	41.92	7.90	18.30	54/14
	75	11.38	48.35	3.83	36.44	
0.5	15	29.85	46.15	5.64	18.36	65/22
	75	10.10	47.86	3.39	38.65	
1.0	15	34.92	40.12	9.99	14.97	71/25
	75	13.86	37.89	4.32	43.93	
2.0	15	35.48	38.80	8.98	16.75	69/20
	75	14.64	38.12	5.70	41.53	
3.0	15	35.42	34.19	7.83	22.57	70/23
	75	13.09	37.22	4.12	45.57	

Table D.15. XPS atomic composition and water contact angle (θ_A/θ_R) data for adsorption studies of PF$_3$E onto Si wafers from 50:50 THF:toluene solution as a function of polymer concentration.

Concentration (mg/ml)	θ_T (degrees)	Atomic Composition (%)				θ_A/θ_R (degrees)
		C	O	F	Si	
0	15	33.82	46.90	-	19.28	30/15
	75	10.99	48.71	-	40.30	
0.1	15	31.39	41.15	9.82	17.64	48/16
	75	11.63	44.36	5.06	38.95	
0.5	15	30.80	38.98	12.70	17.52	59/23
	75	12.01	44.41	8.05	35.53	
1.0	15	35.32	31.81	16.22	16.65	72/24
	75	13.55	34.87	6.77	44.81	
2.0	15	32.16	36.76	15.31	15.77	72/18
	75	15.22	34.99	7.51	42.27	
3.0	15	39.52	29.54	14.06	16.89	70/24
	75	14.05	35.20	6.23	44.51	

APPENDIX E

ABBREVIATIONS

215

AIBN	azo(bisisobutyronitrile)
AFM	atomic force microscopy
ATR IR	attenuated total reflectance infrared
BPO	benzoyl peroxide
Bu_3SnH	tributyltin hydride
DSC	differential scanning calorimetry
GPC	gas permeation chromatography
HD	hexadecane
LLDPE	linear low density polyethylene
MAH	maleic anhydride
mm	mmHg
PAH	poly(allylamine hydrochloride)
PCTFE	poly(chlorotrifluoroethylene)
PCTFE-Ester	ester-functionalized poly(chlorotrifluoroethylene)
PCTFE-PEAA	acetal-functionalized poly(chlorotrifluoroethylene)
PCTFE-OH	alcohol-functionalized poly(chlorotrifluoroethylene)
PCTFE-OCOC$_3$H$_7$	butyrate-functionalized poly(chlorotrifluoroethylene)
PCTFE-OCOC$_{17}$H$_{35}$	stearate-functionalized poly(chlorotrifluoroethylene)
PCTFE-OCOC$_3$F$_7$	heptafluorobutyrate-functionalized poly(chlorotrifluoroethylene)
PCTFE-OH-PAH	polyallylamine adsorbed on alcohol functionalized poly(chlorotrifluoroethylene)
PF$_3$E	poly(trifluoroethylene)

PF$_3$E-g-MAH	maleic anhydride grafted poly(trifluoroethylene) or maleated poly(trifluoroethylene)
PMP	poly(4-methyl-1-pentene)
PSS	poly(sodium styrenesulfonate)
PTFE	poly(tetrafluoroethylene)
SC-CO$_2$	supercritical carbon dioxide
TGA	thermal gravimetric analysis
THF	tetrahydrofuran
TLC	thin layer chromatography
WAXS	wide angle x-ray scattering
XPS	x-ray photoelectron spectroscopy

BIBLIOGRAPHY

Aclar Technical Data, Allied-Signal Chemical Corp. Morristown, New Jersey.

Amouroux, J.; Goldman, M.; Revoil, M. F. *J. Polym. Sci. Polym. Chem. Ed.* **1982**, *20*, 1373.

Anand, M.; Cohen, R. E.; Baddour, R. F. *Polymer* **1981**, 22, 361.

Andrade, J. D.; Smith, L. M.; Gregonis, D. E. In *Surface and Interfacial Aspects of Biomedical Polymers*, Andrade, J. D., Ed., Plenum: New York, 1985; Vol.1, Chap. 7, pp 249-292.

Arnett, E. M. *Prog. Phys. Org. Chem.* **1963**, *1*, 223.

Ashley, J. C. *IEEE Trans. Nucl. Sci.* **1980**, *NS-27*, 1454.

Atre, S. V.; Liedberg, B.; Allara, D. L. *Langmuir* **1995**, *11*, 3882.

Bain, C. D.; Whitesides, G. M. *J. Am. Chem. Soc.* **1988**, *110*, 3665.

Bain, C. D.; Whitesides, G. M. *J. Am. Chem. Soc.* **1988**, *110*, 6560.

Bain, C. D.; Whitesides, G. M. *Langmuir* **1989**, *5*, 1370.

Bain, C. D.; Whitesides, G. M. *Science* **1988**, *240*, 62.

Bee, T. G. *Ph.D. dissertation* University of Massachusetts, **1993**.

Bee, T. G.; McCarthy, T. J. *Macromolecules* **1992**, *25*, 2093.

Bell, C. M.; Arendt, M. F.; Gomez, L.; Schmehl, R. H.; Mallouk, T. E. *J. Am. Chem. Soc.* **1994**, *116*, 8374.

Bening, R. C.; McCarthy, T. J. *Macromolecules* **1990**, *23*, 2648.

BlaakMeer, J.; Böhmer, M. R.; Cohen Stuart, M. A.; Fleer, G. J. *Macromolecules* **1990**, *23*, 2301.

Böhmer, M. R.; Evers, O. A.; Scheutjens, J. M. H. M. *Macromolecules* **1990**, *23*, 2288.

Borsig, E.; Hrckova, H., L. *J. M. S.-Pure Appl. Chem.* **1994**, *10*, 1447.

Brennan, J. V.; McCarthy, T. J. *Polym. Prepr.(Am. Chem. Soc. Div. Polym. Chem.)* **1989**, *30(2)*, 152.

Brown, H. C.; McDaniel, D. H.; Hflinger, O. In *Determination of Organic Structures by Physical Methods*; Braude, E. A., Nachod, F. C., Eds; Academic Press: New York, 1955; p 567.

Cadman, P.; Gossedge, G.; Scott, J. D. *J. Electron Spectr.* **1978**, *13*, 1.

Cais, R. E.; Kometani, J. M. *Macromolecules* **1984**, *17*, 1932.

Cassie, A. B. D. *Discuss. Faraday. Soc.* **1948**, *3*, 11.

Chen, W.; McCarthy, T. J. *Macromolecules* **1997**, *30*, 78.

Chen, W.; McCarthy, T. J. *Polym. Prep. (Am. Chem. Soc. Div. Polym. Chem.)* **1996**, *37(1)*, 457.

Cheung, J. H.; Fou, A. C.; Rubner, M. F. *Thin Solid Films* **1994**, *244*, 985.

Cimmino, S.; Mancarella, C.; Martuscelli, E.; Palumbo, R.; Ragosta, G. *Polym. Eng. Sci.* **1984**, *24*, 48.

Clark, D. T.; Fok, Y. C. T.; Roberts, G. G. *J. Electron Spectrosc.* **1981**, 22, 173.

Clark, D. T.; Thomas, H. R. *J. Polym. Sci., Chem.* **1977**, *15*, 2843.

Clark, D. T.; Thomas, H. R.; Shuttleworth, D. *J. Polym. Sci., Polym. Lett.* **1978**, *16*, 465.

Clark, D. T.; Wilson, R. *J. Polym. Sci. Polym. Chem. Ed.* **1983**, *21*, 837.

Cohen Stuart, M. A.; Cosgrove, T.; Vincent, B. *Adv. Colloid Interface Sci.* **1986**, *24*, 143.

Collin, G. C. S.; Lowe, A.C.; Nicholas, D. *Eur. Polym. J.* **1973**, 9, 1173.

Cooper, T. M; Campbell, A. L.; Crane, R. L. *Langmuir* **1995**, *11*, 2713.

Cosgrove, T.; Obey, T. M.; Vincent, B. *J. Colloid Interface Sci.* **1986**, *111(2)*, 1986.

Costello, C. A.; McCarthy, T. J. *Macromolecules* **1987**, *20*, 2819.

Cross, E. M.; McCarthy, T. J. *Macromolecules* **1990**, *23*, 3916.

Cross, E. M.; McCarthy, T. J. *Macromolecules* **1992**, *25*, 2603.

Csernica, J.; Rein, H.; Baddour, R. F.; Cohen, R. E. *Macromolecules* **1991**, *24*, 3612.

Decher, G. "Multilayer Films (Polyelectrolytes)" in "Polymeric Materials Encyclopedia: Synthesis, Properties, and Applications;" Salamone, J.C., Ed., vol. 6, CRC Press, Inc.: Boca Raton, 1996, 4540.

Decher, G.; Hong, J. D.; Schmitt, J. *Thin Solid Films* **1992**, *210/211*, 831.

de Gennes, P. G. *Macromolecules* **1982**, *15*, 492.

Dettre, R. H.; Johnson, R. E., Jr. *J. Phys. Chem.* **1965**, *69*, 1507.

Dias, A. J.; McCarthy, T. J. *Macromolecules* **1984**, *17*, 2529.

Dias, A. J.; McCarthy, T. J. *Macromolecules* **1985**, *18*, 1826.

Dias, A. J.; McCarthy, T. J. *Macromolecules* **1987**, *20*, 2068.

Dorinson, A.; Ludima, K. C. *Mechanism and Chemistry in Lubrication*; Elsevier Applied Science Publishers: Amsterdum, 1985.

Elman, J. F.; Gerenser, L. J.; Goppert-Berarducci, K. E.; Pochan, J. M. *Macromolecules* **1990**, *23*, 3922.

Evans, S. D.; Sharma, R.; Ulman, A. *Langmuir* **1991**, *7*, 156.

Evers, O. A.; Fleer, G. J.; Scheutjens, J. M. H. M.; Lyklema *J. Colloid Interface Sci.* **1986**, *111(2)*, 446.

Ferreira, M.; Rubner, M. F. Macromolecules **1995**, *28*, 7107.

Fleer, G. J.; Lyklema, J. In *Adsorptions from Solution at the Solid/Liquid Interface*; Chapter 4; Parfitt, G. D.; Rochester, C. H., Eds.; Academic Press: New York, 1983.

Fou, A. C.; Ontisuka, O.; Ferreira, M.; Rubner, M. F.; Hsieh, B. R. *Mat. Res. Soc. Symp. Proc.* **1995**, *369*, 575.

Fou, A. C.; Rubner, M. F. Macromolecules **1995**, *28*, 7115.

Franchina, N. L.; McCarthy, T. J. *Macromolecules* **1991**, *24*, 3045.

Gabara, W.; Porejko, S. *J. Polym. Sci. (A-1)* **1967**, *5*, 1547.

Gao, M.; Kong, X.; Zhang, X.; Shen, J. *Thin Solid Films* **1994**, *244*, 815.

Gaylord, N. G. *J. Macromol. Sci. Chem.* **1989**, *A26*, 1211.

Gaylord, N. G.; Mehta, R.; Deshpande, A. B. In *New Advances in Polyolefins*, Chung, T. C., Ed.; Plemum Press: New York, 1993; p 115.

Gaylord, N. G.; Mehta, M.; Mehta, R. *J. Appl. Polym. Sci.* **1987**, *33*, 2549.

Gaylord, N. G.; Mehta, R.; Mohan, D. R.; Kumar, V. *J. Appl. Polym. Sci.* **1992**, *44*, 1941.

Hall, S. M.; Andrade, J. D.; Ma, S. M.; King, R. N. *J. Electron Spectrosc.* **1979**, *17*, 181.

Hammond, P. T.; Whitesides, G. M. *Macromolecules* **1995**, *28*, 7569.

Harrick, N. J. *Internal Reflection Spectroscopy*, Wiley Interscience: New York, 1967.

Hayes, H. J.; McCarthy, T. J. *Polym. Prep. (Am. Chem. Soc. Div. Polym. Chem.)* **1997**, 38(2), in press.

Holmes-Farley, S. R.; Reamey, R. H.; Nuzzo, R. G.; McCarthy, T. J.; Whitesides, G. M. *Langmuir* **1987**, *3*, 799.

Hong, H.; Davidov, D.; Avny, Y.; Chayet, H.; Faraggi, E. Z.; Neumann, R. *Adv. Mater.* **1995**, *7*, 846.

Israelachvili, J. N.; Gee, M. L. *Langmuir* **1989**, *5*, 288.

Johnson, R. E., Jr.; Dettre, R. H. *J. Phys. Chem.* **1964**, *68*, 1744.

Johnson, R. E., Jr.; Dettre, R. H. In *Contact Angle, Wettability and Adhesion*, Fowkes, F. M., Ed.; Advances in Chemistry Series No. 43; American Chemical Society: Washington, D. C.,1964.

Johnson, R. E., Jr.; Dettre, R. H. In *Surface and Colloid Science*, Matijevic, E., Ed., Wiley-Interscience: New York, 1969.

Johnson, R. E., Jr.; Dettre, R. *Surface Colloid Sci.* **1979**, *11*, 1.

Keller, S. W.; Kim, H. -N.; Mallouk, T. E. *J. Am. Chem. Soc.* **1994**, *116*, 8817.

Kleinfeld, E. R.; Ferguson, G. S. *Science* **1994**, *265*, 370.

Knutson, K.; Lyman, D. In *Surface and Interfacial Aspects of Biomedical Polymers*, Andrade, J. D., Ed., Plenum: New York, 1985; Vol.1, Chap. 6, pp 197-247.

Kong, W.; Zhang, X; Gao, M. L.; Zhou, H.; Zhang, X.; Li, W.; Shen, J. C. *J. Chem. Soc., Chem. Commun.* **1994**, 1297.

Kotov, N. A.; Dekany, I.; Fendler, J. H. *J. Phys. Chem.* **1995**, *99*, 13065.

Laibinis, P. E.; Bain, C. D.; Whitesides, G. M. *J. Phys. Chem.* **1991**, *95*, 7017.

Laibinis, P. E.; Marye, A. F.; Folkers, J. P.; Whitesides, G. M. *Langmuir* **1991**, *7*, 3167.

Laibinis, P. E.; Whitesides, G. M. *J. Am. Chem. Soc.* **1992**, *114*, 1990.

Laibinis, P. E.; Whitesides, G. M.; Allara, D. L.; Tao, Y. -T.; Parikh, A. N.; Nuzzo, R. G. *J. Am. Chem. Soc.* **1991**, *113*, 7152.

Langmuir, I. *J. Am. Chem. Soc.* **1916**, *38*, 2221.

Langmuir, I. *Science* **1938**, *87*, 493.

Lee, K. -W.; McCarthy, T. J. *Macromolecules* **1988**, *2*, 309.

Lee, K.-W.; McCarthy, T. J. *Macromolecules* **1988**, *21*, 2318.

Levӓsalmi, J. -M. *Ph.D. dissertation* University of Massachusetts, **1996**.

Levӓsalmi, J. -M.; McCarthy, T. J. *Macromolecules* **1995**, *28*, 1733.

Levӓsalmi, J. -M.; McCarthy, T. J. *Macromolecules* **1997**, *30*, 1752.

Lovinger, A. J.; Cais, R. E. *Macromolecules* **1984**, *17*, 1939.

Lovinger, A., J.; Davis, G. T.; Furukawa, T.; Broadhurst, M. G. *Macromolecules* **1982**, *15*, 323, 329.

Lvov, Y.; Ariga, K.; Kunitake, T. *Chem. Lett.* **1994**, 2323.

Lvov, Y.; Decher, G.; Möhwald, H. *Langmuir* **1993**, 9, 481.

Lvov, Y.; Decher, G.; Sukhorukov, G. *Macromolecules* **1993**, 26, 5396.

Lvov, Y.; Essler, F.; Decher, G. *J. Phys. Chem.* **1993**, 97, 13773.

Lvov, Y.; Haas, H.; Decher, G.; Möhwald, H. *J. Phys. Chem.* **1993**, 97, 12835.

Lvov, Y.; Haas, H.; Decher, G.; Möhwald, H. *Langmuir* **1994**, 10, 4232.

Mao, G.; Tsao, Y.; Tirrell, M.; Davis, H. T. *Langmuir* **1993**, 9, 3461.

Mirabella, F. M. Jr. *Applied Spectroscopy Reviews* **1985**, 21(1&2), 45.

Mitsuaki, N.; Masuasu, A. *J. Chem. Soc. Jpn.* **1970**, 70, 1432.

Mittal, K. L., Ed.; *Adhesion Aspects of Polymeric Coatings.*;
Plenum Press: New York, 1983.

Mohr, J. M.; Paul, D. R.; Pinnau, I.; Koros, W. J. *J. Membr. Sci.* **1991**, 56, 77.

Mohr, J. M.; Paul, D. R.; Taru, Y.; Mlsna, T. E.; Lagow, R. J.
J. Membr. Sci. **1991**, 55, 149.

Muller, G.; Abraham, K.; Schaldach, M. *Applied Optics* **1981**, 20(7), 1182.

Nakagawa, T.; Yamada, S. *J. Appl. Polym. Sci.* **1972**, 16, 1997.

Napper, D. *Polymeric Stabilization of Colloidal Dispersions*;
Academic Press: London, **1983**.

Nuzzo, R. G.; Allara, D. L. *J. Am. Chem. Soc.* **1983**, 105, 4481.

Oster, G.; Shibata, O. *J. Polym. Sci.* **1957**, 26, 233.

Penning, J. F. M.; Bosman, B. *Colloid Polym. Sci.* **1979**, 257, 720.

Porejko, S.; Gabara, W.; Kulesza *J. Polym. Sci. (A-1)* **1967**, 5, 1563.

Porter, M. D.; Bright, T. B.; Allara, D. L.; Chidsey, C. E. D. *J. Am. Chem. Soc.*
1987, 109, 3559.

Roover, B. D.; Sclavons, M.; Carlier, V.; Devaux, J.; Legras, R.; Momtaz, A.
J. Appl. Polym. Sci. **1987**, 33, 2549.

Rossman, K. *J. Polym. Sci.* **1956**, 19, 141.

Samay, G.; Nagy, T.; White, J. L. *J. Appl. Polym. Sci.* **1995**, 56, 1423.

Sanderson, R. D.; du Toit, F. J.; Carstens, P. A. B.; Wagner, J. B.
Thermal Analysis **1994**, 41, 563.

Sathe, S. N.; Rao, G. S. S.; Devi, S. *J. Appl. Polym. Sci.* **1994**, *53*, 239.

Scheutjens, J. M. H. M.; Fleer, G. J. *J. Phys. Chem.* **1979**, *83*, 1619.

Scheutjens, J. M. H. M.; Fleer, G. J. *J. Phys. Chem.* **1980**, *84*, 178.

Schonhorn, H.; Hansen, R. H. *J. Appl. Polym. Sci.* **1968**, *12*, 1231.

Shimada, J.; Hoshino, M. *J. Appl. Polym. Sci.* **1975**, *19*, 1439.

Shoichet, M. S.; McCarthy, T. J. *Macromolecules* **1991**, *24*, 982.

Silverstein, R. M.; Bassler G. C.; Morrill, T. C. *Spectrometric Identification of Organic Compounds*, John Wiley and Sons: New York, 1981, pp 107.

Snyder, R. G.; Hsu, S. L.; Krimm, S. *Spectrochim. Acta, Part A*, **1978**, *34*, 395.

Stockton, W. B.; Rubner, M. F. *Polymer Prepr. (Am. Chem. Soc. Div. Polym. Chem.)* **1994**, *35*, 319.

Tadras, T. F. In *Polymer Colloids* ; Corner, T.; Buscall, R., Eds.; Elsevier Applied Science Publishers: New York, 1984.

Tam-Chang, S. -W.; Biebuyck, H. A.; Whitesides, G. M.; Jeon, N.; Nuzzo, R. G. *Langmuir* **1995**, *11*, 4371.

Timmons, C. O.; Zisman, W. A. *J. Colloid Interface Sci.* **1966**, 165.

Troughton, E. B.; Bain, C. D.; Whitesides, G. M.; Allara, D. L.; Nuzzo, R. G.; Porter, M. D.*Langmuir* **1988**, *4*, 365.

Van der Schee, H. A.; Lyklema, J. *J. Phys. Chem.* **1984**, *88*, 6661.

Wang, H.; Zhang, Q. M.; Cross, L. E.; Sykes, A. O. *J. Appl. Phys.* **1993**, *74*, 3394.

Wu, C. -J.; Chen, C. -Y.; Woo, E.; Kuo, J. -F. *J. Polym. Sci. Polym. Chem.Ed.* **1993**, *31*, 3405.

Xanthas, M. *Polym. Eng. Sci.* **1988**, *28*, 1392.

Yagi, T. *Polymer J.* **1979**, *11*, 711.

Yamada, T. K., Kitayama, T. J. *J. Appl. Phys.* **1981**, *52*, 6859.

Yamamoto, F.; Yamakawa, S. *J. Polym. Sci. Polym. Chem. Ed.* **1979**, *17*, 1581.

Yasuda, H.; Sharma, A. K.; Yasuda, T. *J. Polymer Sci., Phys.* **1981**, *19*, 1258.

Young, T. (a) *Phil. Trans.* **1805**, 95, 65., (b) *Phil. Trans.* **1805**, *95*, 82.